Application of Suction Stress Concept to Partially Saturated Compacted Soils

Dissertation

as a requirement of the degree of
Doktor-Ingenieur (Dr.-Ing.)

at the Faculty of
Civil and Environmental Engineering
Ruhr-Universität Bochum

submitted by
Alborz Pourzargar
from Esfahan, Iran

Reviewers
Prof. Dr.-Ing. habil. Tom Schanz
Prof. Dr.-Ing. Gunnar Heibrock
Prof. Dr.-Ing. Maria Datcheva

Bochum, December 2017

Vorwort des Herausgebers

Die vorliegende Promotion von Herrn Alborz Pourzargar beschäftigt sich mit einem der zentralen Themen der modernen Bodenmechanik. In den 30er Jahren des letzten Jahrhunderts befasste sich Karl v. Terzaghi mit dem Begriff der "effektiven" Spannung in trockenen oder vollständig wassergesättigten Materialien. Die auf diesen klassischen Forschungsarbeiten aufbauenden Arbeiten sind zahlreich und die eingeschlagenen Wege und ihre Methodik ist vielfältig.

In den 50er Jahren wurde erstmals von Bishop et al. versucht den Begriff der effektiven Spannung, auf teilgesättigte Böden zu erweitern. Seither gibt es wiederum die unterschiedlichsten Konzepte, die sich grundsätzlich in zwei Gruppen unterteilen lassen: Arbeiten mit zwei Spannungsgrößen bzw. Arbeiten mit nur einer effektiven Spannungsgröße. Letzteren Ansatz versucht diese Arbeit zu validieren, und zwar für den Bereich der Scherfestigkeit teilgesättigter feinkörniger Böden.

Grundlegender Ansatz der Promotion ist der Versuch das sogenannte "suction stress concept" (SCC) nach Lu Likos mittels experimenteller Untersuchungen in verschiedenen Versuchsgeräten zu validieren. Betrachtet werden hierzu ausschließlich Ergebnisse zur Scherfestigkeit. Gegenübergestellt werden die aus den Scherversuchen rückgerechneten effektiven Spannungen den unabhängig aus der Saugspannungs-Sättigungs-Beziehung (SWCC) ermittelten Werten. Es ergeben sich sowohl im Vergleich der Scherversuche als auch in deren Vergleich mit den Werten mittels der SWCC erhebliche Abweichungen. Diese Ergebnisse wurden international hochrangig publiziert. Ursache für diese Abweichungen sind jedoch nicht ausschließlich Defizite der Theorie, sondern möglicherweise auch Besonderheiten der Versuchsdurchführung. Die Scherversuche wurden sowohl im Triaxialversuch, als auch im direkten Zugversuch und einem neuartigen Versuchsgerät (Hohl-Zylinderversuch) durchgeführt. Alle diese unterschiedlichen Versuchsgeräte erfordern unterschiedliche Versuchskörpergeometrien, dies ist unumgänglich und generell beherrschbar, der Aufwand jedoch sehr umfangreich. Zur Herstellung der Proben für diese Versuche wurde die Methode der dynamischen Verdichtung verwendet. Die Proben zur Bestimmung der SWCC wurden aber überwiegend statisch verdichtet. Bei diesem Vorgehen ergeben sich auf Grund der unterschiedlich resultierenden Mikrostruktur, auch bei identischer Porenzahl und identischem Wassergehalt, unterschiedliche hydro-mechanische Eigen-

schaften. Dieses ist bei dem Vergleich der Ergebnisse zu berücksichtigen.

Herr Pourzargar beschäftigt sich in seiner Promotion mit der Untersuchung des Begriffs der "effektiven" Spanning in teilgesättigten, verdichteten Böden. Als theoretische Grundlage verwendet er die wegweisenden Arbeiten von Lu Likos, welche das sogenannte "suctions stress concept" einführten. Die ursprüngliche Anwendung betraf teilgesättigte granulare Böden. Herr Pourzargar erweitert seine Untersuchungen in den Bereich der verdichteten, feinkörnigen Böden.
Die Arbeit umfasst überwiegend experimentelle Elemente. Neben dem umfangreichen Versuchsprogramm mit nicht einfachen, aber bereits bewährten Versuchstechniken, unternimmt Herr Pourzargar erste Schritte, ein neuartiges Versuchsgerät zu validieren und dadurch die Aussagekraft zum Zusammenhang zwischen der effektiven Spannung und der Zugfestigkeit zu untermauern.

Bochum, Oktober 2017

Tom Schanz

This work is dedicated to my beloved parents

Mohammad and Tayebeh and my wife Sahar

Acknowledgements

All praises and thanks be to God for giving me strength and courage to achieve one of the challenging tasks of my life. This PhD thesis is a result of five years of research work carried out at Chair for Foundation Engineering, Soil and Rock Mechanics, Ruhr-Universität Bochum. I would like to thank first and foremost my supervisor, Prof. Tom Schanz, who gave me the opportunity to start my PhD and provided his continues support over all these years. My sincere gratitude goes to Dr. Diethard König, who helped me during my research and for his comments and suggestions throughout these years.

I want to express my sincere thanks to Prof. Maria Datcheva, for all the support and encouragement she gave me.

I would like to thank Prof. Gunnar Heibrock for his support during this study. At many times of this research project I benefited from his advice, particularly so when exploring new ideas.

I hereby express my special thanks to the Central Scanning Electron Microscope and the Chair for Building Materials of Ruhr-Universität Bochum for their kind cooperation and technical supports.

My gratitude should also be extended to all my current and former colleagues, laboratory staffs, and to all parties who indirectly assisted me during my period of stay in Bochum.

Last but not least, I wish to gratitude my family for the whole support they have always given to me. Without their helps I would not be able to accomplish this work.

Alborz Pourzargar

Bochum, Germany

November 2017

Abstract

To date there is an ongoing discussion about how to describe the effect of soil- water interaction (in terms of suction) when dealing with the mechanical behavior, especially the shear strength, of partially saturated soils. One approach is to describe the effect of matric suction on the state of stress in terms of effective stress. This approach has the fundamental advantage of extending classical soil mechanic work to unsaturated soil conditions. The growing number of laboratory tests indicates that the effective stress concept is sufficient to describe macroscopic effects from soil- water interaction when dealing with shear-strength related problems. However, systematic experimental study of the effective stress with taking into account a wide range of suction as well as different failure modes and different kind of soils is still missing.

The purpose of the research work is to examine the effective stress concept with respect to different failure modes observed in tensile and shear tests. This means that different failure modes are used to determine suction stress. The materials used to study the effective stress concept were including pure sand, two sand-kaolin mixtures, and pure kaolin (fine to coarse grained).

The experimental study allows to investigate failure at tensile to high compression stress conditions, as well as taking into account the entire suction range. The values of suction stress derived by different experimental methods were compared with those predicted via SWCC on drying curve and the reason for observed deviations in suction stress derived from different methods are discussed.

To estimate the magnitude of different interparticle stresses on suction stress, the capillary stress and physicochemical stress have been determined and measured by mechanics based model and van der Waals stresses respectively. Observation of the soil structure as influenced by variation in degree of saturation was studied qualitatively and quantitatively in the process of drying and saturation.

Although the tensile behavior of materials can be obtained by the direct tensile method, many researchers have questioned the validity of the direct tensile strength in the past. To escape from the difficulties of the direct tensile test a different way has been worked out for determination of tensile strength by an indirect method which is called Hollow Cylinder. Comparisons of results obtained for suction stress show good agreement between the determined values derived from hollow cylinder with those predicted via SWCC and direct tensile test experiments.

The results showed the suction stress values derived by tensile tests and triaxial tests were consistent for samples with low matric suction. Predicted values of the suction stress using the SWCC were found to be significantly higher as compared to the suction stress values obtained based on tensile and triaxial tests and this method failed for sample with higher amount of fine content.

One reason for the observed deviations in suction stress values derived from tensile tests and triaxial tests may be that suction stress at different levels of saturation and failure modes is dominated by different interparticle stresses. In addition the upscaling function to predict suction stress from SWCC does not consider the contributions of different interparticle stresses originating e.g. from capillary effects and physico-chemical stresses varying with degree of saturation. Also changes in micro structure of the soil samples during drying and wetting may influence the suction stress, which is not reproduced by SWCC.

Zusammenfassung

Das mechanischen Verhalten von teilgesättigten Böden wird durch die Wechselwirkung zwischen der Wasserphase und dem Korngerüst (Saugspannung) maßgeblich bestimmt. Wie diese Wechselwirkung bei der Beschreibung des mechanischen Verhaltens und insbesondere der Scherfestigkeit solcher Böden zu berücksichtigen ist, wird nach wie vor diskutiert. Eine Vorgehensweise ist, den Einfluss der Saugspannung auf das mechanische Verhalten im Rahmen des Konzeptes der effektiven Spannungen zu beschreiben. Dieses hat den Vorteil, die klassischen bodenmechanischen Berechnungsansätze auch auf teilgesättigte Böden anwenden zu können. Zahlreiche experimentelle Untersuchungen weisen darauf hin, dass bei der Anwendung des Konzeptes der effektiven Spannungen die makroskopische Wirkung der Interaktion zwischen Wasser und Bodenteilchen in Form einer "suction stress", welche den wirksamen Anteil der Saugspannungen, d.h. deren Anteil an den effektiven Spannungen, ausreichend berücksichtigt. Eine umfassende experimentelle Studie hierzu, welche einen großen Saugspannungsbereich, verschiedene Versagensformen und verschiedene Bodenarten abdeckt, liegt bisher nicht vor. Das Ziel dieser Arbeit ist es, die Anwendbarkeit des Konzeptes der effektiven Spannungen bei teilgesättigten Böden unter Berücksichtigung verschiedener Versagensformen in Zug und Scherversuchen zu untersuchen. Die Wirkung der Saugspannung auf die effektiven Spannungen, die "suction stress", wird aus Versuchen mit unterschiedlichen Versagensformen bestimmt. Es werden Versuchsdaten an Sand, an zwei Mischungen aus Sand und Kaolin und an Kaolin einbezogen. Die experimentellen Untersuchungen erfassen Versagenszustände unter Zugspannungen bis hin zu großen Druckspannungen und unter einer großen Bandbreite von Saugspannungen. Die aus den Versuchen abgeleiteten Werte für die "suction stress" werden "suction stress" gegenübergestellt, welche aus der Saugspannungs-Sättigungsbeziehung (SWCC) auf dem Trocknungspfad berechnet werden. Die sich ergebenden Abweichungen werden diskutiert. Um die Größe der unterschiedlichen Komponenten, welche auf der Mikrostrukturebene zur "suction stress" beitragen, abschätzen zu können, werden die Kapillarspannungen und die physikalisch-chemischen Spannungen, hier infolge van der Walls Kräfte, durch theoretische Ansätze bestimmt. Zusätzlich werden Veränderungen in der Mikrostruktur der Böden infolge der Wassergehaltsänderungen untersucht. Direkte Zugversuche an Böden beinhalten zahlreiche versuchstechnische Schwierigkeiten und die Aussagekraft solcher Versuche wird in der Literatur oft in Frage gestellt. Eine Alternative bildet die Bestimmung der Zugfestigkeit in einem Hohlzylin-

dergerät unter speziellen Randbedingungen. Ein entsprechendes Hohlzylindergerät wird im Rahmen dieser Arbeit entwickelt und getestet. Die aus den Ergebnissen der Versuche im Hohlzylindergerät abgeleiteten "suction stress" liegen in vergleichbaren Größenordnungen wie die, welche auch mit den direkten Zugversuchen und den Scherversuchen ermittelt wurden. Der Vergleich der aus den Zug- und Scherversuchen abgeleiteten "suction stress" zeigt, dass sich diese bei kleinen Saugspannungen entsprechen. Die aus der SWCC berechneten "suction stress" liegen oberhalb der aus den Experimenten bestimmten, wobei die Abweichungen mit zunehmender Saugspannung stark ansteigen. Ein Grund für die Abweichungen ist, dass die "suction stress" bei verschiedenen Wassergehalten und Versagensformen von unterschiedlichen Mechanismen auf der Mikrostrukturebene bestimmt werden. Diese unterschiedlichen Mechanismen werden bei der Berechnung der "suction stress" aus der SWCC nicht berücksichtigt, wie auch die Änderungen in der Microstruktur der Böden unter Austrocknung und Sättigung durch die SWCC nicht ausreichend abgebildet werden.

Contents

List of Figures

List of Tables

Nomenclature

σ_1	Maximum principal stress
σ_2	Intermediate principal stress
σ_3	Minimum principal stress
σ'_1	Maximum principal effective stress
σ'_2	Intermediate principal effective stress
σ'_3	Minimum principal effective stress
σ_n	Total normal stress
σ'_n	Effective total normal stress
σ_t	External stress, propagate through the granular skeleton
σ_{pc}	Physicochemical stresses
σ_C	Particle to particle contact stress
σ_{cap}	Capillary stress
σ_{vdw}	Van der Waals stress
σ_{C0}	Physicochemical stress at the saturated state or apparent tensile stress at the saturated state
$\Delta\sigma_{pc}$	A change in physicochemical stress due to desaturation
σ^s	Suction stress
σ_{tit}	Isotropic tensile strength in non linear M-C failure envelope

σ_{tut} Uniaxial tensile strength in non linear M-C failure envelope

σ_{tia} Isotropic tensile strength

σ_{tua} Uniaxial tensile strength

$(\sigma_n - u_a)$ Net normal stress

σ_r Radial stress

σ_θ Tangential stress

σ_z Axial stress

σ_t Tensile strength

σ_d, q Deviatoric stress, $\frac{\sigma_1 - \sigma_3}{2}$

$\sigma^s_{isotropic\ tensile}$ Suction stresses derived from isotropic tensile stress

$\sigma^s_{direct\ tensile}$ Suction stresses derived from direct tensile strength

σ^s_{SWCC} Suction stresses derived from SWCC

p Mean stress, $\frac{\sigma_1 + \sigma_3}{2}$

p' Effective mean stress

ϵ_1 Maximum principal strain

ϵ_3 Minimum principal strain

u Pore water pressure

u_a Pore air pressure

u_w Pore water pressure

$f(u_a - u_w)$ Function of matric suction

χ Effective stress parameter

X An upscaling factor describing the average portion of forces acting on a microscopic level

c	Cohesion
c'	Effective cohesion
c_t	Cohesion at low stress regims
φ	Friction angle
φ'	Effective friction angle
φ_t	Friction angle at low stress regims
φ'_t	Friction angle of the saturated condition at low stress regims
Ψ_{AEV}	Suction corresponding to air entry value
Ψ_r	Residual suction
α	Empirical fitting parameters (inverse of air entry pressure)
n	Empirical fitting parameters (pore size distribution parameter)
F_t	External force, propagate through the granular skeleton
F_{pc}	Physicochemical forces
F_C	Particle to particle contact force
F_{cap}	Capillary force
H_c	Hamaker constant
h	Thickness of the adsorbed layers
J	Unit of energy
ω	Gravimetric water content
S_a	Specific surface area
ρ_w	Mass density of water
s	Distance of two particles

R	Water bridge exists between two particles
F	Capillary bonding force
T_s	Surface tension force
θ	Contact angle
β	Filling angle
R_1 and R_2	Two radii of water bridge curvature
V_{bridge}	Volume of the water bridge
k	Mean coordination number
ρ_{sol}	Particle density
ρ_{liq}	Liquid density
ϕ	Porosity
Sr	Actual degree of saturation
Sr_e	Effective degree of saturation
Sr_r	Residual degree of saturation
$\sum F_p$	Sum of the interparticle forces
T	Width of the loading strip
D	Diameter of the specimen
P	Applied pressure in bending test
M	Bending moment
$\bar{y}$	Distance of the tensile surface of the beam from the neutral axis
I	Moment of inertia
p_o	Outer pressur

p_i Inner pressur

p_{cr} Critical pressure

$p_{plastic}$ Fully plastic state pressure

a, b and c Inner, outer and plastic radius

r At any point of a radial distance

A Grain surface

A_a Dry portions of the grain surfaces

A_w Wetted portions of the grain surfaces

w_{opt} Optimum proctor water content

s_t Total suction

R_g Universal gas constant

T_a Absolute measured temperature

M_w Molecular weight of water

e Void ratio

d_1 Diameter assign to volume of mercury

d_2 Diameter assign to additional volume of mercury

h_0 Initial height of specimen

Δh Change in height of specimen

Δh Change in height of specimen

1. Introduction

1.1. Background

Geotechnical research firmly established that the mechanical aspects of a soil (i.e. the change in volume and shear strength) can be described in terms of the strength parameters and state of stress. In saturated soil, the state of stress can be described by total stress and pore pressure, unified under the concept of effective stress.
A statement about the effective stress principle was given by Terzaghi (1936) at the first international conference on soil mechanics and foundation engineering as follow:

"The stresses in any point of a section through a mass of soil can be computed from the total principal stresses, σ_1, σ_2, σ_3, which act in this point. If the voids of the soil are filled with water under a stress u, the total principal stresses consist of two parts. One part, u, acts in the water and in the solid in every direction with equal intensity. It is called the neutral stress (or the pore water pressure). The balance $\sigma'_1 = \sigma_1 - u$, $\sigma'_2 = \sigma_2 - u$, and $\sigma'_3 = \sigma_3 - u$, represents an excess over the neutral stress u, and it has its seat exclusively in the solid phase of the soil. This fraction of the total principal stresses will be called the *effective principal stresses*. Porous materials (such as sand, clay, and concrete) react to a change of u as if they are incompressible and their internal friction are equal to zero (Terzaghi 1936). All the measurable effects of a change of stress, such as compression, distortion and a change of shearing resistance are exclusively due to changes in the effective stresses σ'_1, σ'_2 and σ'_3."
The effective stress concept has been well accepted and studied for saturated soils. Numerous attempts have been made to develop a similar concept of effective stress for partially saturated soils. However, partially saturated soils are more complex, and it has been more difficult to arrive at an agreement with regards to the description of the effective stress.
Bishop (1959) was one of the first who tried to extend the concept of effective stress to partially saturated soils:

$$\sigma'_n = (\sigma_n - u_a) + \chi(u_a - u_w) \tag{1.1}$$

Here, χ is a parameter related to the degree of saturation (effective stress parameter). The magnitude of the χ parameter is unity for a saturated soil and zero for a dry soil. $(\sigma_n - u_a)$ is the net normal stress and $(u_a - u_w)$ is matric suction. This approach has the fundamental advantage that classical soil mechanics principles can be applied to partially saturated soils. Examination of the proposed effective stress concept has led many researchers to suggest the use of $(\sigma_n - u_a)$ and $(u_a - u_w)$ to describe the mechanical behavior of partially saturated soils (Jennings & Burland 1962, Aitchison 1965, Blight 1967, Fredlund & Morgenstern 1977).

A growing number of lab tests indicate that the effective stress concept is sufficient to describe macroscopic effects from soil water interactions when dealing with a limit state e.g. shear strength related problems and, the complex behavior of partially saturated soils might be described using classical soil mechanic principles. However, existing studies have limitations e.g. in terms of suction range and failure mode investigated and systematic experimental study of the effective stress taking into account a wide range of suction as well as different failure modes and different kind of soils is still missing.

1.2. Objectives and scopes of the work

The primary objective of this research is to examine the suction stress and therefore effective stress concept with respect to different failure modes observed in tensile and shear tests. This means that different modes of failure are used to determine suction stress. The experimental study allows to investigate failure at tensile to high compression stress conditions (full mechanical stress) as well as to take into account dry to saturated conditions (full suction range).

To estimate the possible order of magnitude of different interparticle stresses on suction stress, capillary stresses and physicochemical stresses are calculated as functions of saturation using existing approaches. In addition, as a first indicator for changes in microstructure during drying and wetting, environmental scanning electron microscopy (ESEM) and mercury intrusion porosimetry (MIP) are performed.

The materials used to study the effective stress concept were sand, two sand-kaolin mixtures (70-30 and 50-50) and pure kaolin. Due to the complex and time consuming tests when dealing with partially saturated soils, experimental studies of the effective stress concept are limited in terms of soil type and suction range investigated. To overcome

these limitation, direct tensile and triaxial tests are performed on two sand-kaolin mixtures and the experiments of Lu et al. (2007) and Alabdullah (2010) on pure sand and experimental results by Heibrock (1997) and Brueggemann (1998) on pure kaolin are used to study of the effective stress concept.

The specific scope of the work includes (Fig. 1.1):

- Determination of the basic properties of the materials used.
- To examine the behavior of partially saturated soils under different failure modes by performing and analyzing tensile and shear tests at different degrees of saturation (box 1).
- To study the effective stress concept by using the data from the experiments performed within this study (box 2).
- Conducting experiments to obtain data for main drying, wetting and scanning soil water characteristic curves (SWCC) and back analyzing this data against known mathematical models of SWCC (box 3).
- Investigation of the soil structure and pore system by means of ESEM and MIP (box 3).
- To estimate the importance of the interparticle stresses for defining suction stress employing existing methodology and test data (box 4).
- Comparing the values of the suction stresses derived from the experimental tests with those predicted via SWCC and existing models.
- Design of new hollow cylinder device to study tensile strength under matric suction controlling on pure sand (box 1).

1.3. Organization of Thesis

This dissertation consists of eight chapters. The first chapter gives an introduction to the thesis explaining the motivation and main objectives. The second chapter presents the basics of partially saturated soil mechanics and the effective stress concept for partially saturated soils. Different methods for the determination of suction stresses via tensile tests, shear tests and predictions from SWCC are summarized. The interparticle stresses, which act in partially saturated soils and the models formulated on a microstructure level

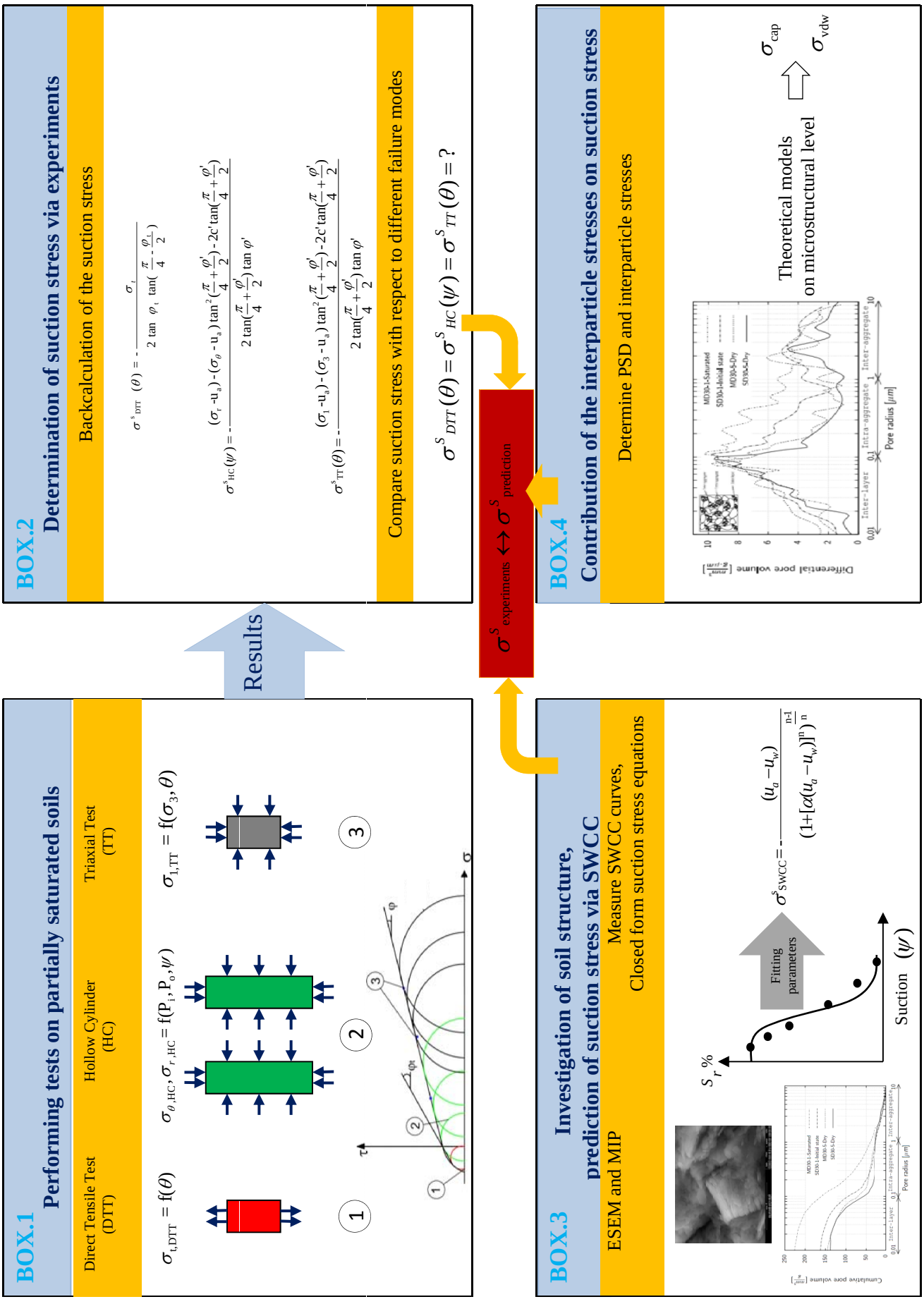

Figure 1.1.: The specific scope of the work

for the determination of them are also discussed. Direct and indirect methods for the determination of tensile strength are introduced and the advantages of the hollow cylinder for determination of the tensile strength and the principle of the cavity expansion theory are explained.
The basic properties of the materials used, experimental techniques, sample preparation and test procedures are discussed in chapter 3.
The results of SWCC, direct tensile tests, triaxial tests and observed formation and evolution of the soil structure during wetting-drying processes by using ESEM and MIP methods are presented in chapter 4.
In chapter 5, the values of the suction stresses derived from direct tensile test and shear tests for materials used (sand, two sand-kaolin mixtures and pure kaolin) are presented. In addition, the suction stress is predicted from closed form equation employing SWCC equation.
In chapter 6, by using the results of the MIP and the theoretical relationship introduced in chapter 2, the interparticle stresses (van der Waals stress and capillary stress) are determined. The suction stress values derived using data from different experimental methods are compared with those predicted via SWCC and the existing models on microstructure level. The reason of the difference between the values of the suction stress using different methods is discussed.
Setup and calibration of the new hollow cylinder device are presented in chapter 7. In this chapter, the results of the hollow cylinder are compared with experiments and those predicted from SWCC and theoretical method.
Chapter 8, includes the conclusions derived from this study.

2. State of the art

2.1. Overview

In this chapter the basics of partially saturated soil mechanic relevant to this study are briefly presented, along with a survey on the soil-water characteristic curve and different methods for measuring suction. Concepts of effective stress, stress state variables, tensile and shear strength of partially saturated soils are discussed. Suction stress, as a consequence of the interparticle stresses is considered and different methods for determination of the suction stress are explained. Different methods for determination of tensile strength in terms of direct and indirect methods are briefly described and the advantages of hollow cylinder compared to other conventional methods used for the determination of the tensile strength is accounted for. The procedure for elasto-plastic analysis of a cavity subjected to the radial and tangential stresses is explained.

2.2. Basics of partially saturated soils mechanic

2.2.1. Background

From the beginning of the twentieth century, geotechnical science has focused on the characterization of soil as a two-phase material (solid and water or solid and air). However, a considerable proportion of geotechnical engineering problems are involved with partially saturated (or unsaturated) soils, which have three phases (solid, water, and air), with significant behavioral differences from a two-phase system. Due to the existence of air and water in the pore space, phenomena that are impossible to observe in two-phase media, such as surface tension of water at a water-air interface, affect both soil parameters and behavior. As a result, unsaturated soils present a variety of engineering challenges that require tools that are beyond those available for saturated soil mechanics. Examples of challenges include problems associated with failure due to rainfall (especially in slopes),

expansive soils, and problematic soils in semi-arid regions. Interest in such problems started in the late 1950's, and has increased in the last decades.

2.2.2. Soil suction components

Soil suction can be defined as the potential for a partially saturated soil to attract or retain water in terms of pressure. If gravity, temperature, and inertial effects are neglected, the mechanisms for this attraction are capillary, short-range hydration and osmotic mechanisms (Mitchell 1976). The capillary mechanism occurs only in partially saturated soil but hydration and osmotic mechanisms can exist in either saturated or partially saturated conditions (Lu & Likos 2004). The capillary effect in a partially saturated system is due to the physics of air-water interfaces. Soil has small pores to store water. Some energy (in the form of negative pressure) has to be applied to withdraw the water, which is held in place by the potential energy of the tensile forces created due to curved air-water interfaces. These forces are termed the capillary potential. Therefore, the capillary effects in partially saturated system include the curvature of the air-water interface and the associated negative pore water pressure (Lu & Likos 2004). Short-range hydration effects conceptually arise from both the surface area and charge properties of the solid and are more important in fine-particle soils and include the van der Waals attraction and electrical double layer repulsion. Osmotic effect is produced due to salts and other solute concentration differences and can be provided with soluble materials. The soil suction components can also be defined using the thermodynamic relationship between the free energy state of the soil water (or the soil suction) and the partial pressure of the pore water vapor.
The matric suction is defined as the equivalent suction derived from the measurement of the partial pressure of the water vapor in equilibrium with the soil water, relative to the partial pressure of the water vapor in equilibrium with a solution identical in composition with the soil water. In pressure terms, matric suction can also be expressed as $(u_a - u_w)$, where u_a is the pore-air pressure, and u_w is the pore-water pressure.

2.2.3. Suction measurement

Soil suction measurement techniques can be classified as either laboratory or field methods and by the component of suction that is measured, e.g. matric suction or total suction.

Laboratory measurements require undisturbed specimens to account for the sensitivity of suction to soil structure. Disturbance effects become less critical at higher values of suction (Delage & Lefebvre 1984). Table 2.1 summarizes common suction measurement techniques and applicable measurement ranges.

Table 2.1.: Common techniques for measuring soil suction in laboratory and field conditions (Schanz et al. 2004 and Agus & Schanz 2005).

Suction Component Measured	Technique/Sensor	Practical Suction Range [kPa]	Lab/Field
Matric Suction	Tensiometers	0-100	Lab and Field
	Axis Translation	0-1500	Lab
	Electrical/thermal conductivity sensors	0-400	Lab and Field
	Contact filter paper	0-1000000	Lab and Field
Total Suction	Thermocouple psychrometers	100-8000	Lab and Field
	Chilled-mirror hygrometers	1000-450000	Lab
	Resistance/capacitance sensors	0-1000000	Lab
	Isopiestic humidity control	10000-600000	Lab
	Two-pressure humidity control	10000-600000	Lab
	Non-contact filter paper	1000-500000	Lab and Field

2.3. Soil-water characteristics curve (SWCC)

The relationship between the amount of water in the soil and the associated suction in pore water is described by the Soil-Water Characteristic Curve (SWCC). SWCC is one of the most useful characteristics in partially saturated soil mechanics and related to many geotechnical and hydromechanical properties of a soil, such as hydraulic conductivity, effective stress, and volume change (Fredlund & Rahardjo 1993). This curve represents

the soil's ability to retain water at different suctions levels. The amount of water can be expressed by any of the parameters showing the wetness of soil (i.e. degree of saturation, volumetric water content, or gravimetric water content). A typical SWCC curve is shown in Figure 2.1, which presents a relationship between degree of saturation and suction (Leong & Rahardjo 1997).

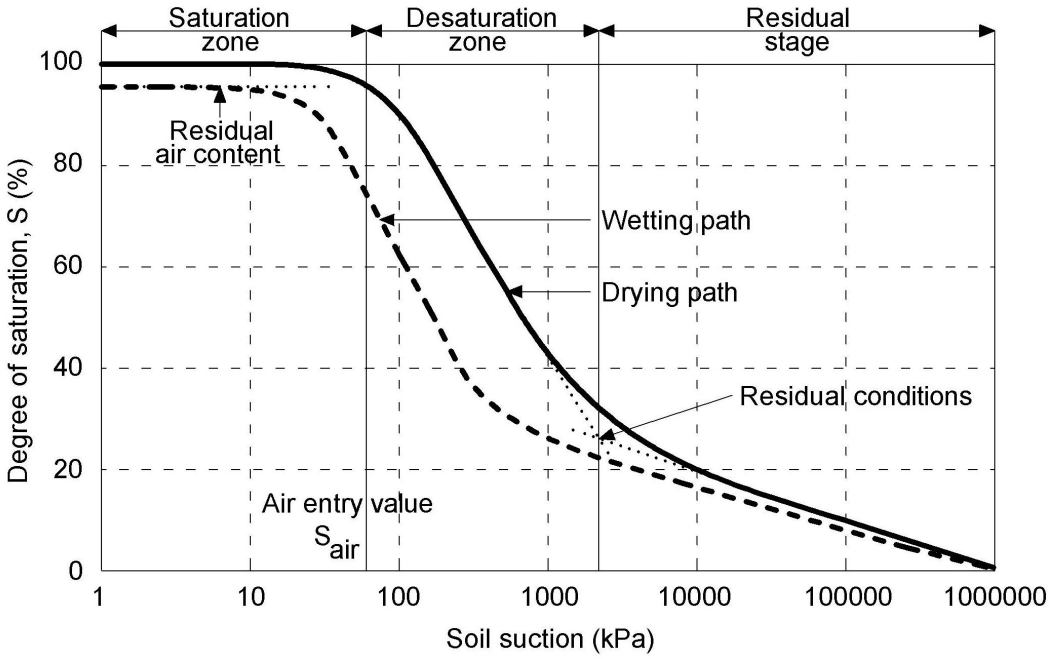

Figure 2.1.: A typical SWCC (Leong & Rahardjo 1997)

SWCC shows different paths for wetting and drying conditions. If a saturated soil sample is subjected to suctions starting from a very low value, it loses water content and follows the drying path which is also called the drainage path. The reverse (i.e. wetting or imbibition path) is the process whereby the water content of soil increases with a decrease in suction. If a dried sample is subjected to suction decreasing, starting from a very high suction level, the soil starts absorbing water.

The suction corresponding to the oven-dried condition is about 1000 MPa, as found by Croney & Coleman (1961). Fredlund & Morgenstern (1977) also found, from the gravimetric water content versus suction relationship for various sand-clay soils, that at zero water content the suction approaches a value of approximately 980 MPa. This value is also supported by thermodynamic considerations (Richards 1966).

Based on the proposed method by Fredlund & Xing (1994) air entry value and residual condition are defined as follows:

- Air entry value, Ψ_{AEV}: describes the suction on the drying path where air first starts to enter the soil's largest pores and desaturation commences.
- Residual suction, Ψ_r: describes the condition where the pore water resides primarily as isolated pendular menisci and extremely large changes in suction are required to remove additional water from the system.

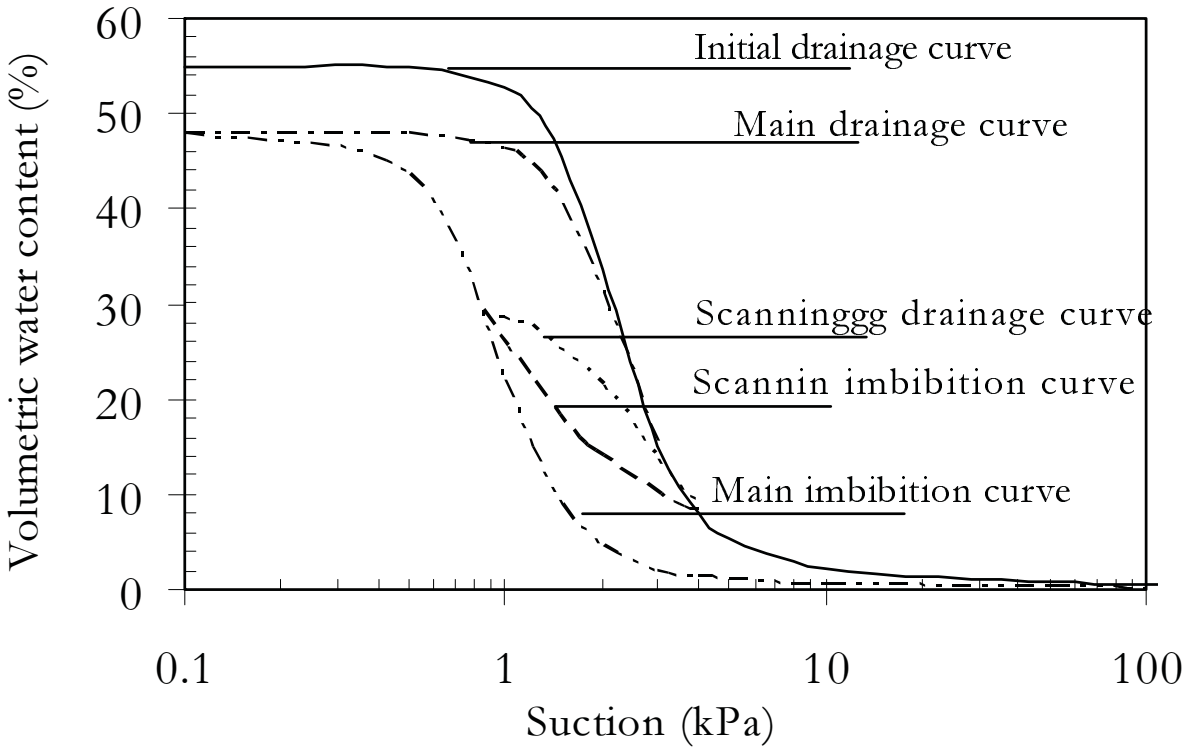

Figure 2.2.: Soil-water characteristic curve showing the initial drainage curve, main imbibition curve, main drainage curve and scanning curves (Lins 2009)

Soil water characteristic curve depends on the soil suction history. Therefore, it is required to distinguish between drying and wetting characteristics of the soil. During the drying process, more water is retained by a soil than during the wetting process for the same suction value. Thus, the relation between water content and suction is hysteretic and is presented by the existence of the initial drainage curve, main drainage and imbibition curves, as well as an infinite number of scanning curves in between the main drying and imbibition curves (Figure 2.2).

2.3.1. SWCCs model

A large number of empirical equations have been proposed by various researchers to best fit experimental data of the soil-water characteristic curve. The parameters in the empirical equations are usually related to the air-entry value and the rate of desaturation of the investigated soil. In this study the proposed model by van Genuchten (1980) has been used to fit the laboratory data over the entire soil suction range. A well known SWCC equation is that given by van Genuchten (1980):

$$Sr_e = \left\{ \frac{1}{1 + [\alpha(u_a - u_w)]^n} \right\}^{\frac{(n-1)}{n}} \tag{2.1}$$

"where n and α are empirical fitting parameters of partially saturated soil properties, with α being the inverse of air entry pressure for water saturated soil and n being the pore size distribution parameter (Lu et al. 2010)".

2.4. Interparticle stresses in partially saturated soils

Lu & Likos (2006) proposed that physicochemical stress can exist in the form of (i) van der Waals stress (ii) electrical double layer repulsion, and (iii) chemical cementation. Meanwhile, dewatering leads to form capillary stress in terms of (i) negative pore water pressure, and (ii) surface tension. The cross section in Fig. 2.3 shows the interparticle forces for partially saturated conditions. As it could be seen F_t related to the external loading that propagate through the granular skeleton. F_{pc} arises from physicochemical forces and is the summation of the van der Waals forces, electrical double-layer repulsion and chemical cementation forces. F_C is particle to particle contact force providing a passive counterbalance via physicochemical forces. Water pressure forces $u_w(A - A_a)$ act on the wetted portions of the grain surfaces near the interparticle contacts, and air pressure forces $u_a A_a$ on the dry portions of the grain surfaces (Mitchell 1976). Mechanical equilibrium among all types of forces leads to (Lu & Likos 2006):

$$F_t + F_{pc} + F_{cap} - F_C - u_w(A - A_a) - u_a A_a = 0 \tag{2.2}$$

$$\frac{F_t}{A} + \frac{F_{pc}}{A} + \frac{F_{cap}}{A} - \frac{F_C}{A} + u_w \frac{(A - A_a)}{A} - u_a \frac{A_a}{A} = 0 \tag{2.3}$$

$$\sigma_C = \sigma_t - u_a + \sigma_{pc} + \sigma_{cap} + (u_a - u_w)(1 - \frac{A_a}{A}) \tag{2.4}$$

$(u_a - u_w)(1 - \frac{A_a}{A})$, has been suggested to form the physical basis for Bishops treatment of the contribution of matric suction to effective stress (e.g., Mitchell 1976), therefore:

$$\sigma_C = \sigma_t - u_a + \sigma_{pc} + \sigma_{cap} + \chi(u_a - u_w) \tag{2.5}$$

If the physicochemical stress at the saturated state σ_{C0} is used as a reference, a change in physicochemical stress $\Delta\sigma_{pc}$ due to desaturation can be introduced into Eq. 2.5 as follows:

$$\sigma_C = \sigma_t - u_a + \sigma_{C0} + \Delta\sigma_{pc} + \sigma_{cap} + \chi(u_a - u_w) \tag{2.6}$$

Considering the preceding microscopic interparticle force and stress analyses (Eqs. 2.3 2.4), leads to:

$$\sigma_C = \sigma' = \sigma_t - u_a + \sigma'_s + \sigma_{C0} \tag{2.7}$$

where σ'_s is herein defined as "suction stress" and is conceptualized as the resultant of interparticle physicochemical stresses attributable to cementation, van der Waals attraction, double-layer repulsion, capillary stress arising from surface tension, and negative pore-water pressure.

$$\sigma'_s = \sigma_{pc} + \sigma_{cap} + \chi(u_a - u_w) - \sigma_{C0} \tag{2.8}$$

It could be also written:

$$\sigma'_s = \sigma_s - \sigma_{C0} \tag{2.9}$$

where σ'_s= suction stress; σ_s= "uncorrected" suction stress; and σ_{C0}= apparent tensile stress at the saturated state.

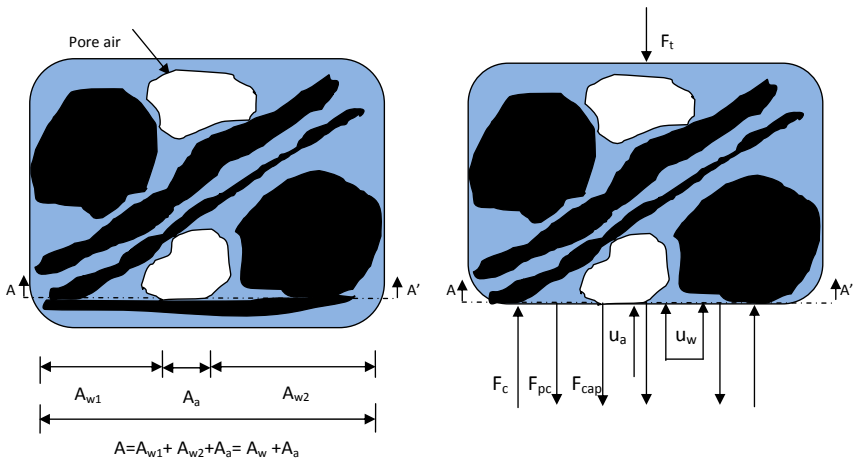

Figure 2.3.: Interparticle forces equilibrium for partially saturated soil system (adopted from Lu & Likos 2006)

2.4.1. Van der Waals stress

The van der Waals stress dominates for low degree of saturation and increases towards its maximum value at 0% saturation (Lu & Likos 2006). Electrical Double-layer repulsion is most pronounced in saturated clay soils and generally decreases with a reduction in degree of saturation (van Olphen 1991, Lu & Likos 2006, Baille et al. 2014). Cementation is more related to salts and other solute concentrations between the particles (Santamarina 2001). The following approximation, describing van der Waals stress, was proposed by Tuller et al. (1999):

$$\sigma_{vdw} = \frac{H_c}{6\pi h^3} \tag{2.10}$$

Where H_c is Hamaker constant and h is the thickness of the adsorbed layers. Tuller et al. (1999) proposed a value of $H_c = -6 \times 10^{-20} J$ for soils. Assuming a complete coverage of all the clay surface area by adsorbed water, the gravimetric water content ω [%] can be evaluated by the following expression:

$$\omega = 100 S_a h \rho_w \tag{2.11}$$

where $S_a\,[m^2/kg]$ is the specific surface area of the minerals and mass density of water is ρ_w=$10^3\ kg/m^3$. By eliminating h among equations 2.10 and 2.11, the resulting stress can be determined as follows:

$$\sigma_{vdw} = 10^6 (\frac{A\rho_w^3}{6\pi})(\frac{S_a}{\omega})^3 \tag{2.12}$$

For the materials used in this study, it is assumed that the cementation is essentially nonexistent and for dry samples the physicochemical stresses arise from van der Waals stress (Lu & Likos 2006).

2.4.2. Capillary stress

In Figure 2.4, the symmetric liquid bridge between two equal spheres is illustrated.
For a given interface geometry, the capillary stress is formed by surface tension (T_s) of water. This acts along the water particle contact line and the effect of negative pore water pressure ($u_a - u_w$) acting on the cross sectional area (Rumpf 1961 and Schubert 1984). As shown in Figure 2.4 a water bridge exists between two particles of radius R and is separated by a distance of *2s*. For such conditions the capillary bonding force, due to surface tension and negative pore water pressure, can be expressed as:

$$F = 2\pi R T_s \sin\beta[\sin(\beta + \theta) + \frac{R}{2}\sin\beta(\frac{1}{R_1} - \frac{1}{R_2})] \tag{2.13}$$

Where β is filling angle, T_s and θ are the surface tension and contact angle, respectively. R_1 and R_2 are the two radii of curvature of the water bridge and can be determined as:

$$R_1 = \frac{R(1-\cos\beta)+\frac{T_s}{2}}{\cos(\beta+\theta)} \tag{2.14}$$

$$R_2 = R\sin\beta + R_1[\sin(\beta+\theta)-1] \tag{2.15}$$

Kim & Sture (2008) proposed that by knowing the water content (w) the volume of the water bridge V_{bridge} can be determined by equation2.16:

$$V_{bridge} = \frac{8\pi w R^3}{3k}\frac{\rho_{sol}}{\rho_{liq}} \tag{2.16}$$

Where k is the mean coordination number, ρ_{sol} and ρ_{liq} are the water and particle densities, respectively. In addition, by assuming that R_1 remains constant Pietsch & Rumpf (1967) provided the following expression for the determination of the water volume bridge:

$$V_{bridge} = 2\pi[2R_1^2+R_2^2]R_1\cos(\beta+\theta) - \frac{R_1^3\cos^3(\beta+\theta)}{24R^3} - \frac{R_1^2}{8R^3}(R_1+R_2)$$
$$\cos(\beta+\theta)\sin(\beta+\theta)(\tfrac{\pi}{2}-\beta-\theta) - \tfrac{1}{24}(2+\cos(\beta)(1-\cos\beta)) \tag{2.17}$$

By knowing the water content, densities of the water and solid particle and choosing the mean coordination number (k), the volume of the water bridge for a specific radius of the spherical particles can be determined by equation 2.16. By assuming θ, seperate distance and radius of the spherical particles, for different magnitudes of the filling angle (β), the two radii of the curvature R_1 and R_2 can be calculated. When using equation 2.16, the volume of the water bridge is known, the filling angle β related to different water contents can be extracted from equation 2.17. Equation 2.18 is proposed by Rumpf (1961) for the prediction of the tensile strength for non-contacting monosized spherical particles. The model assumes that all the particles are spheres with the same size and distributed uniformly. The model also assumes that the bonds are statistically distributed along the surface and in all directions. Lastly, the capillary bonding forces are distributed by a mean value that can be used in the calculation (Kim & Sture 2008). Based on these assumptions, Rumpf (1961) proposed an expression for tensile strength due to capillary bonding forces (σ_{cap}) in the pendular state:

$$\sigma_{cap} = \frac{1-\phi}{\phi}\frac{F}{4R^2} \tag{2.18}$$

where ϕ is porosity, R is the particle radius, and F is the bonding force related to the capillary force between two monosized spherical particles. By replacing F from Equation 2.13 in Eq. 2.18 the tensile strength can be determined as follows (Kim & Sture 2008):

$$\sigma_{cap} = \frac{1-\phi}{\phi}\frac{F}{4R^2} = \frac{1-\phi}{\phi}\frac{\pi T_s}{2R}\sin\beta[\sin(\beta+\theta) + \frac{R}{2}\sin\beta(\frac{1}{R_1} - \frac{1}{R_2})] \tag{2.19}$$

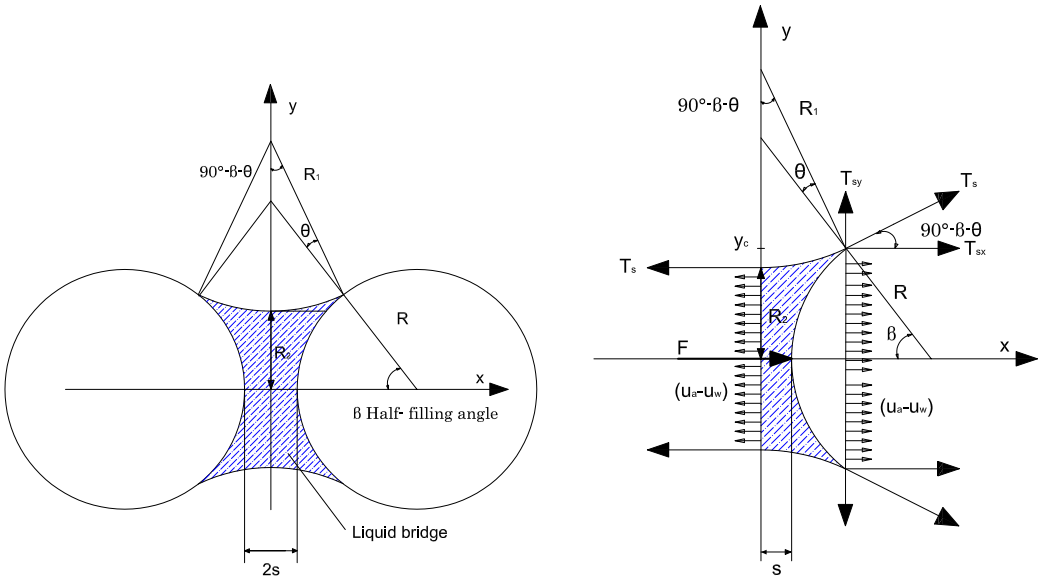

Figure 2.4.: (a) Symmetric liquid bridge between two equal rigid smooth spheres with a separation of 2s to account for actual surface roughness (b) illustration of geometry of right-hand side of liquid bridge (Molenkamp & Nazemi 2003)

2.4.3. Effective stress in unsaturated soils

Bishop (1959) was the first who tried to express the concept of effective stress σ' for unsaturated soil in the following form:

$$\sigma' = (\sigma_n - u_a) + \chi(u_a - u_w) \tag{2.20}$$

Where σ_n is the total normal stress (average normal stress applied to surface of Representative Elementary Volume "REV" in soil), u_a describes the pore air pressure and u_w the pore water pressure. $(\sigma_n - u_a)$ is the net normal stress and the interaction of water and soil is illustrated in terms of matric suction $(u_a - u_w)$. Thus effective stress σ' is defined as

the excess of net normal stress $(\sigma_n - u_a)$ over an "equivalent" suction $\chi(u_a - u_w)$ (equivalent means that at higher suctions $(u_a - u_w)$ is no longer a direct measure of pore water pressure but a measure of the energy state of soil water (Nuth & Laloui 2008)). From this point of view χ may be interpreted as an upscaling or transfer function describing the average portion of equivalent suction that results in effective stress. It is assumed that this stress describes stresses at solid particle contacts. In the following years numerous experimental studies have been performed to measure χ (e.g. Jennings 1961, Oberg & Sallfors 1997, Tarantino & Tombolato 2005, etc.). It is a common assumption that the effective stress parameter is related to the degree of saturation in representing the shear strength of soils (Bishop & Donald 1961 and Oberg & Sallfors 1997). In elasto-plastic constitutive relationships (Hassanizadeh & Gray 1990, Houlsby 1997, Gray & Schrefler 2001, Gallipoli et al. 2003, Wheeler et al. 2003, Tamagnini 2004, Nuth & Laloui 2008, Alonso & Romero 2011). This assumption may not work well for some soils, and relatively large discrepancies have been observed in some early studies (Bishop & Blight 1963). Other studies have used the effective saturation $Sr_e = \frac{Sr - Sr_r}{1 - Sr_r}$ (Sr is the actual degree of saturation and Sr_r, related to the residual degree of saturation) as the effective stress parameter successfully to evaluate the shear strength and elastic modulus of unsaturated soils (Vanapalli et al. 1996, Lu et al. 2010, Khosravi et al. 2010 and Khosravi & McCartney 2012). While more complicated functions of the degree of saturation have also been proposed (Toll & Ong 2003 and Sheng et al. 2008) for defining the effective stress parameter, some other studies have shown the utility of empirical relationships. Khalili & Khabbaz (1998) defined the effective stress parameter as a power law relationship involving the ratio of the suction and the air entry suction, which has been applied in constitutive models (Loret & Khalili 2002) and in reexamining data from the literature (Khalili et al. 2004). Khalili & Zargarbashi (2010) performed staged triaxial tests on unsaturated soil specimens during wetting, and they observed that the effective stress parameter is sensitive to hydraulic hysteresis. Further, they found that the use of an effective stress parameter equal to the degree of saturation may not be suitable for all soils during hydraulic hysteresis. The validity of the effective stress concept is still a matter for intense discussion. The most often mentioned shortcomings are:

- Collapse phenomenon cannot be explained by using the effective stress concept (Jennings & Burland 1962).

- Compression behavior resulting from changes in matric suction is different from load induced compression. Matric suction induced hardening is not involved in the effective stress concept when using a single-valued approach (Bishop & Blight 1963,

Modaressi & Abou-Bekr 1994, Bolzon et al. 1996, Loret & Khalili 2000, Loret & Khalili 2002).

- Hysteresis effects (non-reversible swelling and shrinkage behavior) in wetting-drying paths are not considered (Topp & Miller 1966, Poulovassilis & El-Ghamry 1978).
- Theoretical shortcomings from a continuum mechanics point of view, resulting from a combination of the net normal stress $(\sigma_n - u_a)$ acting on a macroscopic scale and matric suction $(u_a - u_w)$ acting on a microscopic scale in one equation (Aitchison 1965, Matyas & Radhakrishna 1968, Brackley 1971, Fredlund & Morgenstern 1977, Gens et al. 1995).

The inability to use the conventional effective stress concept for accurate representation of unsaturated soil behavior resulted in the development of the "independent stress state variable approach". Coleman (1962) explained and described the stress state variables governing the behavior of unsaturated soil. It is supposed that the stress state variables have to be created from the individual force components acting on the solid, water, and air phases. They proposed that the variables are: treating stresses from loads (net normal stress) $(\sigma_n - u_a)$ and matric suction $(u_a - u_w)$. In the same study they validated the concept of stress state variables by carrying out a series of null tests. These experiments have approved that as long as the state variables remain constantly changing the air, water, or the total pressures causes no changes in the state of the soil. Using a new laboratory apparatus, Matyas & Radhakrishna (1968), Fredlund & Morgenstern (1977), Alonso et al. (1990) and Geiser et al. (2006) investigated these variables. Their outcomes confirmed the use of matric suction and the net stress as independent stress variables.

2.5. Suction stress

While the above mentioned approaches have been derived from a macroscopic point of view, Lu & Likos (2006) presented a micromechanically based concept for describing effective stresses. They proposed that effective stress in a section of soil (Fig. 2.3) could be defined as the sum of the interparticle forces $(\sum F_p)$ due to mechanical loading, capillary forces F_{cap} and physicochemical forces F_{pc} (e.g., due to van der Waals, double layer and chemical cementation), per unit area (A) intersecting an REV of the soil. As a result the suction stress can be described as a stress variable which is stablished on the representative elementary volume of partially saturated soil, that describes the contribution of matric suction to effective stress.

Using this approach, they showed that on a microscopic level, the effects of soil-water interactions (in terms of effective stress) can be lumped into a macroscopic stress defined as suction stress (σ^s)

$$\sigma'_n = (\sigma_n - u_a) - \sigma_{pc} - \sigma_{cap} + \chi(u_a - u_w) \tag{2.21}$$

$$\sigma^s = \sigma_{pc} + \sigma_{cap} - \chi(u_a - u_w) = -X(u_a - u_w) \tag{2.22}$$

$$\sigma' = (\sigma_n - u_a) - \sigma^s \tag{2.23}$$

In equation 2.22 X is an upscaling factor. However, X has been widely correlated to the degree of saturation (matric suction) and can be equated to Bishop's effective stress parameter χ (Mitchell & Soga 2006) but does not equal to χ. X is a complex function of water content, matric suction, and the particle and pore size properties. Hence, the effect of the other physicochemical forces (such as van der Waals force) which are dominated in dry conditions can also be placed in upscaling factor of X.
From this point of view, X may be interpreted as an upscaling or transfer factor describing the average portion of forces acting on a microscopic level that results in effective stress, acting on a macroscopic level. An analysis and discussion of effective stress concepts in partially saturated soils can be found in Nuth & Laloui (2008). They show that the listed shortcomings for the validity of the effective stress concept do not result from the concept itself but from ignoring soil plasticity (e.g. the collapse phenomenon is explained by a nonreversible rearrangement of particles) or in choosing the appropriate upscaling function (e.g. hardening or hysteresis effects). They conclude that the stress part of deformation and shear strength behavior of unsaturated soils can be adequately described in terms of what they call a "generalized form" of Bishop effective stress" (defined as the sum of the net normal stress and the effect of the degree of saturation by suction):

$$\sigma' = (\sigma_n - u_a) + X(u_a - u_w, Sr) \tag{2.24}$$

$$Sr = f(u_a - u_w) \tag{2.25}$$

Where X is a function of matric suction and saturation Sr. A collection of proposed equations is given in table 2.2. It can be concluded that using the "generalized form" of effective stress allows us to overcome the listed shortcomings of the effective stress concept. Therefore matric suction induced changes in shear strength can be written as a function of matric suction and saturation:

$$\tau = c' + \sigma' tan\varphi' = c' + (\sigma_n - u_a) - X(u_a - u_w, Sr)\, tan\varphi' \tag{2.26}$$

Assuming that equation 2.26 is valid and knowing a closed form equation for the function X means that classical soil mechanic concepts can be applied to shear strength related

problems. The equations presented in table 2.2 are empirical or semi-empirical equations or result from an idealized model of forces transferred on a particle contact level. Mechanically and or physically more rigorous approaches from theoretical point of view for effective stress equations in unsaturated soils have been presented by (e.g. Houlsby 1997, Murray 2002, Borja 2006, Borja & Koliji 2009, Murray & Sivakumar 2010, Nikooee et al. 2013, Fuentes & Triantafyllidis 2013). These works are of importance since they reveal the assumptions and conditions necessary to make the effective stress descriptions valid.

2.6. Determination of the suction stress

2.6.1. Suction stress derived from SWCC

Lu et al. (2010) proposed the following closed-form equation for the determination of suction stress by using the fitting parameters of the van Genuchten (1980) model:

$$\begin{aligned} \sigma^s &= -(u_a - u_w) && (u_a - u_w) \leq \Psi_{AEV} \\ \sigma^s &= -\frac{(u_a - u_w)}{\{1 + [\alpha(u_a - u_w)]^n\}^{\frac{(n-1)}{n}}} && (u_a - u_w) \geq \Psi_{AEV} \end{aligned} \tag{2.27}$$

where n and α are empirical fitting parameters of unsaturated soil properties, with *alpha* being the inverse of air entry pressure (Ψ_{AEV}) for water saturated soil and n being the pore size distribution parameter. In this form, if the matric suction is lower than the air entry value, the suction stress exhibits a linear relationship with matric suction, and its magnitude is equal to the value of matric suction. But for matric suction higher than the air entry value the magnitude of the suction stress has to be determined from the second part of the Eq. 2.27. Therefore, the effective stress of the unsaturated soil differs from that of the saturated soil when the matric suction is larger than the air entry value.

2.6.2. Suction stress derived from tensile strength

To describe possible methods to derive suction stress from experiments (tensile strength or triaxial tests) within the framework of the effective stress concept, Fig. 2.5 shows the failure envelope describing the shear strength of a partially saturated soil at constant matric suction. The friction angle φ is determined by triaxial tests using saturated samples and corresponding stress levels. φ_t describes possible none linear MC-behaviour at low stress level or tensile stress regimes.

Table 2.2.: Shear strength and tensile strength studies with respect to effective stress

No	Author	Soil type, Test type: Direct shear (DS), triaxial test (TT), uniaxial tensile test (UTT)	"suction controlled (SC), Water content controlled (WCC)	Drying (D) / wetting (W) path	Matric suction, Normal stress p, [kPa]	"suction stress "	Kind (fitting/ predictive), uniqueness of failure surface confirmed
1	Escario (1980)[1]*	Clay, DS	SC	D	0~850[1], 100~800	only validation	- Yes
2	Escario and Sáez (1982) [2]*	Clay, DS	SC	D	0~1000[1], 100~800	only validation	- Yes
3	Gan et al. (1988)	Glacial, DS	SC	D	0~500[1], 100~160	only validation	- Yes
4	Sivakumar (1993)**	Kaolin, TT	SC	N.D	0~300[3], 50~300	only validation	- Yes
5	Wheeler and Sivakumar (1995)	Compacted Kaolin, CL		D	0~300	only validation	- Yes
6	Cui, Delage (1996)**	Silt, TT	SC		0~1500[3], 100~600	only validation	- Yes
7	Shen and Yu (1996)	Evaluated in Goh (2012)	N. D	N.D		$\sigma^s = (u_a - u_w).\frac{1}{1+(u_a-u_w).d}$ d: constant	Fitting -
8	Vanapalli et al.(1996)* Garven &Vanapalli (2006)	Glacial, (CL), 18.7, DS	SC		0~500[3], 25~200	$\sigma^s = (u_a - u_w).Sr_e^k$ (1996) $k = -0.0016.I_p^2 + 0.0975.I_p + 1$ (2006)	Predictive -
9	Geiser et al. (2006)	Silt, UL,TT	SC	D	0~300, 200~1000	Validation only (e.g. Eq. 2.26)	- Yes
10	Öberg and Salfors (1997)	Silt/ Sands	-			$\sigma^s = (u_a - u_w).S_r$ Predicted values compared to literature data	Predictive -
11	Heibrock (1997)	Compacted kaolin, CH, UTT	WCC	D	0~4500	Tensile strength data	-
12	Khalili and Khabaz (1998) Khalili et al (2004)	Natuural CL-ML,	SC	D	0~400, 50~1200	$\sigma^s = (u_a - u_w).\left(\frac{(u_a-u_w)_f}{(u_a-u_w)_b}\right)^{0.55}$ $(u_a-u_w)_f$: matric suction at failure $(u_a-u_w)_b$: AEV for drying curve or expulsion curve for wetting curve	Predictive -
13	Kim (2001)	Sand, Direct shear, UTT	WCC		0~10[4], 0.1~1	Back calculation of shear strength data	-
14	Mioa et al (2002)	Expansive Clay (CH), TT		D	0~200, 50~150	$\sigma^s = (u_a - u_w).S_r$	Predictive -
15	Rahardjo et al. (2004)	compacted Residual soil, CL,14.8, TT	SC	D/W	0~300	Backanalyzed in Goh et al (2010)	-
16	Lee et al. (2005)	Residual soil SM,TT		D		$\sigma^s = [(u_a - u_w) - AEV]\theta^k.[1 + \lambda(\sigma_n - u_a)]$ λ: Constant, θ: normalized volumetric water content	Fitting -
17	Geiser et al.(2006)***	Silt, TT	SC		0~300[4], 200~1000	$\sigma^s = (u_a - u_w).S_r$	Predictive Yes
18	Thu et al (2006)	Compacted kaolin, MH, TT	SC	D/W	0~300	Backanalysed in Goh et al (2010)	-
19	Lu et al (2009)	Sand, UTT	WCC	D		$\sigma^s = \frac{\sigma_{tut}}{2\tan\varphi_t \tan\left(\frac{\pi}{4}-\frac{\varphi_t}{2}\right)}$ σ_{tut}: Uniaxial tensile strength	predictive if tensile strength is known Yes
20	Goh et al (2010)	Compacted Sand/Kaolin Mixtures, ML-CL	SC	D/W	0~300, 50~100	$\sigma^s = [(u_a - u_w) - AEV]b\theta^k$ b, k: constants, θ: normalized volumetric water content	Predictive soil type dependent equations are given Yes
21	Goh (2012)	Compacted sand/kaolin mixtures ML-CL	SC	D/W	0~700, 50~100	Compared different predictive equations, The Garven and Vanapalli (2006) provided good estimations	Predictive Yes/for drying path
22	Lu et al (2010)	Analysis of data m literature				$\sigma^s = (u_a - u_w).S_{r_e}$	Predictive Yes
23	Springman et al (2003), Cassini et al (2011)	Compacted Silty sand, ML,TT	SC	D/W	0~100, 20~80	$\sigma^s = (u_a - u_w).S_r$	Predictive -
24	Zeh and Witt (2006)	Compacted Clay, CH, UTT	WCC	D	0~50000	tensile strength data	- -
25	Vesga (2008)	Compacted Kaolin, CL	WCC	D	0~15000	tensile strength data	- -
26	Heibrock et al (2003)	Compacted Kaolin, CL, UTT	WCC	D	0~ >100000	tensile strength data	- -

*reported in Lu and Likos (2006), **repoorted in Khalili et al. (2004),*** reported in Nuth and Laaloui (2008), [1] $P = \frac{\sigma_1+\sigma_3}{2}$, [2] test results of Escario (1980) and (1986) are different in time of consolidation and the rate of shear, [3] $P = \frac{\sigma_1+2\sigma_3}{3} - u_a$, [4] $P = \sigma_n$

Lu et al. (2009) proposed a procedure to measure limit states at low stresses. They argue that under tension stress conditions suction stress describes interparticle forces. Therefore isotropic tensile strength σ_{tit} in Fig. 2.5 becomes a direct measure of suction stress. Using this assumption, the effective stress equation may be defined as follows:

$$\sigma'_n = (\sigma_n - u_a) - \sigma^s = (\sigma_n - u_a) - \sigma_{tit} \tag{2.28}$$

$$\sigma^s = \sigma_{tit} \tag{2.29}$$

Inspection of the failure envelope shows that suction stress as defined in Eq. 2.29 and therefore the upscaling parameter describing the macroscopic effects of soil water interaction, can be estimated from uniaxial tensile strength (Fig. 2.5, Lu et al. 2009):

$$\sigma^s = \frac{\sigma_{tut}}{2\tan\varphi_t \tan(\frac{\pi}{4} - \frac{\varphi_t}{2})} \tag{2.30}$$

2.6.3. Suction stress derived from shear strength failure

The other alternative to this procedure is to use the results from shear tests to derive the suction stress. In this case, suction stress (σ^s) can be calculated at constant suction using the following:

$$\sigma^s = \frac{(\sigma_1 - u_a) - (\sigma_3 - u_a)\tan^2(\frac{\pi}{4} + \frac{\varphi'}{2}) - 2c'\tan(\frac{\pi}{4} + \frac{\varphi'}{2})}{2\tan(\frac{\pi}{4} + \frac{\varphi'}{2})\tan\varphi'} \tag{2.31}$$

σ_1 and σ_3 are the total principle stresses in vertical and horizontal directions. c' and φ' are the effective cohesion and friction angle at the soil saturation state, respectively.
Equations 2.30 and 2.31 can be used to calculate the effect of soil suction from direct tensile tests and triaxial tests with partially saturated soils. Suction controlled triaxial tests are practically limited to stress conditions, where matric suctions range from 0 to about 1500 kPa and loading stress from 30 kPa to about 500 kPa. Limitations concerning the matric suction result mainly from extremely long times needed to establish equilibrium at high suction values in fine grained soil samples. Limitations concerning the low loading stress are most significant for coarse grained soils where it becomes more difficult to perform the tests at low stresses. The most widely used concept to validate the effective stress procedure is (Geiser et al. 2006, Kim 2001, Cui & Delage 1996, Maatouk et al. 1995, Sivakumar 1993, Escario & Saez 1986, Jennings 1961):

1. To determine limit state lines using triaxial or direct shear tests on samples with different water contents therefore matric suctions.

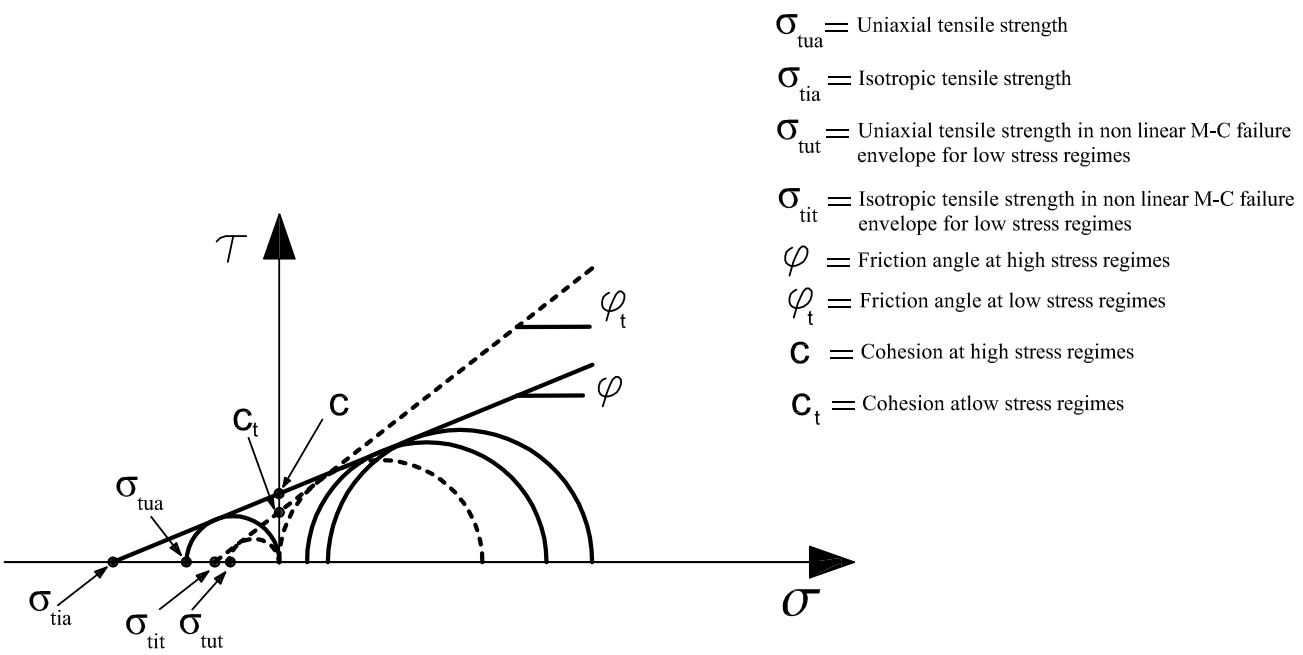

Figure 2.5.: Failure envelope in terms of τ-σ, $(\sigma = \frac{\sigma_1+\sigma_3}{2})$ at constant matric suction with isotropic tensile strength (σ_{tit}), uniaxial tensile strength (σ_{tut}), effective friction angles determined for dry or saturated soil: φ lower friction angle at higher stress regimes, φ_t higher friction angle at lower stress regimes (modified from Lu et al. (2009))

2. To determine suction stress σ^s using e.g. equations 2.30 and 2.31.

3. To plot the test results in p'-q diagrams using the determined effective stresses σ' from Eq. 2.22 and to determine failure envelopes for different suction stresses.

4. To check if these failure envelopes converge to one unique line. If this is true it is generally assumed that effective stress concept is holds.

   Even if this is true the effective stress concept is not necessarily directly applicable because using different kinds of tests (and therefore investigating different failure modes) may result again in a unique effective stress failure envelope but may show differences in suction stresses determined from the test results.
   Therefore to validate a closed form equation for suction stress the following steps have to be added:

5. To assume or derive a specific form of the upscaling function

6. To calculate suction stress and effective stresses resulting in a closed form equation for effective stress (e.g. van Genuchten 1980)

7. To compare suction stresses derived from tensile and triaxial tests with predicted suction stresses using the SWCC curves. If the chosen closed form equation is in accordance with experimental results, the predicted suction stress from SWCC will equal to suction stresses from experiments.

2.6.4. Existing studies validating the effective stress concept and their shortcomings

Due to the complex and time consuming tests when dealing with partially saturated soils, experimental studies of the effective stress concept are limited in terms of soil type and suction range investigated. Table 2.2 summarizes shear strength lab testing series using some kind of effective stress concept. Information on soil type investigated and test type used are listed together with the proposed suction stress equation and a categorization of the proposed equations in terms of being predictive (suction stresses can be predicted from SWCC curves) or fitting-type equations which need measured suction stress data to be applied. In addition, some sources on tensile strength of partially saturated soils are included. The last column indicates if the failure envelopes were unique in cases where this has been investigated explicitly. Inspection of the Table 2.2 shows that:

1. In the cases where the uniqueness of the failure envelope was investigated the uniqueness was proved
2. All studies use one kind of test, in most cases triaxial or direct shear tests, in fact only one kind of failure mode is investigated.
3. In the shear strength related studies only a limited range of relative small suction (in most cases 0-800 kPa, maximum to 1500 kPa) has been investigated.
4. Most of the experiments have been performed at high loading (mechanical) stress (more than 25 kPa), low stress and extension regimes have not been considered.
5. The tensile strength tests cover high suction regions up to air dry conditions. If Eq. 2.30 is applicable, the simple tensile strength experiments could be used to calculate suction stresses and therefore effective stress of partially saturated soils especially for high suction values where suction controlled testing becomes difficult and extremely time consuming in triaxial cell or direct shear testing devices.
6. Most of the suction stress equations can be presented in the form of Equation 2.30.
7. There are no test equipment to perform test in extension and low stresses region via controlling of matric suction.

2.7. Soil fabric and structure

A significant amount of research over the past few decades has focused on the consideration that the structure of the soil governs its response.
In engineering the term *structure* refers to the composition and interparticle forces (Mitchell & Soga 2006).
The influence of the structure as well as the size of the pore spaces, the distributions and orientations of the particles largely influence the mechanical behavior of the soils (e.g. hydraulic conductivity, shear strength and compressibility).
The arrangement of the particle takes a variety of forms in different type of soils. However, in general three main groups of structure elements can be identified (Collins & McGown 1974):

1. Elementary particle arrangement: single forms of particle interaction at the level of individual clay, silt or sand particles.

2. Particle assemblages: Units of particle arrangements. A particle assemblage consists of one or more forms of elementary particle arrangements.

3. Pore spaces.

Additional term is also used commonly in geotechnical engineering is cluster. A cluster is a grouping of particles or aggregates into larger structure units.
The features of the soil structure have been divided in two levels of scale that are typically named microstructure and macrostructure. The interaction of the micro and macrostructure has been created in various fashions as hydraulic, thermal, or mechanical loading processes (Likos & Wayllace 2010).

Barden & Sides (1970) and Sridharan et al. (1971) studied the soil microstructure based on inter-aggregate pores and intra-aggregate pores. This type of microstructure was called a "bimodel-structure" or "double-structure". Different forms of double-structure models have been proposed to relate changes in microstructure and macrostructure to the mechanical response of the soil (e.g., Delage & Lefebvre 1984, Alonso et al. 1987, Coulon & Bruand 1989, Penumadu & Dean 2000, Sivakumar & Wheeler 2000, Cuisinier & Laloui 2004, Li & Zhang 2009, Alonso & Romero 2011, Song et al. 2012 and Tang et al. 2015).
The pore scale at three different levels is illustrated conceptually in Figure (2.6).

- Inter-aggregate porosity refers to the large pore space between the particles and aggregates at a scale of around 1-10 μm.

- Intra-aggregate (inter-particle) accounts for the distribution of the void space in terms of the microstructure between the individual particles within the aggregates at a scale of around 0.1-1 μm

- inter-layer porosity, which includes the pores between the mineral layers within the clay particles at a scale of less than 0.1 μm.

As illustrated in Figure 2.6, pores including the smaller-scale microstructure of compacted mixtures are generally designated as those corresponding to inter-layer separations between expandable mineral layers. Discontinuities between oriented sub-stacks of mineral layers and intra-aggregate voids formed within the larger aggregates of clay particles. These particles contain multiple oriented sub-stacks of mineral layers to form a network of walls within the clay aggregates (Aylmore & Quirk 1971). Pores including the macrostructure are generally considered to be those formed among the aggregates, also referred to as the inter-aggregate void space.

2.8. Tensile strength of soils

The tensile behavior of soils is complex. In general, soils can resist compression but rarely sustain tension. In geotechnical engineering the tensile strength of soil is mostly considered to be insignificant for design purposes. Therefore as a result the tensile testing of soils is seldom performed.
Failure may arise because of increased deviatoric stresses, as in the case of a soil specimen being sheared or as the result of increase tensile stress. Increased deviatoric stresses will damage the soil structure far more than tensile stress. The tensile failure causing a lot of grain debonding and often creates only a single planar fracture with little damage to the adjacent soil particles. Reliable theories and failure criteria that can explain soil behavior under tension are still limited. Moreover, appropriate testing devices that can measure precise tensile stress and strain are not readily available or standardized, and choosing the appropriate sample shape and preparation techniques are difficult.
Tensile behavior of soils is related to slope stability, differential settlement of multilayered embankment dams, landfill liners, rigid and flexible road pavements and airfields. Soil cracking also affect other areas of soil behavior including the rate of moisture loss or gain.

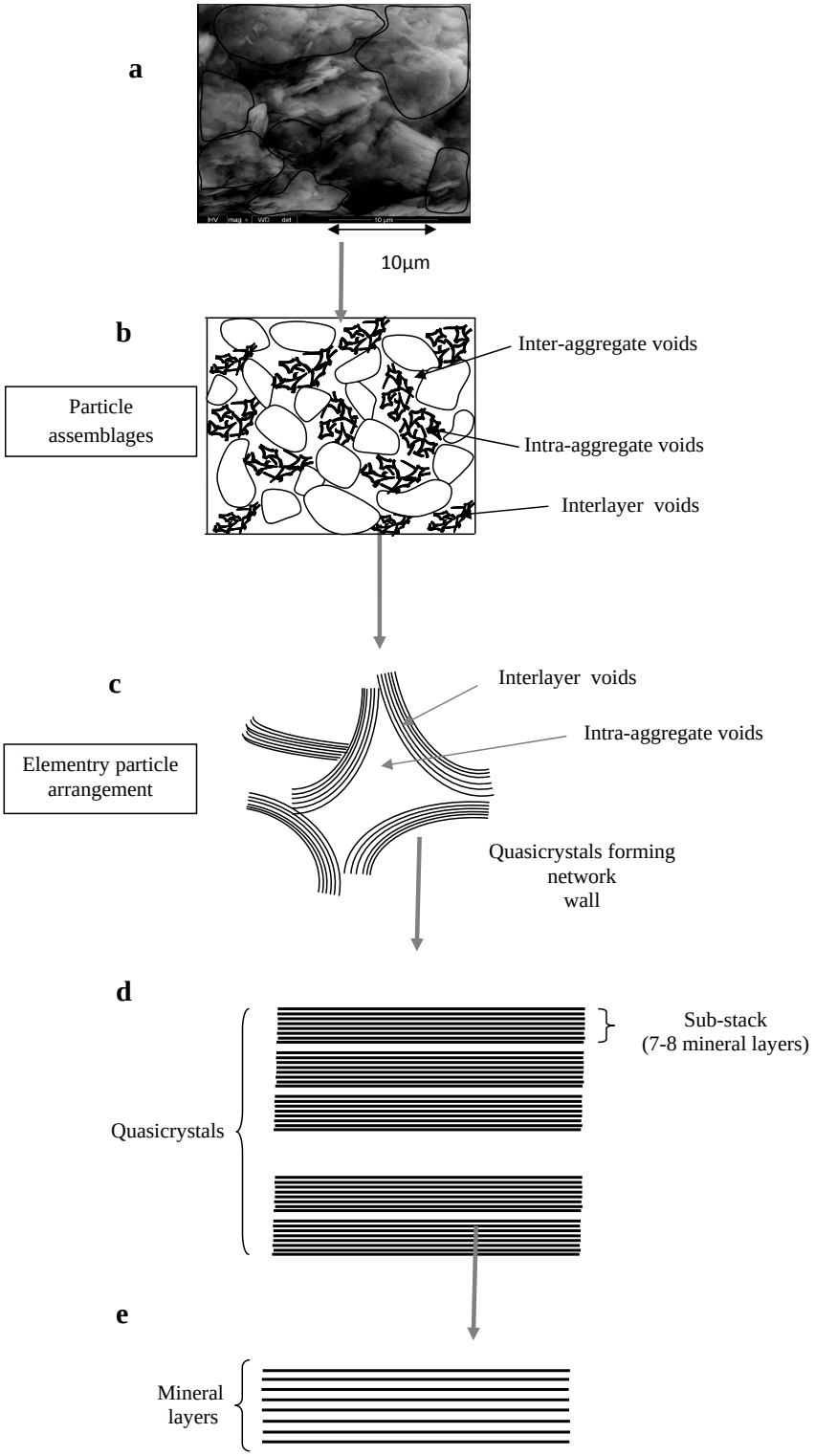

Figure 2.6.: ESEM image (a) showing bimodal porosity of pore spaces on the (b) inter-aggregate scale, (c) intra-aggregate scale,(d) quasicrystal scale, and (e) inter-layer scale (adopted from Likos & Wayllace 2010).

2.8.1. Direct tensile test

The direct tensile test is considered to be the most fundamental and possibly the test that satisfies the condition of true uniaxial tension (Frydman 1967, Vesga 2006, Vesga 2009). Basically, uniaxial tensile tests should subject a specimen to stresses that are uniform throughout. This implies that there should be no bending or torsional stresses, or stress concentration resulting from any geometrical irregularities of the specimen. In this test, as the name applies, the tensile force is directly applied to the specimen along its longitudinal axis until failure occurs. The shape of the specimen is usually a simple geometry, such as a cylinder or prism. The tensile strength can be calculated from the ultimate load sustained by the specimen and the cross sectional area upon which it acts. Although the tensile strength can be obtained by the direct tensile method, many researchers have questioned the validity of the tensile strength in the past. This may arise from the difficulties in the test equipment and loading conditions such as misalignment and stress concentration and significant effect of the inhomogeneity on the test results.

2.8.2. Indirect tensile tests

Several indirect tensile tests were developed as alternative test methods due to a number of limitations and problems associated with direct tensile and bending tests. Misalignment, end gripping or clamping, stress concentration and eccentricities are the main problems in direct tensile tests.

2.8.2.1. Brazilian test

In the Brazilian test, a cylindrical-shaped specimen is horizontally placed between two loading surfaces and compressed steadily along a diametrical plane until failure. The tensile stress field is thus induced at the failure point. The consideration of material properties and relevant assumptions are required to obtain useful results as the stress field in the specimen cannot be derived directly from the known loadings and boundary conditions. Tensile strength is usually calculated from the applied load and the geometry of the specimen using elastic theory as follow:

$$\sigma_t = \frac{2PT}{\pi D} \tag{2.32}$$

Where, σ_t is tensile strength, T is width of the loading strip, D is the diameter of the specimen and P is the applied pressure.

The test is commonly used for pavement materials, cement, concrete, rock and ceramic materials, but using in soil testing is limited (Al-Hussaini & Townsend 1974).

2.8.2.2. Bending test

The bending test involves the application of loads on a compacted or molded beam-shaped sample until failure occurs. The tensile strength can be calculated from the bending moment acting on the beam and the section modulus of the cracked section.The test method is to load a supported beam with a vertical concentrated load. This is positioned either at the center or by two equal loads placed at points a third along the structure from each end to generate a distribution of bending stress, as shown in Figure 2.8.

$$\sigma_t = \frac{M\bar{y}}{I} \tag{2.33}$$

Where, σ_t is tensile strength, M is bending moment, $\bar{y}$ as the distance of the tensile surface of the beam from the neutral axis and I is the moment of inertia.
This test merely measures the modulus of rupture as assumed by beam theory, which assumes that the material is linear-elastic and Young's modulus in both tension and compression are equal. This results in deviation from the actual characteristics of most engineering materials.

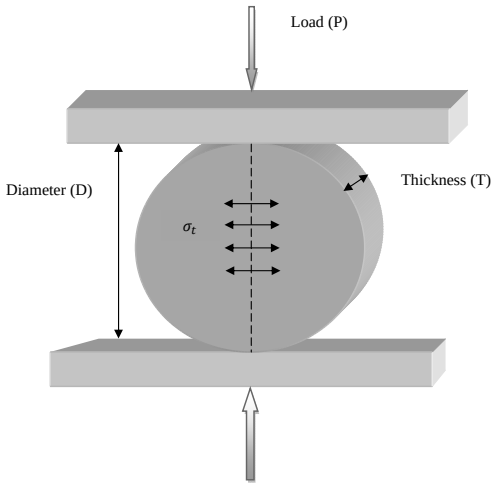

Figure 2.7.: Setup of the Brazilian test

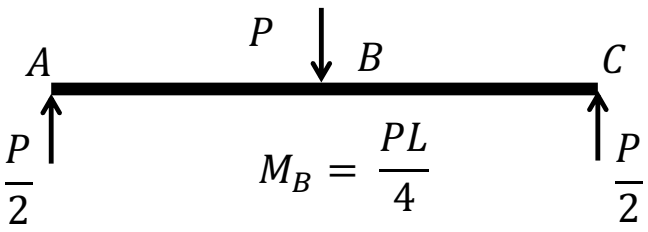

Figure 2.8.: Three point bending test

2.8.2.3. Hollow cylinder

In the hollow cylinder test, an inner pressure is applied to the cavity wall of the hollow cylinder through a flexible membrane, which produces radial and tangential stresses in the cylinder. Radial stress and tangential stress are determined by applying uniformly distributed inner and outer pressures to a circular cylindrical soil specimen with constant wall thickness. The approach is based on the principle of applying pressure to the cavity of the specimen until the specimen fails (see section 2.9).
Considerable previous research subjected to tensile strength of the soils by a hollow cylinder has been mainly conducted on cohesive soils. Al-Hussaini & Townsend (1973), Bai et al. (1982), Hight & Symes (1983), Murdoch (1993a), Ohokal et al. (1997), Ghazi et al. (2000), Alsayed (2002) and Albert NG (2008) used hollow cylinder to measure tensile stress and strain in soils.
In 1973, Al-Hussaini and Townsend designed a hollow cylinder apparatus and conducted a study on tensile strength of compacted soils. Particularly, in this investigation the hollow cylinder tests were performed on clayey soils. Analysis of the tests results was done based on the assumption that the materials are homogeneous, elastic and isotropic.
It was assumed that by keeping the outer pressure (p_o) constant and increasing the inner pressure (p_i), the tangential tensile stress is generated in the soil and when this stress exceeds the tensile strength of the material the specimen fails in terms of tension. During the test, the pressure and deformation of the cylinder cavity were recorded continuously. The test results indicate that failure in the hollow cylinder specimens occurred radially in lines parallel to the axis of the cylinder.

2.9. Cavity expansion theory

2.9.1. Stress distributions in "thick-wall"

It is accepted that for a "thick-wall" hollow cylinder the wall thickness exceeds one-tenth of the inner radius of the hollow cylinder (Nadai 1950, Jaeger & Cook 1979 and Alsayed 1988).
In Fig. 2.9 the thick-wall hollow cylinder specimen is illustrated with the inner and outer radius of a and b respectively. Pressures act uniformly throughout the inner (p_i), and outer (p_o) of the specimen. Increasing the cavity pressure (p_i) and providing vertical displacement restraint, leads to the enforcement of a plain strain deformation to the specimen through the expansion of the cavity.
According to cavity expansion theory, as cavity pressure increases, the radial stress at the inner cavity wall will increase. When the tangential stress becomes equal to the value of the tensile strength, cracks will develop in the radial direction.

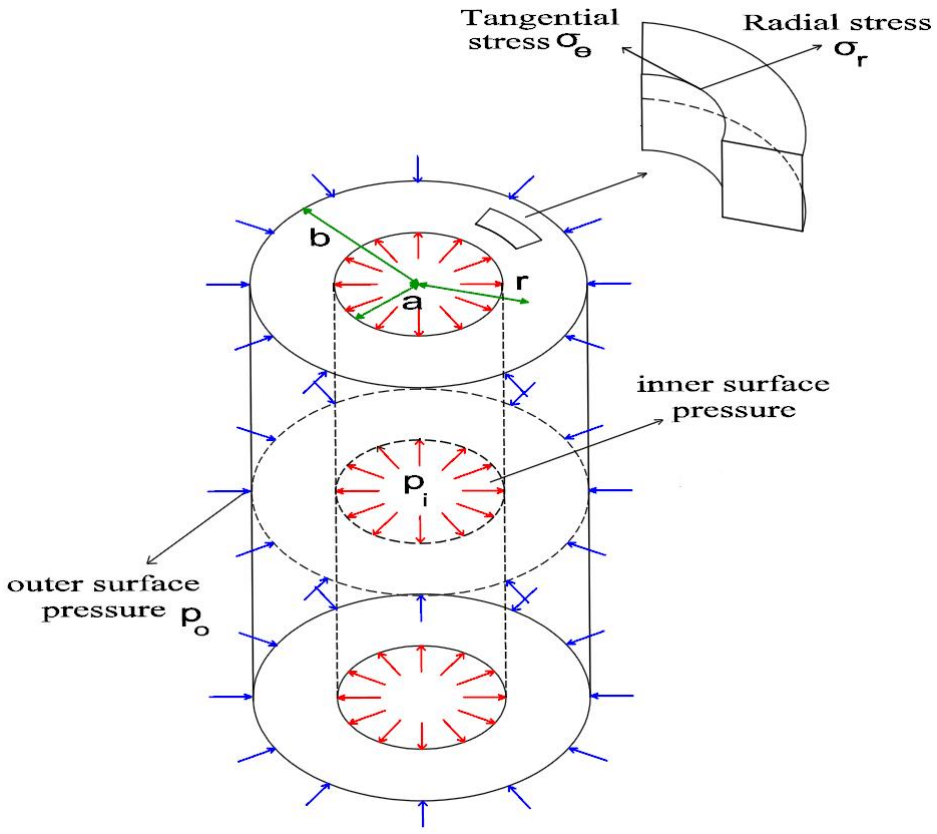

Figure 2.9.: An illustration of a hollow cylinder under inner and outer pressures and the coordinate system used

In other scenarios, as pressure in the cavity increases, the inner pressure may reach shear failure before the tangential stress reaches the tensile strength. A semi-analytical solution by Yu (2000) includes the influence of changing the mechanical properties of the soil on the distribution of the stresses around the cavity and in this research is used to calculate the stress distribution along the cavity wall thickness. A summary of this solution is given herein.

2.9.2. Semi-analytical solution by Yu (2000)

For the expansion of a cylindrical cavity in a finite medium modeled as a elastic-perfectly plastic material (i.e. Mohr-Coulomb model), the radial stress and the tangential stress are expressed analytically in Yu (2000). Depending on the ratio of the inner pressure (p_i) to the outer pressure (p_o) by using conventional cylindrical co-ordinates ($r; \theta; z$) and denoting the principal stresses as radial (σ_r), tangential (σ_θ), and axial (σ_z), increasing the inner pressure (p_i) leads to the formation of three stress state conditions around the cavity wall as follows (Fig. 2.10):

i) Elastic zone

A small ratio of (p_i/p_o) leads to pure elastic behavior over the whole thickness of the wall. In the elastic zone, the radial and tangential stresses can be obtained via a similar procedure, presented in e.g. Den Hartog (1952). The following equations are used to calculate σ_r and σ_θ at any point of a radial distance r:

$$\sigma_r = -p_o + (p_i - p_o)\left(\frac{1}{\frac{b^2}{a^2} - 1} - \frac{1}{\frac{r^2}{a^2} - \frac{r^2}{b^2}}\right) \tag{2.34}$$

$$\sigma_\theta = -p_o + (p_i - p_o)\left(\frac{1}{\frac{b^2}{a^2} - 1} + \frac{1}{\frac{r^2}{a^2} - \frac{r^2}{b^2}}\right) \tag{2.35}$$

In Figure 2.11, the change in radial and tangential stresses along the wall thickness of the cylinder is presented for the elastic region, where a gradual reduction in the tangential and radial stresses from inner to outer radius can be seen. The greatest value of σ_r and σ_θ is found at $r = a$ (inner surface of the cavity wall). Hence, it is expected that the yielding (critical pressure) will begin at the inner surface (Chakrabarty 2006).

ii) Elastic-Plastic zone

By increasing the ratio of (p_i/p_o) the inner pressure (p_i) reaches a critical pressure (p_{cr}) and the soil at the inner surface of the cavity wall starts to behave plastically. However, the outer surface of the wall is still under elastic conditions. Therefore, the stress components

in plastic and elastic zones become different.

$$p_{cr} = p_o + \frac{(b^2 - a^2)[Y + (\alpha - 1)p_o]}{(1 + \alpha)b^2 + (\alpha - 1)a^2} \tag{2.36}$$

Stresses in the plastic region:

$$\sigma_r = \frac{Y}{\alpha - 1} + Ar^{-\frac{(\alpha-1)}{\alpha}} \tag{2.37}$$

$$\sigma_\theta = \frac{Y}{\alpha - 1} + \frac{A}{\alpha} r^{-\frac{(\alpha-1)}{\alpha}} \tag{2.38}$$

Stresses in the elastic region:

$$\sigma_r = -p_o + B(\frac{1}{b^2} - \frac{1}{r^2}) \tag{2.39}$$

$$\sigma_\theta = -p_o + B(\frac{1}{b^2} + \frac{1}{r^2}) \tag{2.40}$$

Where:

$\alpha = \frac{1+\sin\varphi}{1-\sin\varphi}$, $Y = \frac{2c\cos\varphi}{1-\sin\varphi}$

A and B are integration constants, p_i and p_o prescribed at the boundary, c and φ are Mohr-Coulomb failure criteria.

$$A = -[Y + (a - 1)P_o] \times [\frac{1}{a - 1} - \frac{(\frac{c}{b})^2 - 1}{(a - 1)(\frac{c}{b})^2 + a + 1}]c^{\frac{a-1}{a}} \tag{2.41}$$

$$B = \frac{Y + (a - 1)P_o}{\frac{a-1}{b^2} + \frac{1+a}{c^2}} \tag{2.42}$$

iii) Plastic zone

As shown in Fig. 2.11 an increase in inner pressure caused to spread of the plastic radius (c) into the soil mass. Finally by reaching to the fully plastic state pressure ($p_{plastic}$) the entire cylinder becomes plastic ($c = b$).

$$\frac{c}{a} = \left\{ \frac{[(\frac{c}{b})^2 + 1 + \frac{2}{\alpha-1}](Y + (\alpha - 1)p)}{(2 + \frac{2}{\alpha-1})(Y + (\alpha - 1)P_o)}) \right\}^{\frac{\alpha}{\alpha-1}} \tag{2.43}$$

$$p_{plastic} = \frac{Y + (\alpha - 1)p_o}{\alpha - 1}[(\frac{b}{a})^{\frac{\alpha-1}{\alpha}} - 1] + p_o \tag{2.44}$$

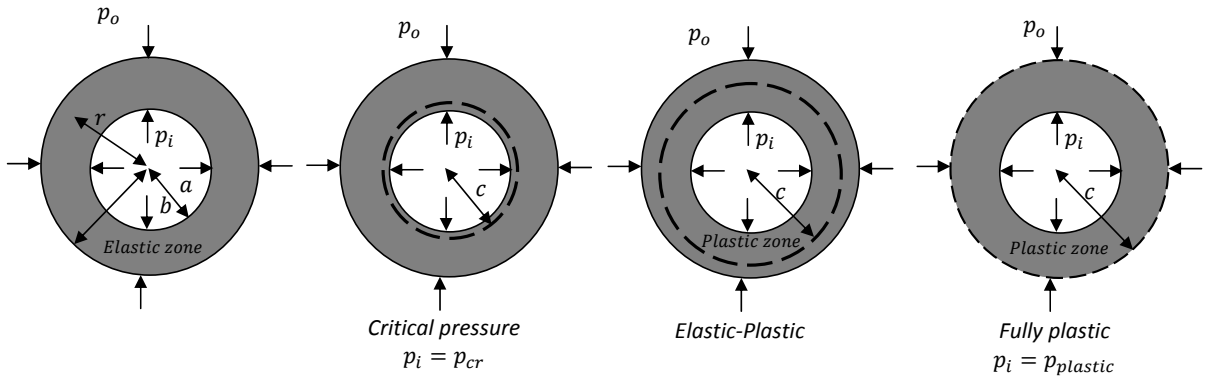

Figure 2.10.: Stresses in the elastic, elastic-plastic and fully plastic region

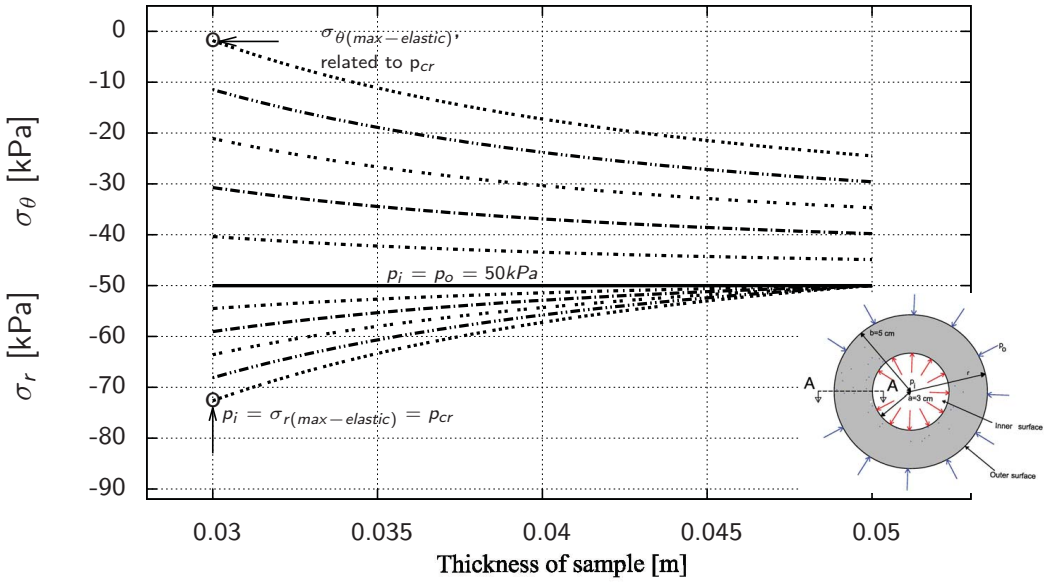

Figure 2.11.: Stress distribution in a thick-wall hollow cylinder, expanded by inner pressure (p_i) in the elastic range

As shown in Figure 2.12, once the soil starts to deform plastically, the magnitude of the radial stress steadily decreases from $r = a$ to $r = b$. The tangential stress, on the other hand, has the greatest value on the elastic/plastic boundary at $r = c$ and the highest value of the tangential stress is found at the outer radius ($r = c = b$) for $p_i = p_{plastic}$.
The value of tangential stress has a smaller value in the plastic region than in the elastic region. This is because the tangential stress has to be decreased to maintain a constant deviator stress with radial stress after elastic failure has occurred (Chakrabarty 2006).

iv Partially saturated condition

In the elastic phase the radial and tangential stresses change by equal and opposite magnitudes. Therefore, in this region the mean net stress remains constant. From this, if a cavity is expanded in the elastic zone, there is no reason to expect any change in suction in the thick-wall (Mair & Wood 1987). There are no important changes in degree of saturation within the plastic region affected by the expansion of the cavity wall. Therefore, one could also expect that matric suction remains constant throughout the expansion of the cavity wall considering both elastic and plastic regions without any restriction imposed on the magnitude of the deformations (Houlsby 1998).

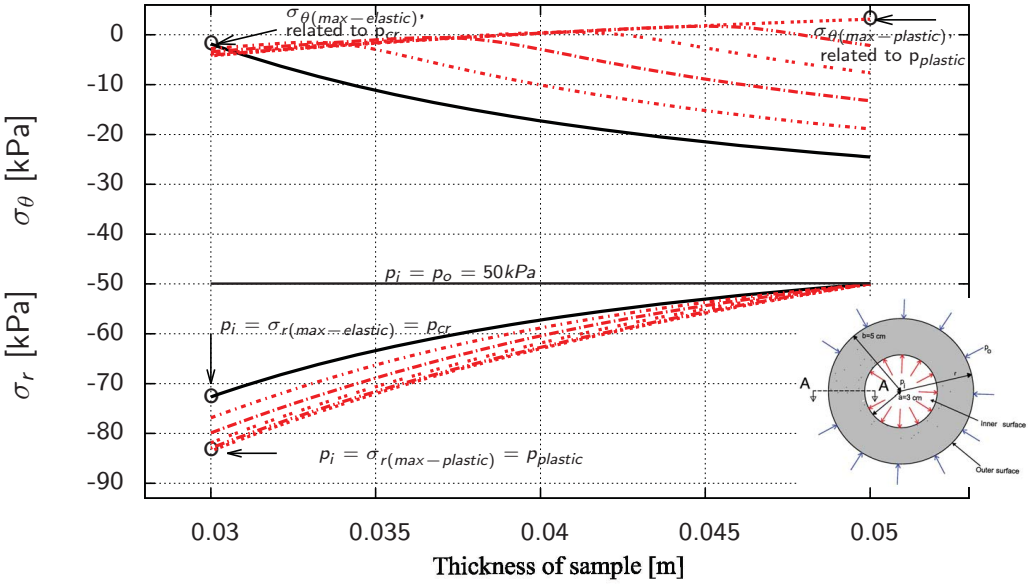

Figure 2.12.: Stress distribution in a thick-wall hollow cylinder, expanded by inner pressure (p_i) in the elastic/plastic range

This evidence could be considered to use the concepts of available cavity expansion theory to be extended to the framework of partially saturated soil behavior and allows to use of the elastoplastic models in partially saturated soil conditions (Schnaid et al. 2004).
In this study it is considered that the expansion of the cavity wall is occurred in fully drained process. In addition, to perform the tests on partially saturated specimens the matric suction has been controlled and as a consequence the suction remains constant during the test. This assumption allows one to use the same stress-strain relationships for partially saturated condition as well as applied for drained analysis in saturated condition.

In addition, this assumption implies that partially saturated soils at constant suction behave qualitatively in the same way as soils in saturated state.

2.10. Summary

Research work during the last decades strongly indicates that the "effective stress concept" may be a suitable concept when dealing with limit state problems in partially saturated soils. If this holds true the well known concepts of critical state soil mechanics in saturated or dry soils could be fully transferred to limit state problems taking into account partially saturated conditions.
Experimental studies indicate that using the effective stress concept allows to determine the parameters needed to describe shear strength behavior of partially saturated soils as well as "suction stress" from shear and tensile tests using partially saturated samples.
Existing studies validating the effective stress concept are mostly performed on one kind of soil and limited to low matric suction regions, do not consider tensile and low mechanical stress regimes and investigate only one kind of failure mode. Therefore a systematic comparison of the effective stress concept on different kinds of soils including the full mechanical stress and suction stress range as well as different kinds of failure modes is still missing.

3. Materials and methods

3.1. Experimental strategy

With regards to the shortcomings depicted in Chapter 2, a systematic experimental study of the effective stress concept to take into account the full mechanical stress and full degrees of saturation as well as different failure modes is still missing. In this study we attempt to study the effective stress concept on different kind of soils (fine to coarse grained) with respect to shear strength of partially saturated soils by considering different modes of failure (direct tensile and shear test), the full range of degrees of saturation, and changes in soil structure during drying and wetting. The materials used and the experimental works are summarized in Fig. 3.1. Four materials, including pure sand, two sand-kaolin mixtures, and pure kaolin (fine to coarse grained) were used in this study. SWCC was determined for two sand-kaolin mixtures and the results of Lins (2009) and Alabdullah (2010) are used to determine SWCC for pure sand and pure kaolin respectively. Direct tensile test of Lu et al. (2007) and the biaxial shear test results of Alabdullah (2010) are used to study the effective stress concept on pure sand. The experiments of direct tensile and triaxial tests as well as ESEM and MIP are performed on two mixtures of sand-kaolin (70-30 and 50-50) by using Spergauer kaolin and Hostun sand. Direct tensile test and triaxial test by Heibrock (1997) and Brueggemann (1998) are performed on a medium plastic kaolin. Investigations on soil microstructure have been done by using two methods, namely ESEM and MIP on two sand-kaolin mixtures in wetting and drying paths.

3.2. Basic properties of the used materials

Investigating the basic properties of the used materials was determined according to DIN and ASTM laboratory standards. Hostun sand is poorly-graded sand with grain sizes

that range from 0.1 mm to 1.0 mm in diameter. It is classified as (SP) in the unified soil classification system (USCS).

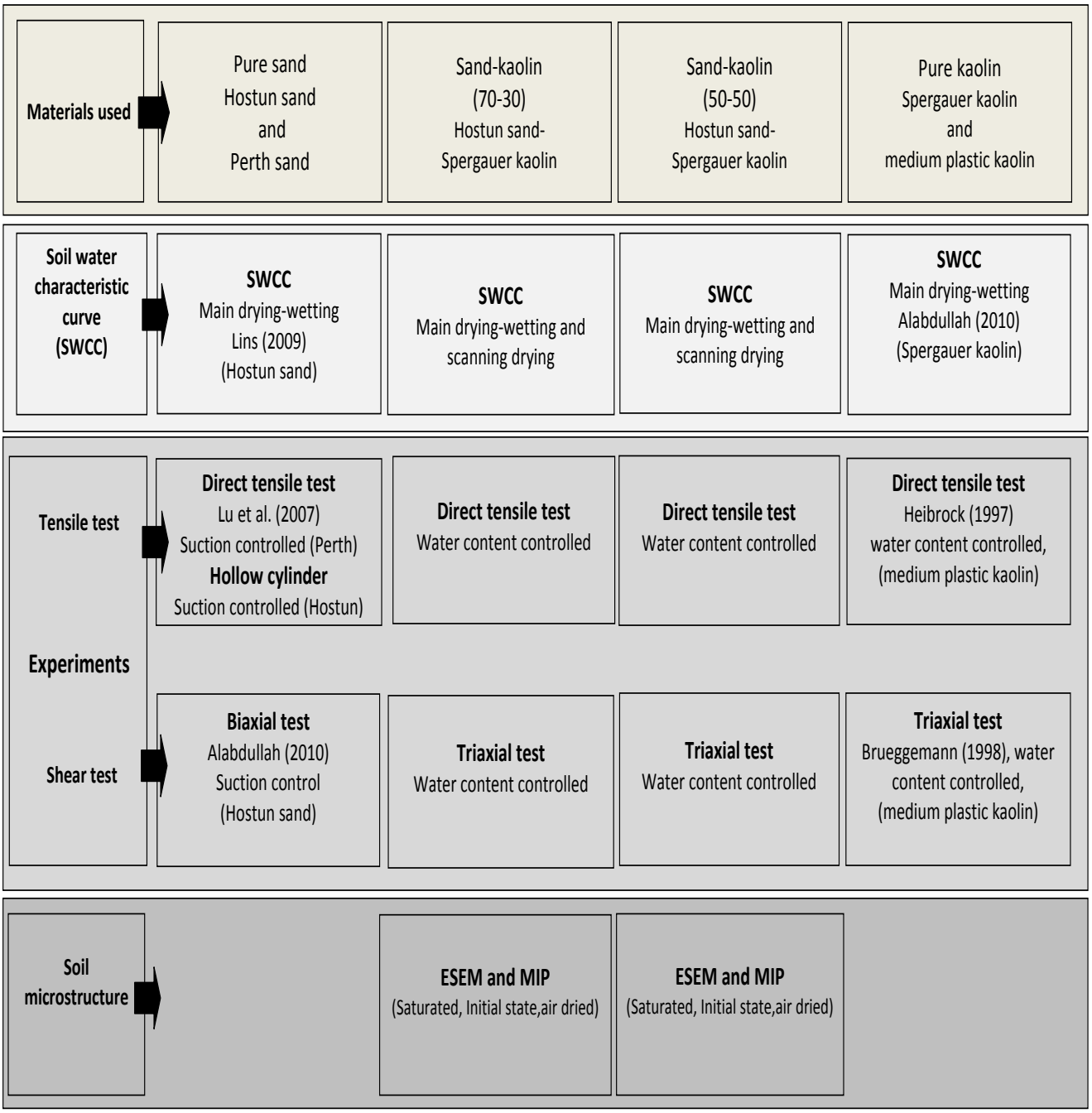

Figure 3.1.: Materials used and the experimental works

Direct tensile test and triaxial tests are performed on two mixtures of sand-kaolin (70-30 and 50-50) by using Spergauer kaolin which is classified by the USCS as (CH) and Hostun sand (SP). Test results of direct tensile and triaxial tests by Heibrock (1997) and Brueggemann (1998) on a medium plastic kaolin are used to study the effective stress concept on clay.

3.2.1. Grain size distribution

The grain size distribution curves are shown in Figure 3.2 for Hostun sand, two sand-kaolin mixtures and Spergauer kaolin. The specific gravity of the soils was determined using DIN 18124 standard methods. The liquid and plastic limit tests were performed according to DIN 18122 standards. The index properties for the soils used in this study are summarized in Table 3.1.

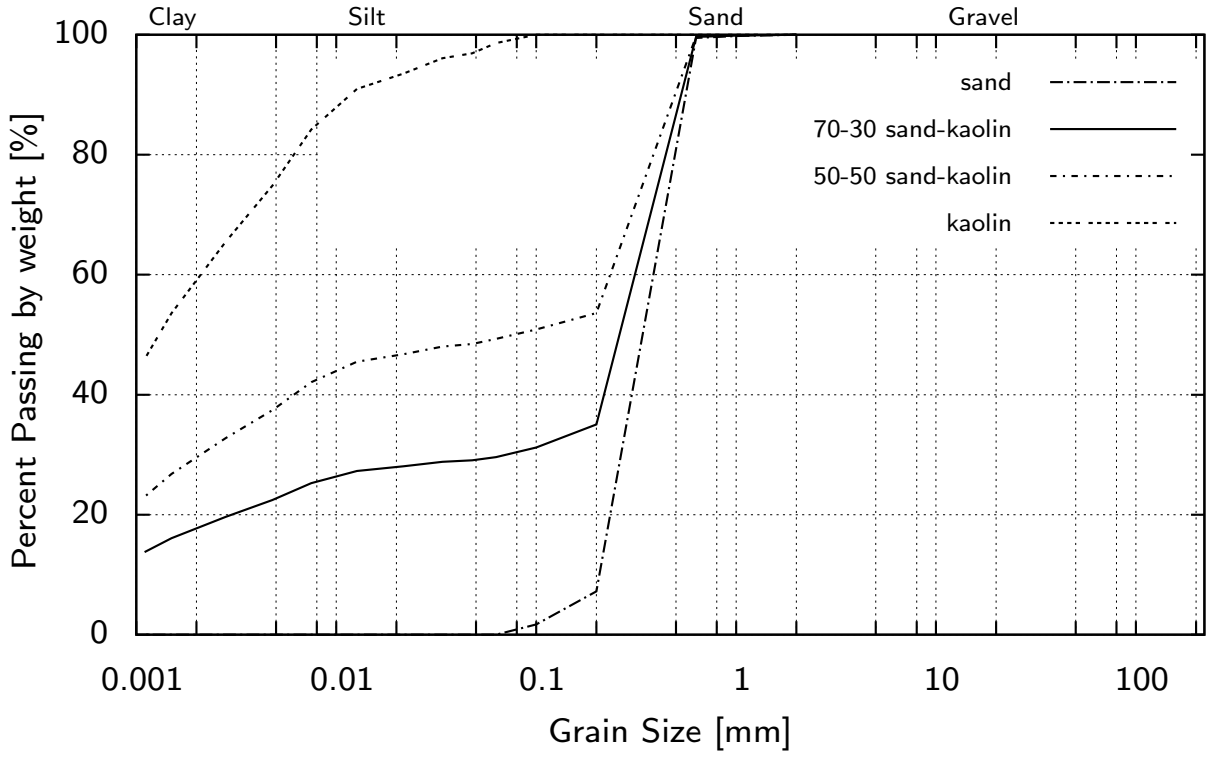

Figure 3.2.: Grain size distribution curves of different soils

Table 3.1.: Index properties of the soils used in this study

Soil type	Hostun sand	Perth sand Lu et al. (2007)	Spergauer kaolin	Mixture of 70%sand 30%kaolin	Mixture of 50%sand 50%kaolin	kaolin Heibrock (1997)
LL [%]	-	-	53.4	33.0	41.2	44.4
PL [%]	-	-	32.3	23.5	25.6	28.1
PI [%]	-	-	21.1	9.5	15.6	16.3
Specific gravity [-]	2.638	2.650	2.617	2.623	2.621	2.707
$d_{10}[mm]$	0.210	0.310	0.001	0.001	0.004	-
$d_{30}[mm]$	0.250	0.400	0.003	0.070	0.022	-
$d_{60}[mm]$	0.39	0.465	0.01	0.31	0.43	-
$c_c[-]$	0.76	1.1	0.82	2.75	0.27	-
$c_u[-]$	1.86	1.5	11.00	40.52	103.93	-
$w_{opt}[\%]$	10.75	-	22.80	12.40	14.60	25.50
Proctor $[g/cm^3]$ density	1.53	-	1.51	1.88	1.79	1.55

3.2.2. Compaction curves

Compaction curve is the relationship between the molding water content of the soil and dry density for a specific soil compacted sample at constant energy. Figure 3.3 shows the determination of maximum dry density and optimum water content (w_{opm}) for compaction tests of the materials used in this study.

3.3. Sample preparation

3.3.1. Sample preparation of SWCC, ESEM and MIP

Fig. 3.4 illustrates the processes of sample preparation for different types of test for two sand-kaolin mixtures. For sample preparation of the SWCC, ESEM and MIP tests, the dry components are mixed well according to mass fractions to make the sample homogeneous. Water equal to w_{opt} was added to the mixtures. The mixtures were then stored for one week to ensure homogenous moisture distribution.

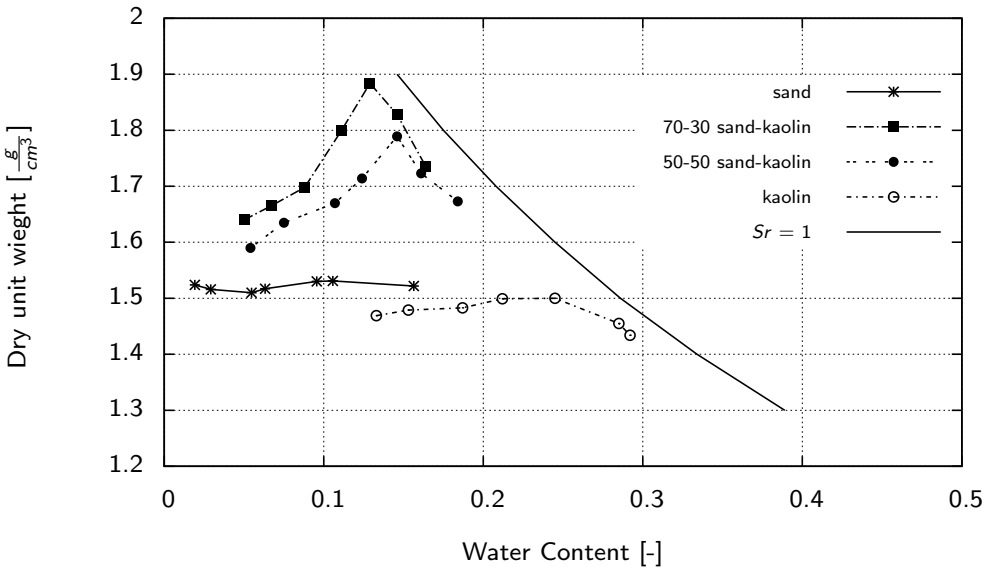

Figure 3.3.: Proctor compaction curves of the used materials

Plexiglas rings with a diameter and height of 50 and 15 mm respectively were filled in two layers and each layer is compacted with a hydraulic jack to the Proctor density. To investigate the influence of compaction, two different methods namely statically and dynamically were used to compact the samples to Proctor density. For static compaction, the samples were compacted to Proctor density by using a hydraulic jack. For dynamic compaction, samples were compacted using a Proctor hammer. As shown in Fig. 3.5, comparison of suction values measured using dynamically and statically compacted samples on scanning drying curves indicates that for the investigated materials used and applied suction the kind of compaction has no significant influence on the SWCC curve.
This finding corresponds with studies of Montanes (2002) and Thom et al. (2007). Montanes (2002) showed that the suction values of the statically compacted samples made on sand-bentonite seem to be in agreement with those obtained from the dynamically compacted samples. It is indicated that the suction seems to be dependent on water content and dry density, rather than on the compaction technique. Thom et al. (2007) investigated the pore size distribution of dynamically and statically compacted kaolin samples and found that although form of compression (static/ dynamic) generally influenced the resulting pore size distribution the differences were small for samples compacted at a water content close to that of an optimum Proctor water content. Once the samples were compacted statically, by optimum water content and Proctor-density (initial state), the weight and dimensions of the sample are measured. For samples on main drying or wetting curves, which are shown by light gray color in Fig. 3.4, the samples were placed in a

deep dish that was filled 2/3 with water and allowed to soak for 2-3 days until complete saturation.

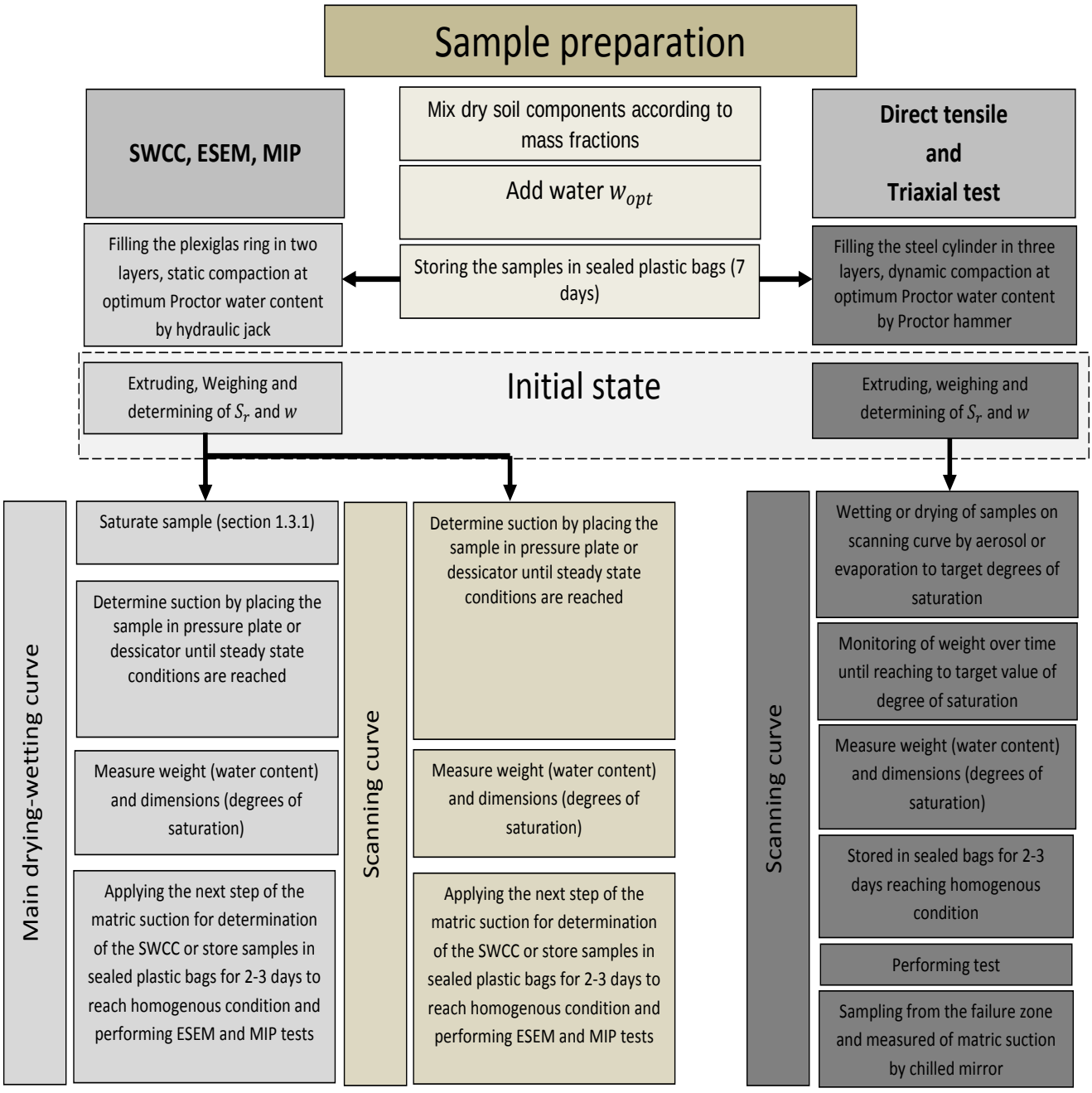

Figure 3.4.: Flow chart of the laboratory processing of sample preparation

On reaching saturation, the samples were subjected to a specific amount of matric suction. The weight of the samples were measured periodically and monitored until no change in weight of the soil samples in the desiccator is observed or when the water flow from the burette into the specimen inside of the pressure plate has stopped.

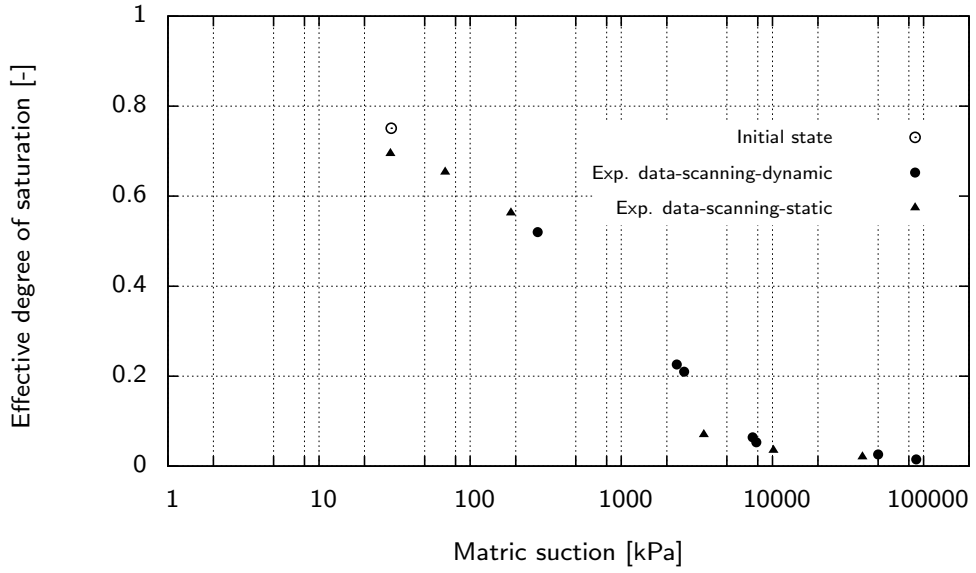

(a)

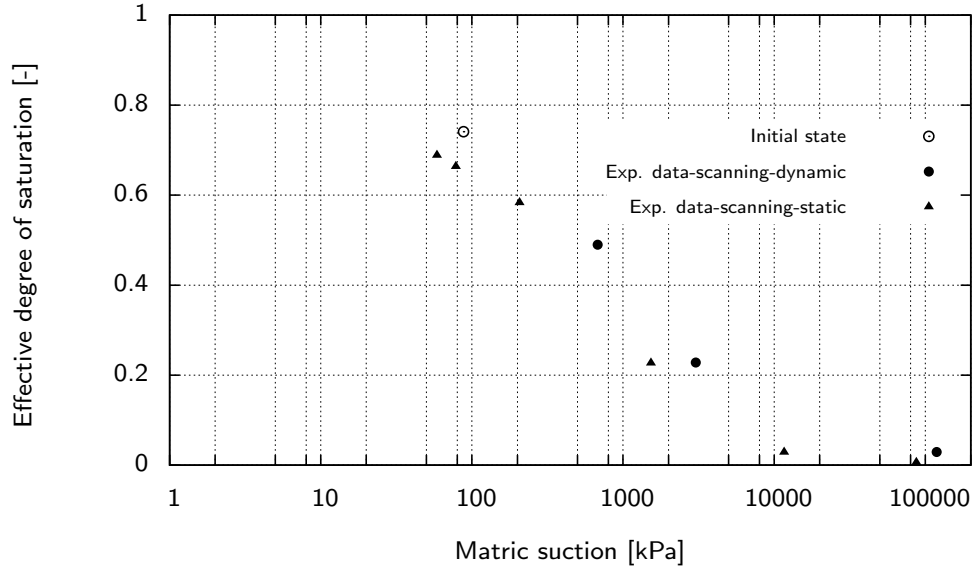

(b)

Figure 3.5.: Suction values measured using dynamically and statically compacted samples on scannig drying curves (a) 70/30 and (b) 50/50 sand−kaolin mixtures

To reach equilibrium, the samples are subjected to the next matric suction for the determination of the SWCC or stored in sealed plastic bags for 2-3 days to reach homogenous condition. ESEM or MIP tests are then carried out to investigate the soil structure. The samples on the scanning curve (see light brown column in Fig. 3.4) were placed in a pressure plate or desiccators and subjected to specific amounts of matric suction. The weight of the samples were measured periodically and monitored until no more change in weight of the soil samples in the desiccator is observed or when the water flow from the burette into the specimen inside of the pressure plate has stopped. To reach equilibrium, the dimensions and weight of the sample are measured to determine the water content and degrees of saturation. The same procedure as explained for the scanning curve was then carried out.

3.3.2. Sample preparation of direct tensile and triaxial tests

All experiments concerning direct tensile and triaxial tests were performed using a homogeneous mixture of sand-kaolin. The water content of these mixtures corresponded to the optimum Proctor water content (w_{opt}) of 70/30 and 50/50 sand-kaolin mixtures respectively (see dark gray column in Figure 3.4).
After mixing the dry soil components according to mass fractions, each mixture was stored for one week to ensure homogenous moisture distribution. Steel cylinder is filled in three layers with the soil sample.
All samples were compacted dynamically in steel cylinders of 50 mm width and 100 mm height using a Proctor hammer. Before adding each new layer, the surface of the previous layers is scratched in order to ensure the uniform distribution of compaction effects. To ensure homogenous compaction of the upper and lower parts of the sample, compaction energy was applied to both sides of the sample. The compaction energy was chosen so that the samples gained Proctor density after compaction. After compaction, samples were extruded from the compaction mold (initial state) (Fig. 3.6).
To prepare samples with lower or higher water contents than w_{opt}, the Proctor-compacted samples were slowly air dried or wetted by using an aerosol. During drying, the weight and dimensions of the samples are measured simultaneously until no further changes in specimen weight are observed. To reach equilibrium the samples were placed in the sealed plastic bags for 2-3 days to ensure even moisture distribution. In addition, after the test, small pieces of sample are taken directly from the failure zone and water content and the matric suction with chilled mirror are measured. In Figure 3.7, the void ratio of the samples during drying showed no significant changes for the 70-30 sand/kaolin mixtures.

By increasing the fine content for the 50-50 sand/kaolin mixture and pure kaolin, the reduction in void ratio through the drying process is more pronounced.

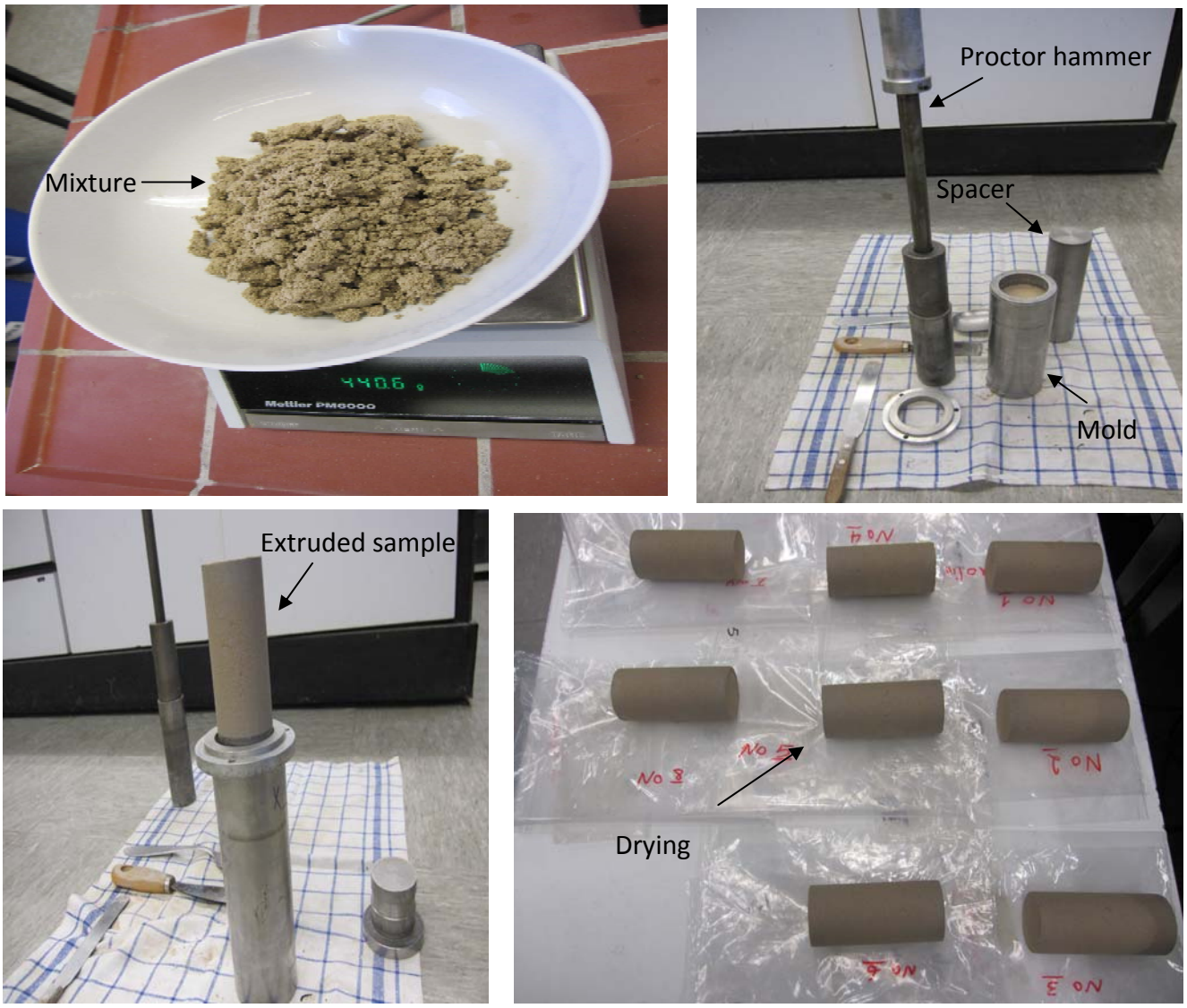

Figure 3.6.: Sample preparation of direct tensile and triaxial tests for two sand-kaolin mixtures

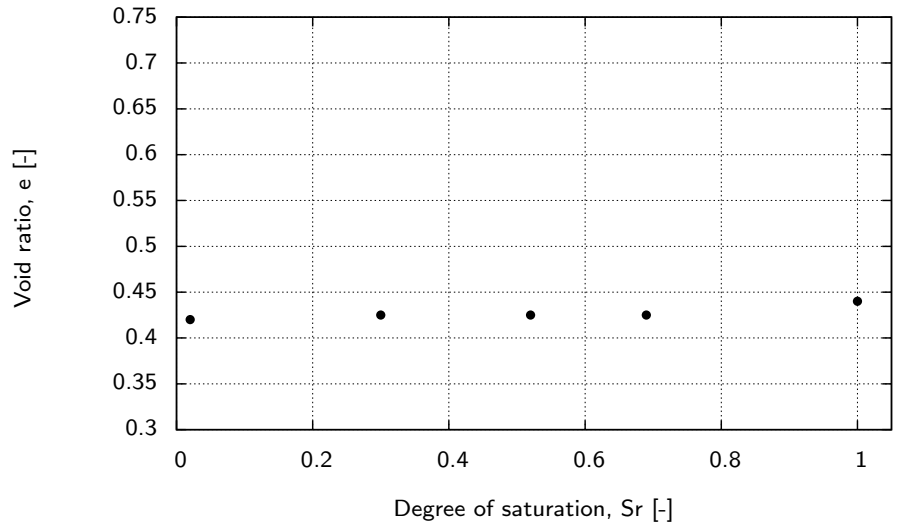

(a)

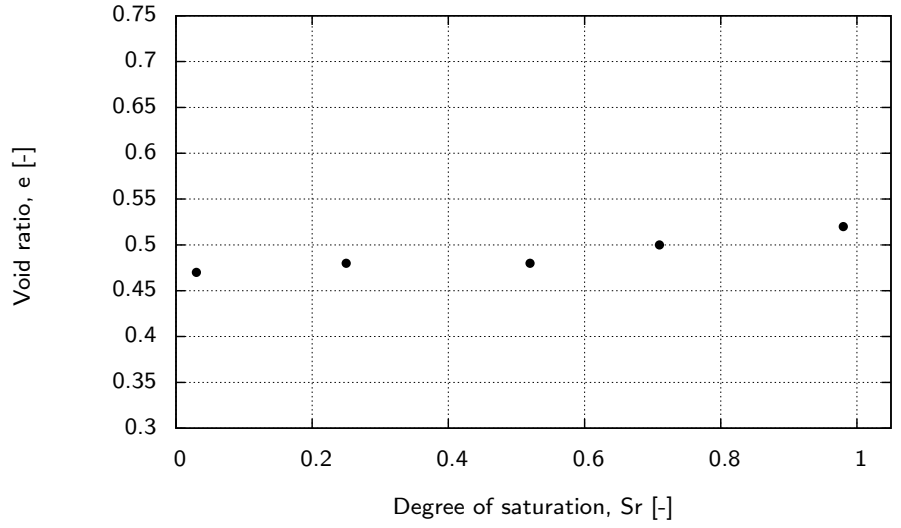

(b)

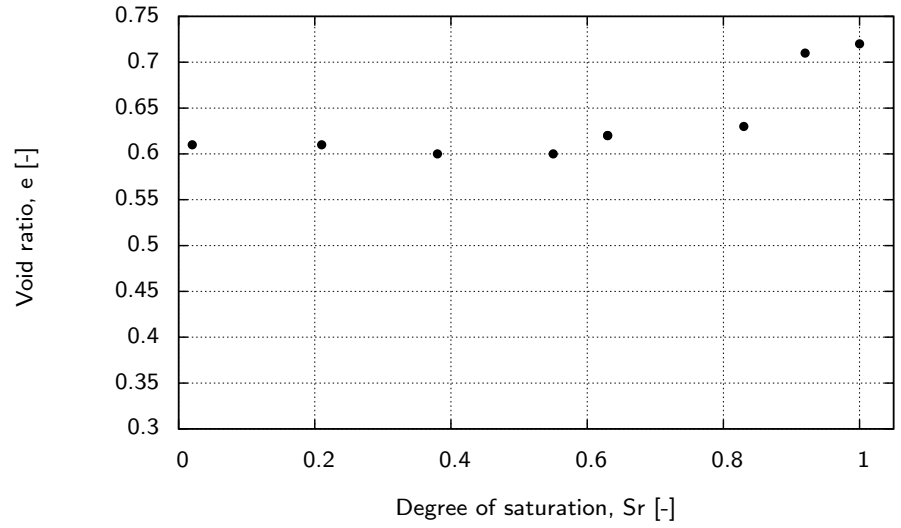

(c)

Figure 3.7.: The void ratio of the specimens during drying and saturation (a) 70-30 sand/kaolin (b) 50-50 sand/kaolin (c) pure kaolin (Alabdullah 2010)

3.4. Techniques and procedures used for SWCC tests

As described in the literature, the soil water characteristic curve (SWCC) represents the relationship between the water content of a soil and its matric suction. Water content in SWCCs determined herein is expressed in terms of the degree of saturation. SWCC includes the main paths, namely drying, wetting and scanning curves, which is placed inside the main drying and wetting loop. In order to draw drying and wetting paths, saturated and dry samples (respectively) must be subjected to constant suctions to lose or receive water until an equilibrium condition is reached. In this study, two methods were implemented to control suction, the Axis Translation Technique (ATT) for suctions <1500 kPa and the Vapor Equilibrium Technique (VET) for suctions > 1500 kPa.

3.4.1. Axis Translation Technique (ATT)

The axis translation technique is the most commonly used technique of controlling suction. Early developments of this technique started by using pressure plate technique. The pressure plate method is the most common direct method used to determine the relationship between the degrees of saturation and suction in soil (ASTM C1699-09). The pressure plate method works on the principle of axis translation, which regulates any difference in pore air pressure and pore water pressure, i.e. the matric suction. The apparatus consists of a high air entry porous ceramic disk contained in a sealed pressure chamber, air pressure supply system and volume measurement via a burette connected to the outlet of the pressure chamber. A schematic diagram of a pressure plate extractor is shown in Figure 3.8. The ceramic disc is kept saturated and in contact with water in a section below the disc. The air entry value of the disc should have a higher suction force than the matric suction of soil to be measured.
The desired matric suction can be achieved by applying air pressure on the specimen within the chamber. Under the applied air pressure the water from the soil and the porous plate is pushed to drain out from the system and collected in the burette. Equilibrium is reached when water is no longer discharged from the specimen. At equilibrium, the applied pressure is equal to the matric suction of the soil.

3.4.2. Desiccators (VET) and chilled mirror technique

Figure 3.9 shows the vapor equilibrium technique schematically. Several salt solutions were used to induce suction to the specimen by changing the relative humidity of the

vapor space in the desiccators. The relative humidity of the vapor above the salt solution was verified using the chilled-mirror hygrometer technique. The chilled mirror hygrometer used in this study was a water activity meter type 3TE produced by Decagon Inc.
The chilled mirror hygrometry technique is used to measure the water potential or suction of soils (Brye 2003, Leong et al. 2003 and Agus & Schanz 2005).

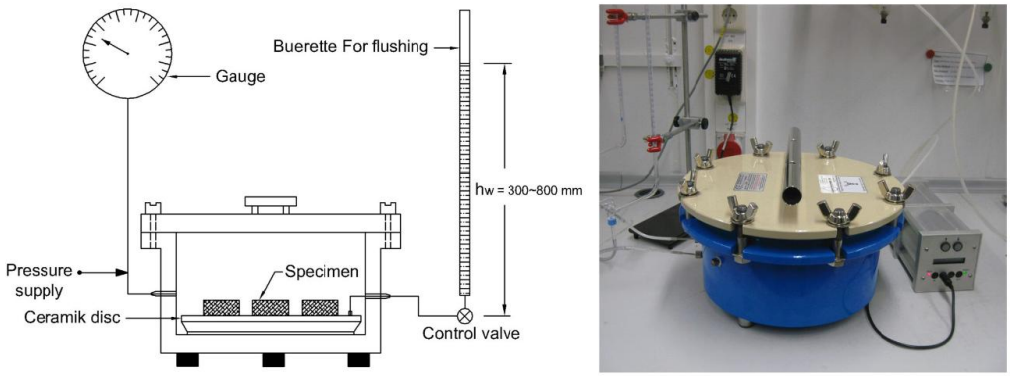

Figure 3.8.: Schematic sketch and a photograph of the pressure plate device

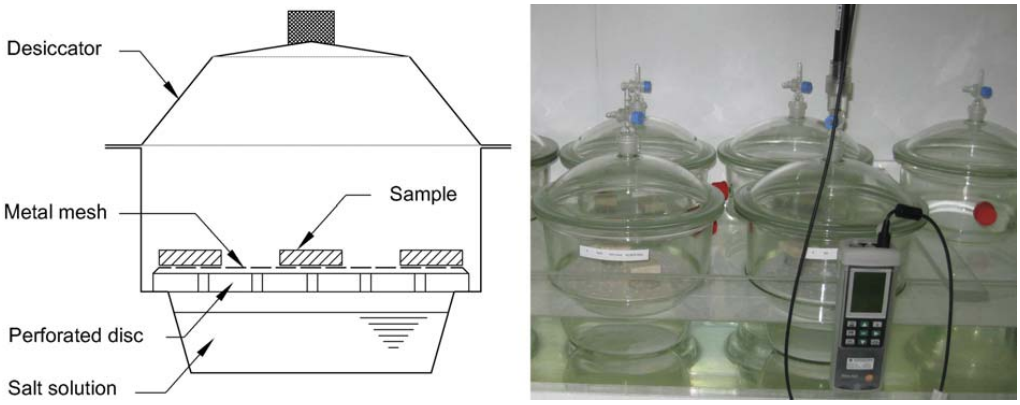

Figure 3.9.: Schematic sketch of VET and photograph of the desiccators used

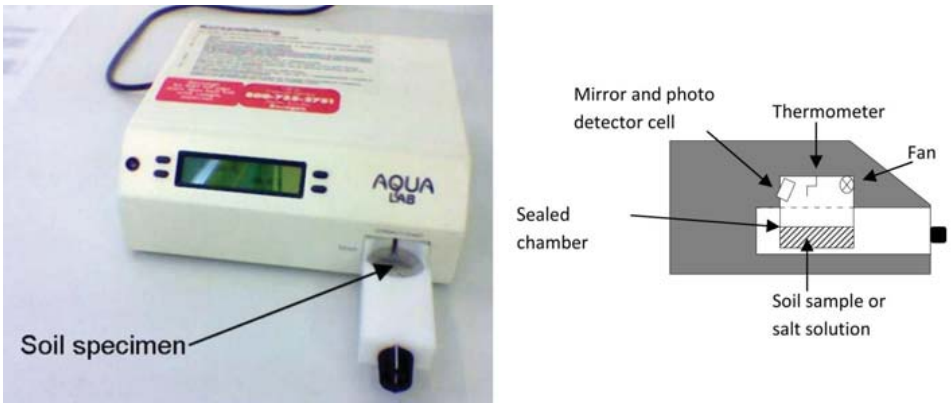

Figure 3.10.: Chilled mirror hygrometer

This technique measures the dew point and temperature of the sealed chamber in which the soil sample is placed. The relative humidity or water activity of the specimen is calculated from the measured dew point and temperature. The temperature of the space is precisely controlled by a thermoelectric cooling system.
As it can be seen in Fig. 3.10 a mirror and photo detector detects the appearance of condensing water. Circulating air over the sample can quicken the process. In this order, a fan is installed inside the chamber. The measured relative humidity can be converted to suction using Kelvin's law as follows (Eq. 3.1):

$$s_t = \frac{-R_g T_a}{M_w(\frac{1}{\rho_w})} \times \ln \frac{RH}{100} \tag{3.1}$$

Where s_t is total suction in kPa, R_g the universal gas constant (i.e. 8.31432 $J/molK$), T_a the absolute measured temperature in degrees K, M_w the molecular weight of water (i.e. 18.016 kg/k.mol), ρ_w the unit weight of water in kg/m^3 as a function of temperature and RH is the measured relative humidity in percent. Chilled mirror technique is mostly applied on samples with relatively low degree of saturation.
Procedures similar to those used in the pressure plate apparatus (ATT) to determine the changes in water content were adopted for vapour equilibrium technique (VET). At the end of the test, the relative humidity of the solution in the desiccator was measured using the chilled mirror technique to compute the actual suction applied to the specimens. In addition, for samples with low water content, the matric suction was measured after direct tensile and triaxial testing using the chilled mirror technique.

3.5. Technique and procedure used for direct tensile tests

In this test, as the name implies, the tensile force is directly applied to the specimen along its longitudinal axis until failure occurs. The tensile strength can be calculated from the ultimate load sustained by the specimen and the cross sectional area upon which it acts. A series of direct tensile tests with degrees of saturation of around 0, 30, 50, 70, and 100% were performed on two sand-kaolin mixtures. The average value related to each degree of saturation was established as the tensile strength.
The experimental test results of Lu et al. (2007) and Heibrock (1997) has been used to investigate the tensile strength on pure sand and pure kaolin respectively. Test setup of the direct tensile tests is shown in Fig. 3.11. Samples were placed in a loading frame using hooks fixed on plastic plates glued to the sample. Tensile tests were performed by applying a strain rate of 0.002, % min^{-1} until sample failure. The corresponding tensile force was measured by a load cell. The maximum measured tensile force was used to define the tensile strength of the sample. In almost all cases, failure occurred in the center of the sample, indicating that no significant stress concentrations took place. Only samples with failure in the middle were used to derive suction stress. The initial water content and the initial void ratio were used to read the corresponding suctions from the SWCC scanning curve. In Tables 3.2, 3.3 and 3.4 the initial conditions for both mixtures of the sand/kaolin and pure kaolin are illustrated.

3.6. Technique and procedure used for triaxial tests

Study of the effective stress concept was done by extruding the failure envelope for triaxial tests. After sample preparation and on reaching the target value of water content (degree of saturation) the samples were placed in conventional triaxial apparatus. Five sets of tests were performed at saturation degrees of around 0, 30, 50, 70 and 100%. Each set included three different confining pressures equal to 25, 50, 100 kPa and 0, 50, 100 kPa for mixtures of 70/30 and 50/50 sand/kaolin respectively. For pure sand, the test results of Alabdullah (2010) are used. The experiments were performed on a biaxial device by using dense specimens ($e_o = 0.66$) under three different confining pressures equal to 10, 50 and 100 kPa. In each set, the net confining pressure ($\sigma_3 - u_a$) was kept constant and the matric suction ($u_a - u_w$) was changed to study the effect of matric suction on the shear strength. The triaxial test results of Brueggemann (1998) are used to study the concept of the effective stress on pure kaolin. The tests were performed on a wide range of degree of

saturation (35, 60, 80, 90 and 100%) and confining pressures of 50, 100 and 200 kPa. To determine the effective friction angle φ' and cohesion c', three consolidated drained triaxial tests were performed using saturated soil samples. The Proctor-compacted samples were saturated in the triaxial cell by applying a small hydraulic gradient and a backpressure of up to 300 kPa. After reaching Skempton's pore water coefficient B values $\geq$95%, isotropic stress conditions were applied to allow for the consolidation of the sample. The samples were then sheared under strain-controlled (0.004 $\%min^{-1}$) conditions. Dried, compacted samples were placed in a conventional triaxial apparatus with an open drainage system. Isotropic stress corresponding to the selected confining pressure was applied. During this procedure, the drainage system, which was connected to the pore space of the sample, was open. After a consolidation time of 24 h, loading was applied to the sample by increasing the vertical strain ϵ_1 at a constant strain rate of 0.004 $\%min^{-1}$ and constant confining pressure σ_3. Several checks were carried out during the tests. After the tests, the partially saturated soil samples were cut into three slices of equal thickness and the water content of each slice was measured. Meanwhile, for a number of samples, the void ratio of the slices was determined using the paraffin wax method. Although no significant changes in water content were observed, the void ratio and therefore the degree of saturation in the shear zone changed significantly. Moreover, after triaxial testing, the matric suction for samples with low water content was measured using chilled mirror technique. For experimental testing on two sand-kaolin mixtures no significant changes in matric suction was found before or after triaxial testing.

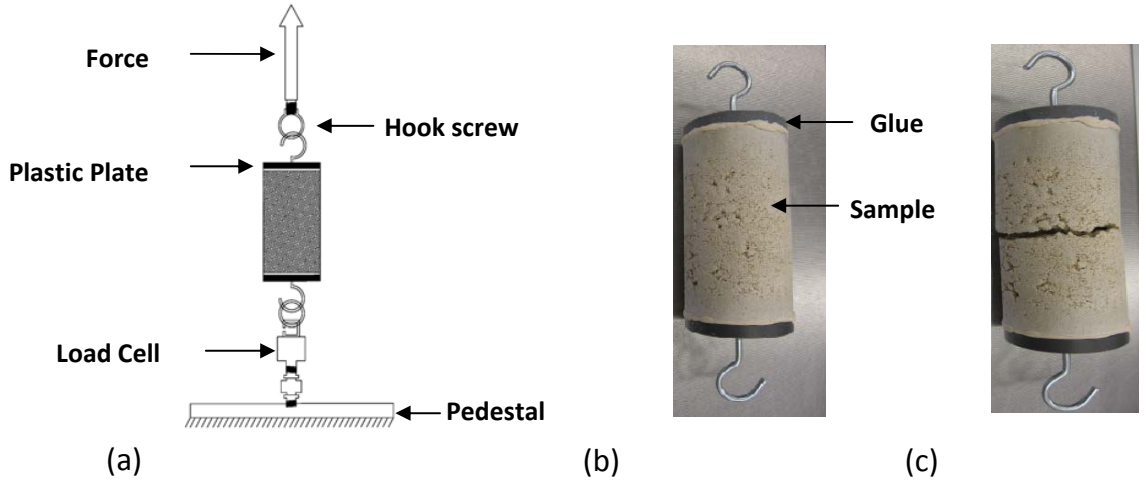

Figure 3.11.: (a) Setup of the direct tensile test for two sand-kaolin mixtures, (b) the specimen before the test, and (c) the specimen after the test

Boundary conditions and information on the samples used for triaxial testing are provided in Tabels 3.5, 3.6 and 3.7.

Table 3.2.: Program of direct tensile tests with initial conditions for mixture sand/kaolin (70/30)

Initial gravimetric water content [-]	Initial void ratio [-]	Initial volumetric water content [-]	Initial degree of saturation [-]	Matric suction [kPa]
0.003	0.42	0.005	0.01	100,000
0.003	0.43	0.005	0.01	100,000
0.003	0.43	0.006	0.02	100,000
0.018	0.42	0.033	0.11	7,000
0.023	0.42	0.042	0.14	7,000
0.054	0.42	0.101	0.35	800
0.054	0.42	0.099	0.34	800
0.053	0.42	0.098	0.34	800
0.083	0.41	0.153	0.53	360
0.081	0.41	0.150	0.51	360
0.081	0.41	0.150	0.51	360
0.080	0.42	0.148	0.51	360
0.116	0.43	0.213	0.71	80
0.113	0.43	0.212	0.70	80

Table 3.3.: Program of direct tensile tests with initial conditions for mixture sand/kaolin (50/50)

Initial gravimetric water content [-]	Initial void ratio [-]	Initial volumetric water content [-]	Initial degree of saturation [-]	Matric suction [kPa]
0.005	0.48	0.009	0.03	120,000
0.005	0.49	0.009	0.03	120,000
0.009	0.49	0.015	0.05	120,000
0.008	0.49	0.014	0.04	120,000
0.044	0.46	0.079	0.25	2,500
0.043	0.46	0.077	0.24	2,500
0.045	0.47	0.081	0.25	2,500
0.095	0.49	0.168	0.51	800
0.096	0.48	0.171	0.53	800
0.095	0.49	0.167	0.51	800
0.095	0.48	0.167	0.51	800
0.135	0.50	0.236	0.70	120
0.134	0.50	0.233	0.70	120

Table 3.4.: Program of direct tensile tests with initial conditions for pure kaolin (Heibrock 1997)

Initial gravimetric water content [-]	Initial void ratio [-]	Initial volumetric water content [-]	Initial degree of saturation [-]	Matric suction [kPa]
0.005	0.61	0.0085	0.02	600,000
0.05	0.61	0.0817	0.20	6,000
0.085	0.59	0.1462	0.38	4,000
0.125	0.6	0.2526	0.55	3,000
0.15	0.62	0.2529	0.63	2,500
0.15	0.62	0.2526	0.63	2,500
0.2	0.63	0.3353	0.83	1,600
0.25	0.71	0.3973	0.92	700
0.31	0.72	0.4952	1.00	1

Table 3.5.: Program of triaxial tests with initial and boundary conditions for mixture sand/kaolin (70/30)

Confining pressure [kPa]	Initial gravimetric water content [-]	Initial void ratio [-]	Initial volumetric water content [-]	Initial degree of saturation [-]
25	0.002	0.43	0.004	0.01
50	0.003	0.42	0.005	0.02
100	0.003	0.41	0.006	0.02
25	0.047	0.43	0.085	0.28
50	0.052	0.42	0.096	0.32
100	0.050	0.43	0.092	0.31
25	0.087	0.43	0.159	0.53
50	0.087	0.43	0.160	0.53
100	0.085	0.43	0.155	0.52
25	0.114	0.43	0.210	0.70
50	0.112	0.43	0.206	0.69
100	0.113	0.43	0.207	0.69
25	0.163	0.43	0.297	1.00
50	0.166	0.44	0.301	0.99
100	0.166	0.44	0.298	0.99

Table 3.6.: Program of triaxial tests with initial and boundary conditions for mixture sand/kaolin (50/50)

Confining pressure [kPa]	Initial gravimetric water content [-]	Initial void ratio [-]	Initial volumetric water content [-]	Initial degree of saturation [-]
0	0.005	0.48	0.01	0.03
50	0.006	0.48	0.01	0.03
100	0.008	0.48	0.01	0.04
0	0.044	0.47	0.08	0.24
50	0.043	0.47	0.08	0.24
100	0.046	0.47	0.08	0.25
0	0.096	0.48	0.17	0.52
50	0.096	0.48	0.17	0.52
100	0.094	0.48	0.17	0.51
0	0.137	0.50	0.24	0.71
50	0.137	0.50	0.23	0.70
100	0.134	0.50	0.23	0.71
0	0.194	0.52	0.34	0.99
50	0.192	0.52	0.33	0.98
100	0.195	0.52	0.34	0.99

Table 3.7.: Program of triaxial tests with initial and boundary conditions for mixture of pure kaolin (Brueggemann 1998)

Confining pressure [kPa]	Initial gravimetric water content [-]	Initial void ratio [-]	Initial volumetric water content [-]	Initial degree of saturation [-]
50	0.085	0.60	0.146	0.35
100	0.085	0.60	0.146	0.35
200	0.085	0.60	0.146	0.35
50	0.150	0.62	0.253	0.63
100	0.150	0.62	0.253	0.63
200	0.150	0.62	0.253	0.63
50	0.200	0.63	0.335	0.83
100	0.200	0.63	0.335	0.83
200	0.200	0.63	0.335	0.83
50	0.250	0.71	0.397	0.92
100	0.250	0.71	0.397	0.92
200	0.250	0.71	0.397	0.92
50	0.310	0.72	0.495	1.00
100	0.310	0.72	0.495	1.00
200	0.310	0.72	0.495	1.00

3.7. Technique and procedure used for biaxial tests

Biaxial device allows for direct and reliable testing of the soil materials under truly plan strain conditions, to evaluate the shear banding and stress-strain parameters under this condition. Effects of matric suction on shear strength were assessed by using the experimental results of Alabdullah (2010) on pure sand. The experiments were performed using a double wall biaxial device under plane strain conditions while applying matric suction. The schematic diagram of the biaxial cell device is shown in Fig. 3.12.
Once saturated samples were prepared, they were subjected to a predetermined level of matric suction by using the axis translation technique (ATT) (see section 3.4.1). Both the pore-air and pore-water pressures were translated into a positive range of pressures, which were applied through porous and ceramic discs. The volume changes on the pore-water phase of the specimens were measured using the burette volume change indicator, which was connected to the ceramic discs. The equilibrium was considered to be achieved when no volume changes were observed in pore-water volume. Boundary conditions and information on the samples used for testing on pure sand are provided in Table 3.8.

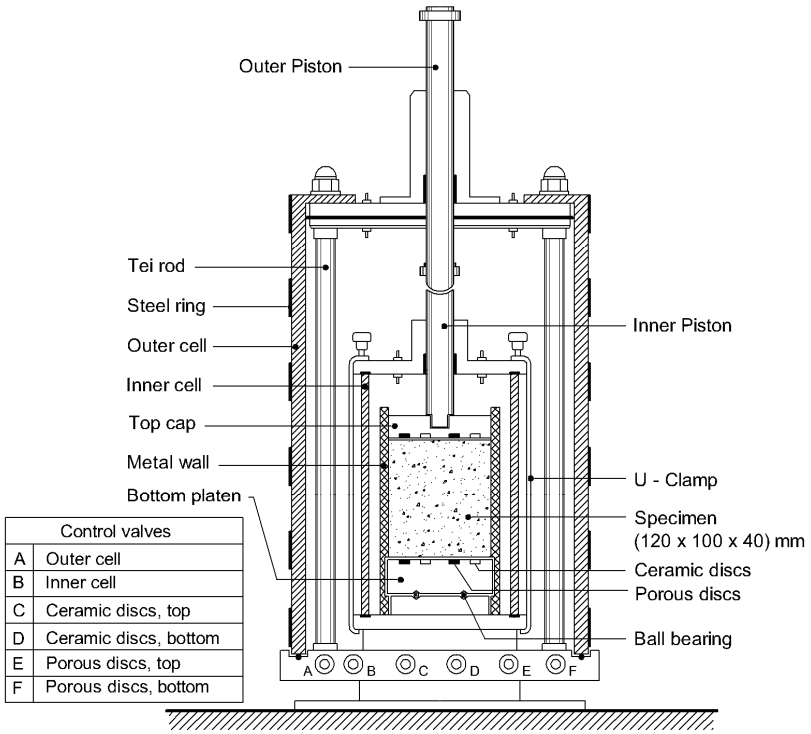

Figure 3.12.: The schematic diagram of the double-wall biaxial cell

Table 3.8.: Program of biaxial tests with initial and boundary conditions for pure sand (Alabdullah 2010)

Confining pressure [kPa]	Matric suction [kPa]	Initial void ratio [-]
10 50 100	Dry	0.66
10 50 100	2	0.66
10 50 100	4	0.66
10 50 100	Saturated	0.66

3.8. Experimental techniques for examining soil structure

Investigations on the microstructure of the studied soils have been conducted qualitatively and quantitatively. Qualitative observations of structures using visual images are done by ESEM, which is the most widely used surface diagnostic tool. The soil microporosity structure is studied by performing MIP that quantifies soil Pore Size Distribution (PSD) by showing the relationship between pore volumes and pore radius. All experiments were performed using mixtures of sand -Kaolin of 70/30 and 50/50 respectively.

3.8.1. ESEM method

This technique employs a narrowly focused beam of high-energy electrons to scan across the surface of a specimen. The beam's interaction with the surface generates a shower of secondary and backscattered electrons that are collected by a detector. The intensity of the emitted electrons varies according to differences in surface topography and/or material composition (Murray & Sivakumar 2010).
The Environmental Scanning Electron Microscope (ESEM) enables us to observe samples in their natural water content state. This helps us to avoid changes in origin structure of the soil.

Tests were carried out at the Electron Microscopy Laboratory in the Department of Materials Science and Metallurgical Engineering of the Ruhr Universität Bochum. The device used was the FEI ESEM Dual BeamTM Quanta 3D FEG. The instrument was equipped with various detectors, monitoring secondary electrons as well as backscattered ones. The configuration of the device is illustrated in Fig. 3.13.
The major components of the vacuum system of the ESEM are illustrated in Figure 3.14. In principle, two pumps control the chamber pressure. The rotary vacuum pump ensures pressure is reduced. The secondary pump is applied through the pressure-limiting hole. Water vapor is used to flood the sample chamber.
Detection in the ESEM is based on the principle of gas ionization. When the sample is placed in the chamber, the primary electronic beam is accelerated towards and collides with the sample, discharging secondary electrons. Positive gas ions are created by the collision of secondary electrons on the specimen surface. A gaseous secondary electron detector is used to detect back-scattered electrons by discriminating against their spurious signals. As a result of the discrimination between secondary electrons and backscatter electrons, the image quality and resolution from the ESEM are improved (Moo-Young & Ochola 1999).

Figure 3.13.: The configuration of the ESEM device

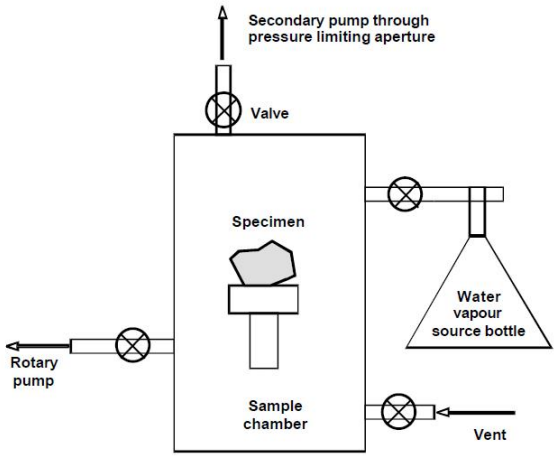

Figure 3.14.: ESEM vacuun system (Montanes 2002)

ESEM method is used to investigate the microstructure of the samples for two mixtures of the sand-kaolin (70/30 and 50/50) at three different states:

1. Saturated state (wetting from initial state)
2. Initial state (Proctor density with optimum water content)
3. Air-dry condition (dewatering from saturated state on main drying path)

3.8.2. MIP method

Pore size distribution can be determined by water desportion, non-polar liquid desportion, nitrogen sorption, micrometric methods (thin section and scanning electron microscopy) and mercury intrusion porosimetry (MIP). The approach used in this study involves the MIP method on two sand-kaolin mixtures using a freeze-dried technique for evaluation of the pore-size distribution on drying and wetting paths. The work was carried out at the chair of building material techniques in Ruhr Universität Bochum. In order to study the pore size distribution of soil using the MIP method, samples at four different states was selected (Figure 3.15):

1. Saturated state (wetting from initial state)
2. Initial state (Proctor density with optimum water content)
3. Air-dry condition (dewatering from saturated state on main drying path)
4. Air-dry condition (dewatering from initial state on scanning drying path)

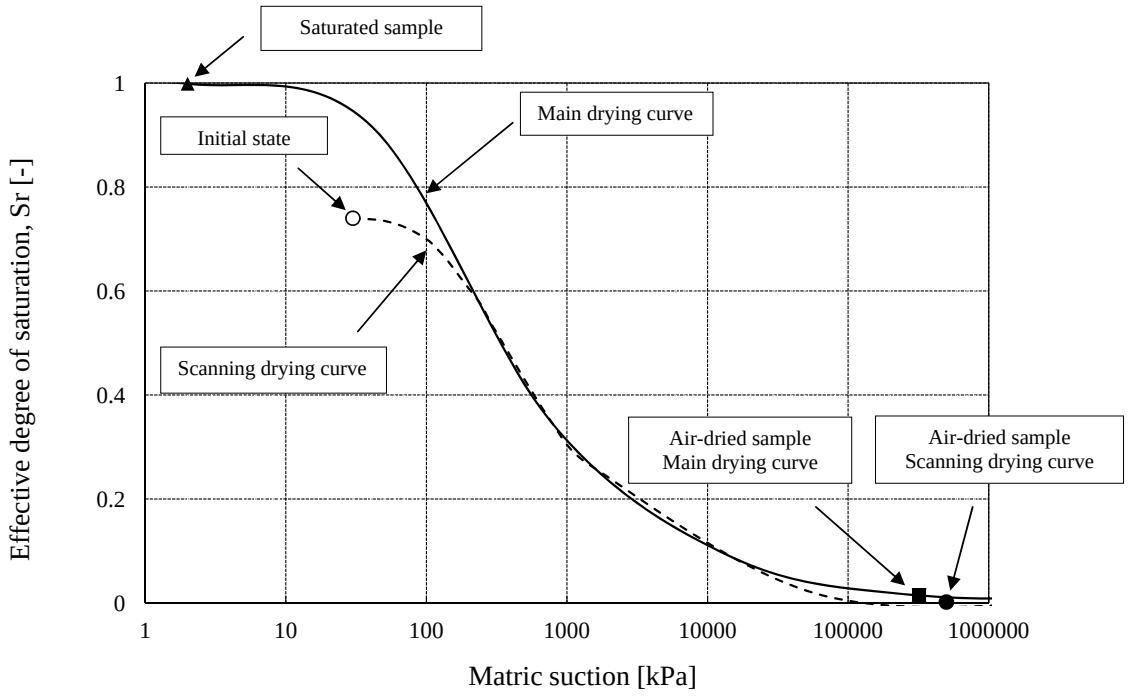

Figure 3.15.: Selected samples for investigation of the soil structure by MIP method

Implementation of MIP is based on the theory that pore-size distribution can be determined by measuring the pressure required to force mercury to intrude the void of a porous material due to the "ink bottle effect" (Fig. 3.16). The relationship between intrusion pressure and equivalent pore diameter could be calculated by Jurin's equation Eq. (3.2):

$$D = \frac{4T_s \cos \alpha}{P} \tag{3.2}$$

Where D is the pore diameter, T_s is the surface tension of mercury, α is the contact angle and P is the applied pressure. In order to convert data to show pore size distribution curves, the surface tension and contact angle of mercury were taken as 472 $\mu m/m^2$ and 135° respectively. Analysis was carried out on specimens were trimmed from the middle of the sample. The pressure porosimeter (Figure 3.17) consists of two devices; a low pressure porosimeter (Figure 3.17a), used for the measurement of pores between 135 μm to 4.5 μm and high pressure porosimeter (Figure 3.17b), which is applicable for the measurement of pores in the size range of 7.7 μm and 0.0012 μm. Dehydrated samples are needed when using the mercury intrusion apparatus. The extraction of the pore water without disturbing the origin structure of the specimen is a very difficult process and there is usually no way to determine the amount of disturbance caused. A rigorous dehydration procedure should use freeze-drying to avoid changes in porosity and the distribution of pore sizes.

In addition, freeze-drying causes less disturbance and shrinkage than air or oven drying.

To freeze-drying the samples, slices in 1 to 2 mm thick were taken from equilibrated samples and put in capsules, which were then placed in a vessel and rapidly frozen by dropping them into the liquid nitrogen (Figure 3.18a) at the freezing temperature about -80° C. After the samples are adequately frozen and all non-condensable gases removed as shown in Fig. 3.18b, a vacuum pump is used to reduce the ambient gas pressure in the vessel for 24 hours.

By determining the weight, the sample was placed in sample holder and vacuum is applied. Applying compressed air leads to flow of the mercury into a cell unit. This procedure was continued until the cell filled completely. The intrusion of the mercury into the sample was monitored during the pressure increment. Once the maximum pressure is reached, cell unit pressure is released into the atmosphere.
High-pressure porosimetery was performed in the pressure range equal to 220 MPa. Pressure was increased until reaching the intrusion equilibrium. Mercury extrusion was then carried out by reducing the pressure at the same rate.

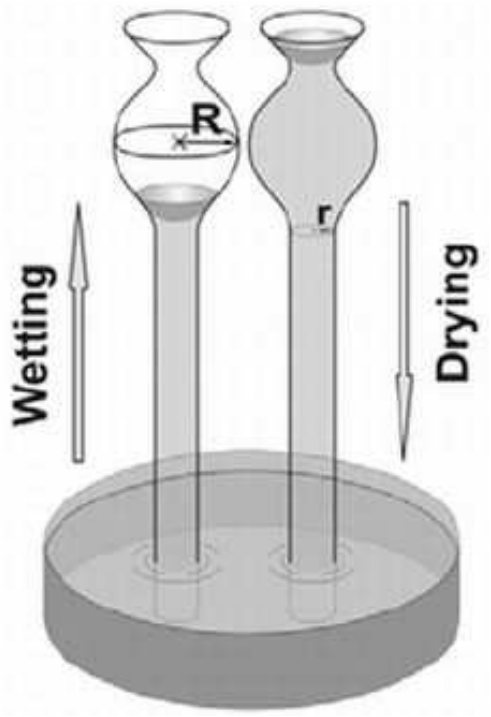

Figure 3.16.: Ink bottle effect

(a) (b)

Figure 3.17.: Thermo electron corporation prosimeter: (a) low pressure porosimeter (b) high pressure porosimeter

(a) (b)

Figure 3.18.: (a) Liquid nitrogen (b) vacuum pump

3.9. Summary

The basic properties of the materials used and the experimental program to study of the effective stress concept have been presented in this chapter. The experiments that are carried out in this study include the SWCC, direct tensile test and shear test. For SWCC tests, which consisted of ATT and VET methods, sample preparation and details of controlling suction have been well explained. The test devices used in this study, test setup, sample preparation and test program for direct tensile, triaxial tests and biaxial shear device are described.

In addition, the experimental techniques for examining the soil structure by ESEM and MIP are explained in details. Based on the explained techniques for performing tests in next chapter the test results are shown.

4. Experimental results

4.1. Presented results

This chapter presents the experimental results of the laboratory test program described in Chapter 3. The test results of direct tensile tests, shear tests and the results of the investigation on soil structure by using the ESEM and MIP methods are presented in this chapter.

4.2. Results of SWCC tests

For suctions in the range of the axis-translation technique (ATT) two samples from each material were prepared. Matric suctions were applied step by step. Once for a certain value of suction the sample reaches equilibrium, the next level of suction was applied to the same sample. However, for the vapor equilibrium technique (VET) for each applied suction value a range identical samples were prepared. The specimens altered in mass, which was monitored over time until this process achieved no further changes in weight. The measured mass of the specimens for 70/30 mixture are given in Figure 4.1 and Figure 4.2. Figure 4.1 illustrates the results of the ATT method at matric suction values of 100 and 600 kPa and Figure 4.2 is for experiments performed by using the VET method, at suction values of 10000 and 100000 kPa.

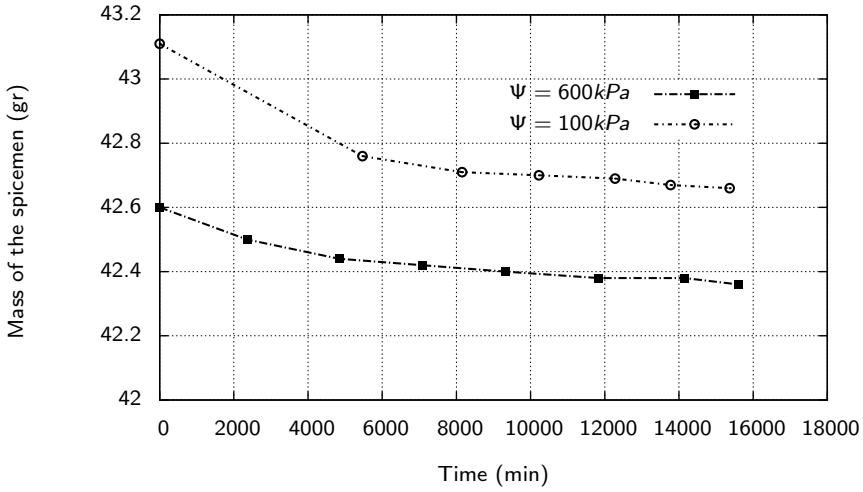

Figure 4.1.: Measured mass of 70/30 sand-kaolin mixture due to applied suction during drying path in the pressure plate extractor (ATT method)

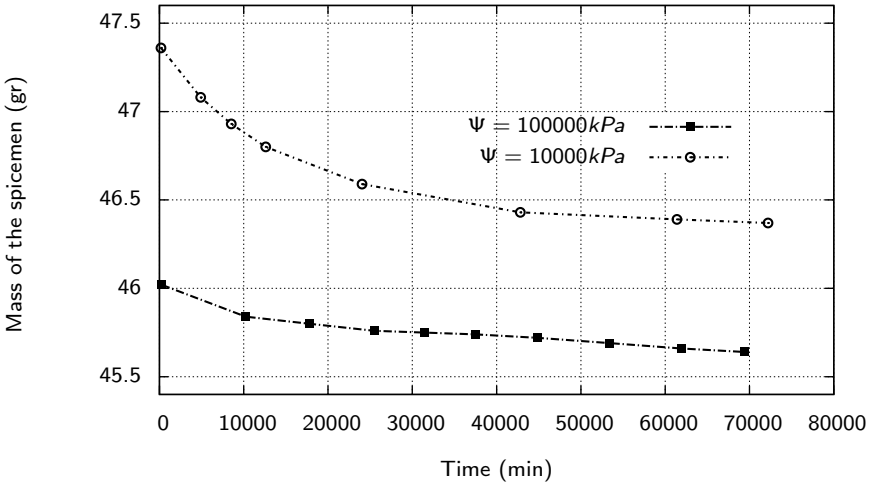

Figure 4.2.: Measured mass of 70/30 sand-kaolin mixture due to applied suction during drying path using vapour equilibrium technique

For all materials the experiments of the soil water characteristic curve on main drying and wetting paths are shown in Figures 4.3 to 4.6 in the form of degrees of saturation versus matric suction. The experimental data related to the scanning drying path for two sand-kaolin mixtures are included in Figures 4.4 and 4.5.
Matric suction of the samples on the scanning-drying path were measured after triaxial testing using the chilled mirror technique for samples with low water content.

To determine the matric suction of samples at initial state (compacted with optimum water content), several samples with initial state conditions were subjected to different matric suctions and the weight of the samples were measured periodically. The applied matric suction to the sample with minimum changes in weight (no drainage or imbibition) was defined as the matric suction related to the initial state.

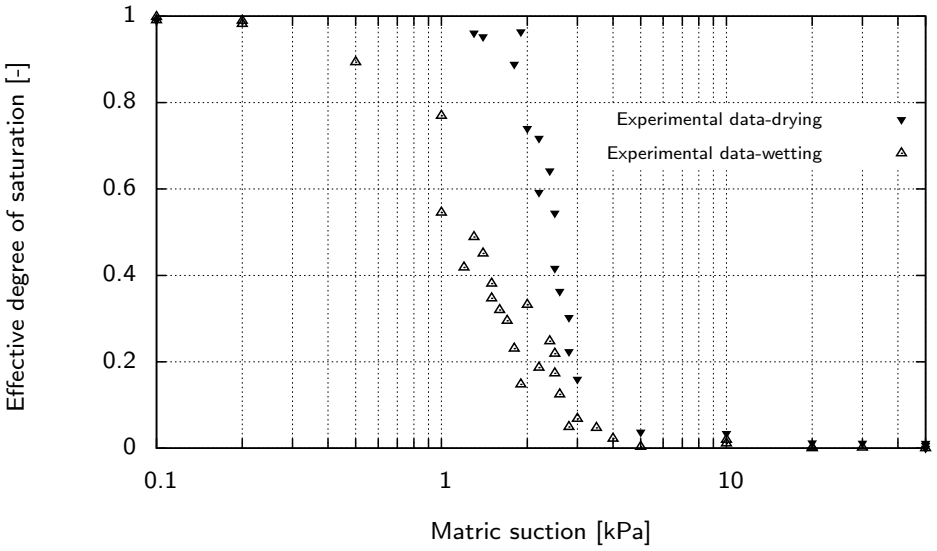

Figure 4.3.: Experimental results of drying and wetting paths for pure sand (Lins 2009)

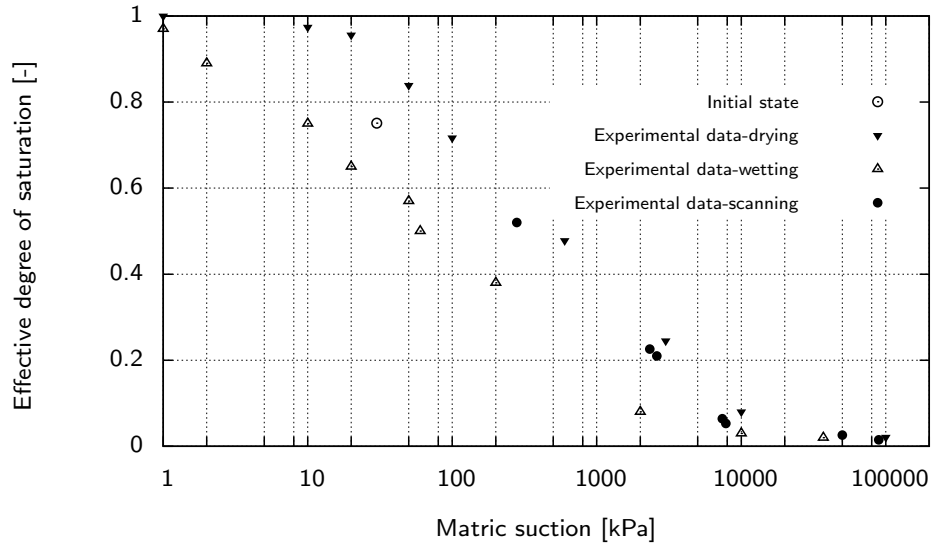

Figure 4.4.: Experimental results of drying, wetting and scanning paths for sand/kaolin (30/70)

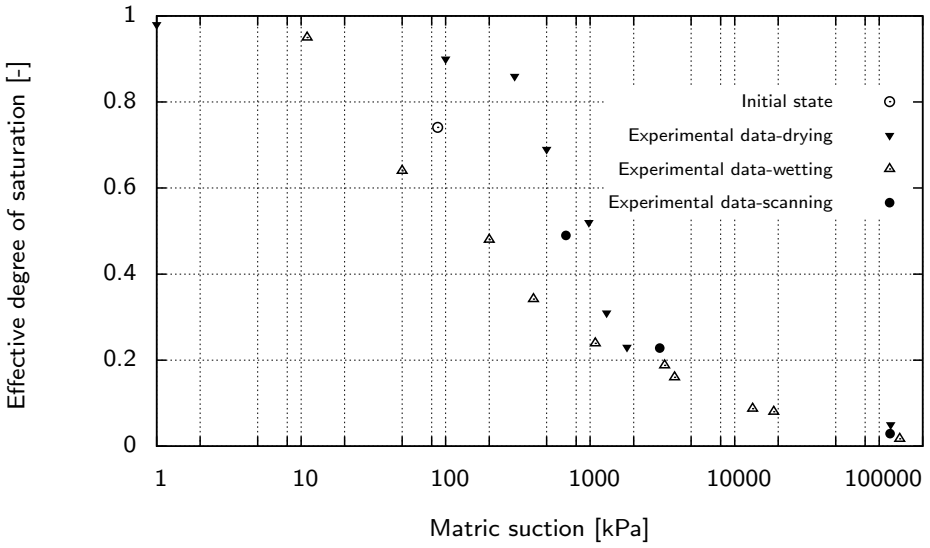

Figure 4.5.: Experimental results of drying, wetting and scanning paths for sand/kaolin (50/50)

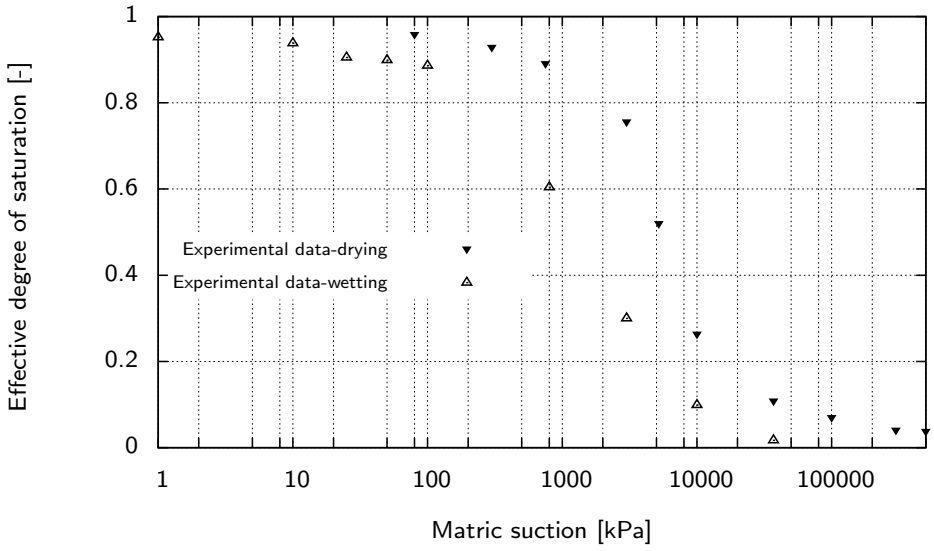

Figure 4.6.: Experimental results of drying and wetting paths for pure kaolin (Alabdullah 2010)

4.3. Results of direct tensile tests

Strain-stress curves obtained from the direct tensile tests of two sand-kaolin mixtures (70/30) and (50/50) are shown in Figures 4.7 to 4.11. These curves were the result of strain measurement by applying a strain rate of 0.002 $\%min^{-1}$ until sample failure. The corresponding tensile force was measured by a load cell. The maximum measured tensile force was used to define the tensile strength of the sample.
Generally, the strain-stress curves show a relatively linear behavior. A detailed discussion on the effect of soil type on the strain-stress characteristics is provided in chapter 5.

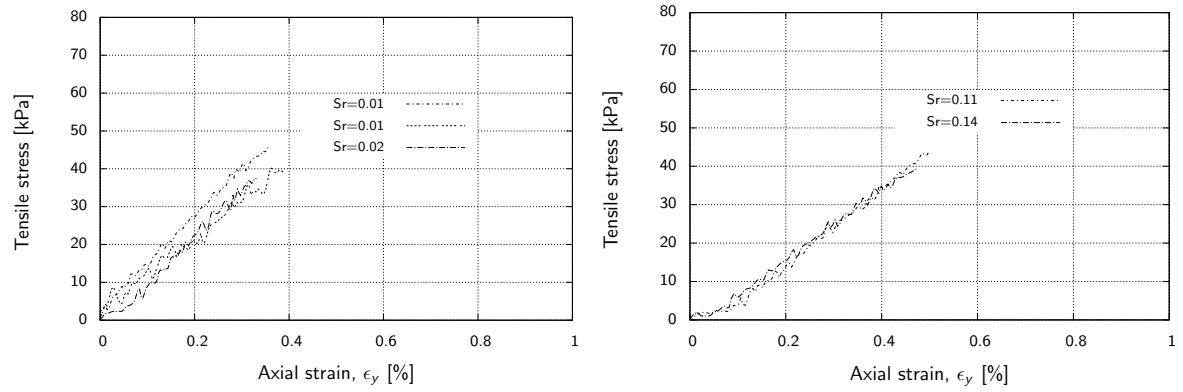

Figure 4.7.: Strain-stress characteristic curves of direct tensile test, for mixture of sand/kaolin (70/30); saturation≈0 and 0.1

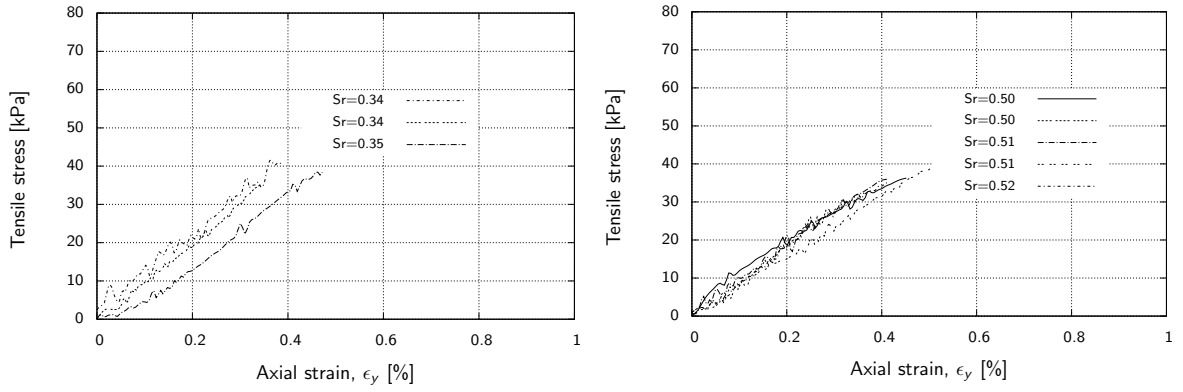

Figure 4.8.: Strain-stress characteristic curves of direct tensile test, for mixture of sand/kaolin (70/30); saturation≈ 0.3 and 0.5

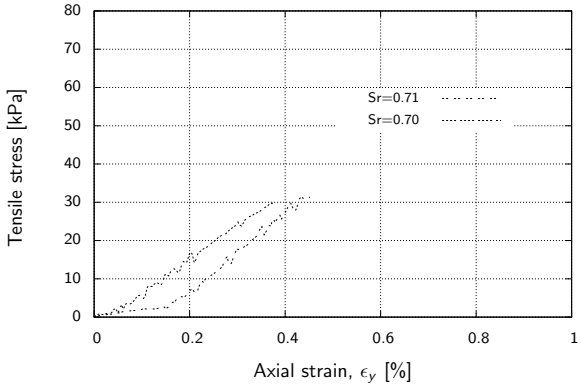

Figure 4.9.: Strain-stress characteristic curves of direct tensile test, for mixture of sand/kaolin (70/30); saturation≈ 0.7

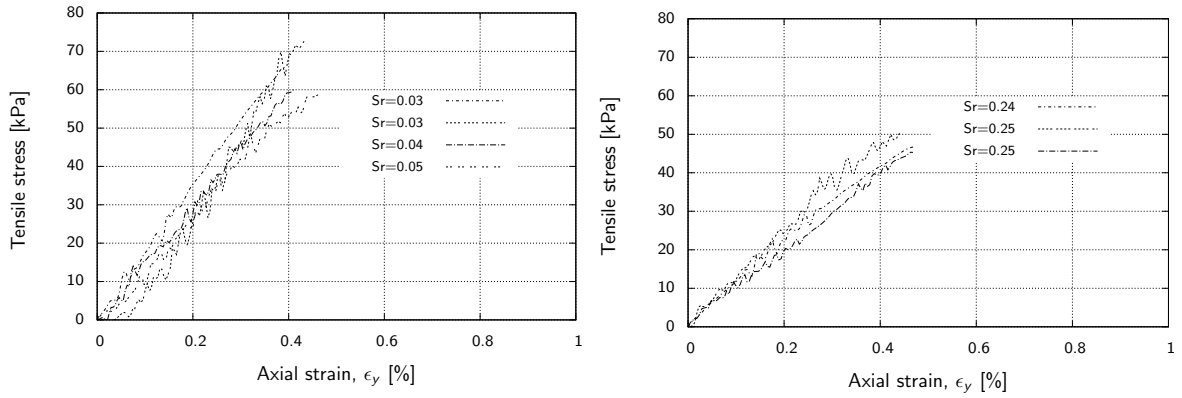

Figure 4.10.: Strain-stress characteristic curves of direct tensile test, for mixture of sand/kaolin (50/50); saturation≈ 0 and 0.25

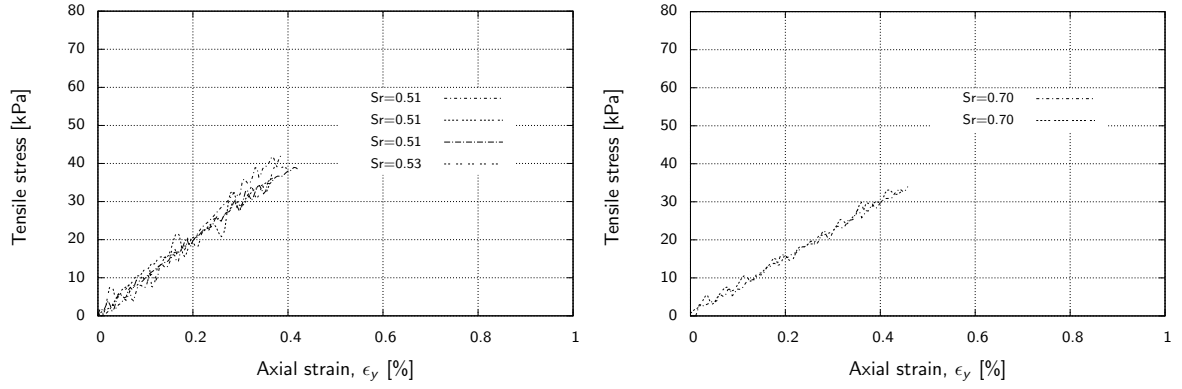

Figure 4.11.: Strain-stress characteristic curves of direct tensile test, for mixture of sand/kaolin (50/50); saturation≈ 0.5 and 0.7

4.4. Results of triaxial and biaxial tests

In this section the results of biaxial shear test on pure sand (Alabdullah 2010), triaxial tests on two mixtures of sand-kaolin (70/30 and 50/50) and triaxial tests for pure kaolin (Brueggemann 1998) are presented.
The axial strain (ϵ_y) are defined using the following equation:

$$\epsilon_y = \frac{\Delta h}{h_0} \tag{4.1}$$

Where Ψ is matric suction of sample, h_0 is initial height of the specimen, Δh is change in height.
The deviator stress σ_d (q) is defined by the following equation:

$$\sigma_d = q = \frac{\sigma_1 - \sigma_3}{2} \tag{4.2}$$

Figures 4.12 to 4.23 show deviator stress (σ_d) versus axial strain (ϵ_y) with different cell confining pressures (σ_3). The biaxial tests (Alabdullah 2010) on pure sand were performed under suction control. Five series of tests were performed on pure sand in dry and saturated conditions, and suction values of 2, 4 and 8 kPa.
Five series of triaxial tests were performed on each mixture of sand-kaolin (70/30) and (50/50) with degrees of saturation 0, 30, 50, 70, and 1. Each series was subjected to three different confining pressures equal to 25, 50, 100 kPa and 0, 50, 100 kPa respectively.
The triaxial results by Brueggemann (1998) included five series of tests that were performed on pure kaolin with degrees of saturation around 30, 50, 70, 90, and 100%. Each series consisted of three single tests with confining pressures of 50, 100, and 200 kPa.
For saturated soils the volume change of the soil specimens can be achieved by measuring the volume of the water expelled from the soil specimen. Because in partially saturated soils it is not possible to measure the volume of water expelled from the sample, therefore, volume change measurement becomes challenging for partially saturated soils. The volume change of the partially saturated sample is measured by monitoring the flow of cell water into or out of the triaxial cell by using a double-walled cell technique (section 7.4.3). Since, the triaxial cell device was not equipped by double-walled system in order to avoid any misinterpretation the volume change of the samples was not measured.

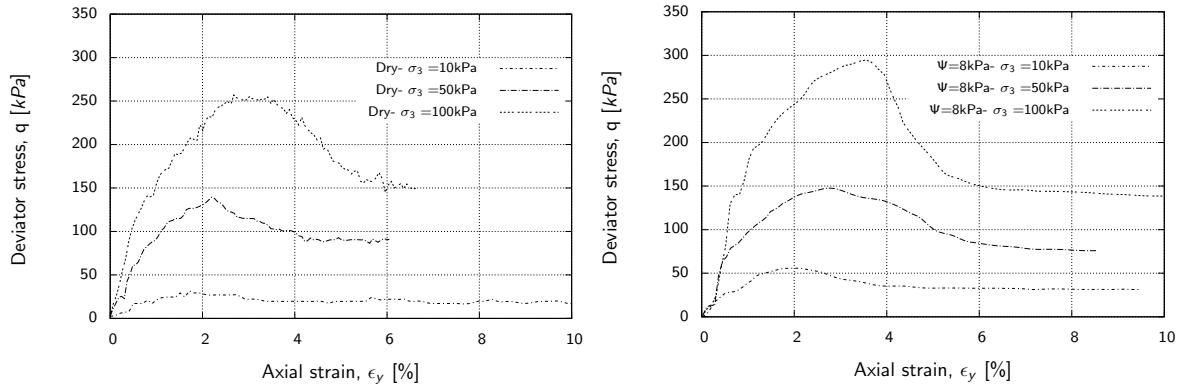

Figure 4.12.: q vs. ϵ_y, for pure sand; dry and Ψ= 8 kPa

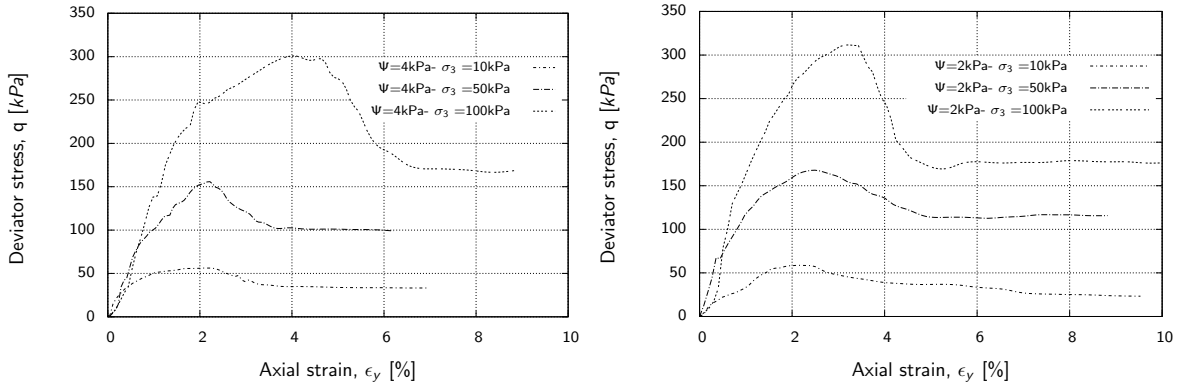

Figure 4.13.: q vs. ϵ_y, for pure sand; Ψ= 4 kPa and 2 kPa

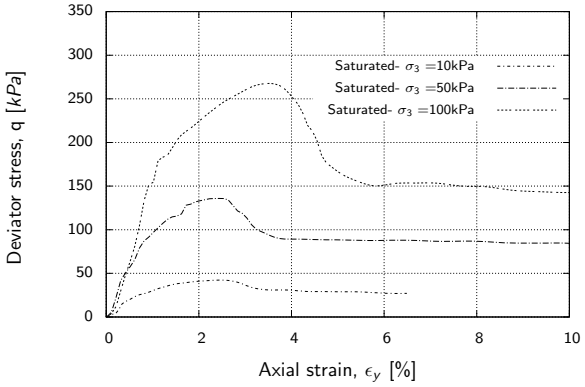

Figure 4.14.: q vs. ϵ_y, for pure sand; saturated

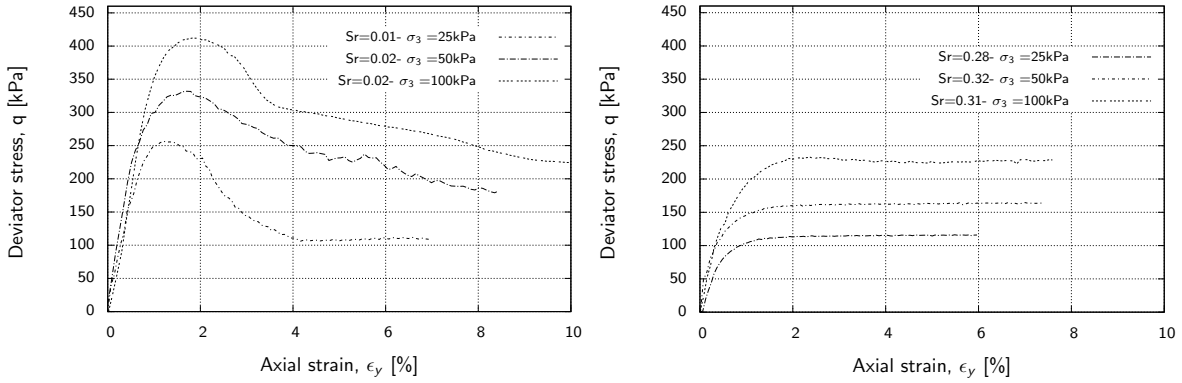

Figure 4.15.: q vs. ϵ_y, for mixture of sand/kaolin (70/30); saturation≈ 0.0 and 0.3

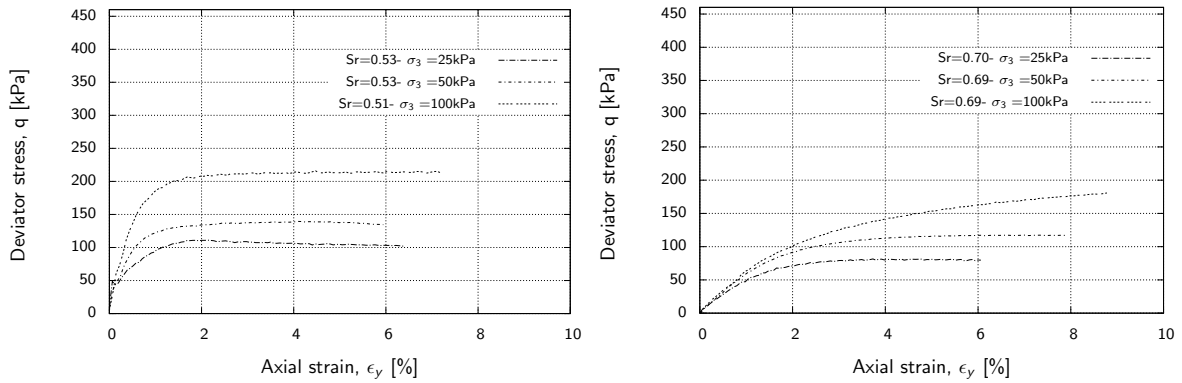

Figure 4.16.: q vs. ϵ_y, for mixture of sand/kaolin (70/30); saturation≈ 0.5 and 0.7

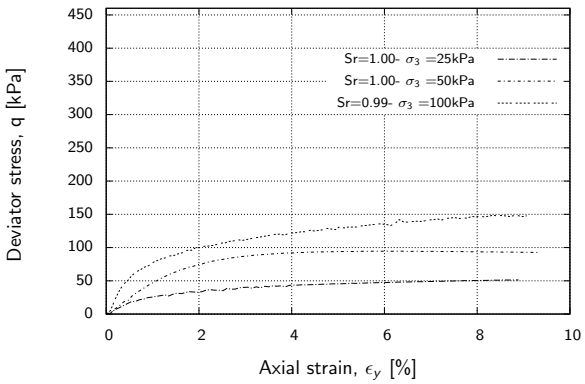

Figure 4.17.: q vs. ϵ_y, for mixture of sand/kaolin (70/30); saturation≈ 1.0

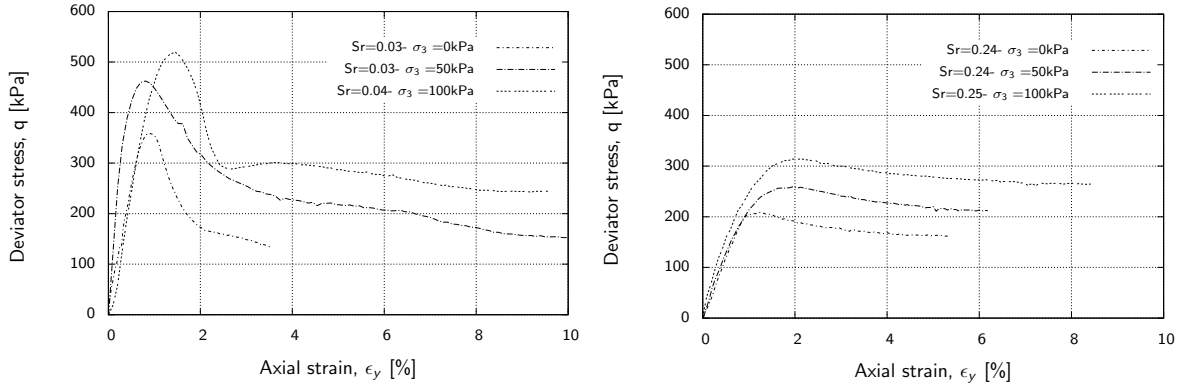

Figure 4.18.: q vs. ϵ_y, for mixture of sand/kaolin (50/50); saturation$\approx$ 0.0 and 0.25

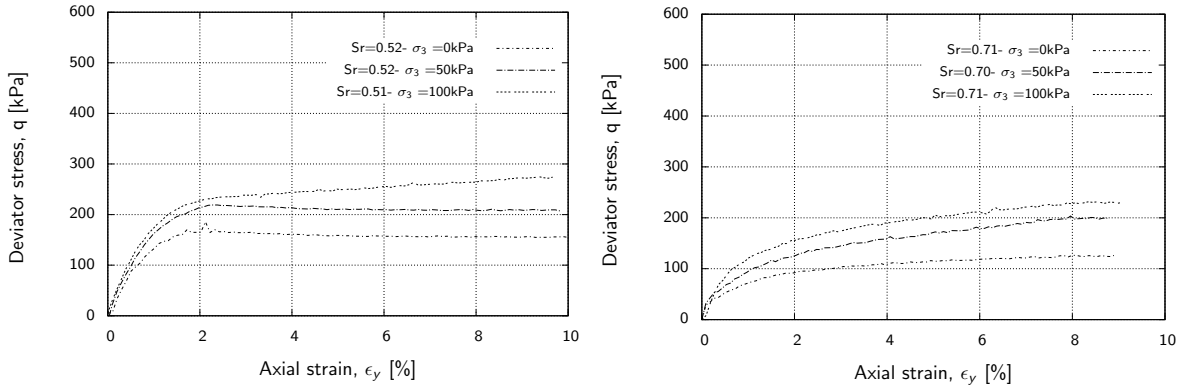

Figure 4.19.: q vs. ϵ_y, for mixture of sand/kaolin (50/50); saturation$\approx$ 0.5 and 0.7

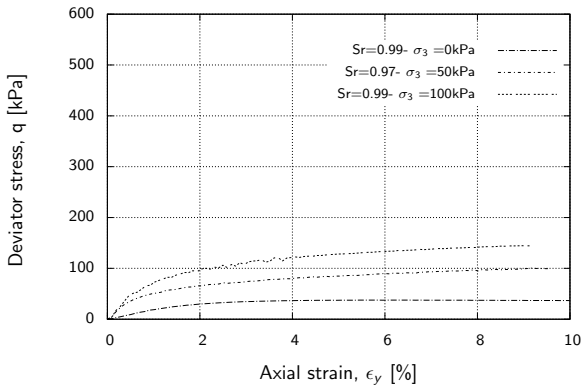

Figure 4.20.: q vs. ϵ_y, for mixture of sand/kaolin (50/50); saturation$\approx$ 1.0

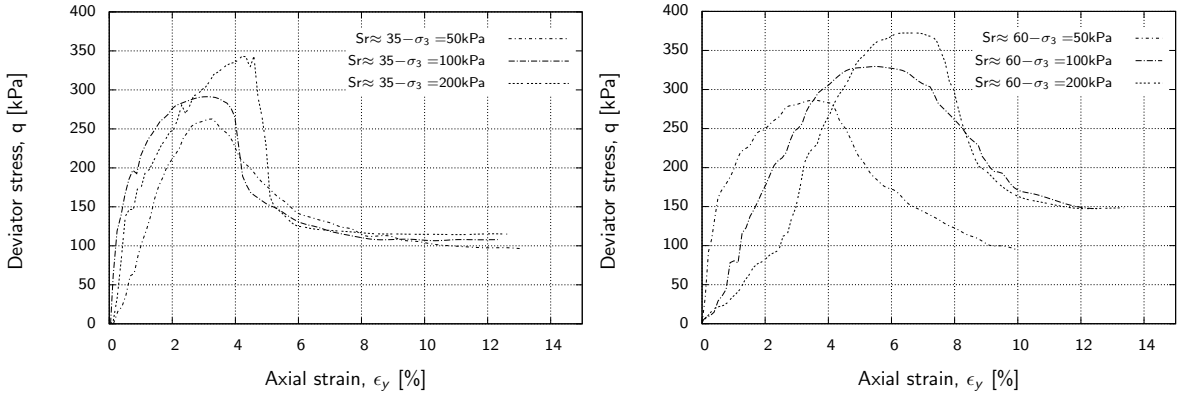

Figure 4.21.: q vs. ϵ_y, for pure kaolin; saturation≈ 0.35 and 0.6

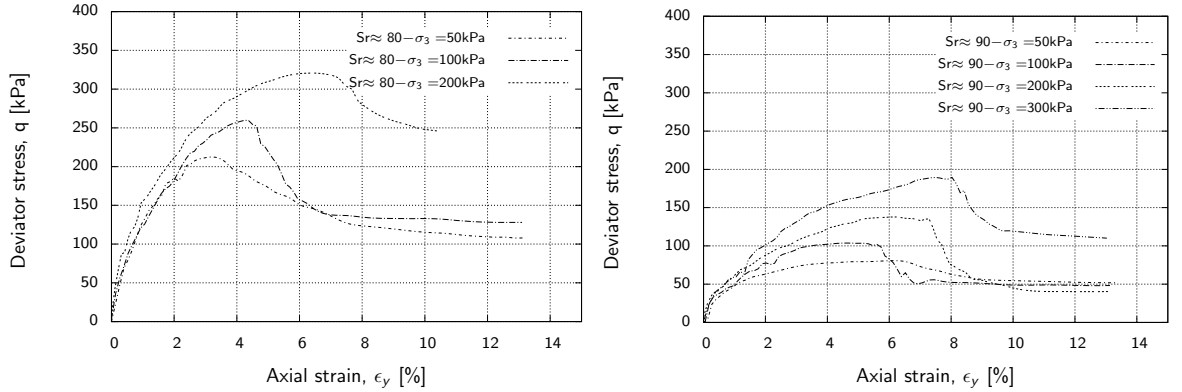

Figure 4.22.: q vs. ϵ_y, for pure kaolin; saturation≈ 0.8 and 0.9

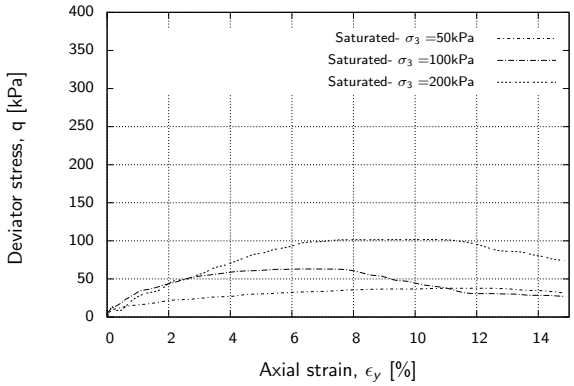

Figure 4.23.: q vs. ϵ_y, for pure kaolin; saturation≈ 1.0

4.4.1. Observation of failure zone in tested samples

Figure 4.24 shows the shear failure modes of the samples with 70/30 sand-kaolin at different degrees of saturation. The failure for relatively dry samples (Sr=0.00 and 0.30) differs from the failure of the saturated and relatively wet samples.
As explained in chapter 3 after the tests, the partially saturated soil samples were cut into three slices of equal thickness and the water content of each slice was measured. Meanwhile, for a number of samples the void ratio of the slices was determined using the paraffin wax method. Although no significant change in gravimetric water content was observed but the void ratio and therefore the degree of saturation in middle part around the shear zone changed extremely. After triaxial testing the matric suction for samples with low water content was measured using chilled mirror technique. In addition the changes in void ratio and degree of saturation measured in the middle part of the sample close to the shear zone as well as the matric suction derived from the measured degree of saturation and the SWCC (scannig curve) determined, are illustrated in Figures 4.25.
The mechanical loading during shearing leads to displacement of particles and distortion of phases. As a result although considerable changes in void ratio and furthermore in degrees of saturation are observed but no significant changes in gravimetric water content and matric suction (by chilled mirror) are indicated in the shear zone (Figures 4.25).

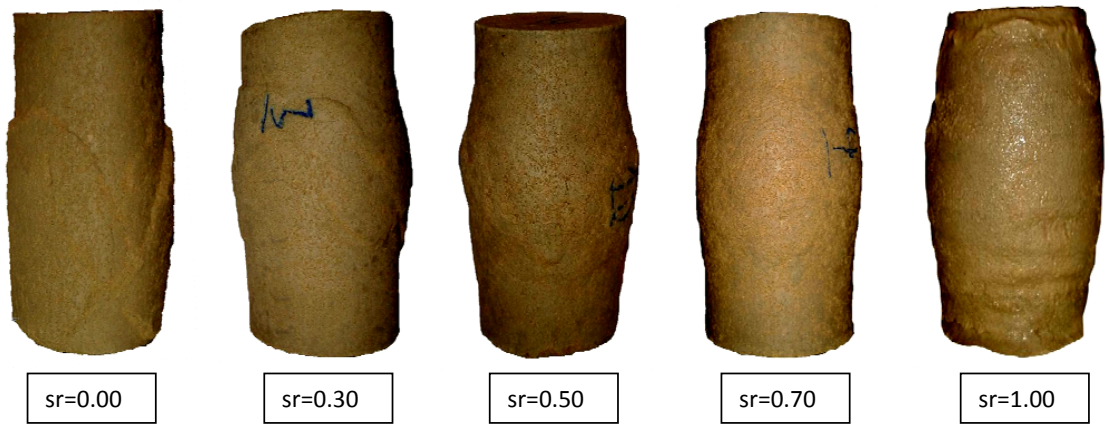

Figure 4.24.: Failure mode under deviatoric loading at different degrees of saturation for 70/30 sand-kaolin mixture

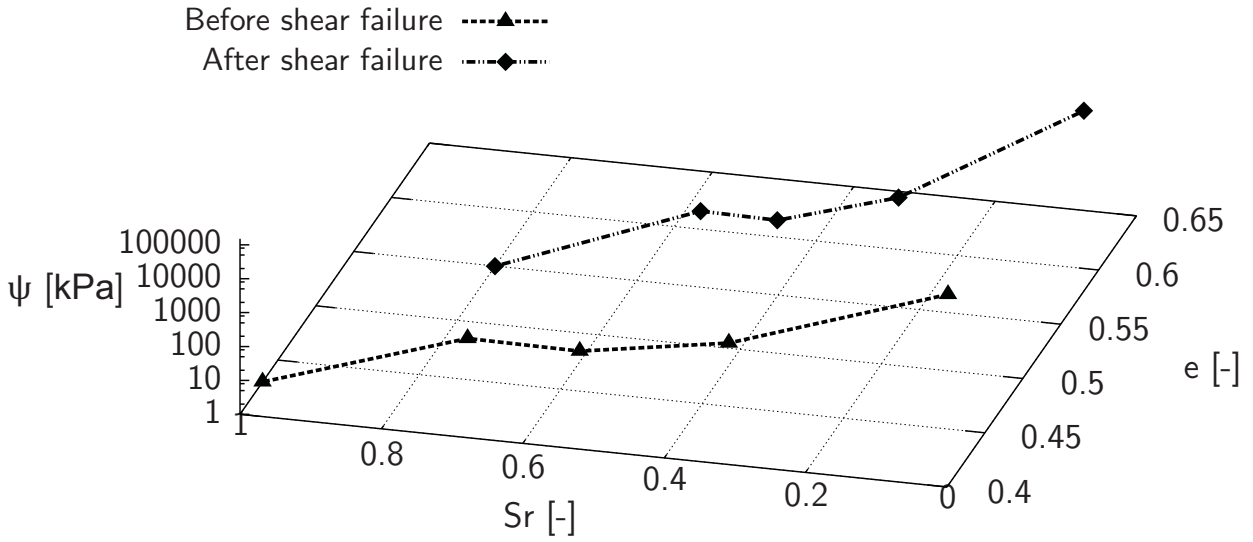

(a)

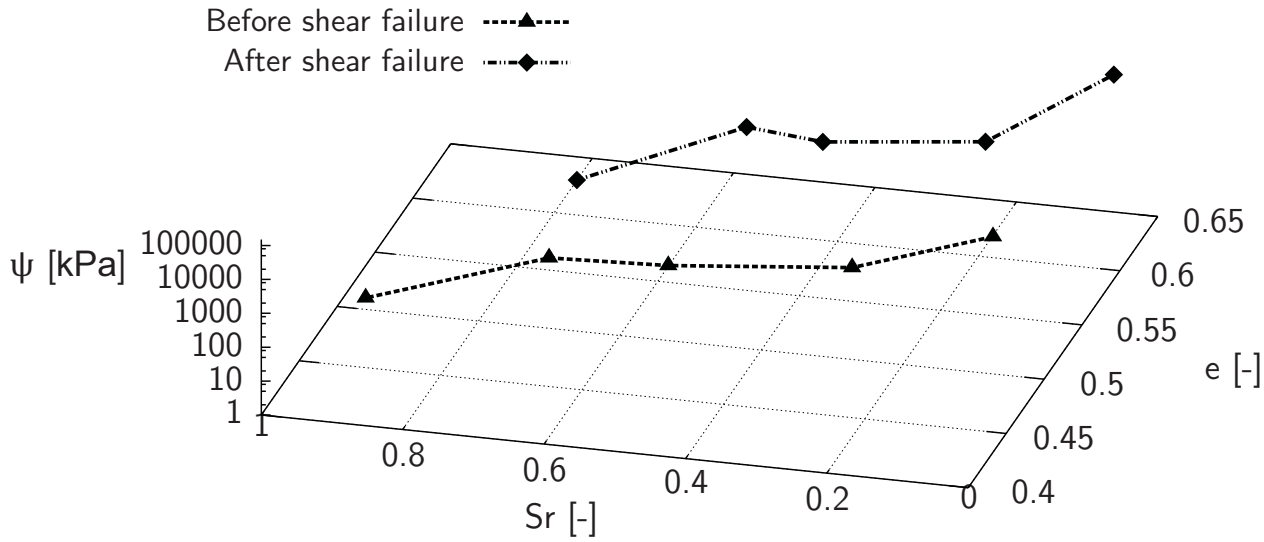

(b)

Figure 4.25.: 3D plots of the triaxial test results related to the shear failure zone for (a) 70/30 and (b) 50/50 in terms of matric suction (Ψ)−degree of saturation (Sr) −void ratio (e); before shear failure and after the shear failure

4.5. ESEM image

In this study the ESEM method is used to investigate the microstructure of the samples for two mixtures of the sand-kaolin (70/30 and 50/50) at three different states (see section 3.8.1).
The ESEM photos were selected from a range of micrographs taken to study the influence of the fine content of kaolin (with 30% and 50%).
Meanwhile, the observation was setup to study soil structure at three different degrees of saturation; in initial state and along the main drying path in saturated, and air dried condition.

4.5.1. Effect of fine content

Assessments of the ESEM micrographs at various contents of kaolin indicate that the configuration of clay particles could occur in one or a combination of "bridging sand particles", "coating or partially coating of the sand particles" and "aggregations of clay in form of cluster" (Montanes 2002) (Fig. 4.26).

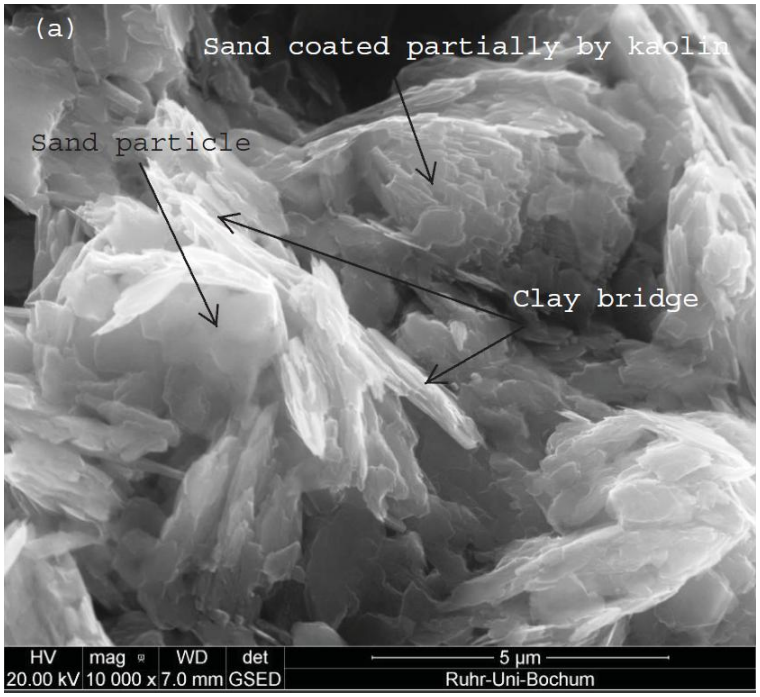

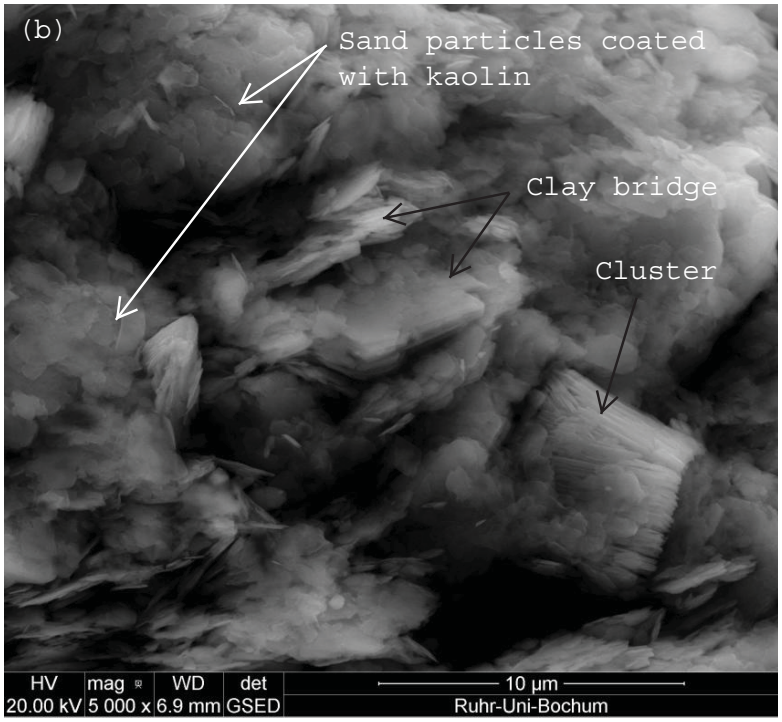

Figure 4.26.: ESEM image of the sand-kaolin particles arrangements in forms of (a) partial coating of sand grains and clay bridging (70-30 sand-kaolin mixture) (b) coating of sand grains and clay cluster (50-50 sand-kaolin mixture)

ESEM micrographs are shown in Figure 4.27 in initial states at different magnifications for two mixtures of sand-kaolin (30-70 and 50-50). These figures were selected to study the influence of kaolin content on soil structure.
In Figure 4.27-a for samples with 30% sand particle bonds are made of clay (i.e clay bridge). For samples with 50% kaolin (Figure 4.27-b) the coating of the sand particle is more effective and the sand particles coating is almost complete. It can be seen as the kaolin content increases for 50-50 sand-kaolin mixture the soil structure is composed by number of clusters.

4.5.2. Effect of wetting and drying

Before wetting, the soil structure in initial state is densely packed and the sand grains are partially or completely coated by the kaolin. After wetting the samples from initial state (Fig. 4.28-2) to saturated state (Fig. 4.28-1) the porosities among the particles become larger and the overall volume of the mixtures are increasing.

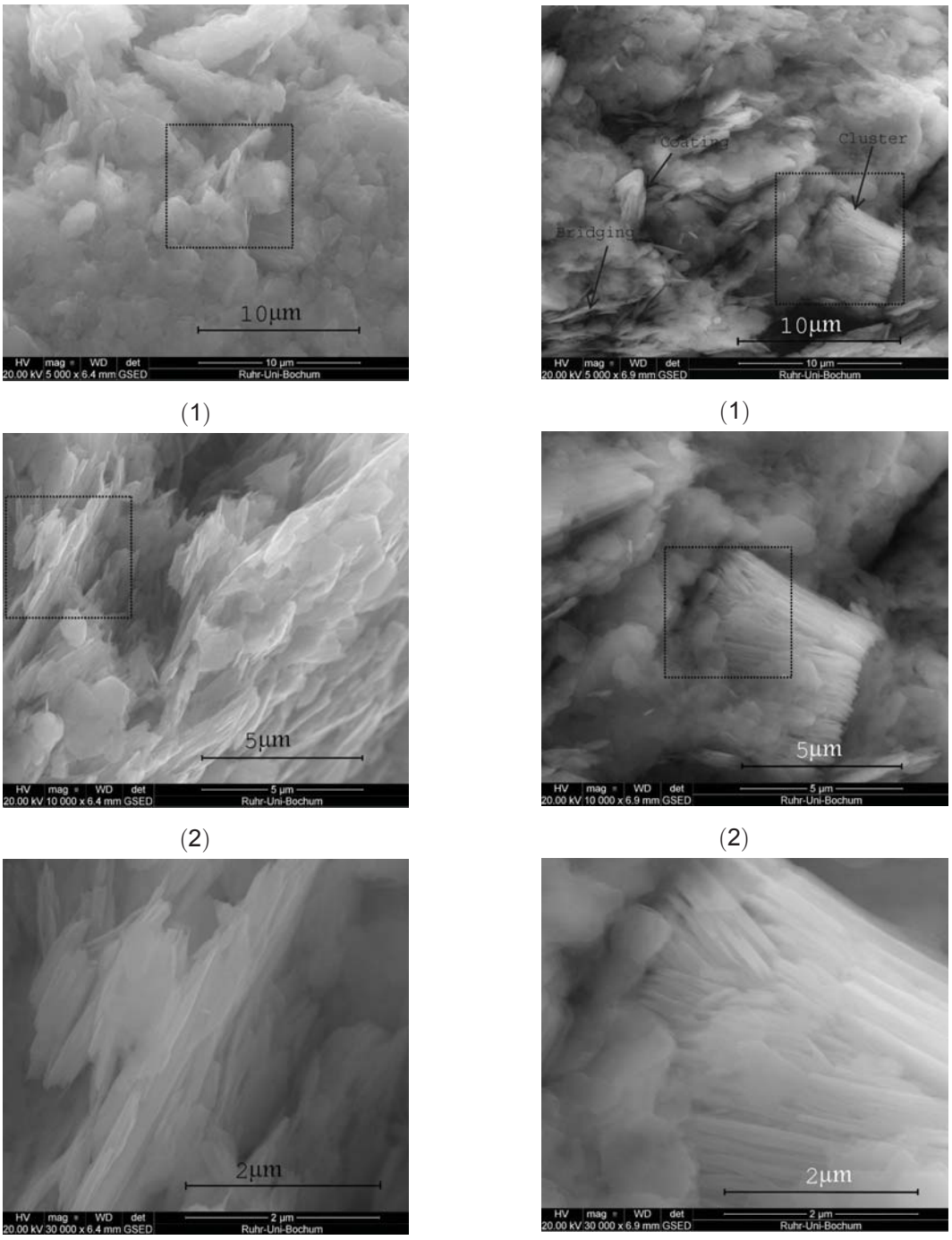

(1) (1)

(2) (2)

(3) (3)

(a) (b)

Figure 4.27.: ESEM image of the sand-kaolin mixture (a) (70-30) and (b) (50-50) in initial state at different magnification (1) 5000X, (2) 10000X and (3) 30000X

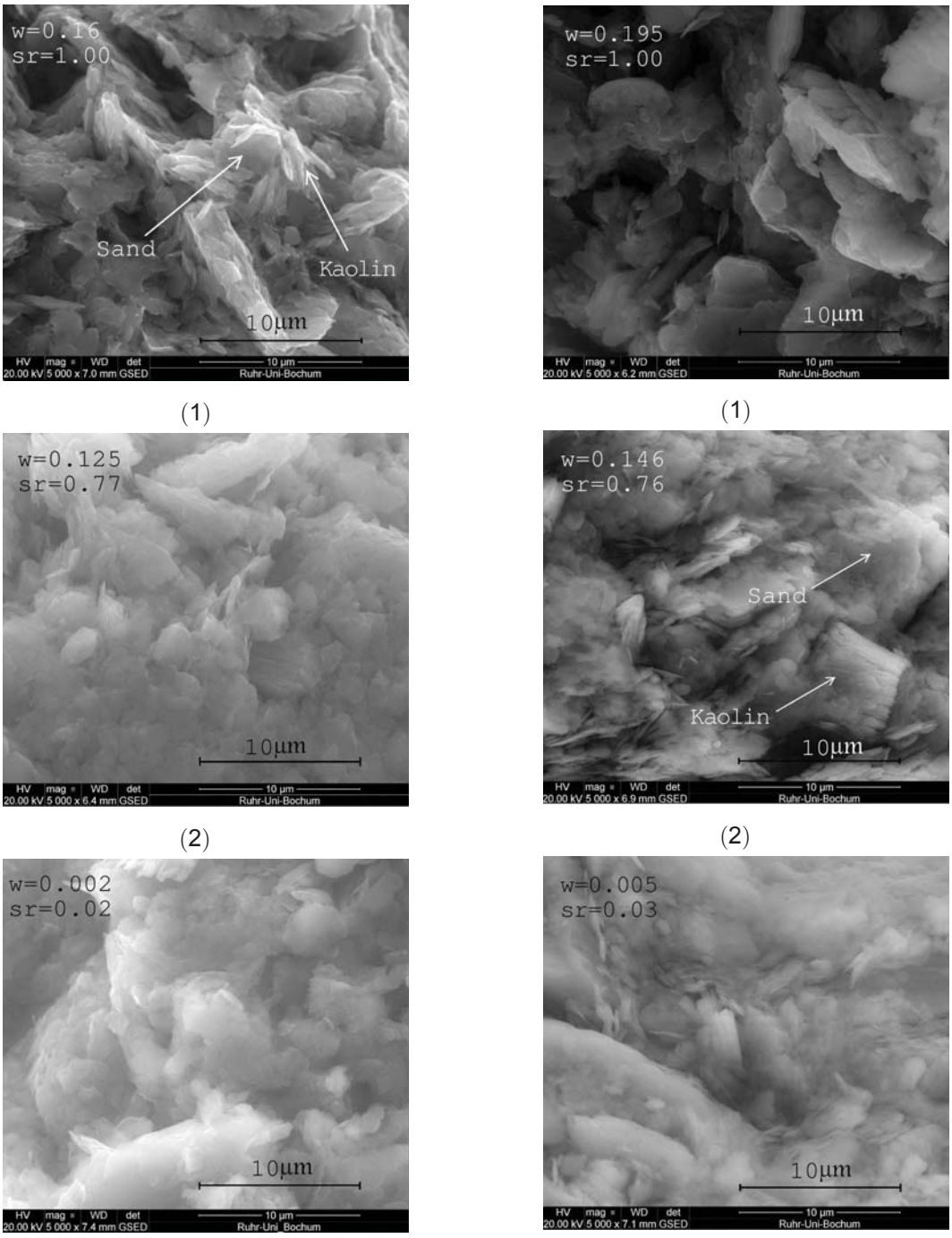

Figure 4.28.: ESEM image of the sand-kaolin mixture (a) (70-30) and (b) (50-50) at different degrees of saturation (1) saturated, (2) initial state and (3) air-dry

After sample preparation in initial state conditions and wetting to saturated condition, samples were air dried along the main drying path. For both mixtures it can be seen in Figures 4.28-3 that by drying the samples from saturated conditions on the main drying path and reaching to air-dry condition, the pore spaces become smaller. However, for the samples in the initial state and air-dried condition no significant changes in pore spaces can be seen. As the soil dries, the aggregates are packed more tightly.
The main limitations for this technique were as follows:

- Because of the granular nature of the soil, it is very difficult to avoid disturbance and protect the original structure of the specimen during sampling.
- The soil sample is not homogeneous and the observation depends on the zone of the sample that is being selected. Therefore, the interpretation of the images is very intuitive and the results may not be representative of the whole sample.
- If the specimen contains relatively large particles, visual spaces are mostly occupied by these particles. Due to the ratio of particle to specimen size it is difficult to observe the soil structure.

4.6. Pore size distribution

In order to study the pore size distribution of soil using the MIP method, samples at four different states were selected (Figure 3.15).

4.6.1. Microstructure investigation by MIP test

Figures 4.29, 4.30 and 4.31 show the pore size distribution of the compacted samples for two mixtures of 70/30 and 50/50 sand−kaolin at four different states.

The pore size distributions are presented in terms of differential and cumulative volumes in semi−logarithmic graphs in Figures 4.29 and 4.30. Volumes of intruded mercury between entrance diameters of 0.01 to 0.1 μm, 0.1 to 1 μm and 1 to 10 μm are also shown in Figure 4.31 for both mixtures.
In this study, a pore size larger than 1 μm refers to inter-aggregate pores, pores around 0.1 to 1 μm as intra-aggregate pores, and pores with radiuses smaller than 0.1 μm as inter-layer pores (Thom et al. 2007, Likos & Wayllace 2010, Monroy et al. 2010).
In Figure 4.29, for initial states (SD30-1, SD50-1) the MIP results clearly display bimodal

pore size distribution.
Two dominate pore groups can be observed, with entrance radius grouped around 2.5 μm and 0.1 μm for 70/30 and 5 μm and 0.08 μm for 50/50 sand-kaolin mixtures.
By wetting the samples from initial state to saturated (MD30-1, MD50-1) the double pore size distribution is no longer observed and the microstructure is dominated by pore sizes corresponding to an entrance radius of around 0.1 μm for both mixtures.
Dewatering the samples and reaching air-dry conditions from a saturated state on the main drying path (MD30-5, MD50-5) and from an initial state on the scanning drying path (SD30-5, SD50-5) leads to changes in the microstructure from a single to the bimodal pore size distribution for both mixtures.
As shown in Figure 4.30, wetting of the samples from initial state to saturated conditions leads to an increase of cumulative pore volumes. By dewatering the samples from initial state (SD30-1 and SD50-1) to air-dry conditions (SD30-5 and SD50-5) on a scanning drying path, a small reduction in cumulative pore volume is detected. Meanwhile, for samples dried from saturated conditions (MD30-1 and MD50-1) to air dried conditions (MD30-5 and MD50-5) on a main drying path an extreme reduction in pore volume is observed.
As seen in Fig. 4.30 the cumulative pore volume for both mixtures in air-dry conditions on main and scanning drying paths are similar. Figure 4.31 shows that by wetting the samples from an initial state (SD30-1, SD50-1) to saturated conditions (MD30-1, MD50-1) the increment of the pore volume for intra-aggregates is larger than the inter-aggregate pores. By dewatering samples and reaching an air-dried condition via a main drying path (MD30-5 and MD50-5) and scanning drying path (SD30-5 and SD50-5), the main changes in pore volume can be observed for the pore size in the range of 0.1 to 1 μm.
Pore volumes of inter-aggregates for initial state and air-dry conditions in both the main and scanning drying paths are similar. For pore sizes 0.1 to 1 μm (intra-aggregate) a reduction in pore volume is still observed between the initial state and air-dry condition - this behavior is more pronounced for the 30/70 sand-kaolin mixture.
It is interesting to note that for pores with a radius smaller than 0.1 μm (inter-layer), for all states the pore volume remains relatively constant.

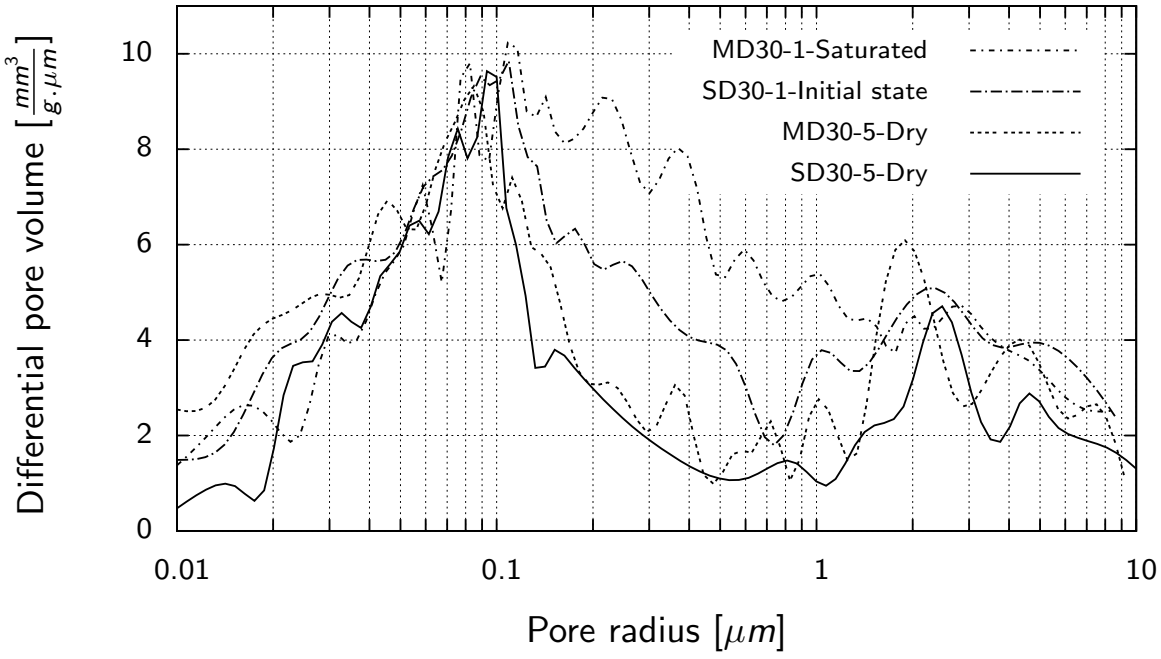

(a)

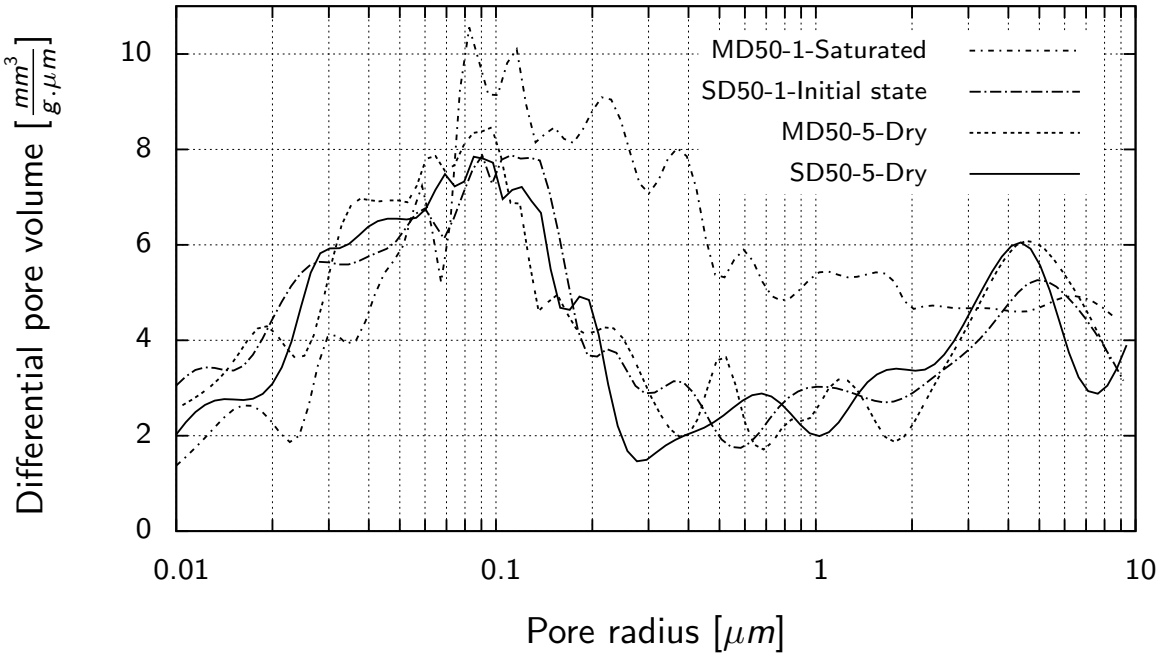

(b)

Figure 4.29.: Differential pore volume versus pore radius of the compacted samples for (a) 70/30 and (b) 50/50 sand−kaolin mixtures at different degrees of saturation (MD: Main drying path; SD: Scanning drying path)

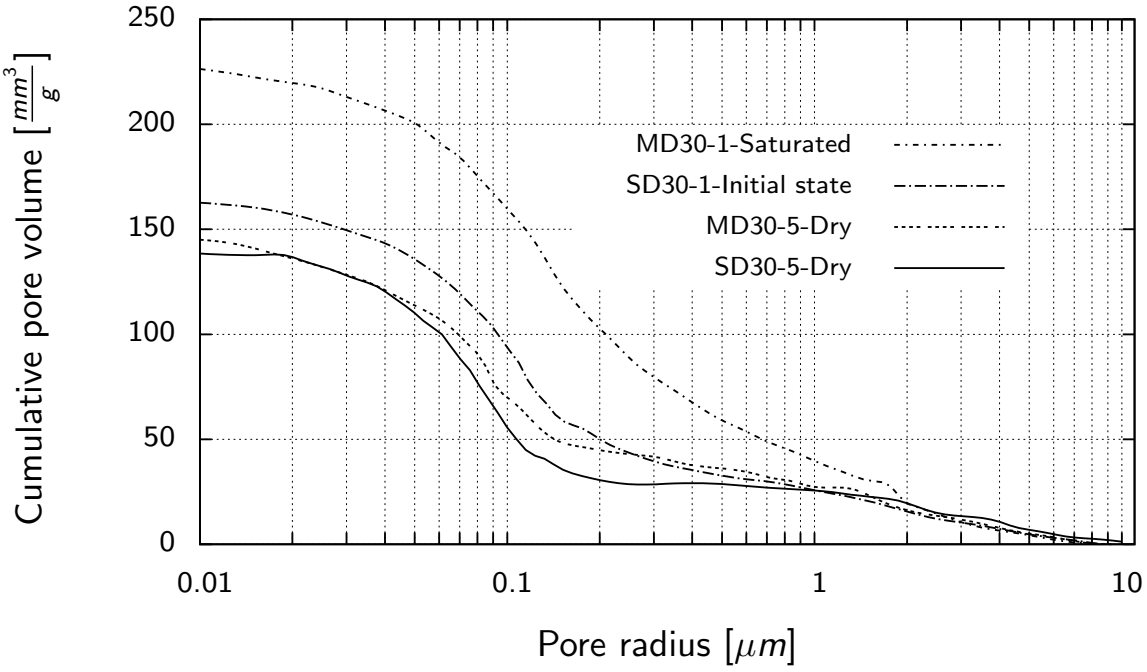

(a)

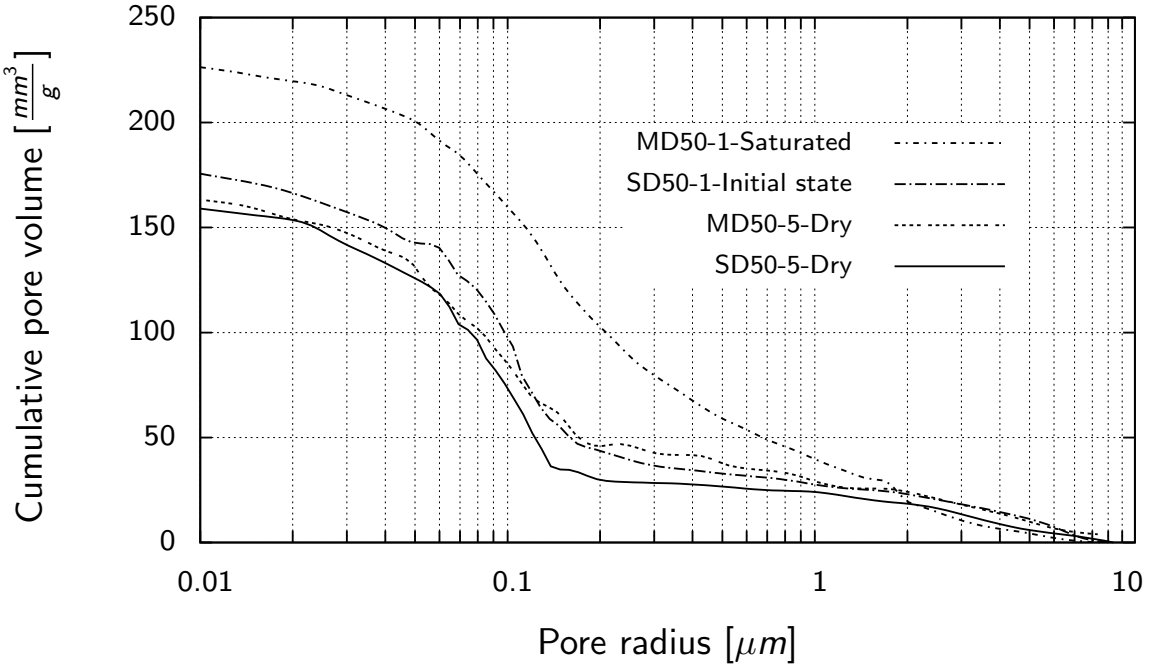

(b)

Figure 4.30.: Cumulative pore volume versus pore radius of the compacted samples for (a) 70/30 and (b) 50/50 sand−kaolin mixtures at different degrees of saturation (MD: Main drying path; SD: Scanning drying path)

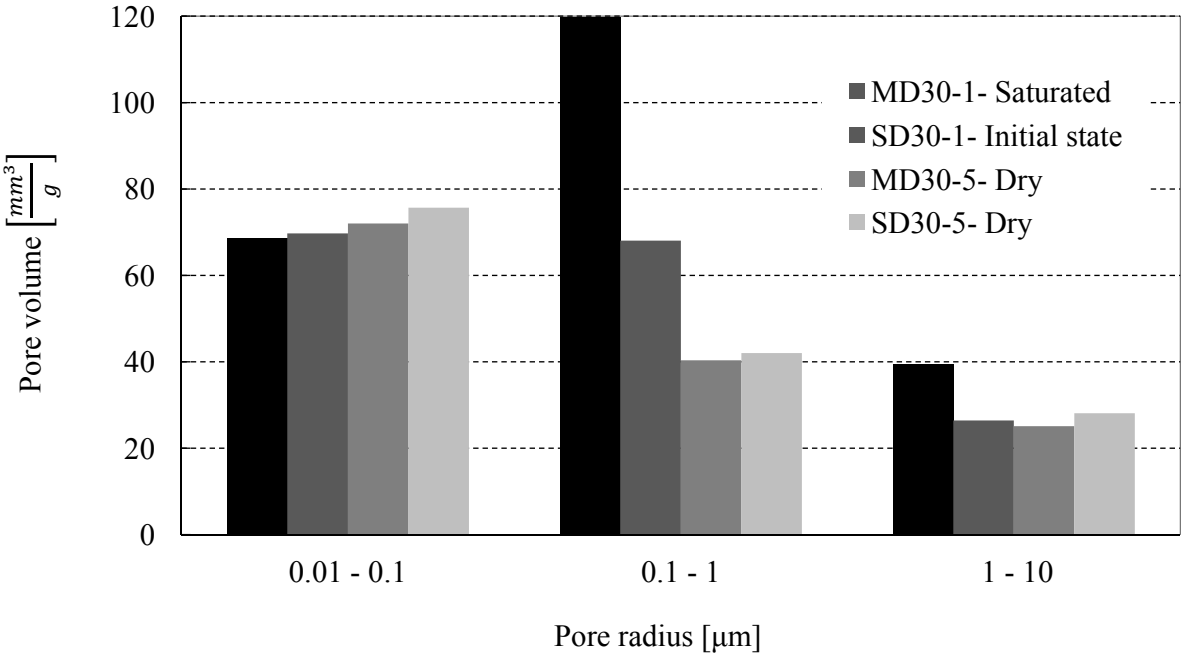

(a)

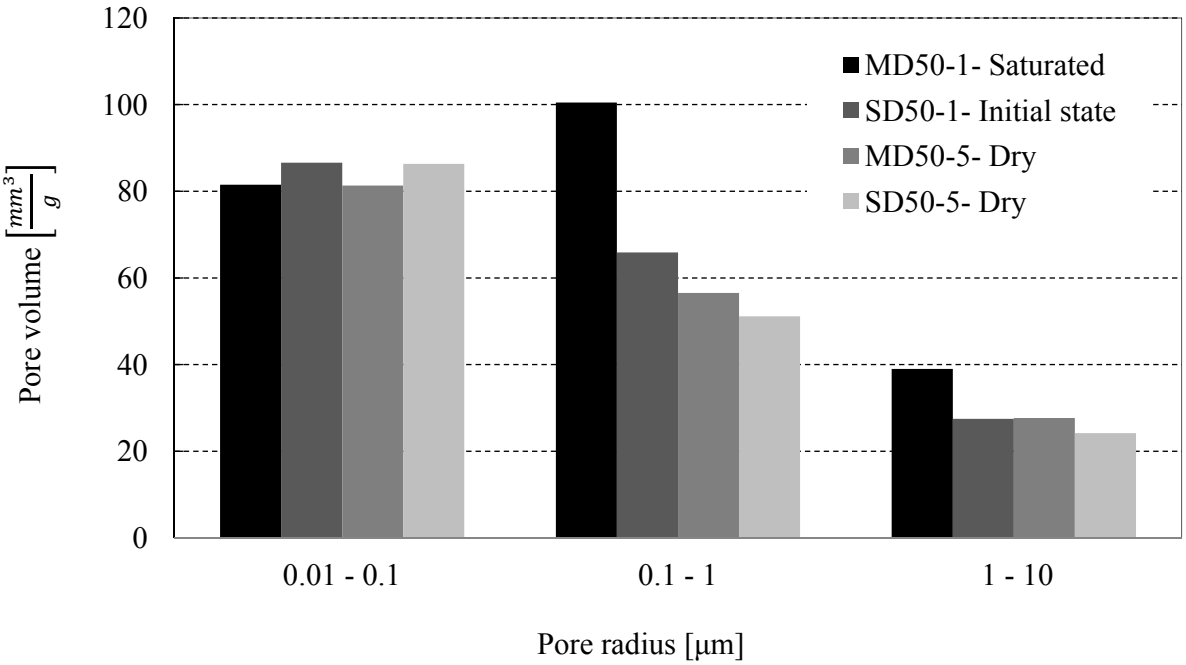

(b)

Figure 4.31.: Variation of the pore volumes of inter-layer, intra-aggregate and inter-aggregate pores at different degrees of saturation for (a) 70/30 and (b) 50/50 sand−kaolin mixtures (MD: Main drying path; SD: Scanning drying path)

Limitations of the MIP technique can be summarized as follows:

- Eq. 3.2 is based on a cylindrical pore model and is not applicable for materials containing pores with different shapes.
- Accessibility to internal pores is constrained by filling external pores. Due to the ink bottle effect, the volume of intruded mercury may be attributed to an incorrect pore size. As pressure is increased, mercury is forced through the pores into adjacent pores (of a larger size). The volume increment is assigned to the smaller pores (De Las Cuevas 1997).
- Due to the overall pressure or to areas of differential pressure within the sample, pores can collapse while measurements are being taken.
- Uncertainty about the values of surface tension and contact angle of mercury can leads to measurement errors (Romero 1999).

4.7. Summary

In this chapter, experimental results of SWCC tests, direct tensile tests and triaxial tests have been presented. Drying and wetting curves of SWCC for investigated soils have been shown. Direct tensile tests were performed on two mixtures of sand-kaolin. The tensile strength versus axial strain for used materials have been presented. Deviator stress versus axial strain has been illustrated for saturated conditions and different levels of saturation and suctions, as well as with three steps of confining pressure for pure sand, two mixtures of sand-kaolin (70/30, 50/50) and pure kaolin. In addition investigation on the microstructure of the sample has been done qualitatively and quantitatively by ESEM and MIP methods to study the influence of the water content variation on the soil structure and shortcoming of each method is discussed.
In chapter 5 by using the experimental results of SWCC, direct tensile and triaxialt test the suction stresses are determined for different types of soils and the failure envelopes are pltted in terms of effective stress by using the suction stresses corresponding to different methods.

5. Determination of suction stress

5.1. Strategy

The chapter describes determination of suction stress using different methods, i.e. the prediction of suction stress using the SWCC-curves and calculating suction stress as the product of suction and corresponding saturation (section 5.2), the determination of suction stress from direct tensile tests (section 5.3) as for as from triaxial tests (section 5.4). Samples were prepared according to the procedure described in section 3.3. Failure envelopes using suction stresses determined from tensile and triaxial test results are presented in section 5.5.

5.2. Prediction of suction stress from SWCC

In Figure 5.1 the SWCC for pure sand, two mixtures of sand-kaolin (70/30 and 50/50) and pure kaolin are illustrated. As shown, the SWCC of Hostun sand is within a narrow range of matric suction, whereas the SWCC of kaolin is within a wide range of matric suction and the SWCC of the two mixtures are between the curves of pure sand and pure kaolin.
The results show that by increasing in amount of the fine content the behavior of the mixtures start differing clearly from the behavior of the sand.
The pure sand (poorly graded soils) have steep soil-water characteristic curves, because the majority of pores are drained at a narrow range of soil suction and show a tendency to desaturate at a fast rate with increasing suction.
The results of SWCC, visual observations of ESEM method (Figs.4.27 and 4.28) and pore size distribution (Fig. 4.31) for 70/30 and 50/50 sand-kaolin mixtures, showed that the microstructure, saturation, and desaturation behavior of these two mixtures are close together. The two mixtures of sand-kaolin, due to having different sized pores, are drained over a wider range of soil suction values in comparison to pure sand.

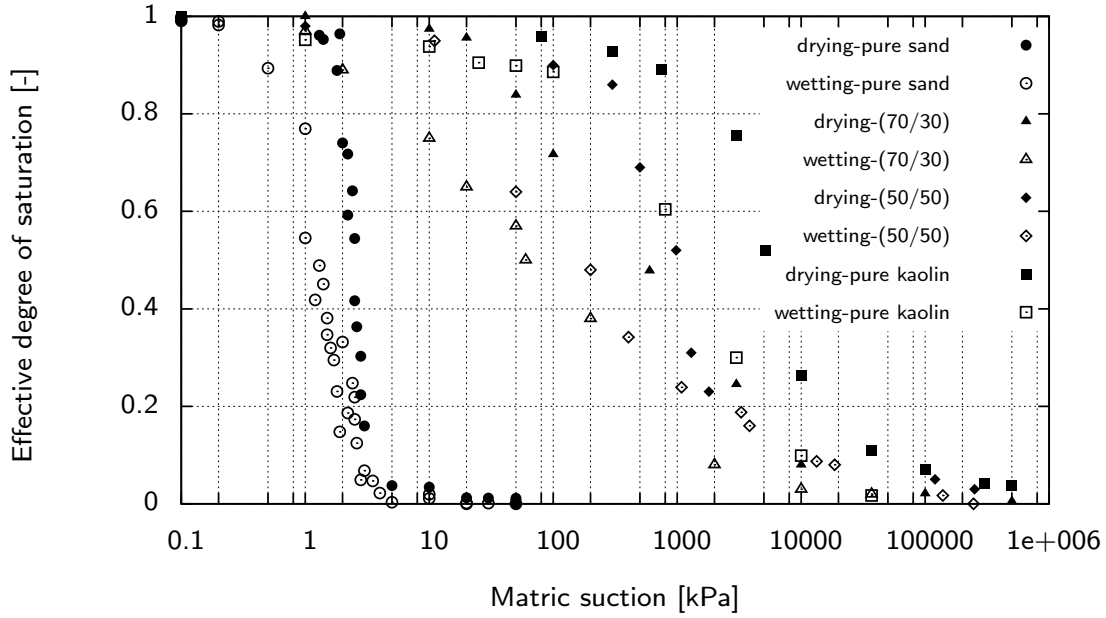

Figure 5.1.: Experimental data of the SWCCs for the materials used

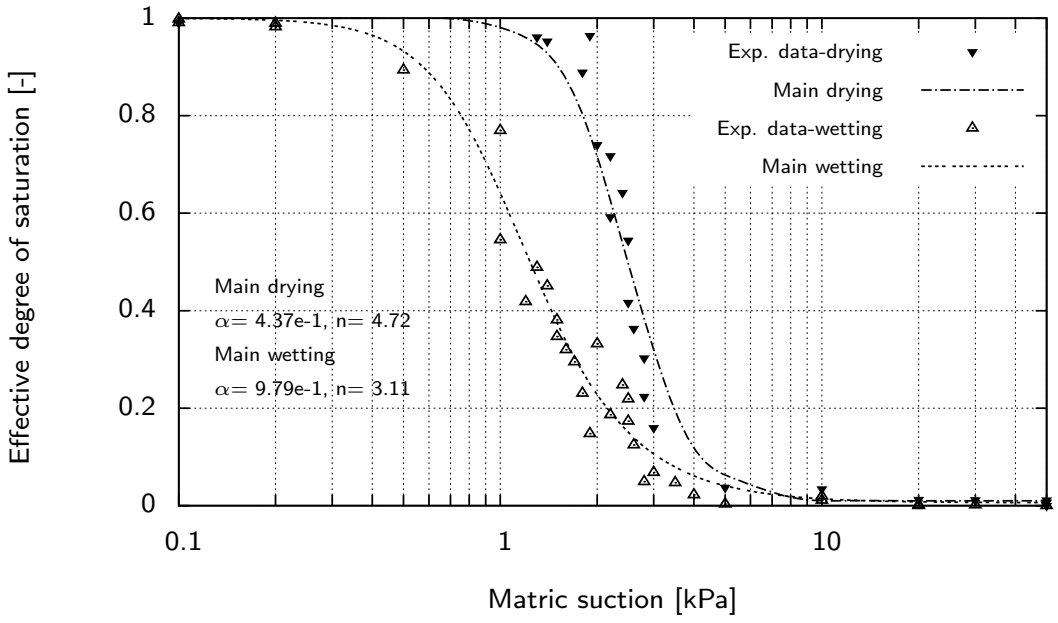

Figure 5.2.: Water retention curves - pure sand, main drying and wetting (Lins 2009)

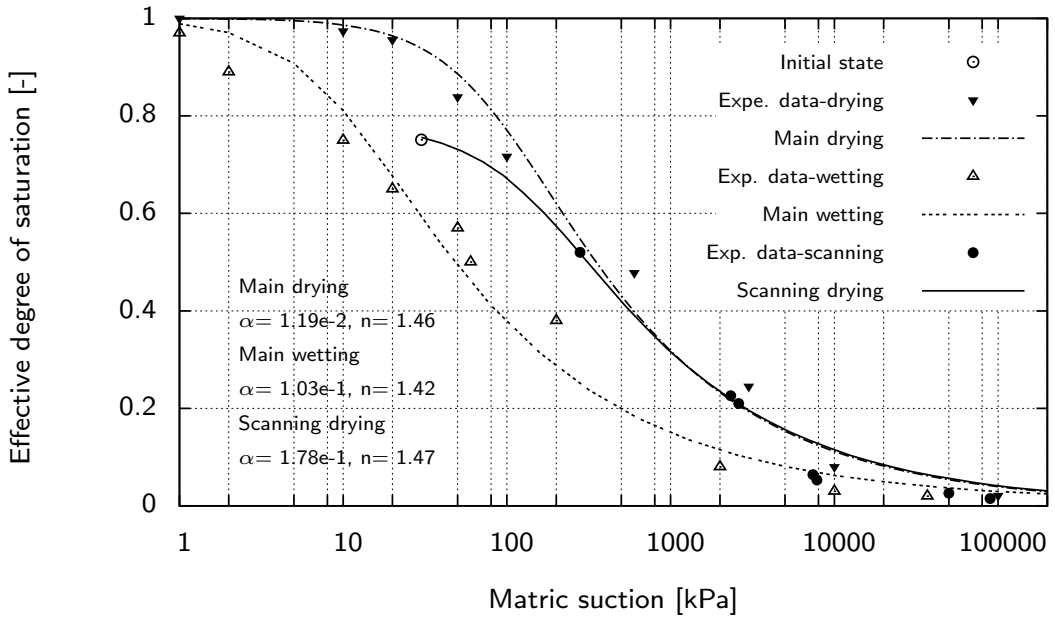

Figure 5.3.: Water retention curves - 70/30 sand-kaolin mixture, main drying, wetting and scanning curves

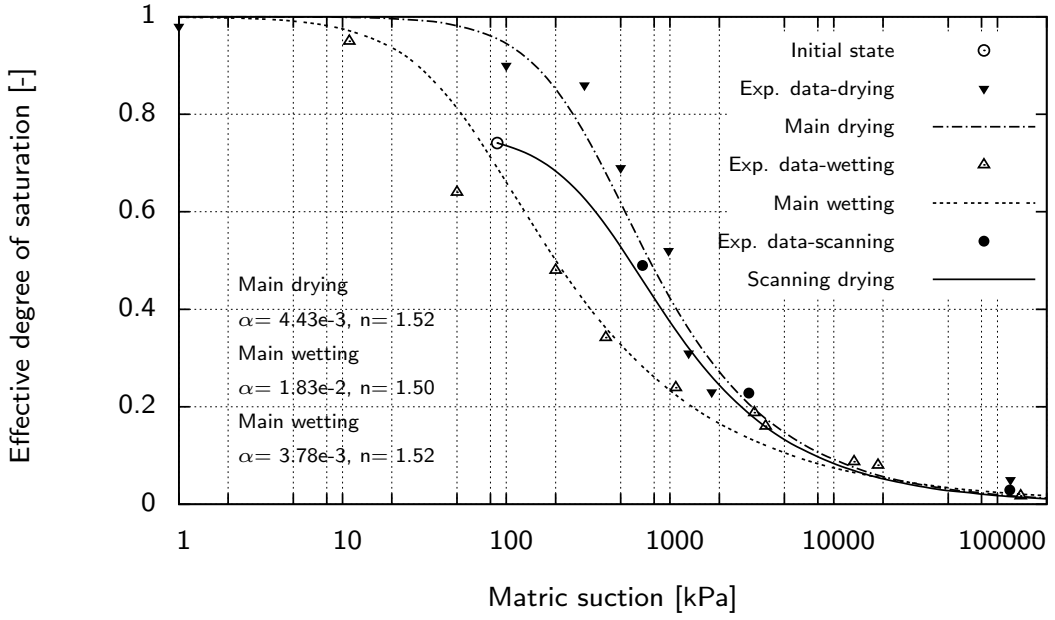

Figure 5.4.: Water retention curves - 50/50 sand-kaolin mixture, main drying, wetting and scanning curves

.

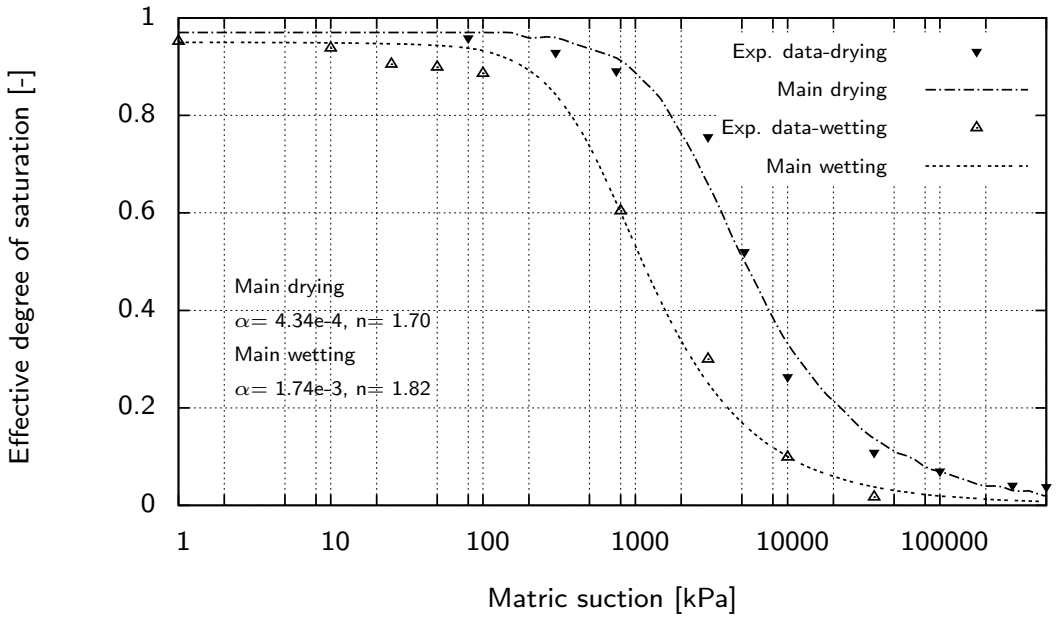

Figure 5.5.: Water retention curves - pure kaolin, main drying and wetting curves (Alabdullah 2010)

Table 5.1.: Fitting parameters of van Genuchten (1980) model for the materials used

Soil sample	α $[kPa^{-1}]$			n $[-]$		
	Main drying	Main wetting	Scanning	Main drying	Main wetting	Scanning
Pure sand	4.37e-1	9.79e-1	------	4.72	3.11	------
70/30 sand-kaolin	1.19e-2	1.03e-1	1.78e-2	1.46	1.42	1.47
50/50 sand-kaolin	4.43e-3	1.83e-2	3.78e-3	1.52	1.50	1.50
Pure kaolin	4.34e-4	1.74e-3	------	1.70	1.82	------

By increasing the amount of fine content for these two mixtures the rate of desaturation decreases. In comparison to sandy soil, flatter soil-water characteristic curves are observed

for these two mixtures. Because of the small pores in clay particles and higher specific surface area, the particles of pure kaolin absorb a greater amount of water in comparison to the sand and two sand-kaolin mixtures. The smaller pores retain the water up to higher matric suction levels. Thus, the capacity of water absorption is higher for clays and their soil water characteristic curves expand over a wide range of soil suctions (Agus & Schanz 2005). Figures 5.2 through 5.5 show experimental results together with predictions of SWCC suggested by the van Genuchten (1980) model.
In Table 5.1 fitting parameters of the materials used are presented.

5.2.1. Suction stress from SWCC

The suction stress can be related to the degree of saturation or matric suction and the relationship is named as the suction stress characteristic curve (SSCC) (Song 2014).
As shown in Eq. 2.27 the equation used to develop the SSCC involves the van Genuchten parameters of the SWCC and matric suction. Figures 5.6 to 5.9 present suction stress in terms of matric suction and degrees of saturation. Figure 5.6a represents the relationship between the suction stress and matric suction for pure sand. The suction stress increased and decreased with an increase of matric suction. For matric suction levels greater than 50 kPa, the suction stress vanishes. In general, for sand, the magnitude of the suction stress shows sinusoidal manner over a relatively small range of matric suction.

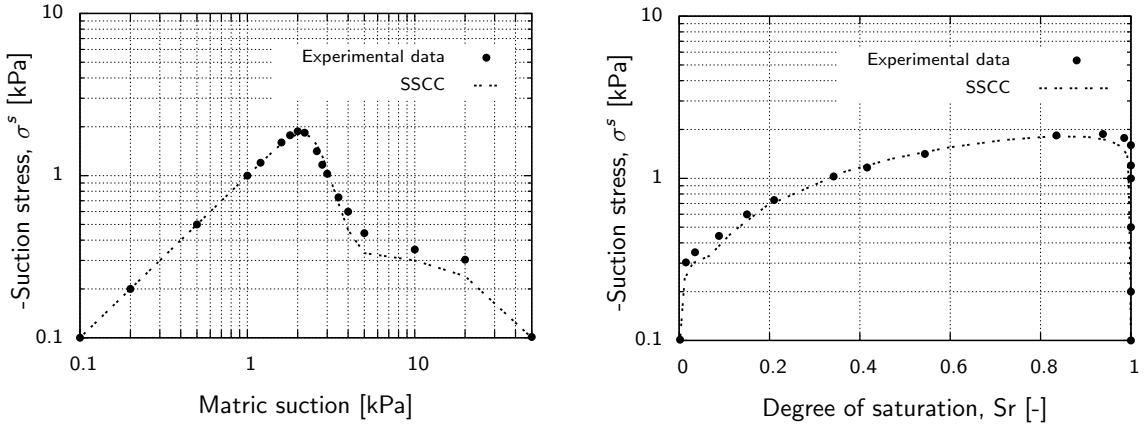

Figure 5.6.: Suction stress characteristic curve of pure sand (a) matric suction - σ^s and (b) Sr - σ^s (obtained from Lins (2009))

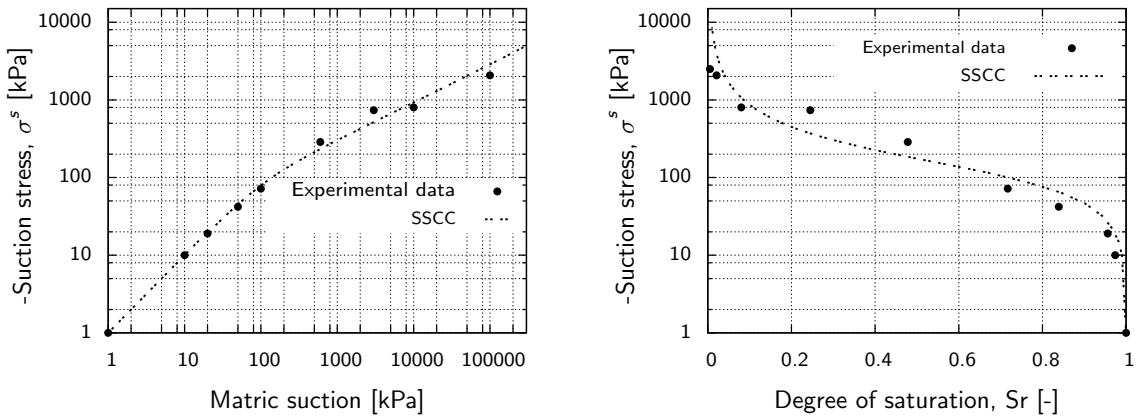

(a) (b)

Figure 5.7.: Suction stress characteristic curve of 70/30 sand-kaolin mixture (a) matric suction - σ^s and (b) Sr - σ^s

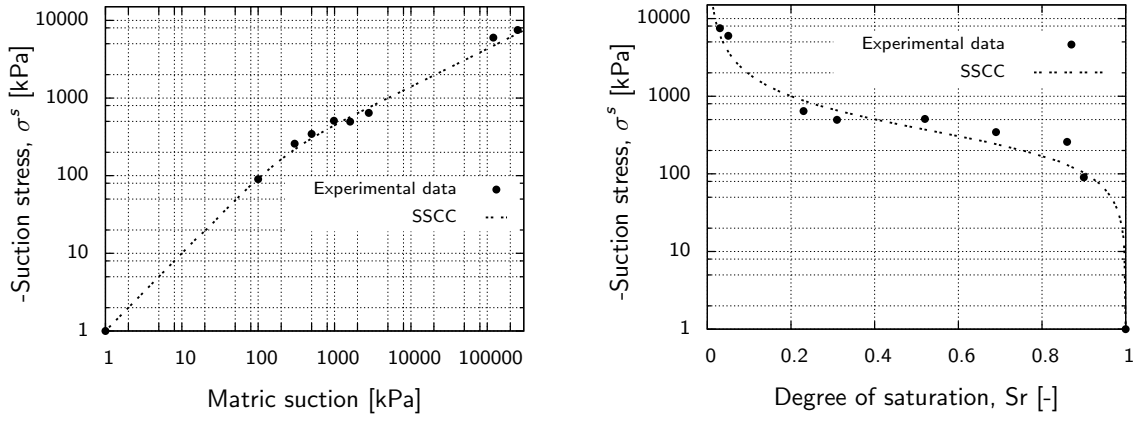

(a) (b)

Figure 5.8.: Suction stress characteristic curve of 50/50 sand-kaolin mixture (a) matric suction - σ^s and (b) Sr - σ^s

In Figures 5.7a and 5.8a suction stresses for sand-kaolin mixtures exhibit different behavior with variations in matric suction in comparison to the development of the suction stress for pure sand.

For sand-kaolin mixtures, as matric suction increased, suction stress increased gradually. An increase in suction stress values is observed even for relatively dry conditions. This behavior is more obvious for 50/50 sand-kaolin mixtures.

Fig. 5.9a shows that the pure kaolin sample obeys the same behavior as sand-kaolin mixtures. Increases in the values of suction stress for high matric suction is more pronounced

in pure kaolin in comparison to the 70/30 and 50/50 sand-kaolin mixtures.
For sand (Fig. 5.6b), in fully dry and saturated conditions, the suction stress is almost zero.
For sand-kaolin mixtures in Figures 5.7b and 5.8b and pure kaolin in Fig. 5.9b the maximum suction stress value is observed in relatively dry conditions.
For mixtures of sand-kaolin at low degrees of saturation the matric suction is reaching to high values. Therefore, according to the Eq. 2.27, even for relatively low degrees of saturation the suction stress shows significantly high values. While for pure sand at low degrees of saturation no significant increasing in matric suction can be seen. As a result at low degrees of saturation, suction stress tends to zero.
Under the proposed framework by Eq. 2.27, suction stress is related to the SWCC. "'The form of these curves is controlled by α and n. The parameter α is a direct indicator of the matric suction at which pore fluid begins to leave a drying soil water system, whereas parameter n reflects the pore size distribution of the soil" (Lu et al. 2010).
Lu et al. (2010) stated that the α parameter dominantly controls the minimum value of suction stress and the suction value corresponding to that minimum, whereas the parameter n exclusively controls the effective degree of saturation corresponding to the minimum suction stress.
In Figures 5.6a to 5.9b it is expected that the SSCC on main drying curve to exhibit two distinct regimes. For sandy soil with $n > 2$, (see Table 5.1), the suction stress shows an up and down behaviour with reduction degrees of saturation.

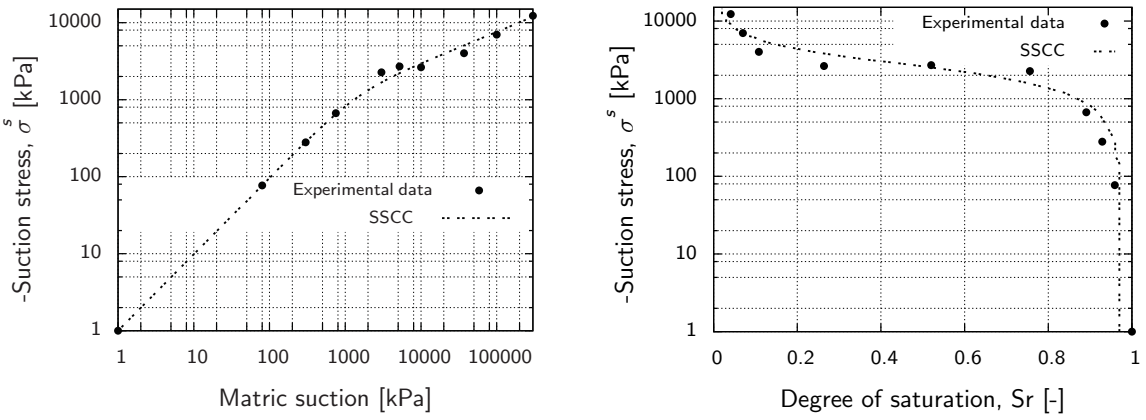

Figure 5.9.: Suction stress characteristic curve of pure kaoiln (a) matric suction - σ^s and (b) Sr - σ^s

For two sand-kaolin mixtures and pure kaolin with $n \leq 2$, suction stress monotonically increases by increasing of matric suction (Lu et al. 2010 and Baille et al. 2014).

5.3. Determination of suction stress via tensile tests

5.3.1. Direct tensile test results

The tensile strength characteristic curve as a function of matric suction and degree of saturation is shown in Figures 5.10 to 5.13 by using the experimental results of Lu et al. (2007) for sand, 70/30 and 50/50 sand-kaolin mixtures and with experimental data from Heibrock (1997) for pure kaolin. The results are summarized in Table A.1 in Appendix A. Tensile strength of Perth sand (Fig. 5.10) characteristically varies with matric suction and saturation in up-and-down as a sinusoidal manner. In general, for partially saturated sand, a non-linear relationship with saturation is observed for tensile strength (Lu et al. 2009).
Dry sand usually has minimal tensile strength close to zero. As sand progressively wets towards full saturation, tensile strength will first increase up to a peak value, which is followed by a reduction to zero at a near fully saturated condition.
For mixtures of 70/30 in Figure 5.11 average tensile strength measurements increase with the reduction in degrees of saturation and increasing of the matric suction. For relatively dry conditions the tensile strength tends to remain almost constant.

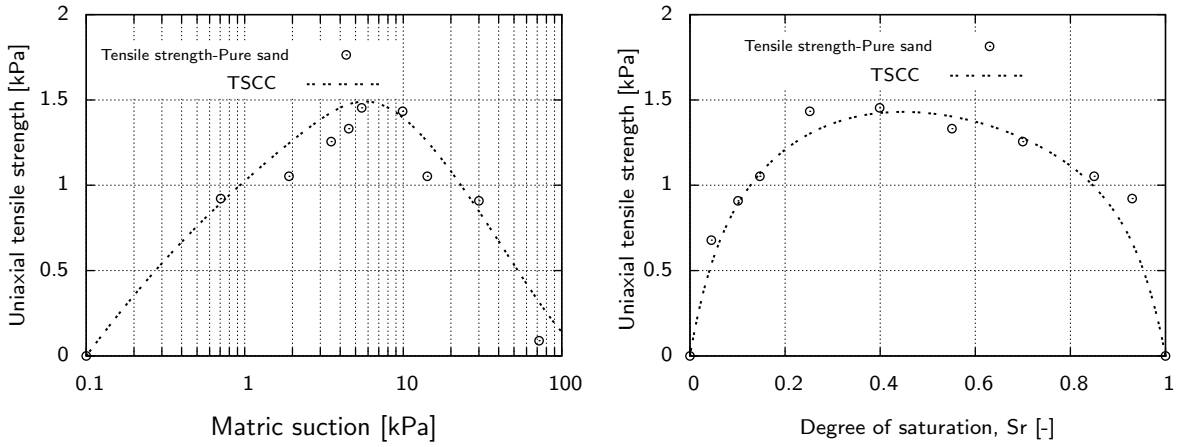

(a) (b)

Figure 5.10.: Tensile strength characteristic curve (TSCC) as a function of (a) matric suction and (b) degree of saturation for pure sand (Lu et al. 2007)

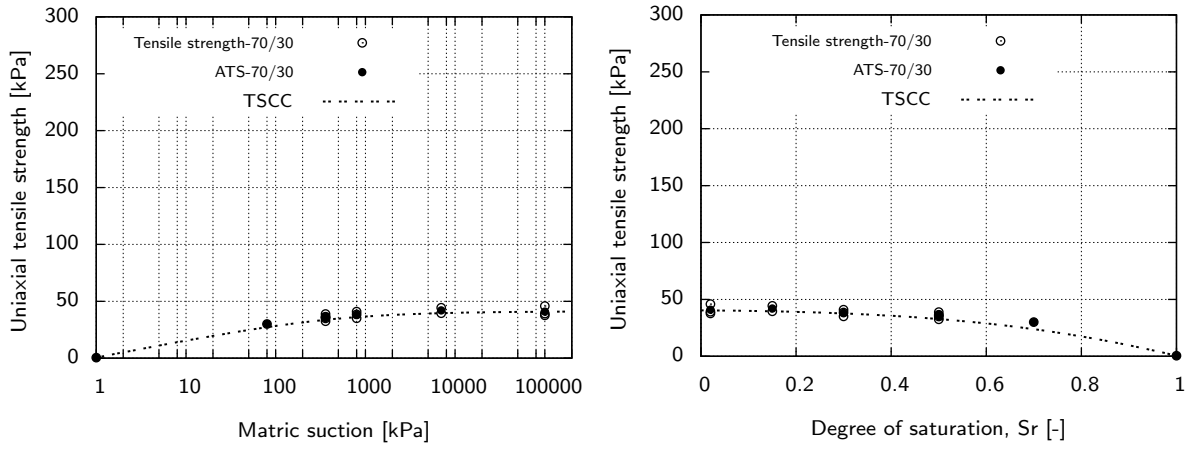

(a) (b)

Figure 5.11.: Tensile strength characteristic curve (TSCC) as a function of (a) matric suction and (b) degree of saturation for 70/30 sand-kaolin (ATS is average tensile strength)

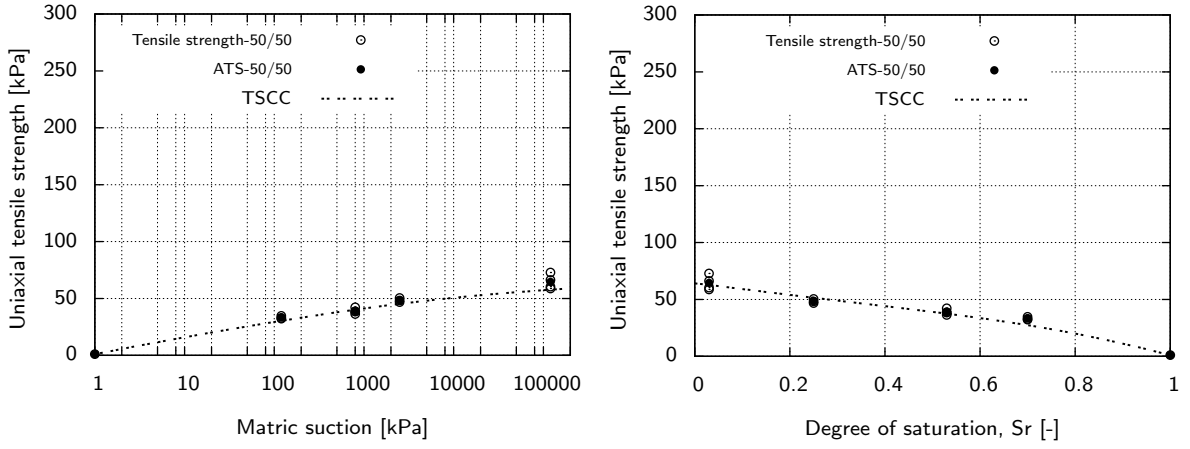

(a) (b)

Figure 5.12.: Tensile strength characteristic curve (TSCC) as a function of (a) matric suction and (b) degree of saturation for 50/50 sand-kaolin (ATS is average tensile strength)

For samples with 50/50 percent sand−kaolin (Fig. 5.12) tensile strength is higher than the 70/30 mixture. This implies that by increasing the amount of the fine content (kaolin) the tensile strength increases. Maximum tensile strengths are measured for 70/30 and 50/50 sand-kaolin mixtures at degrees of saturation close to zero.

The results of pure kaolin in Fig. 5.13 indicate that the degree of saturation has significant effects on the tensile strength. With an increase in the degree of saturation the tensile strength increases and reaches a peak value. With further increases in the de-

gree of saturation the tensile strength decreases. As seen even for saturated conditions the tensile strength for pure clay soils is not zero, which is likely related to some of the physico-chemical stresses that are noticeable at high degrees of saturation (e.g. electrical double layer).

In general, the results correspond to observations from further investigations on the tensile strength of compacted soils. Tamrakar et al. (2007) described the tensile strength measured for three mixtures of compacted clay-silt-sand soils. An increase in the amount of the tensile strength was strongly correlated with an increase in the percentage of fine particles. Increases in tensile strength through increasing the amount of clay was also shown by Barzegar et al. (1995).
The results of tensile strength on compacted "Kanto loam" (LL= 143.5, PL= 74.6) by Tamrakar et al. (2005) show that tensile strength increased with water content and reached to a maximum value of around 50 to 60% of degrees of saturation. Tensile strength decreases with further increases in water content. Tang et al. (2015) carried out laboratory tests on tensile strength on medium plastic clay. The soil samples were prepared by compacting a soil-water mixture of predetermined water content. The soil samples were either wetted or dried to different water contents corresponding to several suction levels. The test results showed an increase in tensile strength with higher suction values.

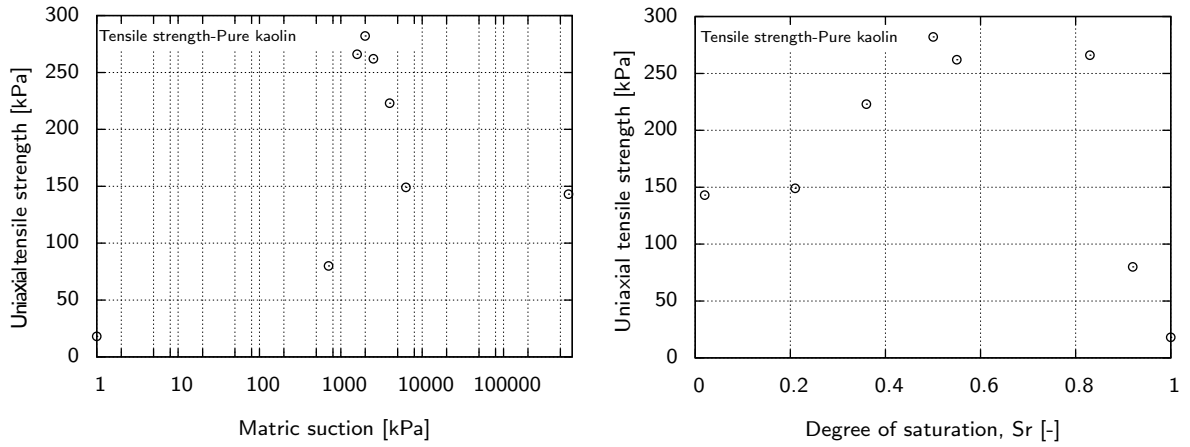

(a) (b)

Figure 5.13.: Tensile strength as a function of (a) matric suction and (b) degree of saturation for pure kaolin (Heibrock 1997)

5.3.2. Suction stress derived from direct tensile and triaxial tests

Because of the difficulties in performing isotropic tensile tests, direct tensile and shear tests at low stress levels are used to predict the isotropic tensile strength (see section 2.6.3).
The suction stress can be derived from the direct tensile and triaxial tests as follow:

1. As it is shown in Figures 5.14 and 5.15 the average of uniaxial tensile strength measurements and the results of the triaxial tests at confining pressures of 25, 50 kPa and 0, 50 kPa for 70/30 and 50/50 sand-kaolin mixtures are used to draw the failure envelopes in terms of p-q.
2. The values of the friction angle φ_t at low stresses are determined for different degrees of saturation and corresponding stress levels. For both sand-kaolin mixtures the values of the friction angle φ_t remain relatively constant. The almost air dry samples are an exception from this trend and show higher friction angle values.
3. The suction stresses ($\sigma^s_{isotropic\ tensile}$) for different degrees of saturation are determined using the average of the direct tensile strength measurement σ_{tut} and the friction angle of the saturated condition φ'_t in Eq. 2.30

The values of the suction stress ($\sigma^s_{isotropic\ tensile}$) for two sand-kaolin mixtures are shown in Table A.2.

5.4. Determination of suction stress from triaxial tests

5.4.1. Triaxial test results

To investigate the relevance of suction stress in relation to shear strength in partially saturated soils, a program of laboratory testing was conducted on two sand-kaolin mixtures (70/30 and 50/50) under different confining pressures and different degrees of saturation. In addition, the results of the shear strength test, via biaxial test, on pure sand (Alabdullah 2010) and the performed triaxial tests by Brueggemann (1998) on pure kaolin are used to evaluate the effects of different matric suctions and degrees of saturation on values of suction stress.
The data from shear tests are summarized in Table A.3 in appendix A. The failure envelopes in terms of the p-q ($p = \frac{\sigma_1+\sigma_3}{2}$, $q = \frac{\sigma_1-\sigma_3}{2}$) diagram and the strength parameters,

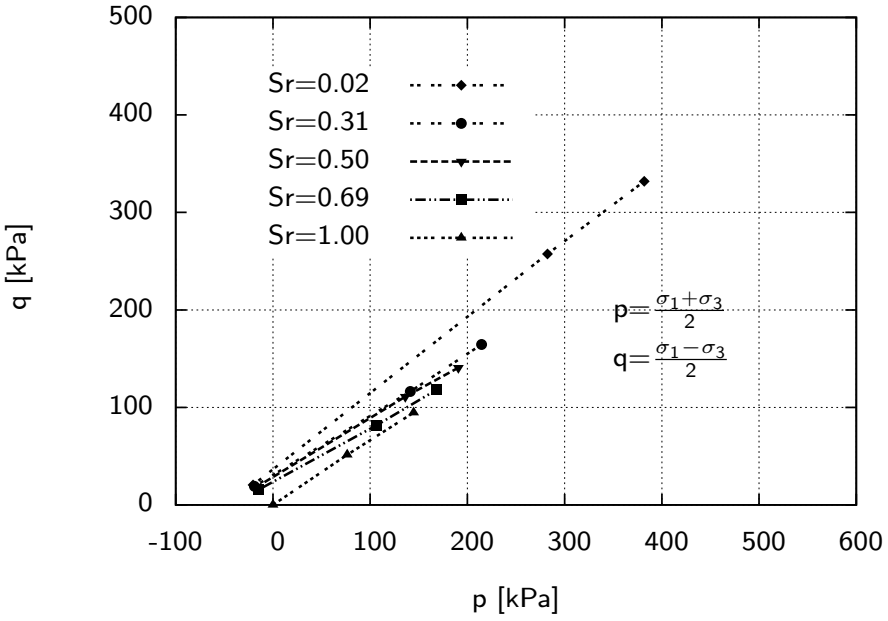

Figure 5.14.: Results of triaxial tests and direct tensile tests in terms of p-q for sand-kaolin mixture (70/30) (Sr is the degree of saturation; σ_3 and σ_1 are the minimum and maximum total principle stresses respectively)

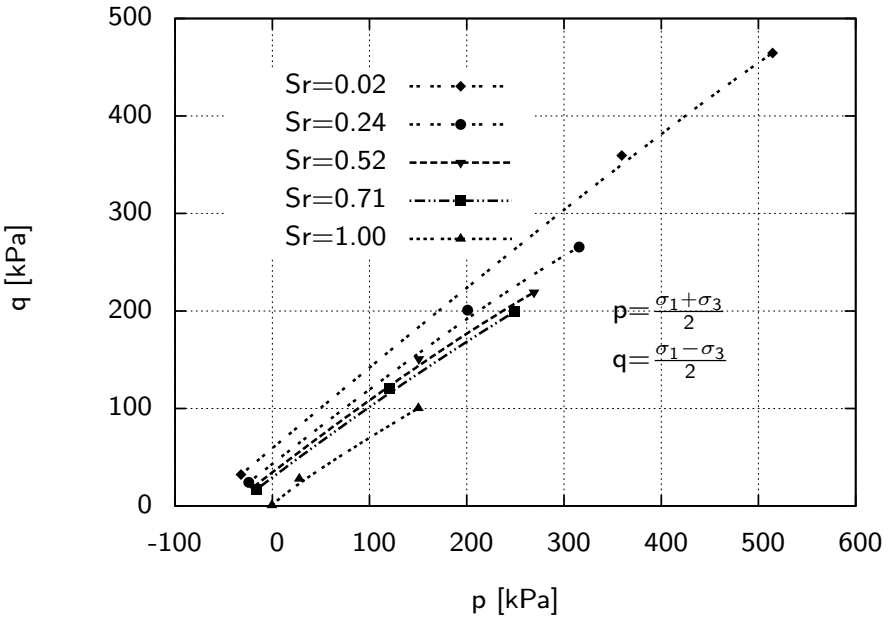

Figure 5.15.: Results of triaxial tests and direct tensile tests in terms of p-q for sand-kaolin mixture (50/50) (Sr is the degree of saturation; σ_3 and σ_1 are the minimum and maximum total principle stresses respectively)

cohesion and friction angle, are shown in Figures 5.16 to 5.22.
Within experimental precision, test results for samples with equal matric suction or degrees of saturation fall on a straight line. For pure sand in Fig. 5.16 it can be observed that the failure envelopes shift upwards slightly through increasing matric suction and reaching maximum value at matric suction equal to 2 kPa. By further increasing matric suction, a reduction is observed for the shear strength of the samples with 4 kPa. For dry samples the failure envelope falls to the saturated failure line.
It is expected that the reason for the reduction in shear strength by increasing matric suction is that the main contribution to soil-water interactions in pure sand comes from capillary stress. Therefore, it is reasonable to argue that by increasing capillary stress the shear strength reaches to its maximum and that further increases in matric suction can lead to reductions in the amount of capillary stress and reduction in shear strength.

Figures 5.17a and 5.17b show that the cohesion intercept exhibits a sinusoidal characteristic over a relatively small range of matric suction and that the friction angle is relatively constant in-line with matric suction variation.
Figures 5.18 and 5.20 show the p-q diagram for two mixtures of sand-kaolin for different degrees of saturation. The experimental results are well fitted with a straight line. A significant increase in peak shear strength can be observed in Figures 5.18 and 5.20 for soils in dry conditions and at degrees of saturation from 30% to 0%. For both mixtures the friction angle of saturated condition and samples with degrees of saturation >30% can be considered constant. The friction angles for dry conditions are significantly larger. The cohesion, c, increases slightly with a reduction in degrees of saturation. The near air dry samples are an exception from this trend and show higher values in terms of cohesion.

Data from Futai (2002) and Reis (2004) are used to compare the experimental results. These authors performed suction-controlled triaxial tests on constant water content and air-dried samples. Figures 5.24 and 5.25 show the shear strength envelopes for the samples tested by Futai (2002) and Reis (2004). Samples in Fig. 5.24 correspond to sandy clay. It can be seen that the cohesion intercept rises with an increase in matric suction.
Figure 5.25 presents the shear strength envelopes on silty sand materials under different values of matric suction. The results show an increase in cohesion intercept and no variation in friction angle with matric suction. For both of the soil tests the air-dried sample is an exception where the cohesion and friction angle are higher than the other experiments.

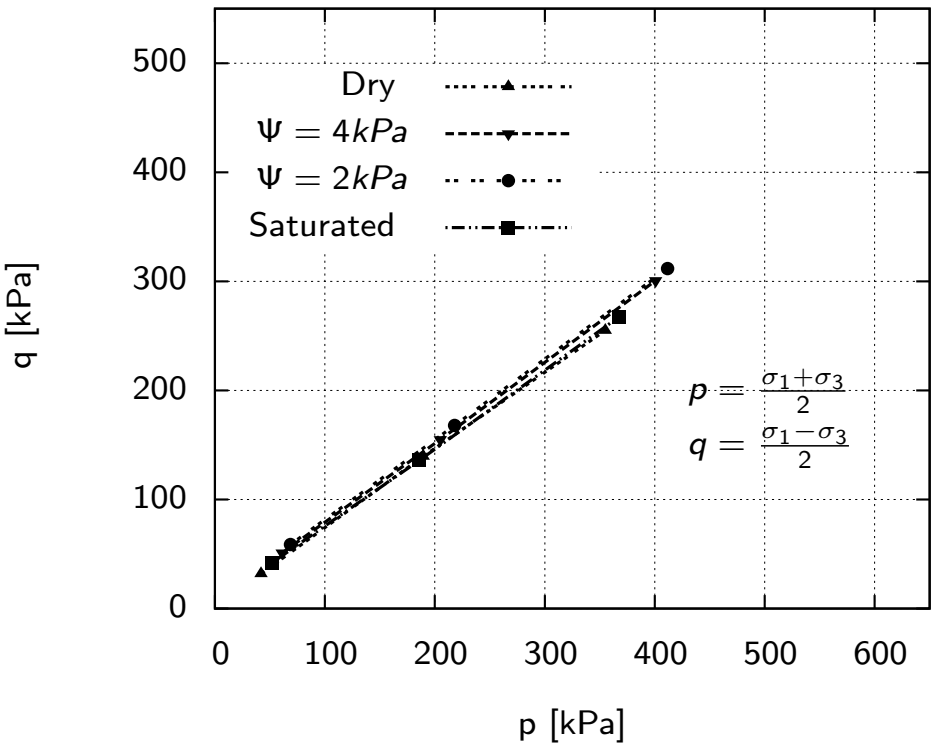

Figure 5.16.: Results of the biaxial tests in terms of p-q for pure sand (Alabdullah 2010) (Ψ is the matric suction; σ_3 and σ_1 are the minimum and maximum total principle stresses respectively)

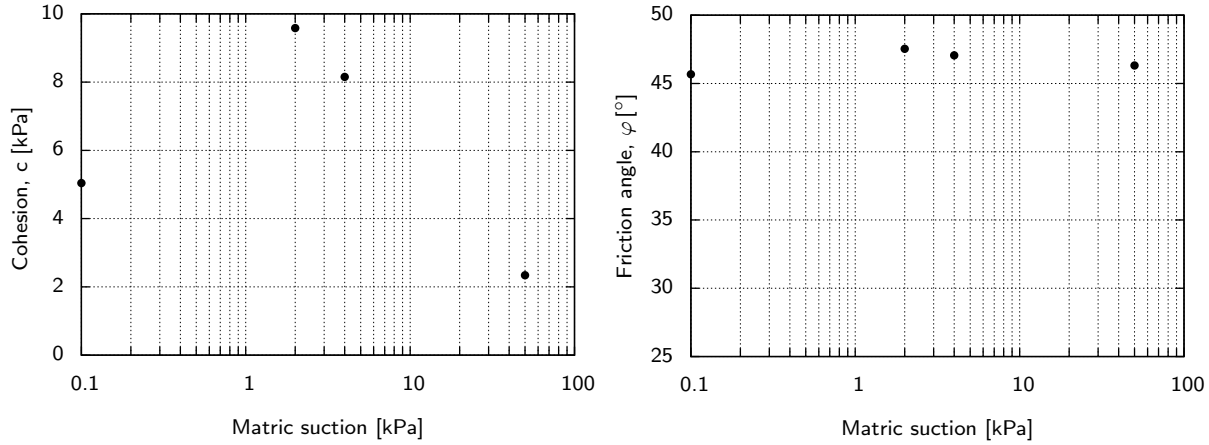

(a) (b)

Figure 5.17.: (a) Cohesion and (b) friction angle for pure sand (Alabdullah 2010) as a function of the matric suction

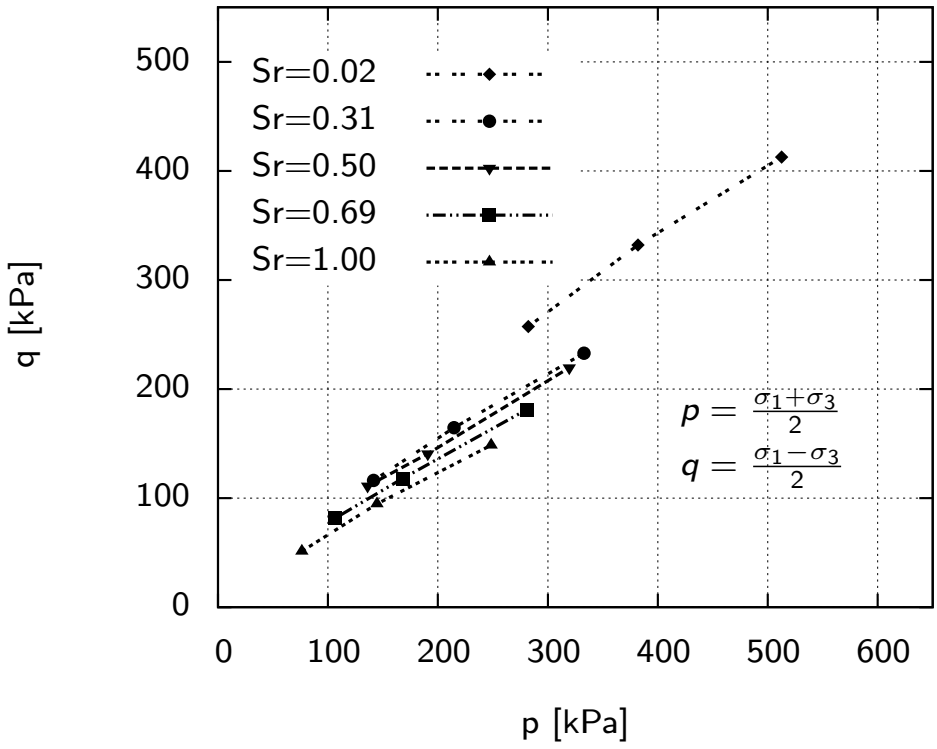

Figure 5.18.: Results of triaxial tests in terms of p-q for sand-kaolin mixture (70/30) (Sr is the degree of saturation; σ_3 and σ_1 are the minimum and maximum total principle stresses respectively)

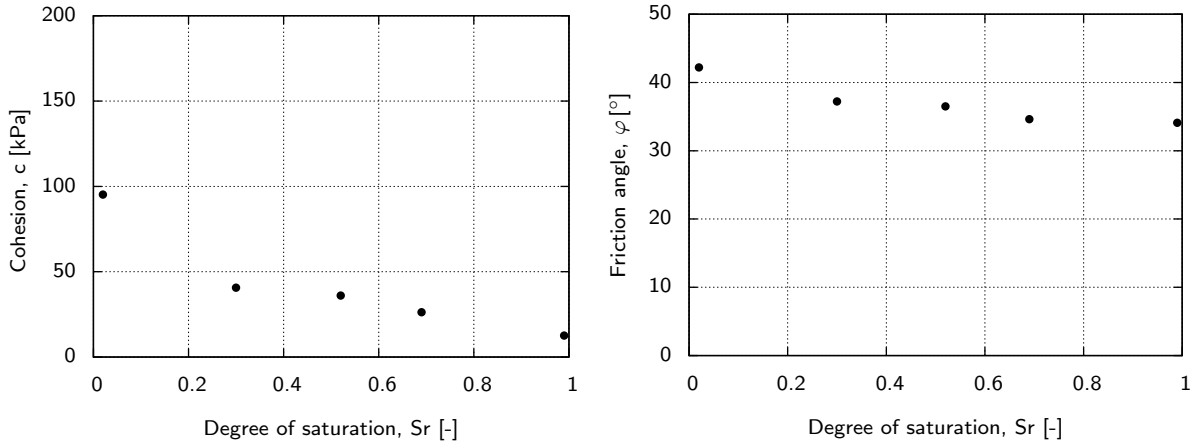

(a) (b)

Figure 5.19.: (a) Cohesion and (b) friction angle for sand-kaolin mixture (70/30) as a function of the degree of saturation

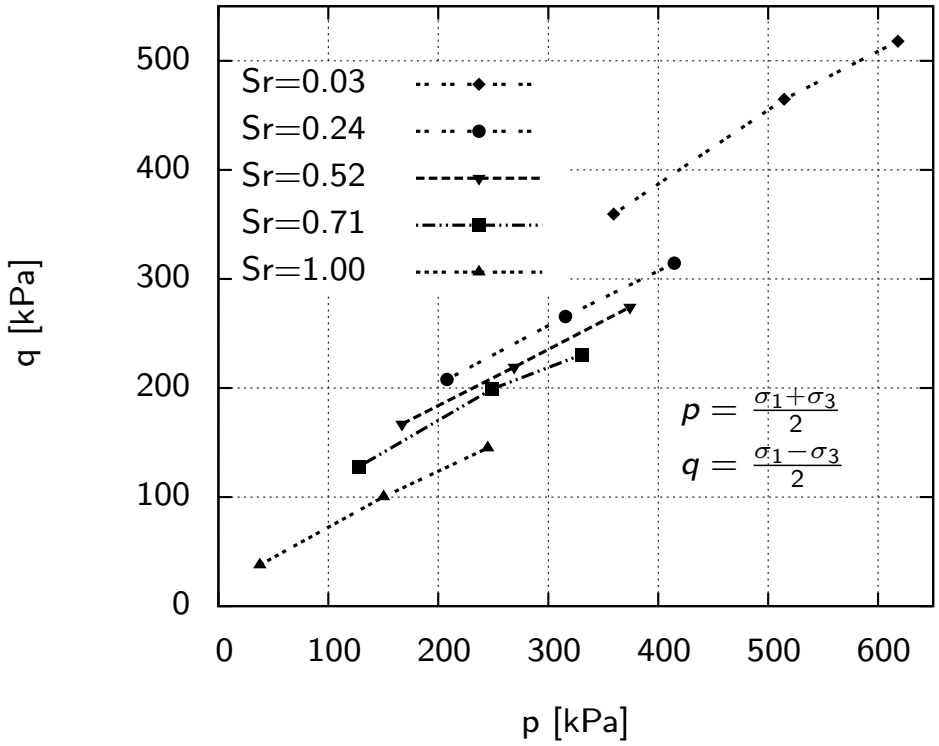

Figure 5.20.: Results of triaxial tests in terms of p-q for sand-kaolin mixture (50/50) (Sr is the degree of saturation; σ_3 and σ_1 are the minimum and maximum total principle stresses respectively)

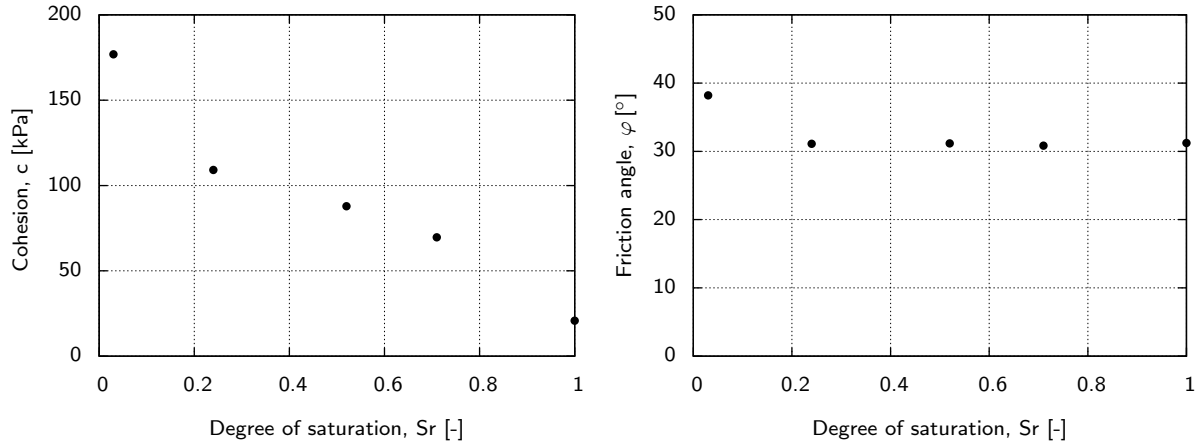

(a) (b)

Figure 5.21.: (a) Cohesion and (b) friction angle for sand-kaolin mixture (50/50) as a function of the degree of saturation

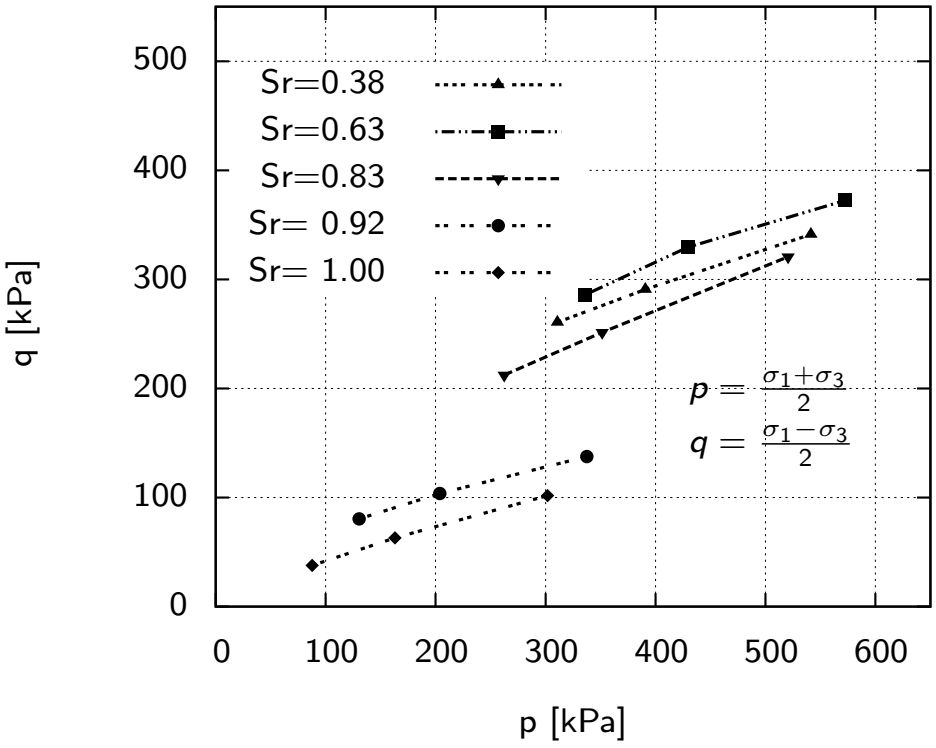

Figure 5.22.: Results of triaxial tests in terms of p-q for pure kaolin (Brueggemann 1998) (Sr is the degree of saturation; σ_3 and σ_1 are the minimum and maximum total principle stresses respectively)

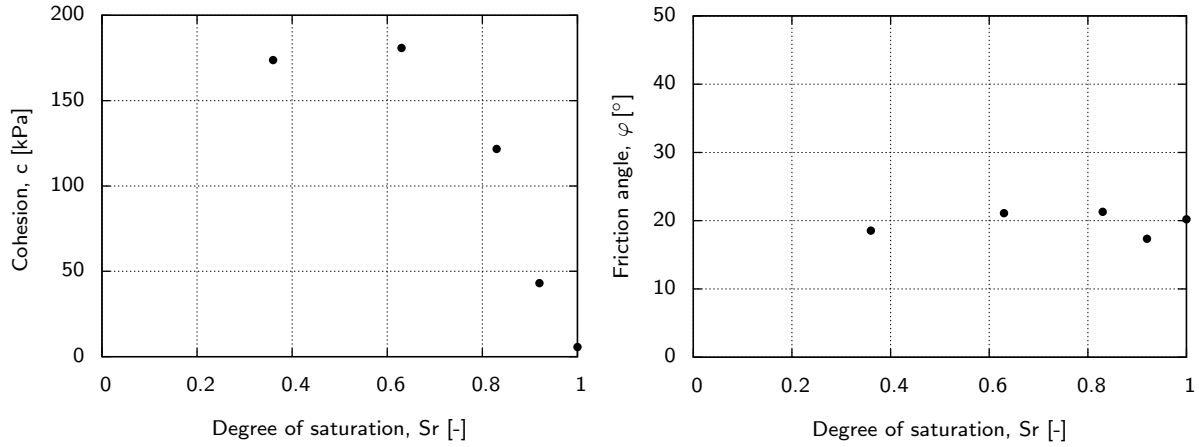

(a) (b)

Figure 5.23.: (a) Cohesion and (b) friction angle for pure kaolin (Brueggemann 1998) as a function of the degree of saturation

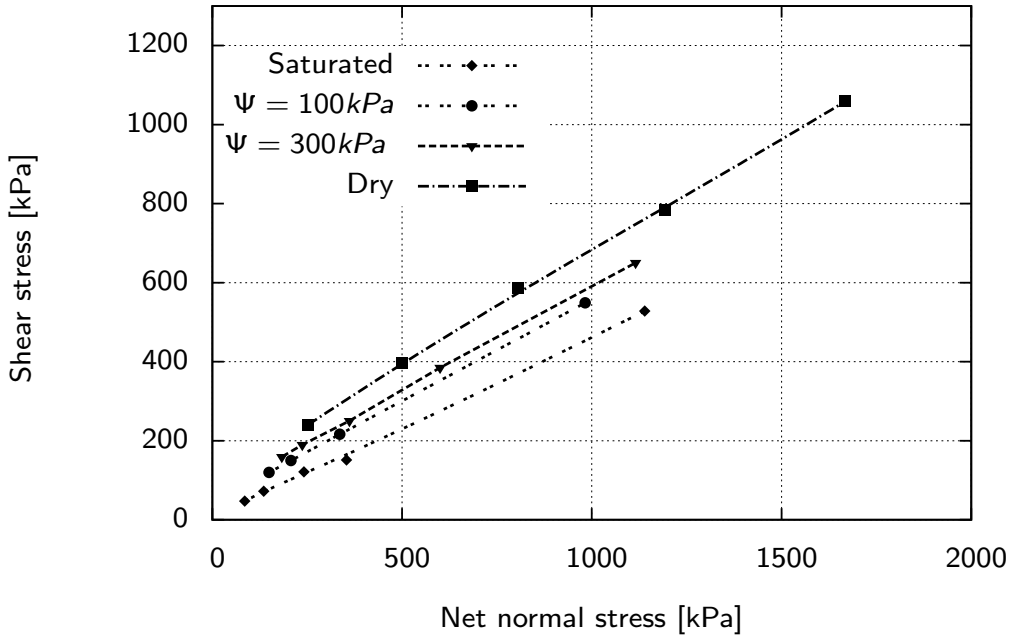

Figure 5.24.: Shear strength envelopes and experimental results on sandy-clay (Futai 2002)

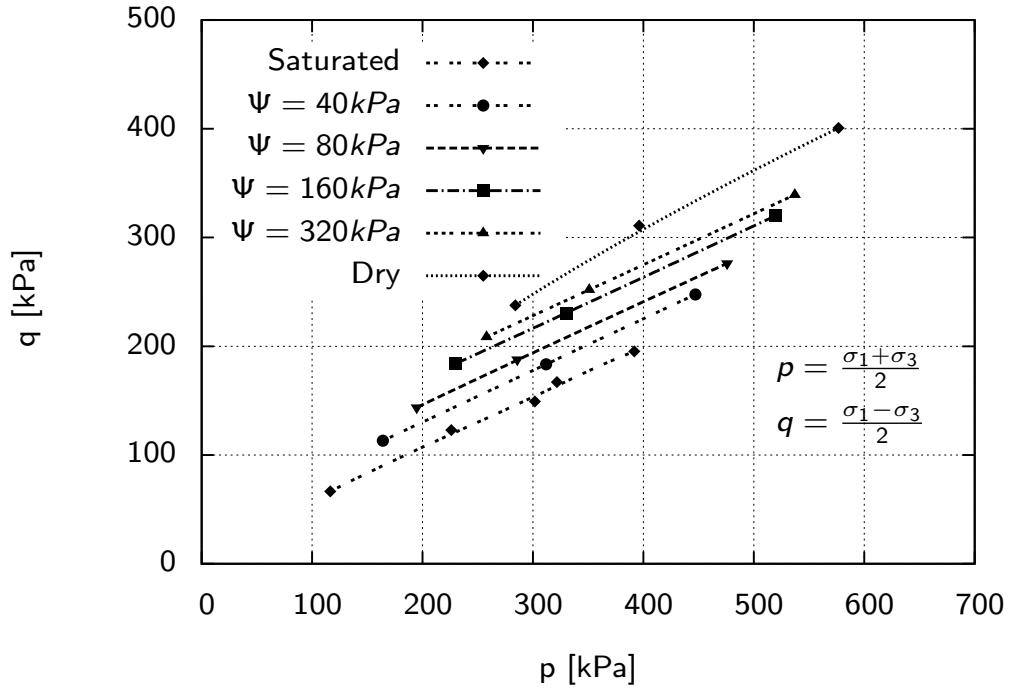

Figure 5.25.: Shear strength envelopes and experimental results on silty sand (Reis 2004)

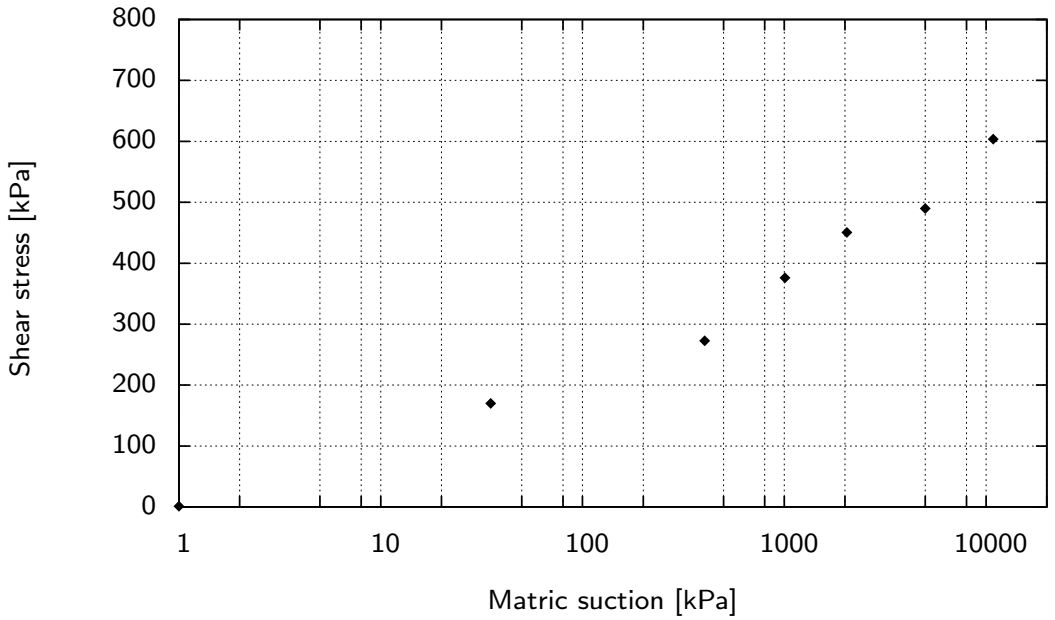

Figure 5.26.: Shear strength and experimental results for one set of tests on clay (Escario & Juca 1989)

Another comparison was made by using data from Escario & Juca (1989), who performed suction-controlled tests on a wide range of matric suction. Escario presented results of direct shear tests on Madrid gray clay taken to 10000 kPa of matric suction. As seen in Fig. 5.26, by increasing matric suction, the shear stress shifts upwards. A set of triaxial tests was performed on silt specimens under saturated and partially saturated conditions by Alsherif & McCartney (2014). In these tests the matric suction was controlled using an automated humidity system. Two sets of triaxial tests were performed on partially saturated specimens at matric suction values of 162 and 291 MPa (corresponding to degrees of saturation of 0.11 and 0.06, respectively) under confining pressures of 100, 200 and 300 kPa. The failure envelopes for the saturated and partially saturated specimens are shown in Fig. 5.27 in terms of net confining pressure.

The experiments indicate that there is a substantial increase in peak shear strength with matric suction for partially saturated soils under high matric suction magnitudes (a 30% increase over a change in suction of 129 MPa).

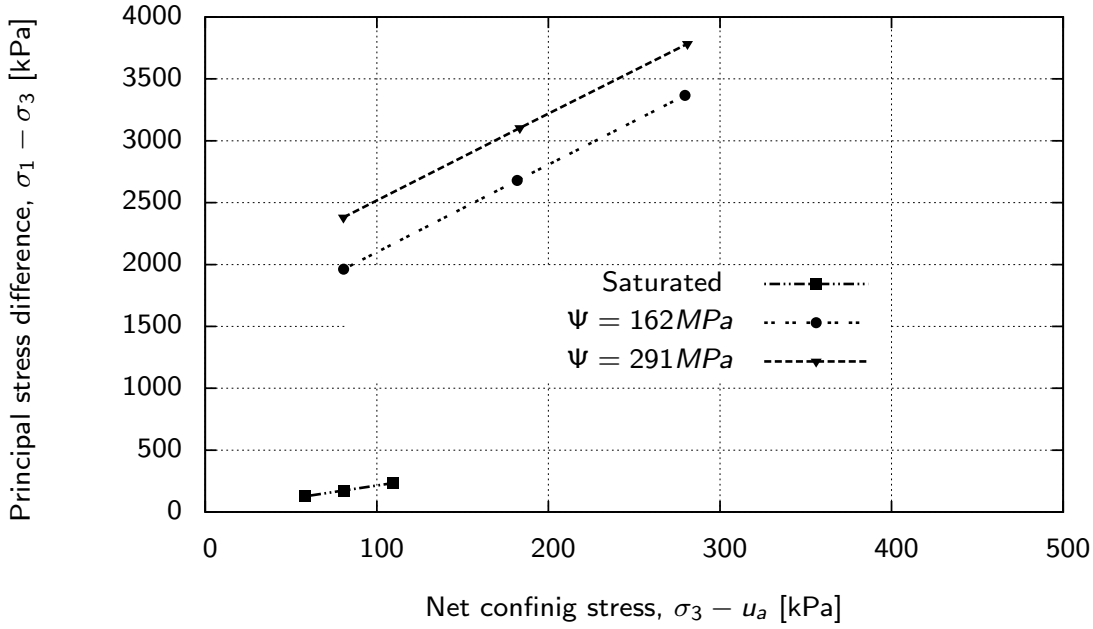

Figure 5.27.: Shear strength envelopes and experimental results on silt specimens (Alsherif & McCartney 2014)

5.4.2. Suction stress derived from triaxial tests

For the determination of suction stress from a triaxial test, the minimum and maximum total principle stresses (σ_3 and σ_1) and c' and φ' (the drained cohesion and friction angle at the soil saturated state) (Table A.3) are integrated into the Eq. 2.31. Figures 5.28 to 5.31 summarize suction stresses determined for pure sand, two sand-kaolin mixtures and pure kaolin.

Figure 5.28 shows that suction stress from the experiments with biaxial devices on pure sand shows an up-and-down behavior over applied matric suction, as well as the predicted values of suction stress from SWCC and tensile tests. The suction stress for two sand-kaolin mixtures is shown in Figures 5.29 and 5.30. A consistent increase in suction stress values is observed with a reduction in degrees of saturation. For both mixtures at relatively low degrees of saturation a significant increase in suction stress values is observed.

Fig. 5.31 illustrates the results of the suction stress for pure kaolin. Reduction in suction stress values can be seen over changes in degrees of saturation, from 0.62 to 0.38. In regards to the test results (Futai 2002, Reis 2004, Escario & Juca 1989, Alsherif & McCartney 2014), it is expected the amount of suction stress rises by reduction in degrees of saturation for fully dry samples.

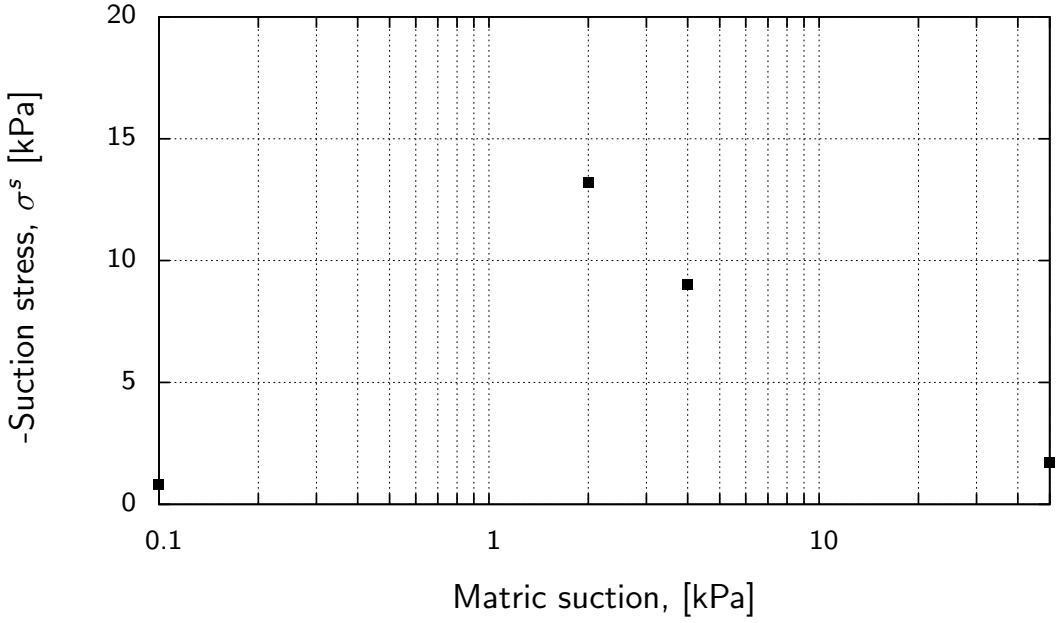

Figure 5.28.: Suction stress derived from biaxial test for pure sand (Alabdullah 2010)

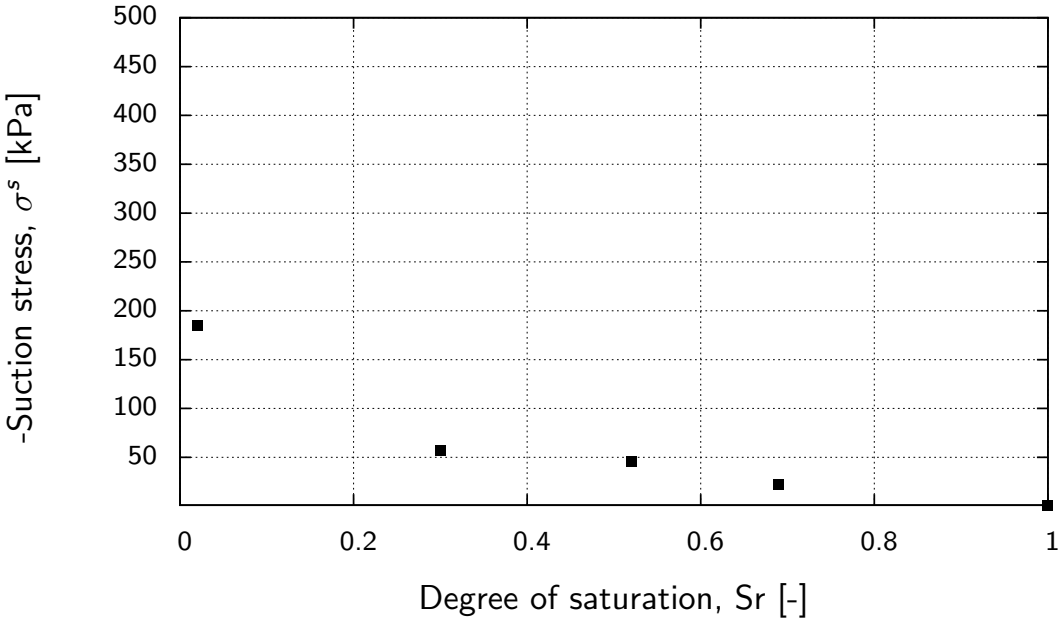

Figure 5.29.: Suction stress derived from triaxial test for 70/30 sand-kaolin mixture

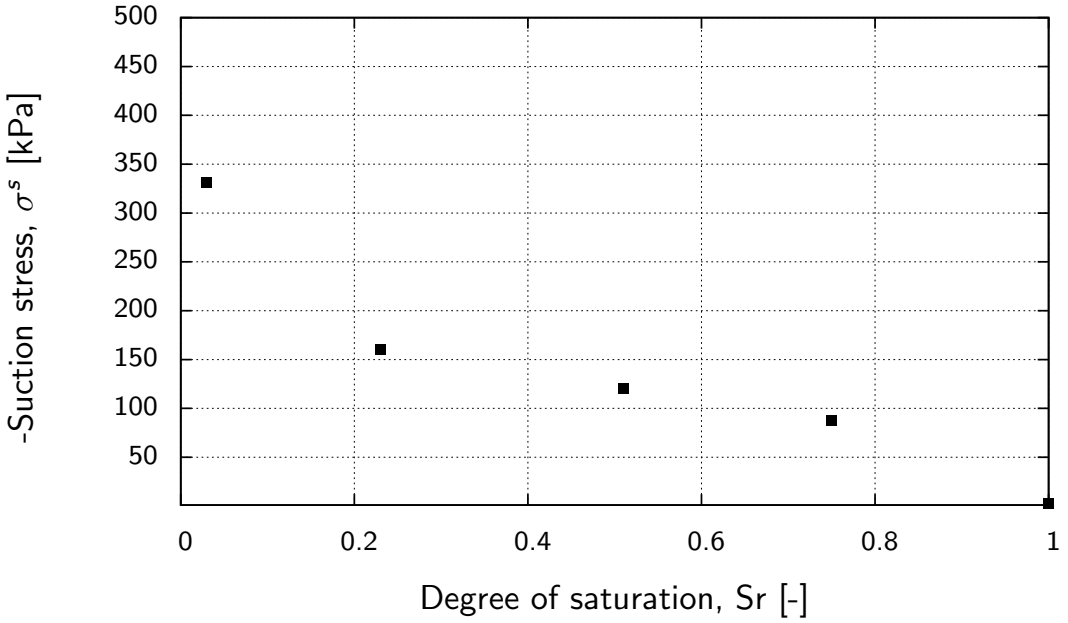

Figure 5.30.: Suction stress derived from triaxial test for 50/50 sand-kaolin mixture

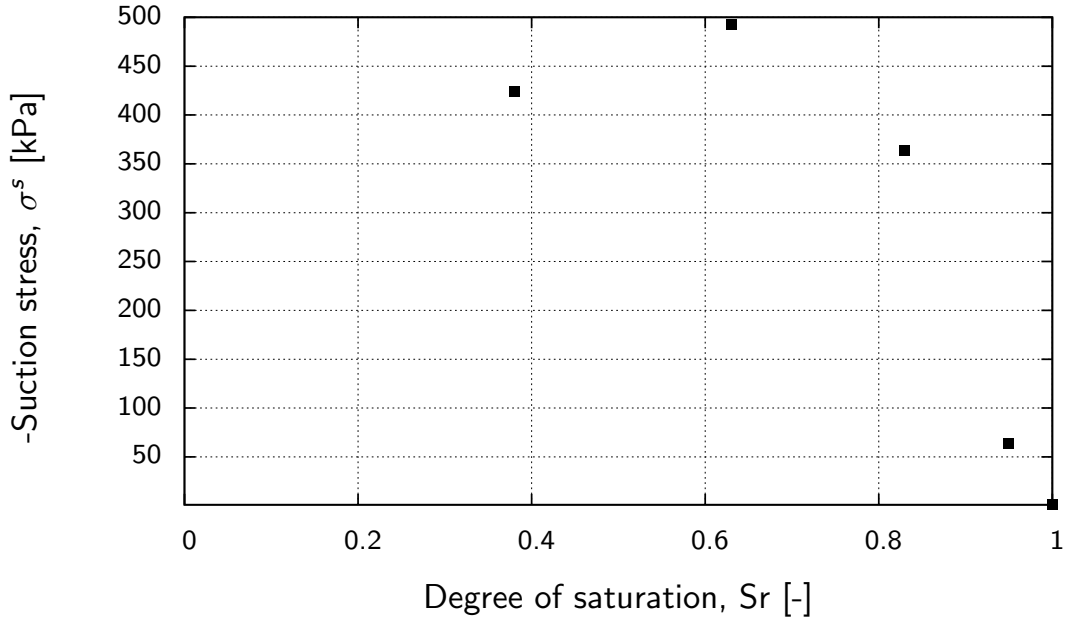

Figure 5.31.: Suction stress derived from triaxial test for pure kaolin (Brueggemann 1998)

5.5. Failure envelopes derived from experiments

With the suction stress value known, the effective stress can be calculated by adding the suction stress to the total normal stress (Eq. 2.28, $u_a = 0$). A p'-q diagram can then be written in terms of effective stress. p' cab be determined as:

$$p' = \frac{(\sigma_1 - u_a) - \sigma^s + (\sigma_3 - u_a) - \sigma^s}{2} = (p - u_a) - \sigma^s \tag{5.1}$$

To compare the proposed expression for effective stress (Eq. 2.28), the values of the suction stress derived from the direct tensile and triaxial tests (section 5.3.2) for two sand-kaolin mixtures Eq. 2.30) are added to the values of total normal stress. Corresponding failure envelopes are then plotted for effective stress. Figs. 5.32 and 5.33 show that the total normal stress failure envelopes for both mixtures converge to a relatively unique effective stress failure envelope. Similar analyses were conducted to examine an alternative expression for effective stress. Figs. 5.34 and 5.35, show effective stress failure envelopes by using direct tensile tests instead of isotropic tensile strength. Suction stress, $\sigma^s_{direct\ tensile}$, for these calculations was set to equal the direct tensile strength. Results in terms of effective stress converge again to relatively unique failure envelope. The convergence of the effective stress failure envelopes by means of direct tensile strength indicates that for the materials used the direct tensile strength measurement can be considered as suction stress in the proposed effective stress concept. To study the effective stress concept for pure kaolin, the measurement of the direct tensile strength was used.

Fig. 5.36 shows the triaxial test results for pure kaolin in terms of effective stress. The total normal stress failure envelope converges to a relatively unique effective stress failure envelope. The fact that the effective stress failure envelopes for the material used are unique supports the effective stress concept defined as the sum of total normal stress and tensile strength.

Using the same procedure, but using the suction stresses derived from the triaxial tests ($\sigma^s_{triaxial}$) (Eq. 2.31), resulted in the p'-q diagram shown in Figures 5.37 to 5.40 for pure sand, two sand-kaolin mixtures and pure kaolin.

It can be observed from Figs. 5.37 to 5.40 that the total normal stress failure envelopes converge to a unique effective stress failure envelope.

Even the failure envelopes (sum of total normal stress and suction stress deriving from shear test results) converge to one unique line but it is not necessarily directly applicable to effective stress. Because although the failure envelopes converge to one unique line the test results indicate differences in suction stresses determined from tensile test and shear test.

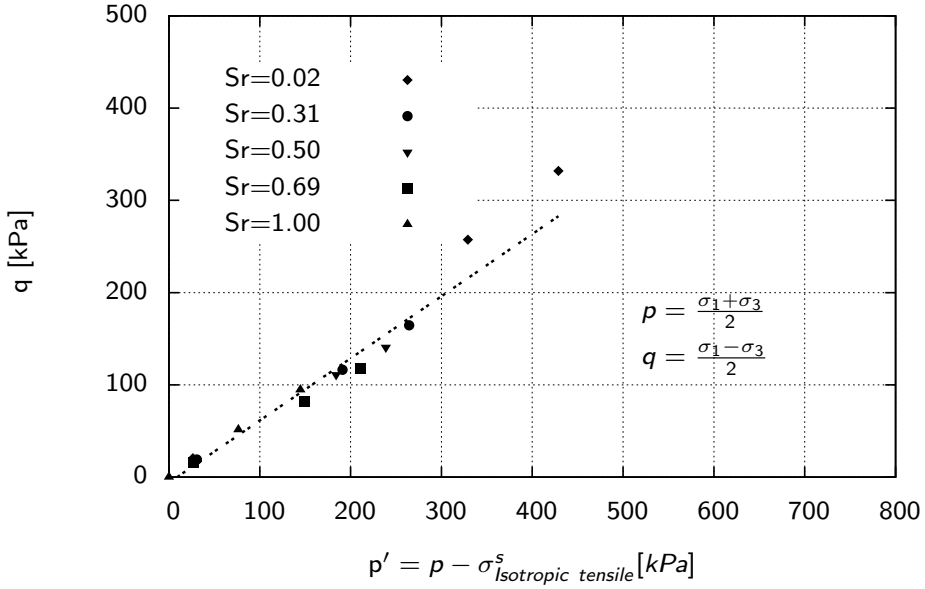

Figure 5.32.: Failure envelope for 70/30 sand-kaolin mixture in terms of effective stress defined as normal stress plus suction stress derived from isotropic tensile strength ($\sigma^s_{isotropic\ tensile}$)

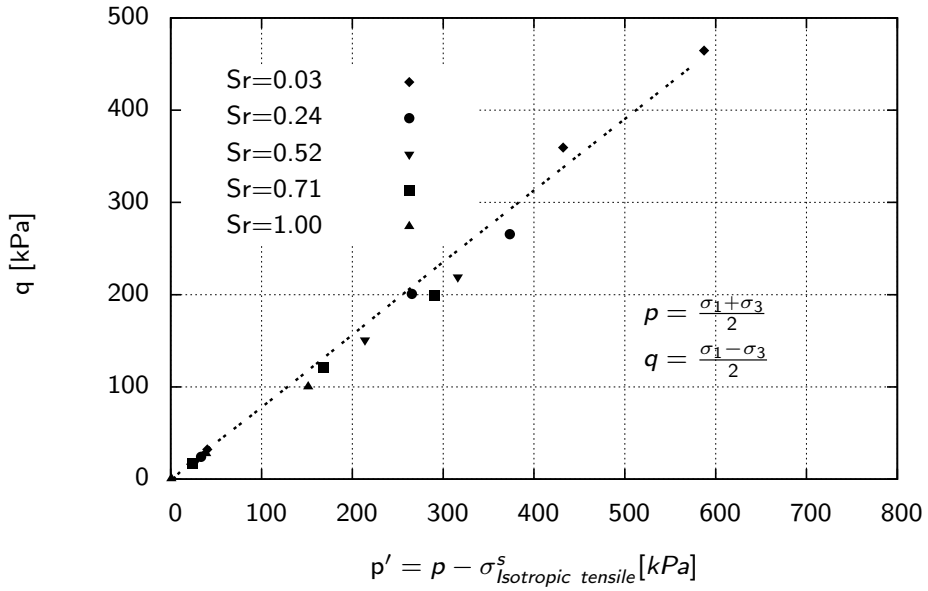

Figure 5.33.: Failure envelope for 50/50 sand-kaolin mixture in terms of effective stress defined as normal stress plus suction stress derived from isotropic tensile strength ($\sigma^s_{isotropic\ tensile}$)

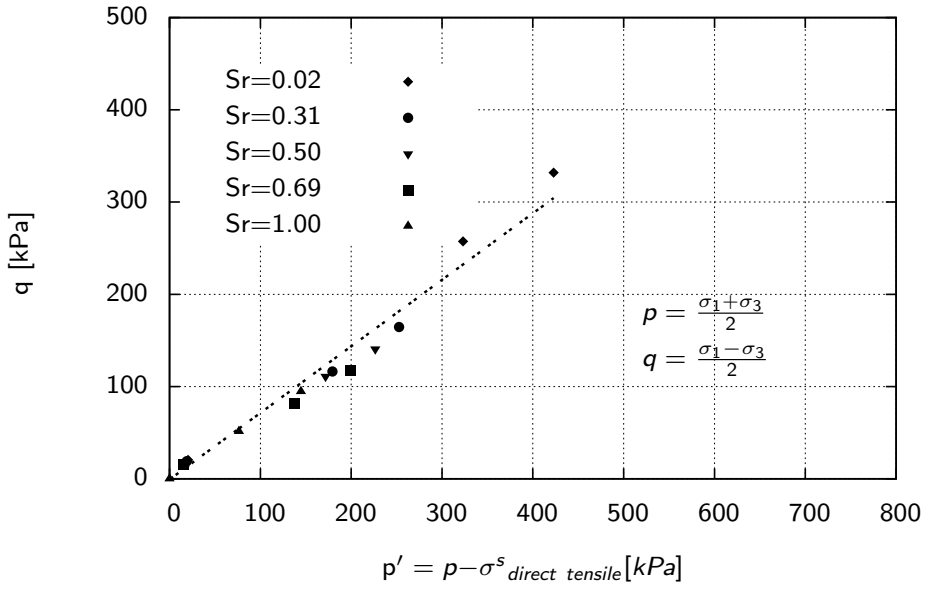

Figure 5.34.: Failure envelope for 70/30 sand-kaolin mixture in terms of effective stress defined as normal stress plus suction stress derived from direct tensile strength ($\sigma^s_{direct\ tensile}$)

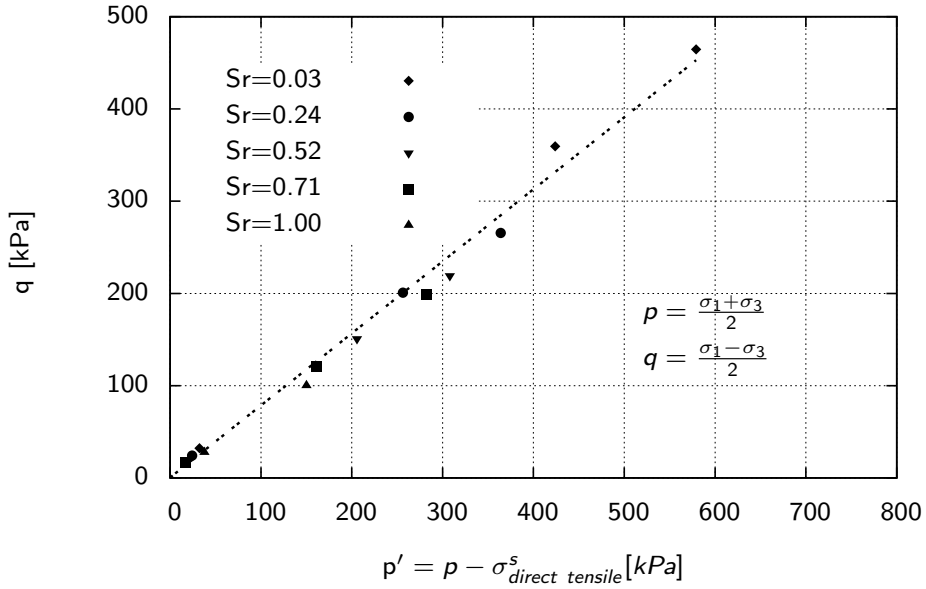

Figure 5.35.: Failure envelope for 50/50 sand-kaolin mixture in terms of effective stress defined as normal stress plus suction stress derived from direct tensile strength ($\sigma^s_{direct\ tensile}$)

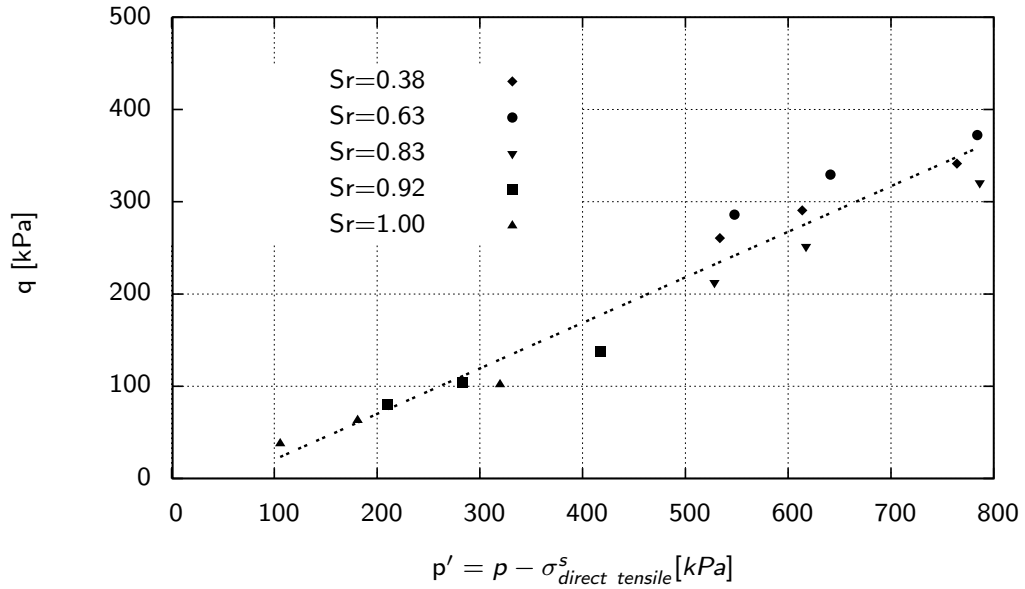

Figure 5.36.: Failure envelope for pure kaolin in terms of effective stress defined as normal stress plus suction stress derived from direct tensile strength ($\sigma^s_{direct\ tensile}$)

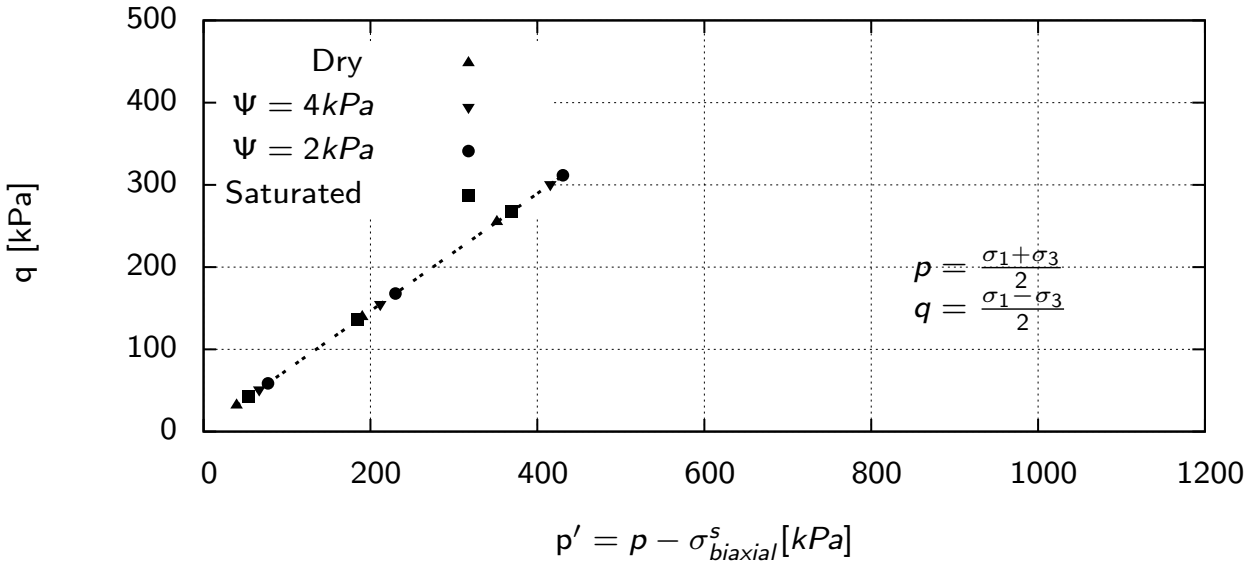

Figure 5.37.: Failure envelope for pure sand in terms of effective stress p′; defined as normal stress p, plus suction stress derived from biaxial test results (Alabdullah 2010)

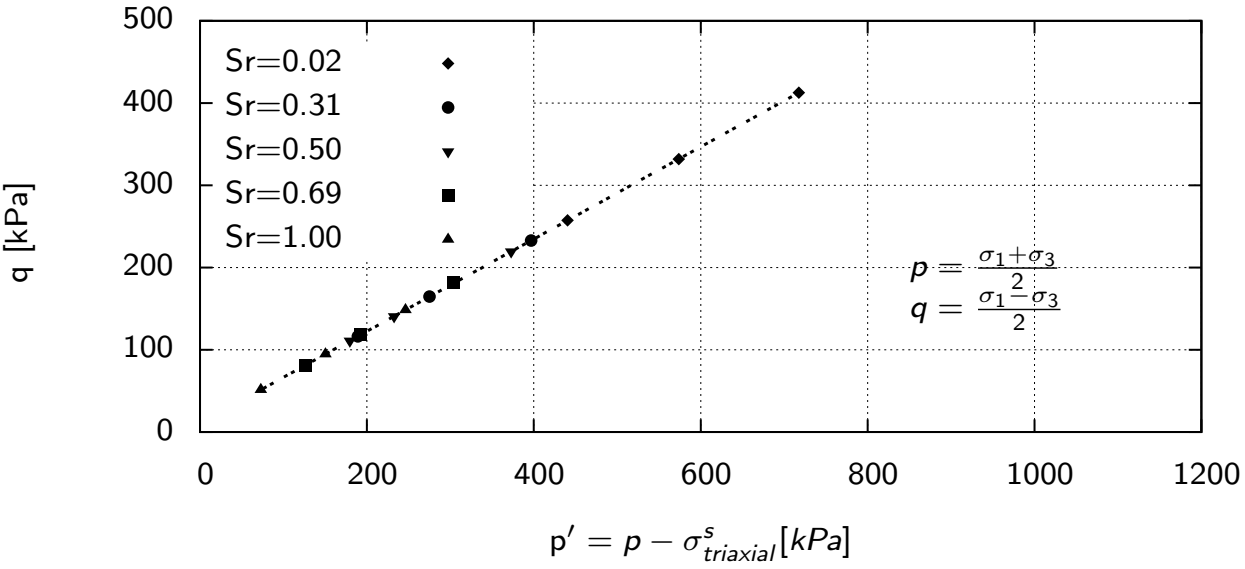

Figure 5.38.: Failure envelope for 70/30 sand-kaolin mixture in terms of effective stress p′; defined as normal stress p, plus suction stress derived from triaxial test results

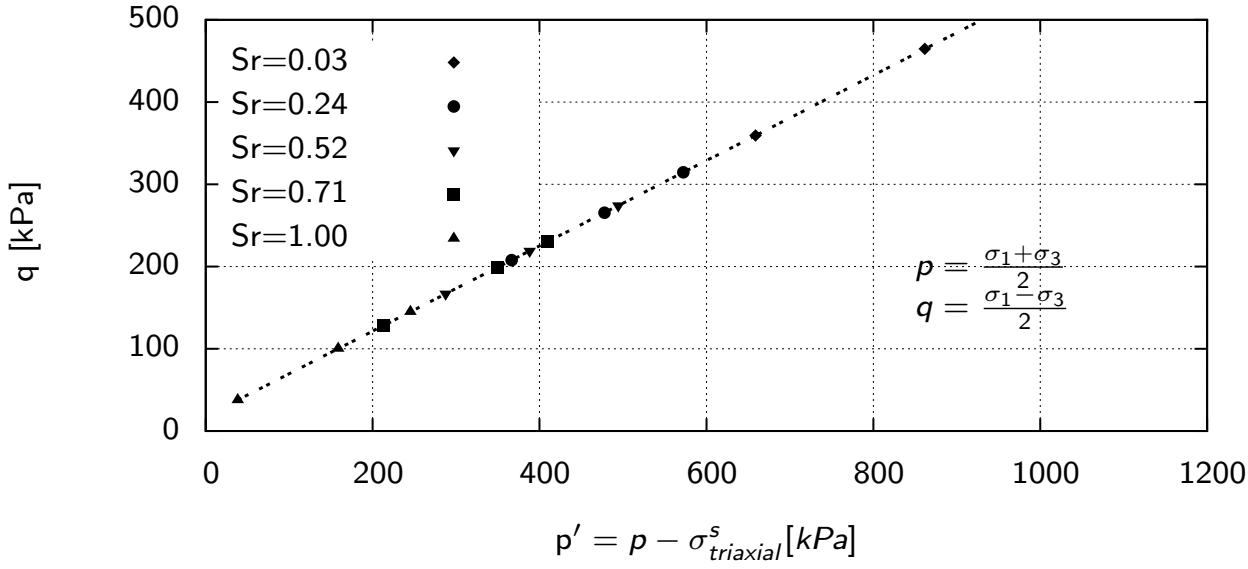

Figure 5.39.: Failure envelope for 50/50 sand-kaolin mixture in terms of effective stress p′; defined as normal stress p, plus suction stress derived from triaxial test results

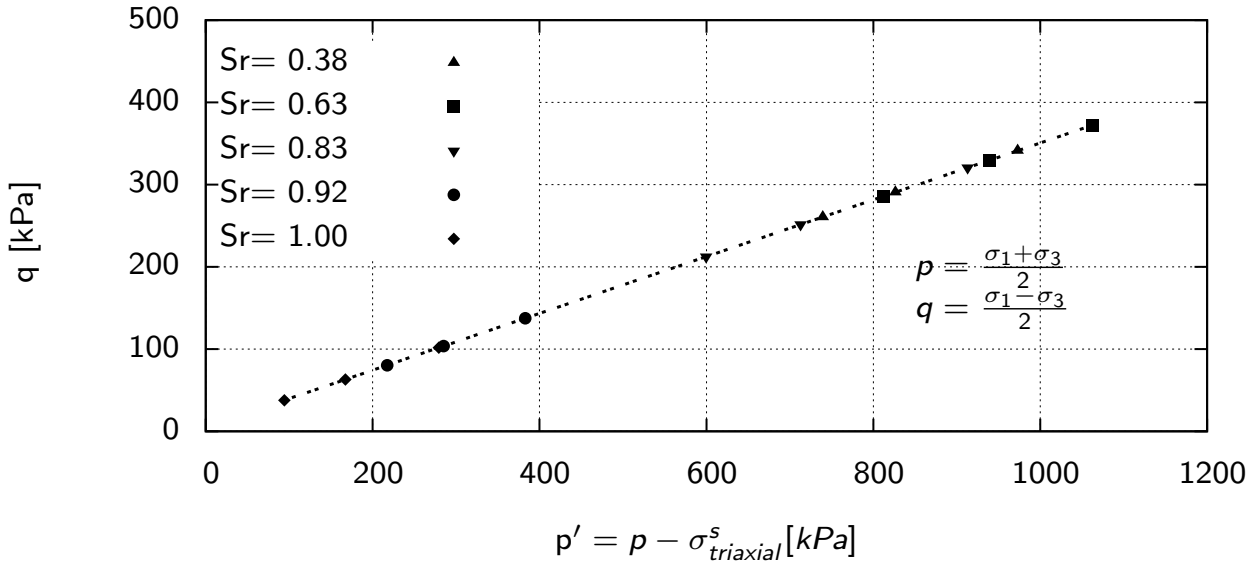

Figure 5.40.: Failure envelope for pure kaolin in terms of effective stress p′; defined as normal stress p, plus suction stress derived from triaxial test results (Brueggemann 1998)

5.6. Summary

Different methods are applied to determine suction stress for sand, kaolin and two mixtures of sand-kaolin (70/30 and 50/50) using different levels of saturation. Direct tensile and triaxial tests were performed to determine suction stress and also the suction stress predicted by SWCC. For sand, the magnitude of the suction stress using different methods shows top-down manner over a relatively small range of matric suction. This shows that for mixtures and pure kaolin the prediction of the suction stress via SWCC are heavily overestimated. This effect seems to become more pronounced with an increasing content of fines and decreasing degree of saturation. It is shown that for materials with fitting parameters, $n¿2$ the curves of suction stress shown sinusoidal manner while for material with $n¡2$ an increasing in suction stress with reduction in degree of saturation is observed. It can be observed from these experiments that the total normal stress failure envelopes converge, resulting in a relatively unique effective stress failure envelope for both results of the direct tensile and shear tests. The fact that the effective stress failure envelopes are unique could be supported the validity of the suction stress measurements via experimental results.

6. Comparison of measured and predicted suction stresses

6.1. Introduction

The results of the MIP are used to estimate the magnitude of different interparticle stresses on suction stress (capillary stresses and physicochemical stresses) by using simple theoretical models.
The results of the experiments are compared with the predicted values by SWCC and models on a microstructural level. The reasons of the deviation between different methods are discussed.

6.1.1. Determination of interparticle stresses via a theoretical method

For the prediction of the interparticle stresses it is assumed that two types of stress act between the particles, physicochemical stresses, which are represented by van der Waals stress as well as capillary stresses.
The van der Waals stress is calculated in line with Eq. 2.12. The specific surface area equal to 50 and 35000 m^2/kg for pure sand and pure kaolin (Pierrat & Caram 1997) and 5500 and 6200 m^2/kg derived from MIP tests for 70/30 and 50/50 sand-kaolin mixtures respectively. The water content amount is determined for different degrees of saturation. The determination of the van der Waals stress for sand, two mixtures of sand-kaolin and pure kaolin is shown in Fig. 6.1. The magnitude of the van der Waals stress highly depends on water content, and it increases towards its maximum values at 0% saturation (Lu & Likos 2006). For high degrees of saturation, the van der Waals stress decreases exponentially.
The capillary stress is the net interparticle stress which has been generated within the

matric of unsaturated granular particles due to the combined effect of negative pore water pressure and surface tension.

Predictions of the capillary force of spherical particles is based on equation 2.13. The liquid−solid contact angle θ is assumed to be equal to zero (Heibrock et al. 2003, Kim & Sture 2008) and the surface tension T_s defined as 0.0728 N/m. To predict the capillary induced tensile strength, the void ratio of 0.65, 0.6, 0.43 and 0.48 are chosen from experiments with pure sand, pure kaolin and two mixtures of sand-kaolin 70-30 and 50-50.

A calculation is done for three different contact numbers "k" equal to 4, 8 and 12. d_{10} was selected as the average particle size. Input data and used parameters for the determination of the capillary tensile strength are shown in Table A.4 and Table A.5 in Appendix B, respectively.

For the determination of the filling angle β, by knowing the water content ω the volume of the water bridge V_{bridge} is determined via equation 2.16.

By choosing a minimum value of β, the two radii of the liquid bridge centers of curvature R_1 and R_2 (Fig. 2.4) are determined through equations 2.14 and 2.15. The obtained values for R_1, R_2 are examined in Eq. 2.17 to check whether the liquid bridge volume between two equal particles from equation 2.17 is fulfilled with the value from equation 2.16. By a systematic increase of β, the minimum value, which satisfies Eq. 2.17, is defined as the filling angle (β) between two monosized particles.

The capillary induced tensile strength was predicted by using Eq.2.18 by changing the fitting parameters, such as the dimensionless separation distance s/R (as illustrated in Fig. 2.4) and the mean number of contact points per particle "k". The response curves that represent the predicted values of capillary induced tensile strength in terms of s/R and k are shown in Figures 6.2 to 6.5 for pure sand, two mixtures of sand-kaolin and pure kaolin.

As seen in Figs. 6.2 to 6.5 for a very low degree of saturation the predicted tensile strength tends to zero. By increasing the dimensionless separation distance (s/R) the curves trend downwards especially at low degrees of saturation. In addition, increasing in the mean number of contact points leads to a reduction of predicted values for tensile strength. In this study, s/R=0.025, 0.0185 and 0.01 are chosen as the separation distance for pure sand, two mixtures of sand-kaolin and pure kaolin respectively. For all materials used $k = 8$ is defined as the contact number.

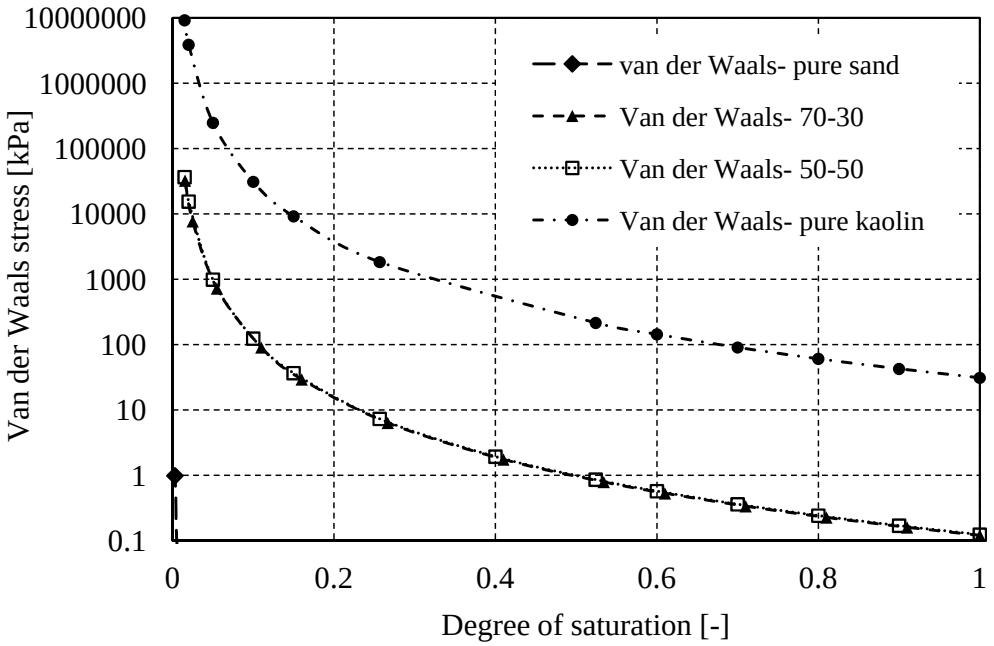

Figure 6.1.: Magnitude of van der Waals stress as function of degree of saturation

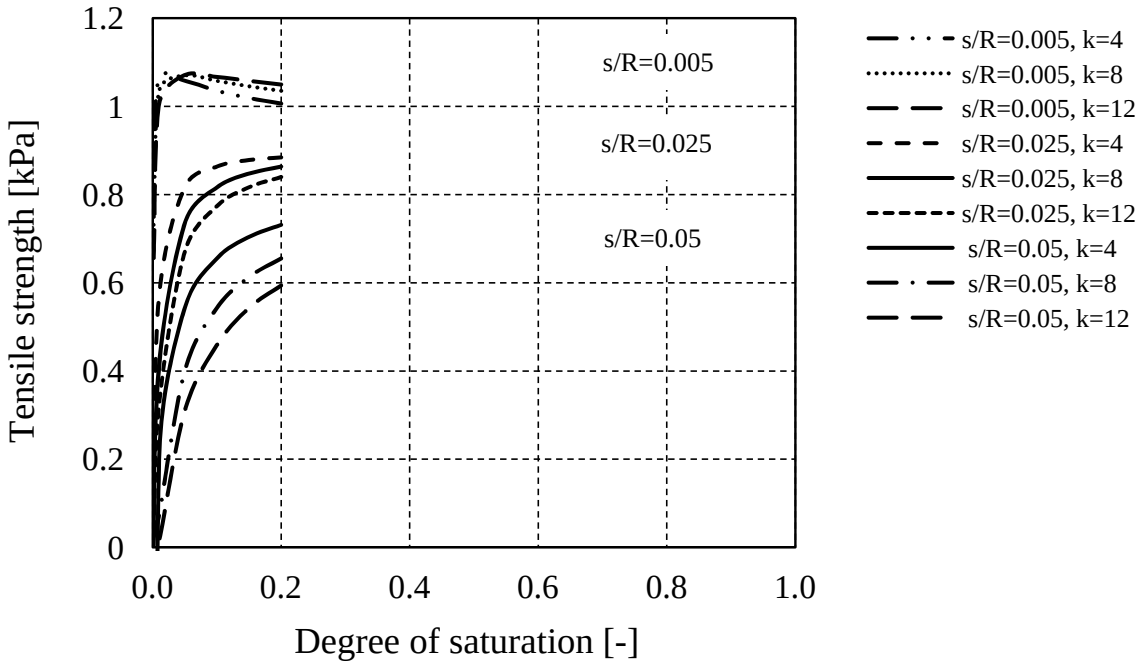

Figure 6.2.: Predicted values of tensile strength for pure sand for s/R= 0.05, 0.025, 0.005 and k= 4, 8 and 10 from capillary theory

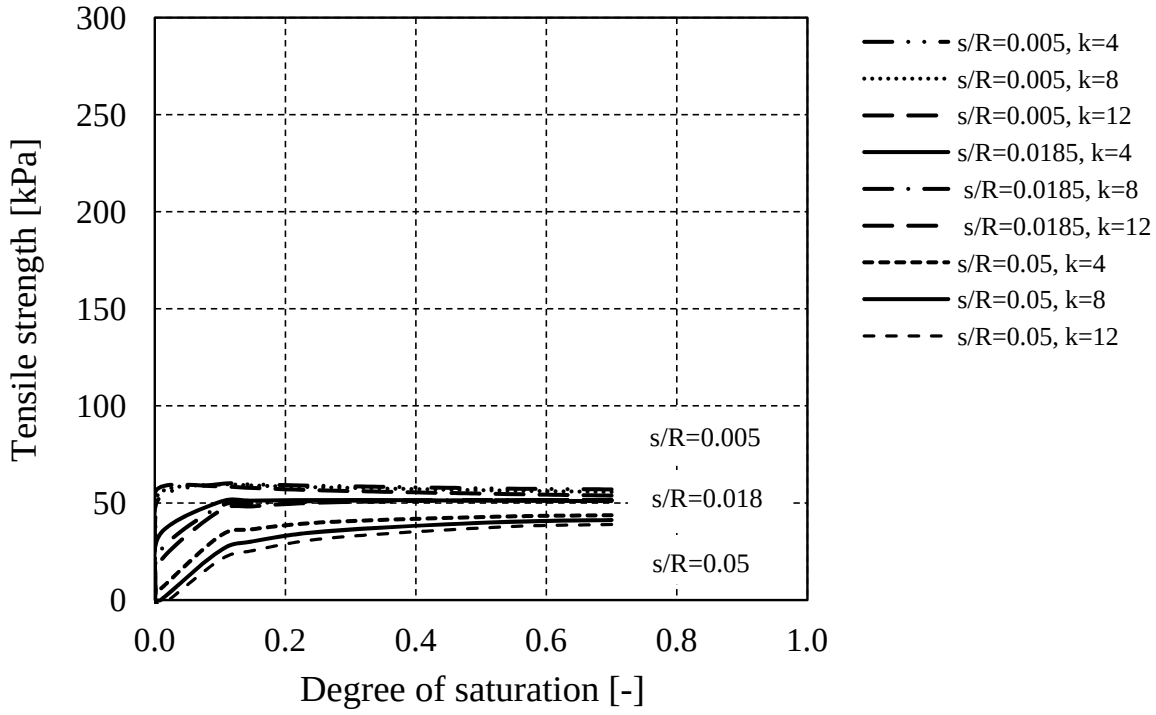

Figure 6.3.: Predicted values of tensile strength for 70/30 sand-kaolin for s/R= 0.05, 0.0185, 0.005 and k= 4, 8 and 10 from capillary theory

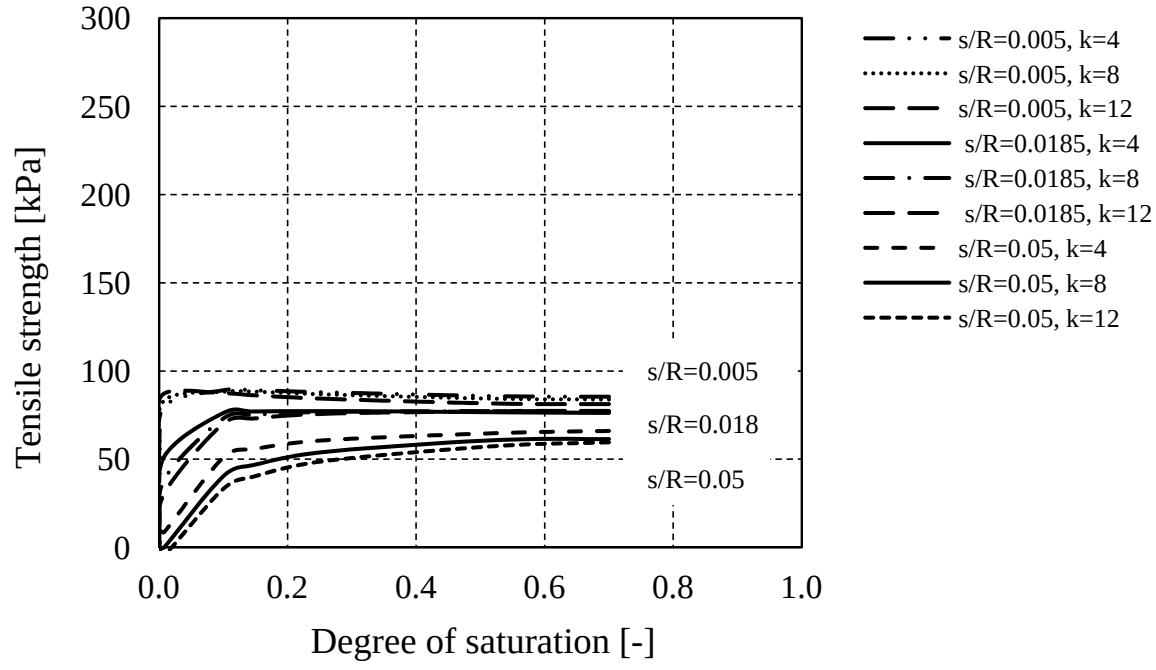

Figure 6.4.: Predicted values of tensile strength for 50/50 sand-kaolin for s/R= 0.05, 0.0185, 0.005 and k= 4, 8 and 10 from capillary theory

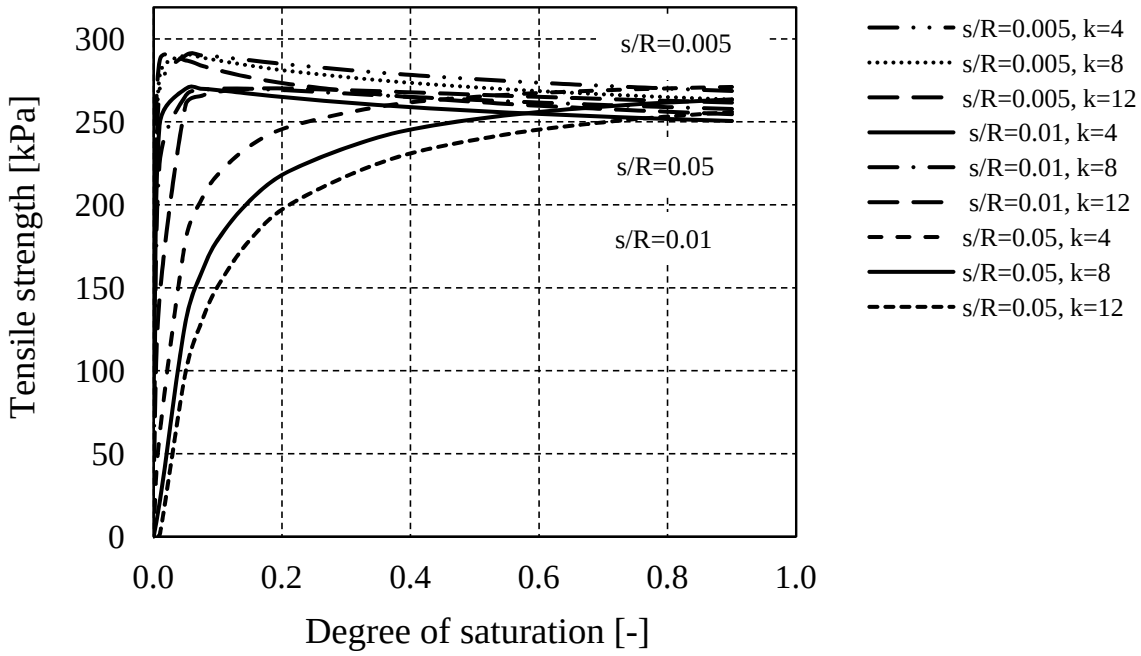

Figure 6.5.: Predicted values of tensile strength for pure kaolin for s/R= 0.01, 0.05, 0.005 and k= 4, 8 and 10 from capillary theory

6.2. Comparison and discussion of models and experimental results

Figures 6.6 to 6.9 summarize the suction stresses predicted from SWCC with Eq. 2.27, and determined values of the suction stress by using the experimental results of the direct tensile test and triaxial test with Eq.2.30 and Eq.2.31 respectively. The suction stress values are compared with the predicted values of the capillary induced tensile strength (Eq.2.19).

All results from the suction stress for pure sand in Fig. 6.6 show sinusoidal manner. The general increase and decrease in suction stress due to a reduction in degrees of saturation can be observed. However, predicted values of suction stress through biaxial shear tests in comparison to other methods are higher, which might be related to the effect of the failure mode. The locations of tensile strength measurements are in line with suction stresses predicted by SWCC. It can be concluded that the suction stress of sand has a magnitude that varies in a sinusoidal manner by changing of the saturation. The results indicate that in the case of sand the van der Waals stress can be safely ignored (Fig. 6.1) and capillary stress is the major reason for suction stress.

Figs. 6.7, 6.8 and 6.9 show that the prediction of suction stress from the drying and scanning SWCC curve and equation 2.27 fails for both sand-kaolin mixtures and pure kaolin. Suction stresses predicted from the SWCC curves severely overestimate the suction stresses derived from tensile and triaxial tests. If the suction stresses derived from experiments are used to define a "suction stress SWCC that gives a good approximation of the derived suction stresses" (see suction stress SWCCs in Figure 6.10) the resulting curve lies outside the SWCC loop composed of the drying and wetting curves of the sample (see Fig. 6.11). This clearly indicates that none of the measured SWCCs (including scanning SWCCs for two sand-kaolin mixtures) can be used to predict suction stresses for compacted samples on the drying path.

The MIP results presented in section 4.6 show that this effect may be partly explained through the test design. This implies that samples used to measure SWCC curves and samples to perform triaxial and tensile tests follow different drying and wetting paths and therefore highlight different soil structures. The main differences occur in the region of pore size between 0.1 to 1 μm. Samples wetted to saturation from a compacted state show a significantly larger volume of pores from the mentioned size compared to the sample at the initial state. When the water content of the saturated sample is lowered again these pores are almost entirely compressed (see Figs. 4.29). Which means that the samples dried from Proctor compacted initial state show significant lower suctions at the same degree of saturation. If the drying path SWCC is used to estimate suction stresses they will be overestimated, as found from the experiments. However this finding remains if not the drying curve but some kind of scanning curve is used to predict suction stress (Figs. 6.7 and 6.8). Independent from the differences found the discussion shows that when using SWCC curves to predict suction stress, the "drying/wetting history of the sample has to be taken into account.

Comparison of suction stress derived from direct tensile tests and triaxial tests in Figs. 6.7 and 6.8 shows that for the 70/30 sand-kaolin mixture, the values of the suction stresses were close to one another for samples with saturations $S_r >$ 0.1 to 0.3. This no longer holds true for the almost air-dry sample where suction stress derived from triaxial tests ("triaxial suction stress") is almost 4 times higher than suction stress derived from tensile tests ("tensile suction stress"). With an increasing the amount of fines to 50 % this effect becomes even more pronounced. For the air dry sample the triaxial suction stress is about 6 times higher than the tensile suction stress. Even for samples with higher saturation rates of about 0.5 or 0.7, this ratio is higher than 2.
For pure kaolin in Fig. 6.9, there are significant differences between the suction stress

through direct tensile and triaxial tests. Fluctuations have been observed for both sets of experimental results. The experimental results show a reduction in the magnitude of tensile strength for relatively dry conditions. It is expected that the suction stress derived from triaxial test result increases for dry condition (Escario & Juca 1989, Futai 2002 and Alsherif & McCartney 2014).

The difference between the suction stress measured by tensile and triaxial tests may result in differences in soil induced structures and kinematics during failure and the fact that the soil-water interactions at different levels of saturation are dominated by different forces. Investigation of the failure zone showed no changes in void ratio or water content (compared to initial state) for tensile test samples, while significant changes in void ratio and no changes in water content and suction were depicted for the triaxial samples (Fig. 4.25).
These differences may contribute towards the observed differences. This result may be interpreted as an indicator for a scale effect. It seems that the tensile failure is dominated by larger scale structures (inter-aggregate pores), while, the smaller scale structures (intra-aggregate pores) have more contribution in shear failure. For relatively dry samples the suction value seems to be dependent on the water content and the changes in void ratio in failure zone has no significant effects on the magnitude of the matric suction.

Figs. 6.3, 6.4 and 6.5 show capillary induced tensile strengths calculated from the model described in section 2.4.2. Depending on the assumptions concerning the contact conditions capillary induced stresses show a more or less constant trend with decreasing saturation until the capillary stress drops towards zero for saturations lower than about 0.1.
The order of magnitude of the calculated stresses correspond to the measured values, supporting the hypothesis that changes in suction stresses with saturation can be explained through capillary phenomena. However, as already mentioned, for the 70-30 mixture tensile and triaxial suction stresses match for saturations higher than 0.3. The values calculated from the capillary model under predict suction stresses derived from triaxial tests and somewhat over predict those from tensile tests. These differences maybe explained in number and the type of contacts that dominate in shear and tensile failure modes. In addition, at various degrees of saturation different interparticle stresses dominate. These differences seem to become more pronounced with increasing content of fines for the 50-50 mixture and pure kaolin.

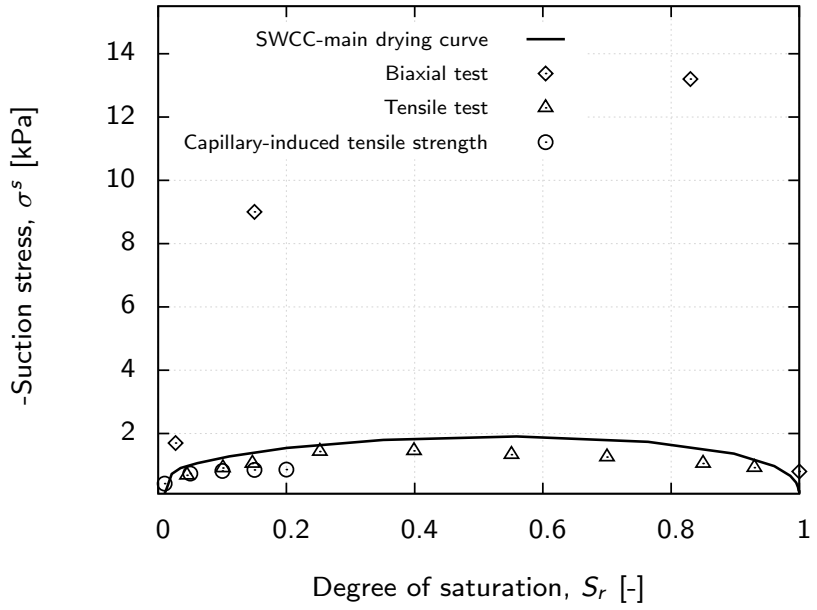

Figure 6.6.: Comparison of suction stress for pure sand, derived from SWCC, biaxial test, direct tensile test and by theoretical method in terms of capillary induced tensile strength

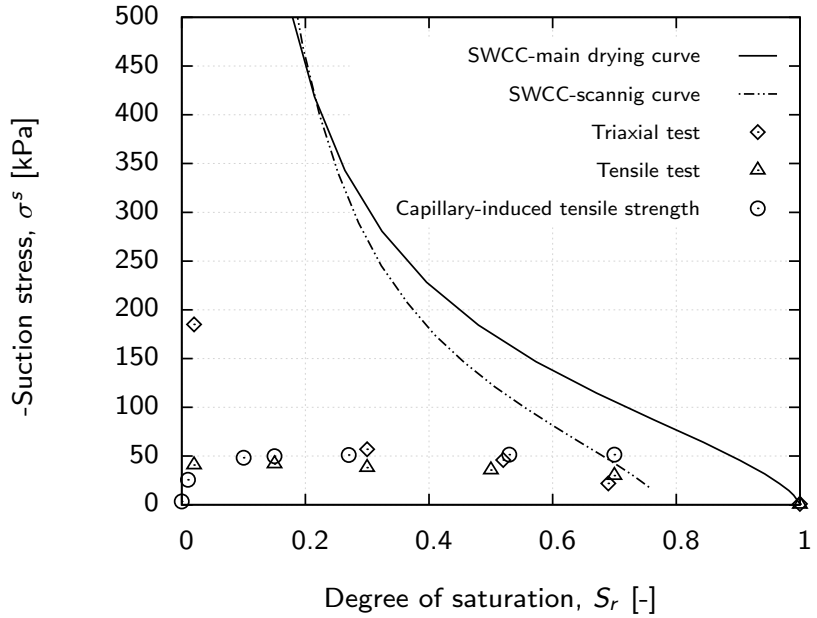

Figure 6.7.: Comparison of suction stress for 70/30 sand-kaolin mixture, derived from SWCC, triaxial test, direct tensile test and by theoretical method in terms of capillary induced tensile strength

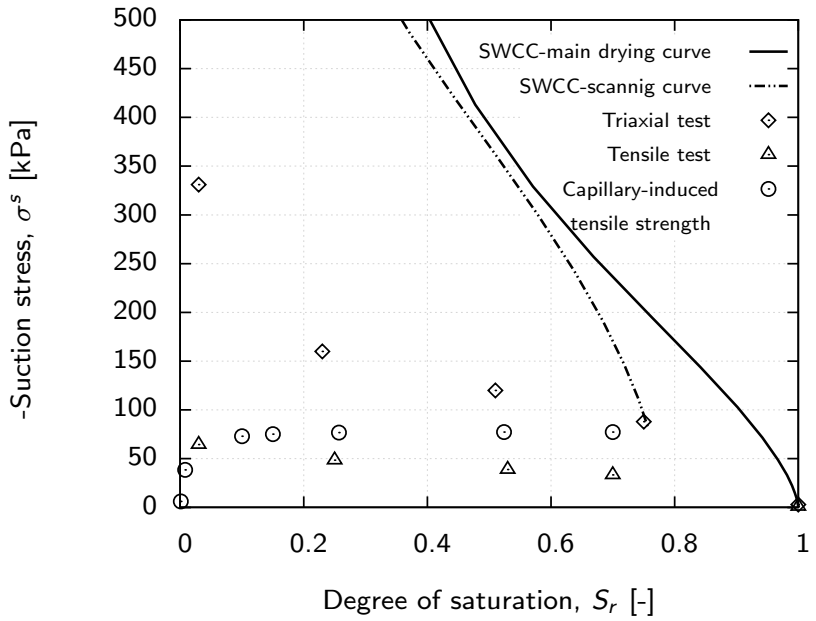

Figure 6.8.: Comparison of suction stress for 50/50 sand-kaolin mixture, derived from SWCC, triaxial test, direct tensile test and by theoretical method in terms of capillary induced tensile strength

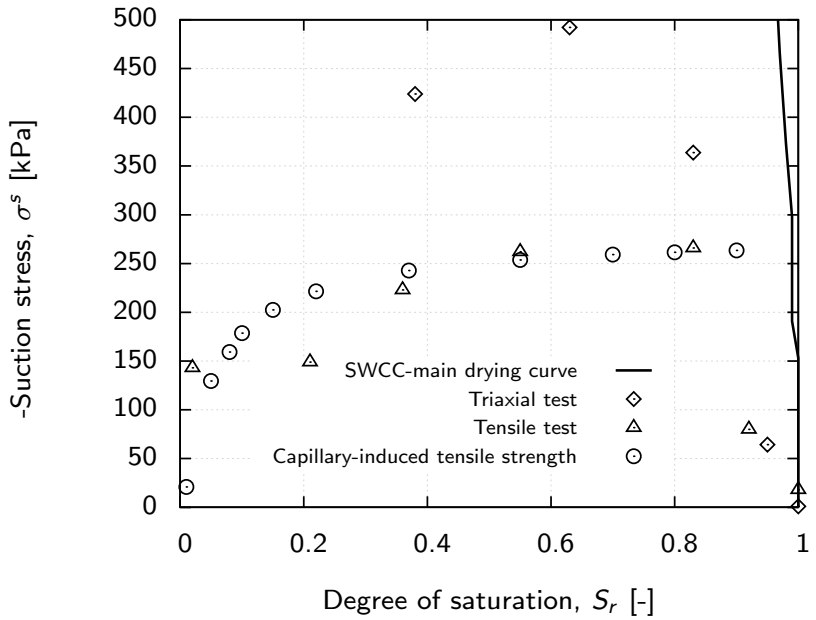

Figure 6.9.: Comparison of suction stress for pure kaolin, derived from SWCC, triaxial test, direct tensile test and by theoretical method in terms of capillary induced tensile strength

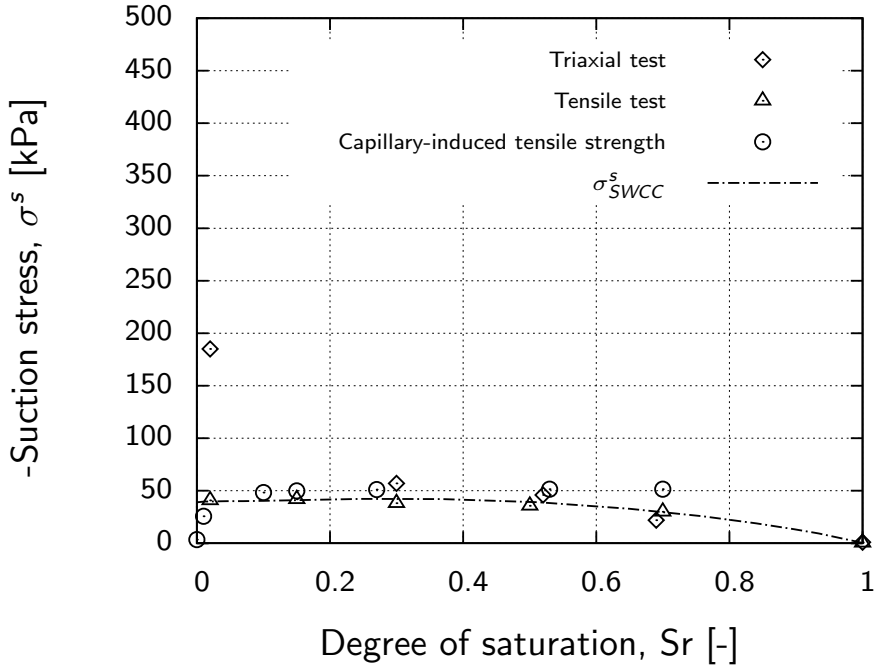

(a)

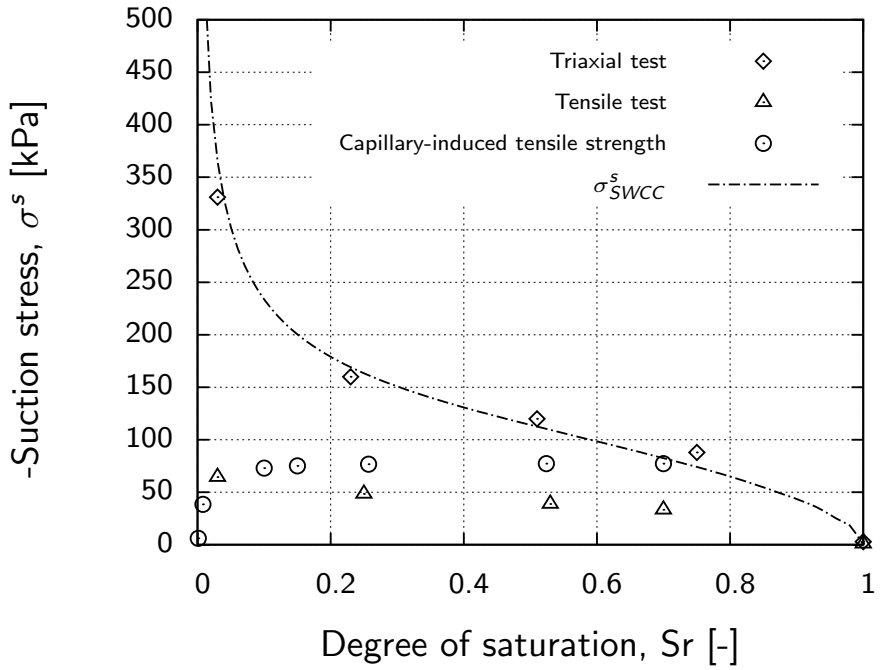

(b)

Figure 6.10.: Determination of suction stress for 70/30 (a) and 50/50 (b) derived from triaxial tests (Eq. 2.31), from direct tensile test (Eq. 2.28), and predicted from the SWCC by back-calculation

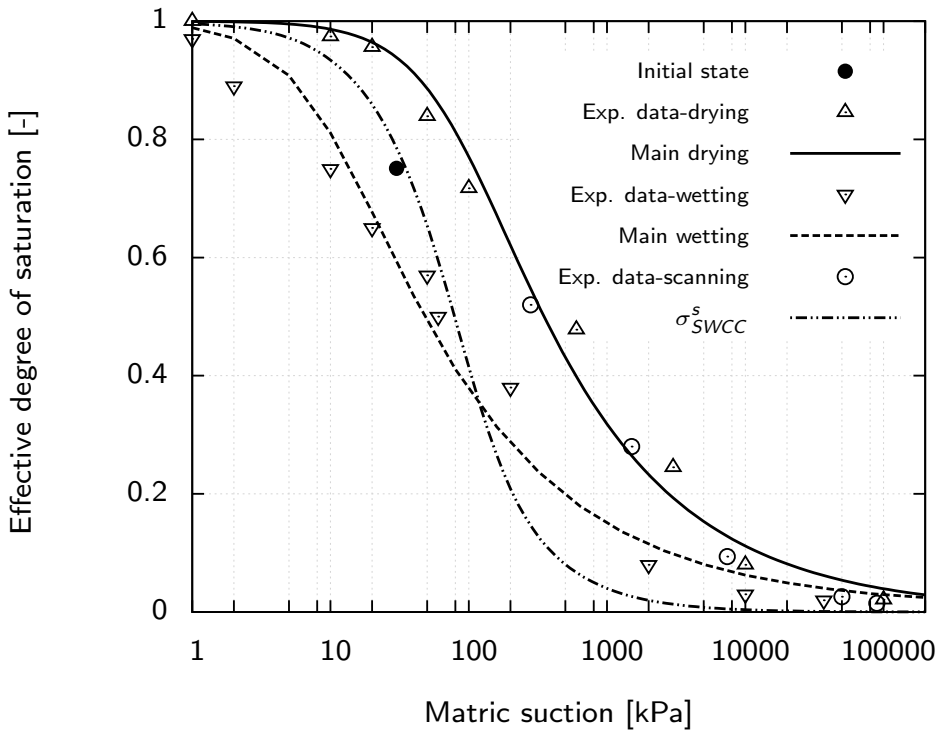

(a)

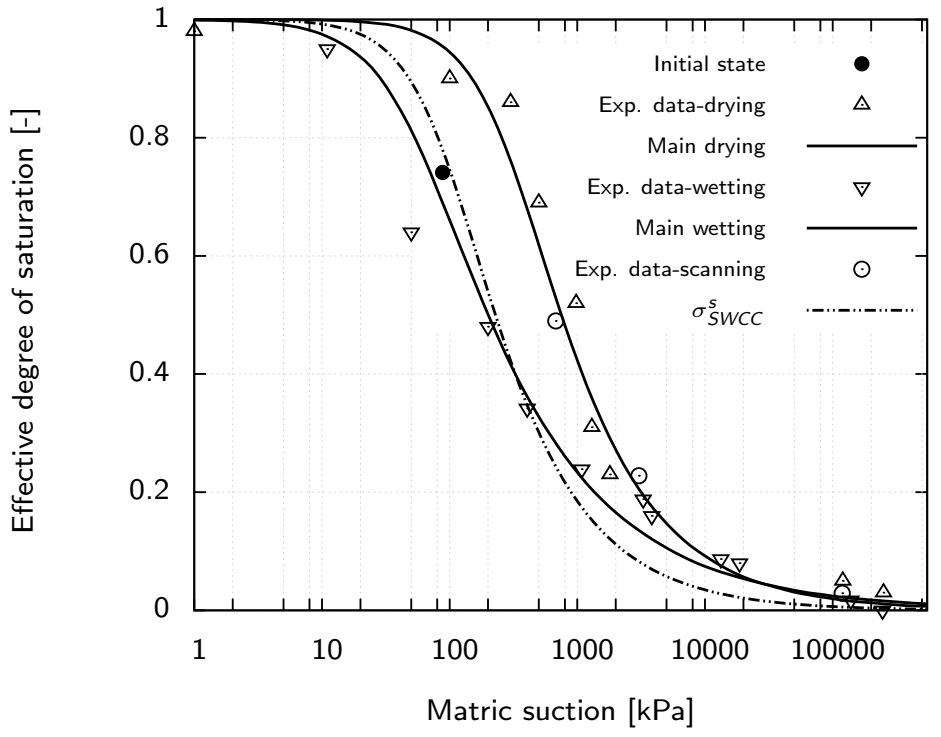

(b)

Figure 6.11.: Determination of SWCCs for 70/30 (a) and 50/50 (b) (drying-wetting) and suction stress SWCCs (best fit to measured suction stress, see Fig. 6.10)

The measured values do not show a decreasing trend for samples with low saturations. Although the analysis maybe somewhat over simplifying but this may be explained by the fact that for two sand-kaolin mixtures at saturations lower than 0.2 the van der Waals stresses increase (see Fig. 6.1) and may start to contribute to suction stress significantly. Generally, for two sand-kaolin mixtures changes in suction stress with saturation seem to be dominated by physicochemical stresses for saturations significantly lower than about 0.2. At saturations higher than about 0.2, changes in suction stress seem to be dominated by capillary stresses.

6.3. Summary

To discuss deviations between predicted suction stresses calculated from SWCC with experimental results, changes in soil pore size distribution with water content have been investigated using the MIP method and experimentally derived suction stresses are compared to suction stresses calculated from simple theoretical models describing the effect of capillary and van der Waals stresses. The suction stress predicted via SWCC is significantly over estimated. The MIP-test results show that this effect may be partly connected to changes in the microstructure of the soil which are not covered by the prediction method using the SWCC. The soil-water interaction at different degrees of saturation is dominated by different interparticle stresses.
Suction stresses derived from tensile and shear tests differ significantly for the samples with a higher content of fines and are more pronounced for low degrees of saturation. Different failure modes and different impacts of suction stress on these modes maybe the reason for differences between the suction stresses derived from tensile and shear tests.

7. Development of Hollow cylinder

7.1. Intention

Although the tensile behavior of materials can be obtained by the direct tensile method, many researchers have questioned the validity of the tensile strength in the past. This may be due to the difficulties in the test equipment and loading conditions such as misalignment and stress concentration. The volume change and creep due to sustained load and the lack of suction controlling are the other negative points in this test. To escape from the mentioned problems a different method concept has been worked out for determination of tensile strength by an indirect method which is called Hollow Cylinder. This chapter presents a new double wall hollow cylinder device for suction controlled testing at low stress levels. The hollow cylinder cell was designed to perform expansion tests in annular soil specimens, with measurements of pressure and volume changes related to the injected water into the cavity wall and volume changes in the inner cell. The device allows one to perform drained and undrained tests.
The majority of hollow cylinder devices developed to date, are using for soil testing under dried or fully saturated conditions. The main feature of the new device is to facilitate the application of the matric suction to use in partially saturated soil via hanging column or axis-translation technique. In addition, for accurate measurement of the volume changes of sample in partially saturated condition, the device is equipped by double wall cell system. The equipment calibration, testing procedures and analysis of typical expansion tests on dry, saturated and partially saturated dense sand are discussed.

7.2. Description of the hollow cylinder apparatus

Figures 7.1 and 7.2 show a schematic view and setup of the new hollow cylinder device that is designed and manufactured at the Ruhr Universität Bochum. The apparatus is capable of testing specimens with 3 cm inner hole radius and 5 cm outer radius.

There are two methods for applying suction to the specimen. Low suctions (up to 20kPa) are applied by using a hanging column with controlled outflow, described by Haines (1930). Higher suctions can be applied with Axis-Translation Technique (Hilf 1956) by applying pore air pressure and pore water pressure through the porous stones and ceramic discs, respectively (see section 3.4.1).

Both top and bottom caps are equipped with two porous stones and two ceramic discs (Fig. 7.3). The ceramic discs are glued to the metal plates using an epoxy resin on periphery. A tight seal between the ceramic disc and metal plate ensures that air will not leak into the water compartment under the ceramic disc. The specimen is placed between two annular platens and the inner and outer of the specimen is covered by two thin rubber membranes. The required connections and valves for the inner and outer of the sample, outer cell pressure and pore-air and water pressures are provided. The outlet has a conical shape and the location of the bleed port on the high point of the top cap also provides the facility to completely remove air bubbles while filling the cavity with water. A desktop computer is linked to the hollow cylinder cell via Pressure Volume Controller (PVC) (Fig. 7.4) (Menzies 1984, Sheahan et al. 1990). The controller precisely regulates and measures pressure and volume change of de-aired water injected to the cavity. The inner cell pressure is applied through the burette volume change indicator. The burette volume change indicators are also employed to measure the overall volume change of the specimen under saturated conditions (back pressure) and for applying suction by hanging column technique. Data are collected by a data logger connected to a computer.

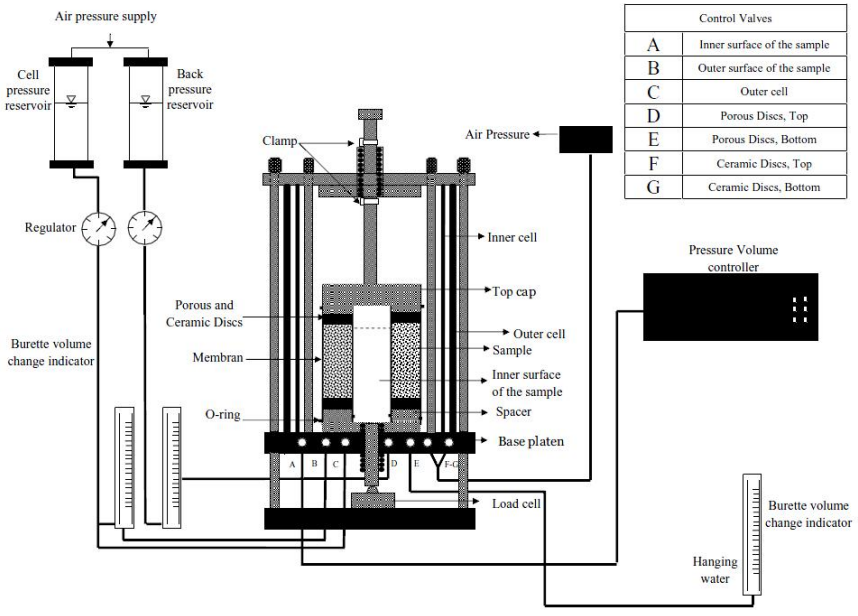

Figure 7.1.: Hollow cylinder test setup (schematic diagram)

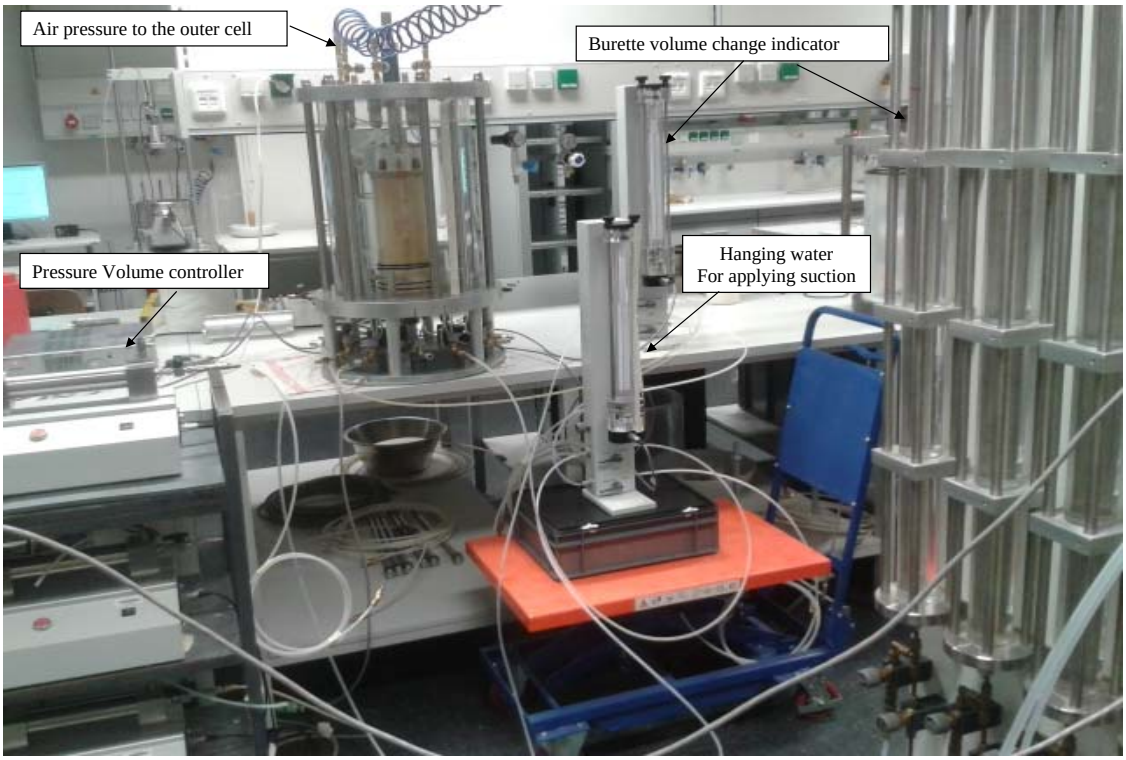

Figure 7.2.: Hollow cylinder test setup

(a)

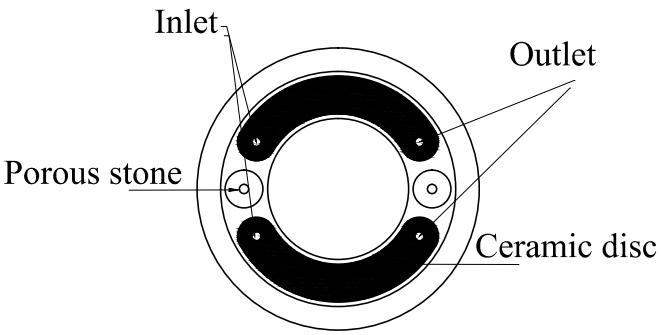

(b)

Figure 7.3.: The bottom view includes the ceramic disc and porous stone

7.3. Used material

The experimental program for this study was conducted on Hostun Sand. Hostun Sand is quartz sand with grain sizes ranging from 0.1 mm to 1.0 mm in diameter. According to the USCS classification, the material is poorly-graded medium sand (SP). The physical properties of the material used are given in Table 3.1 (Lins 2009).
To determine the stress distribution in elasto-plastic region, the shear strength parameters of the sample are needed. In this study the results of the biaxial tests (Table A.3) on sandy soils in dry, partially saturated (matric suction= 2 kPa) and saturated condition are used (Alabdullah 2010).

7.4. System calibration

To enable the new hollow cylinder device to be used accurately in soil testing, it was calibrated for the volume change due to the application of cell pressure. In addition, system components such as a volume change indicator and pressure volume controller were carefully calibrated.

7.4.1. Calibration of volume change indicator

A twin-burette volume change indicator was used to measure the volume changes of the inner cell. The calibration of this device was conducted by filling the burette stepwise with de-aired water and recording the corresponding electrical reading of the data logger connected to the volume change indicator. The calibration was conducted in case of filling and emptying the burette. The relationship between the electrical reading, R_e (mv), and the burette reading, R_b (cm^3), are shown in Figures 7.5a and 7.5b, which are used for the determination of the volume changes in inner cell and samples (back pressure).

7.4.2. Calibration of pressure volume controller

PVCs are digital microprocessor-controlled actuators (Fig. 7.4). The PVCs precisely regulate and measure pressures and volume changes.
This device is ideal for pumping at a constant flow rate.

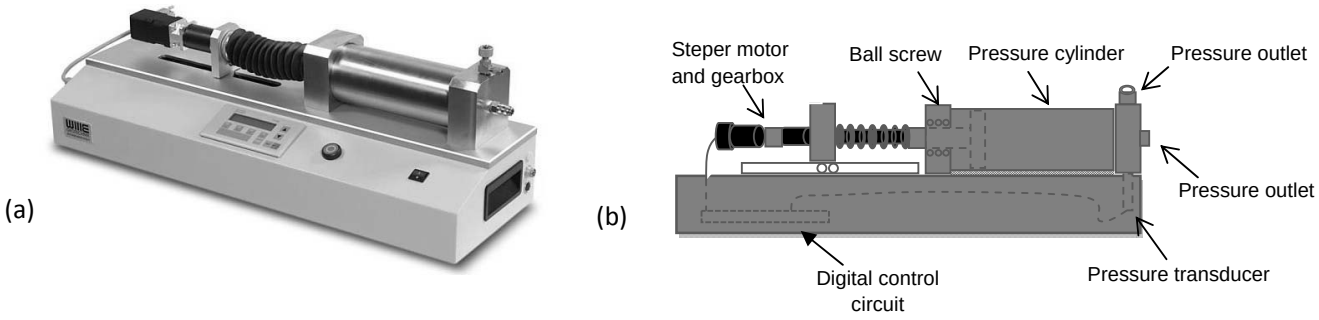

Figure 7.4.: (a) Automatic pressure/volume controller (b) principles of operation of PVC

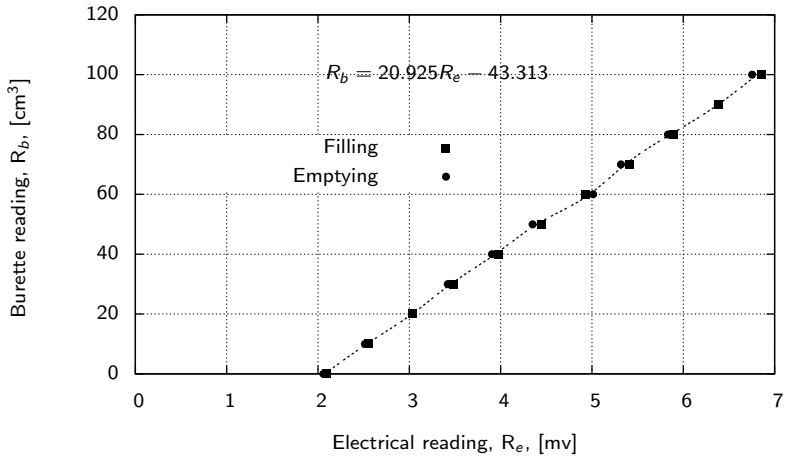

(a)

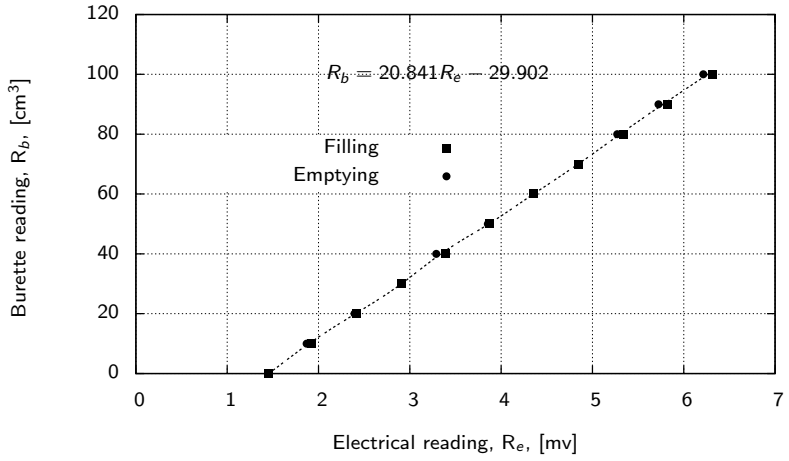

(b)

Figure 7.5.: Calibration of the volume change indicator: (a) inner cell (b) back pressure

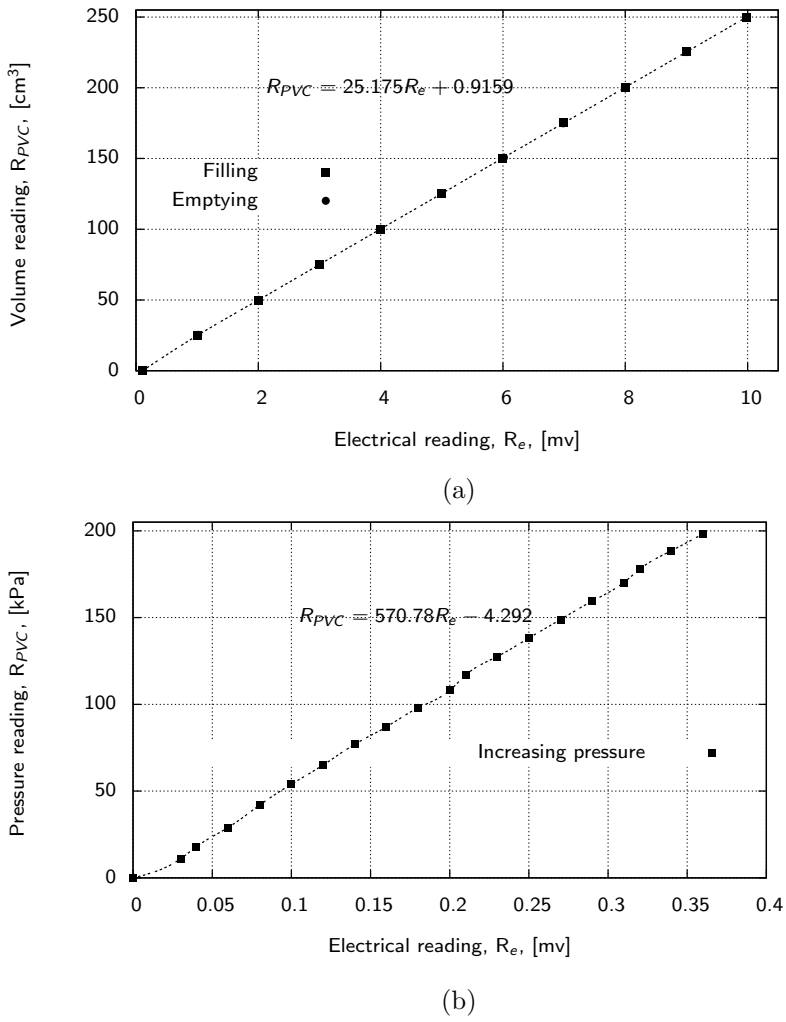

Figure 7.6.: Calibration of the pressure volume controller: (a) volume change (b) pressure

Constant pressure can also be used to provide a constant gradient pressure, as well as to determine volume changes. PVC can be considered as a desired device to be replaced with traditional laboratory pump sources and volume change gauges. De-aired water in a cylinder is pressurized and displaced through a piston moving in the cylinder to reach the target value. The piston is actuated by a ball screw turned in a captive ball nut by a stepping motor and gearbox that move rectilinearly on a ball slide.

The calibration of this device for determination of the volume changes in the cavity wall was conducted by filling and emptying of the pressure cylinder with de-aired water and recording the corresponding electrical reading of the data logger connected to the pressure volume controller.

The calibration of the device for pressure was also conducted by pressurizing the pressure

cylinder and comparing with reference manometer. The relationship between the electrical reading, R_e (mv), and the PVC reading, R_{PVC} in terms of (cm^3) and (kPa), is shown in Figure 7.6.

7.4.3. Calibration of the inner cell using a saturated soil specimen

To perform partially saturated testing double wall cell method is provided in this study (Fig. 7.7). Double wall cell system enables variable suctions to be applied whilst providing accurate measurement of soil volume change. The double wall cell arrangement allows the inner and outer cell pressures to be kept at the same value and to produce zero expansion of the inner cell and to measure the volume change from a volume change of the inner cell. The reliability of the system was checked by testing a saturated sample under expansion. For a saturated sample, the total volume change of the specimen during the test (i.e., difference of the volume change in cavity and inner cell) is equal to the volume of water drained out of the specimen.
In this study p_i is related to the applied pressure to the cavity or inner surface of the sample and the pressure in the inner cell or outer surface of the sample is called p_o (Fig. 7.7). The volume change of the saturated specimen was measured using two methods, namely A and B. In method A, the double wall cell technique was used. The difference of the injected water to the cavity and outflow of water from the inner cell is measured. In method B, the volume of water expelled from the specimen was measured using a burette. Figure 7.8 shows the volume changes measured by two methods versus the differential of the cavity and inner cell ($p_i - p_o$). The measurements showed similar results between the volume changes measured by method A and B.

7.5. Experimental program

The laboratory tests consist of program to investigate the behavior of dry and saturated samples by using the new hollow cylinder device. Additionally, the influence of applied matric suction on the mechanical behavior has been studied.
Table 7.1 summarizes the applied confining pressure and matric suction in the tests performed on dry, saturated and partially saturated Hostun sand.

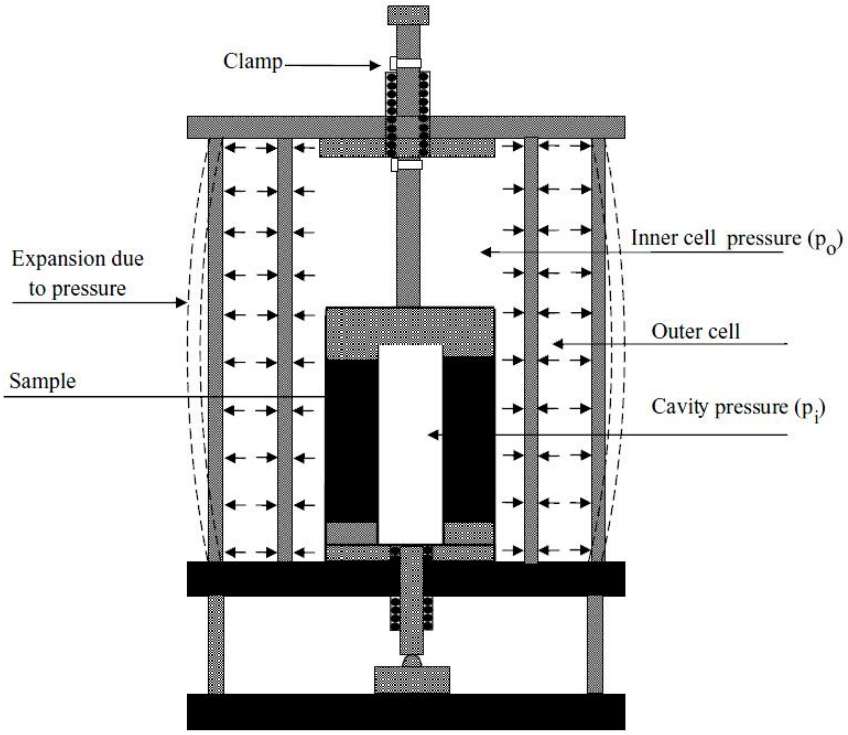

Figure 7.7.: The concept of the double-wall call

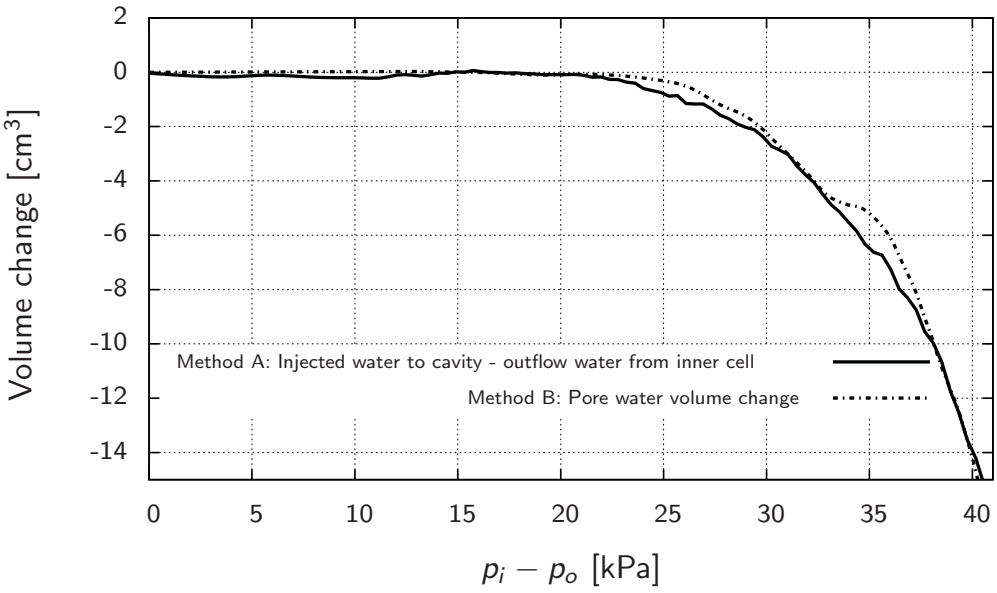

Figure 7.8.: Volume changes of saturated sample measured by two methods: A and B

Table 7.1.: Summary of tests performed by the hollow cylinder device

Dense Hostun sand ($e_0 = 0.7$)		
Condition	Confining pressure [kPa]	Matric suction [kPa]
Saturated	50	-
Partially saturated	50	2
Dry	50	≥ 20

7.6. Sample preparation

1. The inner membrane of 60 mm in diameter and 200 mm in length was put to the bottom of the base pedestal. Three bolts were used to seal the inner membrane. Inner split mold was stood on the base supported (Fig. 7.9-1).
2. An outer membrane of 100mm in diameter and 200mm in length was put outside the base pedestal using two rubber O-rings (Fig. 7.9-2).
3. The outer mold was assembled by screwing on the base pedestal. The outer membrane was stretched against the outer mold. The vacuum is applied to the outer mold (Fig. 7.9-3).
4. Weighted soil for the required relative density was poured into the cavity using the dry funnel pluviation method and distributed uniformly (Fig. 7.9-4).
5. The top cap was gently seated on the top of the specimen. Then outer and inner membranes were rolled up around the top cap and sealed with O-rings, two for the outer membrane, one for the inner membrane. Vacuum was imposed by the bottom drainage tube to prevent the specimen from collapsing. The inner mold was pulled out (Fig. 7.9-5).
6. The top cover was positioned on the top cap and tightened using four bolts. After this, the outer mold was removed (Fig. 7.9-6).
7. After the specimen was set up, the final height and outer diameter of the specimen were measured Fig. 7.9-7).

8. By placing the loading piston in contact with the specimen the cell chambers were brought down and tightened. The cavity, outer and inner cells were filled with water. The pressure is applied to the inner and outer cells and into the cavity, then the vacuum was removed from the specimen (Fig. 7.9-8).

7.7. Test procedure

7.7.1. Initial state

7.7.1.1. Dry sample

After preparing dry soil sample, the cavity, inner cell and outer cell were pressurized to the same pressure. This was done to eliminate any possible changes in the applied pressures (Fig. 7.10 - sample preparation). The pressure to the cavity and inner cell was applied by an air supply pressure through two separate volume change indicators. For the outer cell (where the volume change is not of interest) the cell pressure was applied through conventional air supply pressure.

7.7.1.2. Saturated sample

To prepare saturated sample de-aired water was flushed through the specimen from the lower pore water pressure tube to the upper pore water pressure tube. The pressures in the cavity (p_i) and inner cell (p_o) were applied by an air supply pressure through of two volume change indicators (Fig. 7.10 - sample preparation). For the outer cell, the cell pressure was applied through conventional air supply pressure. The back pressure (p_b) was applied through a volume change indicator which is connected to a separate pressure controller system.
The pressures in the cavity, inner cell, outer cell and back pressure were increased simultaneously to reach target values. The difference between the cavity and inner cell with back pressure is defined as confining pressure ($p_{i,o} - p_b$). The sample was left a couple of hours for saturation (Fig. 7.10 - saturation). After saturation, the Skempton's B-value assessment was used to check the degree of saturation.

(1)

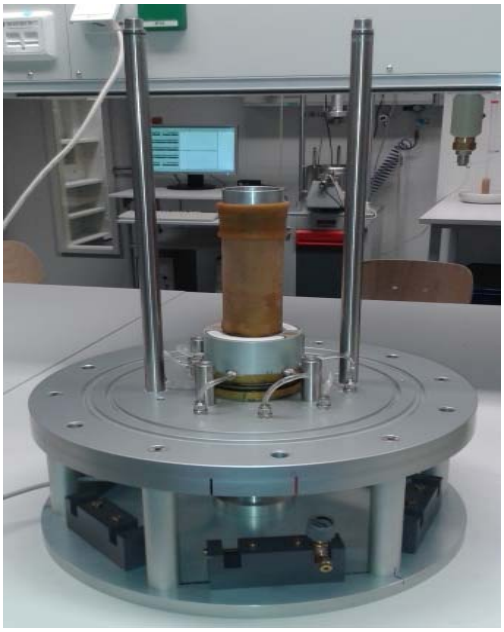

(2)

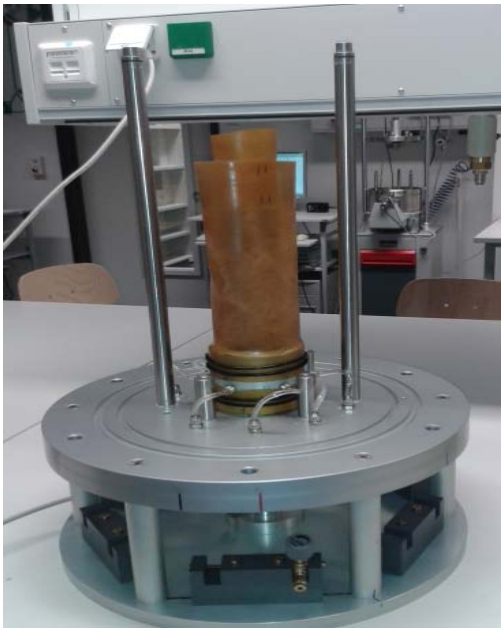

(3)

(4)

(5)

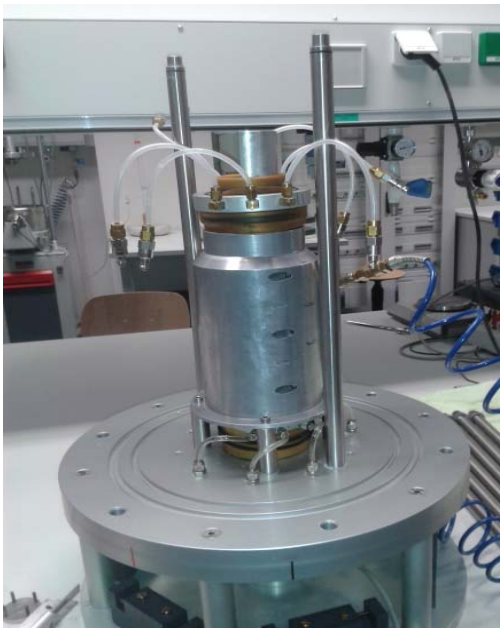

(6)

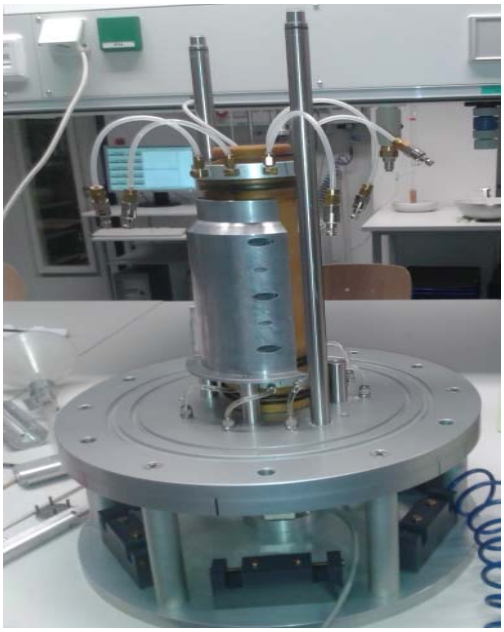

(7)

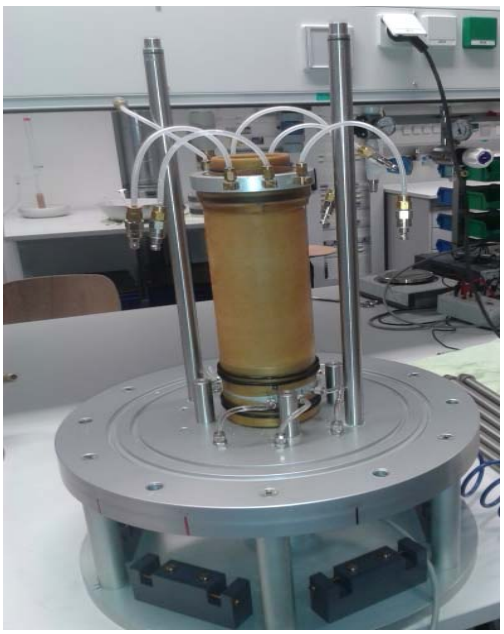

(8)

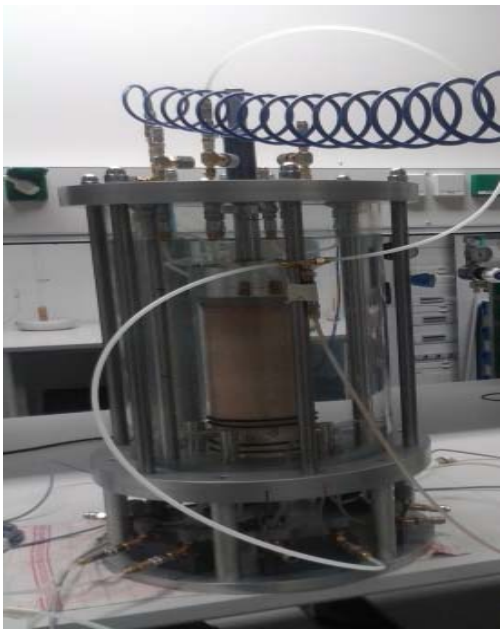

Figure 7.9.: Sample preparation

7.7.1.3. Partially saturated sample

The application of suction to partially saturated samples was conducted with the hanging water column technique. After saturation of the sample, while the difference of pressure between the cavity and inner cell with back pressure was kept constant, pressures was reduced gradually up to back pressure equal to zero.

The pore air pressure in the soil specimen is connected to atmosphere, so it is considered to be zero. The pore water pressure in the specimen is controlled using the hanging column technique with controlled outflow (Haines 1930, McCartney et al. 2008). With the hanging column technique, a static column of water is maintained below a water-saturated porous disc. The height of this column of water corresponds to the matric suction at the bottom of the specimen. Although the matric suction varies linearly with height within the specimen, this is currently the best approach to accurately control matric suction in partially saturated sands due to their low air-entry suction (Khosravi et al. 2010). When there are no more outflows and the water level in the burette becomes constant, the sample has reached the applied suction value (Fig. 7.10 - applying suction using a hanging column).

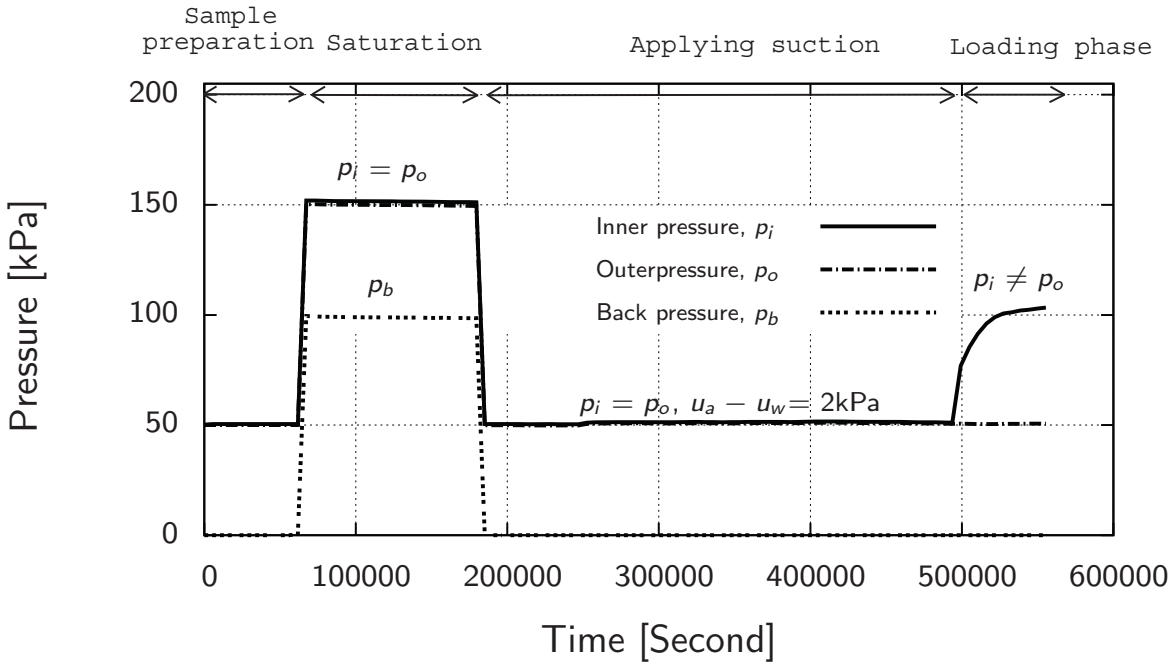

Figure 7.10.: Pressure variations throughout the test procedure

7.7.2. Loading phase

Upon reaching consolidation, the Pressure Volume Controller (PVC) was connected to the cavity and set to the applied pressure (p_i). By synchronizing the pressure in the cavity and PVC, the pressure applied was shifted from the air supply pressure to the PVC. The volume change of the inner cell was measured by the burette volume change indicator through the air pressure controller.

While the pressure in the outer (p_o) (inner cell) of the sample and outer cell was held constant, water injection rate of 0.1 (cm^3/min) was set to the cavity.
Injection of water to the cavity leads to an increase in pressure and volume change. Under this condition, the pressure and volume changes in the cavity and inner cell were monitored continuously by PVC and volume change indicator.
The maximum applied pressure to the cavity was recorded for each test.

7.8. Test results

A series of tests were performed on isotropically consolidated samples ($p_i = p_o = 50\,kPa$) under saturated, partially saturated (matric suction= 2 kPa) and dry conditions. In Fig. 7.11, the differential cavity pressure ($p_i - p_o$) and volume change of the sample ($\Delta V_{CH} - \Delta V_{IC}, \Delta V_{CH}$ is the injected water to the cavity, ΔV_{IC} is the outflow of water from the inner cell) is illustrated in the loading phase.
Figure 7.12, shows the difference between the inner and outer pressure ($p_i - p_o$) versus volumetric strain; $(\Delta V_{CH} - \Delta V_{IC})/V_{Initial}$, where $V_{Initial}$ is the initial volume of the specimen.
By increasing of the cavity pressure from $p_i = p_o$= 50 kPa, the specimen shows linearly elastic behavior. Then it reaches the yield point (critical pressure) at relatively small volumetric strains (see section 2.9.2). The deformation of the soil at the beginning is purely elastic. As the cavity pressure (p_i) increases further, a departure from linearity can be observed (Karner et al. 2003; Moller et al. 2006; Amanullah Marri 2010). This behavior occurs at relatively small volumetric strains (Fig. 7.12).
By reaching the cavity pressure to the critical pressure (initial yielding), further increasing of the differential pressure ($p_i - p_o$) leads to the extension of the plastic zone along with the peak cavity pressure.

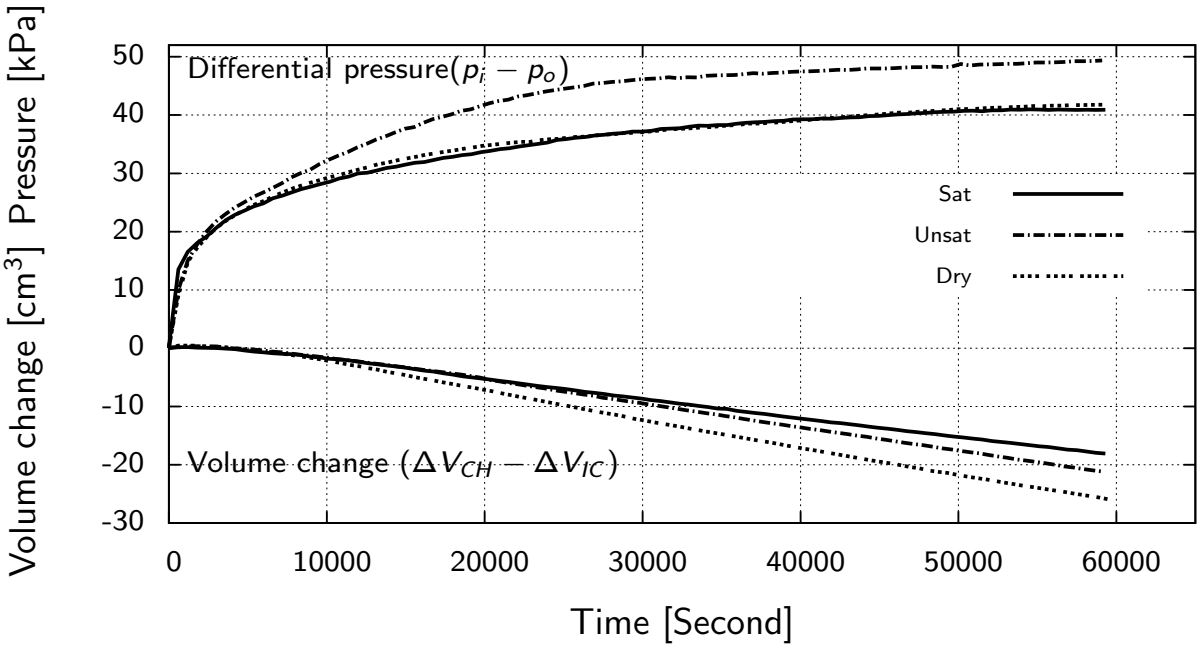

Figure 7.11.: Differential cavity pressure and volume change ($i = 0.1cm^3/min$)

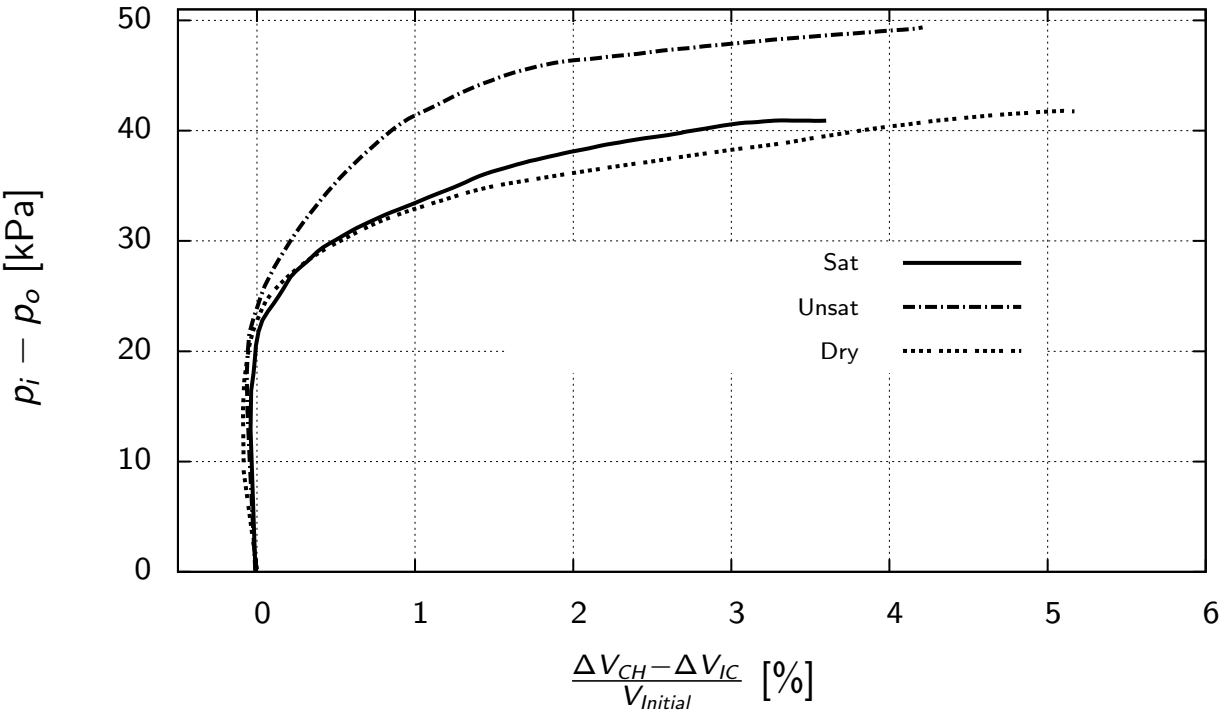

Figure 7.12.: Variation of differential cavity pressure and volume changes in expansion process ($i = 0.1cm^3/min$)

In saturated state, all voids are filled with water, by applying matric suction the capillary neck is formed at the contact points between neighboring particles which lead to capillary stresses and an increase in peak cavity pressure.

Through reduction in water content and upon reaching a dry condition capillary stresses between particles will be lost leading to a reduction of peak cavity pressure. As a result it is possible that the sand behaves in different ways, depending on the distribution of air and water. This all impacts the overall peak cavity pressure of sand.

7.9. Analysis of the test results

The estimation of radial and tangential stresses in elastic and elastic-plastic zones is estimated with a semi analytical solution proposed by Yu (2000) (see section 2.9.2).
When the cavity pressure (p_i) increases from the initial condition ($p_i = p_o$= 50 kPa), the material initially behaves elastically. When $p_i - p_o$ reaches a critical pressure (p_{cr}) (Eq. 2.36) the plastic zone starts at the inner surface of the cavity wall and the plastic region spreads within the sample. The radius of the plastic region extends outwards by increasing differential cavity pressure.

When the differential cavity pressure reaches a state of full plasticity ($p_i - p_o = p_{plastic}$) (Eq. 2.44) the plastic region extends to the outer of the cavity wall. Fig. 7.13 shows the propagation of the plastic radius (black points) along the thickness of the sample when the differential cavity pressure for saturated, partially saturated and dry samples is increased. For a fully plastic state, the greatest magnitude of tangential stress (Eq. 2.38) occurred at the outer radius of the sample.

The radial and tangential stresses on the outer side of the cavity wall for saturated, partially saturated and dry specimens related to the fully plastic state, are illustrated in Figure 7.14. As seen under the partially saturated condition, and under the fully plastic state, tangential stress reaches the tension zone.

Based on the proposed solution, the determined values of radial and tangential stresses are summarized in Table 7.2. As a general trend, the values of the theoretically predicted critical pressure (p_{cr}), and fully plastic pressure ($p_{plastic}$) are lower than the measured values by the hollow cylinder device.

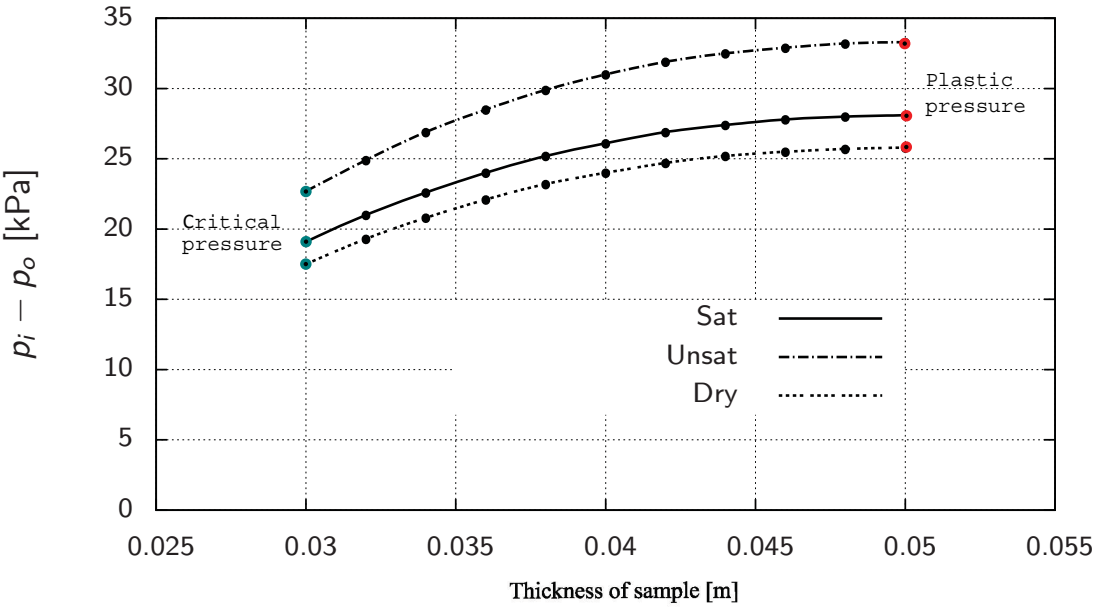

Figure 7.13.: Variation of plastic zone (c) with differential cavity pressure ($P_i - P_o$)

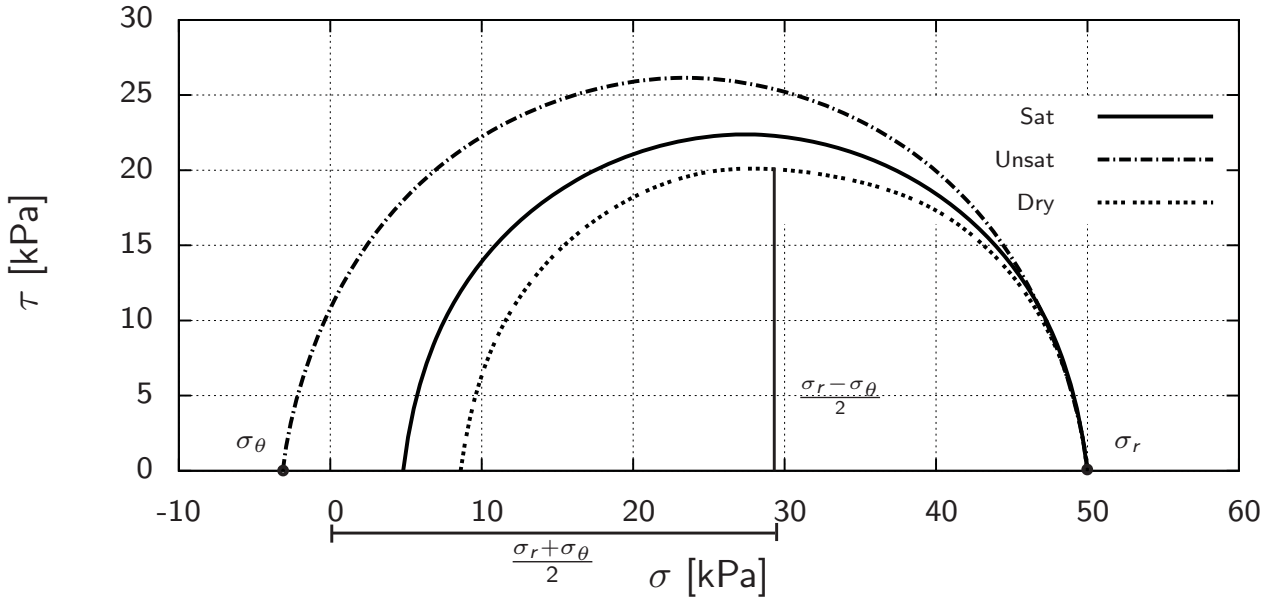

Figure 7.14.: Mohr circle representation of stresses in saturated, partially saturated and dry condition for fully plastic state

Table 7.2.: Theoretical and experimental values of σ_θ, critical pressure and fully plastic pressure

Sample	Confining pressure P_o $[kPa]$	Theoretical Critical pressure P_{cr} $[kPa]$	Theoretical σ_θ in plastic region $[kPa]$	Theoretical fully plastic pressure $[kPa]$	Experimental Failure pressure P_i $[kPa]$
Saturated	50	69.1	-4.8	78.1	90.92
Unsaturated	50	72.7	3.1	83.2	99.1
Dry	50	67.5	-8.6	75.8	92.04

7.10. Determination of the suction stress

In the cavity expansion test, when the tangential stress (σ_θ) reaches tensile strength, the failure will occur in tensile mode. Therefore, based on the concept of suction stress proposed by Lu & Likos (2006), the tangential stress in cavity expansion tests can be replaced by suction stress in tensile failure mode (see section 2.6.2).

In Fig. 7.15 the suction stress is predicted from SWCC by using the closed-form equation 2.27, proposed by Lu et al. (2010). Meanwhile, the maximum value of tangential stress under a fully plastic state in partially saturated condition is implemented for suction stress. In addition, the suction stress determined by biaxial tests (Alabdullah 2010) and direct tensile test (Lu et al. 2007) are compared with those predicted via the models on microstructure level (section 6.1.1).

As observed in Fig. 7.15, all results of the suction stress for pure sand show sinusoidal behavior similar to an up-and-down behavior. While suction stress values determined by biaxial tests are often higher than values produced by other methods, the experiments by direct tensile test are in good agreement with the predicted values of the suction stress with SWCC and the theoretical model.

The location of tangential stresses determined by hollow cylinder in dry, saturated and partially saturated conditions are in line with suction stresses predicted via SWCC, direct tensile test experiments and the theoretical model.

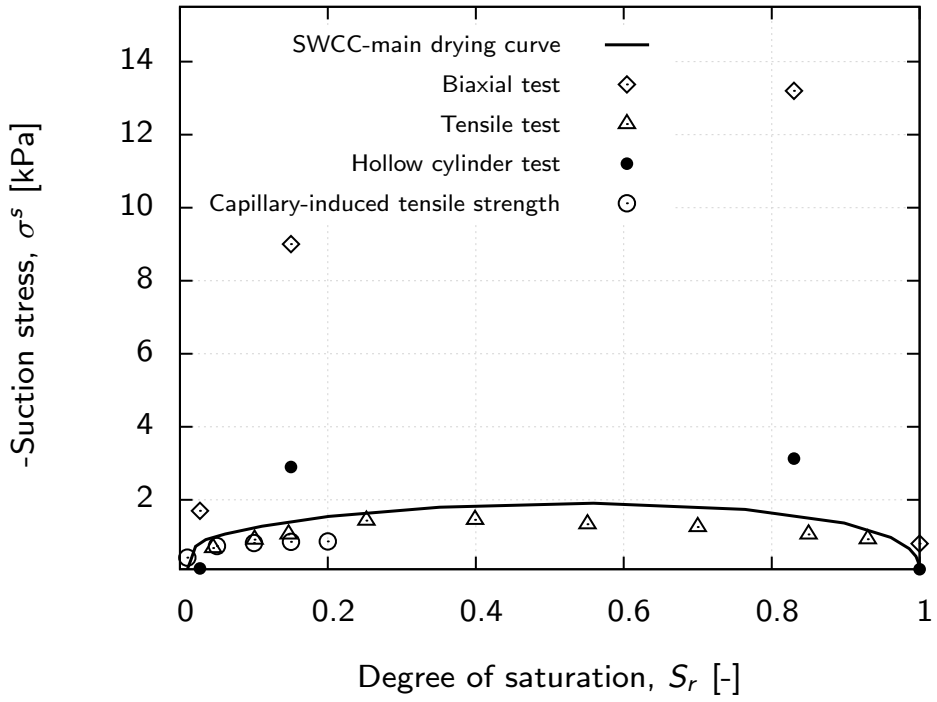

Figure 7.15.: Suction stresses in terms of degree of saturation

7.11. Summary

A new hollow cylinder apparatus was developed to perform expansion tests on cylindrical soil specimens. This was designed to measure tensile strength in thick-wall cylinders. The fully automated apparatus is equipped with a double wall cell to minimize any volume change between the inner and outer cell. Meanwhile, the arrangement of the ceramic disks in the top and bottom caps, and the facility for applying suction via the hanging water column technique, makes it appropriate for performing partially saturated tests. The principles of the process of cavity expansion in sandy soils have been studied using laboratory experiments and analytical solutions. Tests are performed on saturated, partially saturated and dry, dense sand under a confining pressure of 50 kPa.

By increasing the water injection pressure to the cavity, the specimen shows a linearly elastic behavior. It then reaches the yield point at a relatively small volumetric strain. The radial and tangential stresses in the elastic and elastic-plastic region have been determined by the analytical procedure proposed by Yu (2000).

As a general trend, the magnitude of the theoretically predicted critical pressure (p_{cr}), and fully plastic pressure ($p_{plastic}$) are lower than the values measured by the hollow cylinder

device. Comparisons of results obtained for suction stress show complimentary results between the determined values derived from hollow cylinder with those predicted via SWCC and theoretical methods and direct tensile test experiments.
The results indicate that for partially saturated conditions the tension failure has been reached and for saturated and dry conditions no tensile failure observed.
A comparison of the experimental results with theoretical solutions based on cavity expansion theory, indicates that the design tool has the potential to provide a reasonably accurate assessment of tensile strength for sandy soils.
Although, the test results of hollow cylinder show a good agreement with the experiments and theoretical approach but there are some shortcomings which should be considered:

- As the sandy soil is unstable, sample preparation for performing unconfined and low stress expansion test on this soil is very difficult.
- The small volume changes of the specimen in comparison to the volume of the inner cell can lead to difficulty in accurate measurement of volume changes. To overcome this problem it is recommended to reduce the volume of the inner cell.
- The maximum permissible size of aggregate in the hollow cylinder test specimen is smaller than in that of direct tensile test.
- Assumptions such as material is either linear elastic or plastic are required in order to calculate the stress distribution. These assumptions are not an exact description of actual material.
- According to the proposed solution of Yu (2000), the stress distribution in elasto-plastic region has to be calculated by using the parameters c and φ.
- The compressive stresses on any point in the failure plane are non negligible. This indicates that tensile stress is not strictly applied and the soil specimen in this test is not in a state of pure tension.

8. Summary and conclusion

This research was focused to examine the suction stress (as a consequence of the inter-particle stresses) and therefore effective stress concept with respect to different failure modes observed in tensile and shear tests by using different kind of soils (fine grained to coarse grained) and taking into account the entire suction range. The experimental study allows to investigate failure at tensile to high compression stress conditions. The values of suction stress derived by different experimental methods were compared with those predicted via SWCC on drying curve and the models on microstructure level and the reason for observed deviations in suction stress derived from different methods are discussed.
The experimental studies includes fine to coarse grain material as well as pure sand (Lins 2009), two mixtures of sand-kaolin (70% sand-30% kaolin; 50% sand-50% kaolin) and pure kaolin (Heibrock 1997).

In addition, as a first indicator for changes in microstructure during drying and wetting, environmental scanning electron microscopy (ESEM) and mercury intrusion porosimetry (MIP) are performed.
The direct tensile tests are quite easy to perform, but show several shortcomings e.g. stress concentrations may occur at transfer areas between sample and hook and there is no suction control during the test that may result in inaccuracies. A hollow cylinder device allows performing tests at low stress regions avoiding the mentioned shortcomings. Within this work a new hollow cylinder device was calibrated and a first series of tests in annular pure sand specimen with suction control was performed.

It was planned to design and manufacture a new hollow cylinder device and to perform series of tests .

The major conclusions obtained from this research are: **Comparison of suction stress derived from experiments and predicted from SWCC**

- Plotting the test results in p'-q diagrams using the calculated σ' from Eq. 2.22 and determine failure envelopes for different suction stresses (using Eq. 2.29 and 2.31) of tensile and triaxial tests shows that the test results converge fairly well into a straight line. The unique failure criterion of the experimens by triaxial and tensile tests indicates that the principle of the effective stress concept defined as the sum of total normal stress and suction stress is valid and the suction stress can be extracted from the shear strength of tensile tests.

- According to the boundary conditions, the material used and type of the failure modes, there is a difference between the values of the suction stress derived from tensile and triaxial tests (see chapter 6). These discrepancies are more pronounced for smaller degrees of saturation and fine grain materials. Results may indicate that the reason for deviations in suction stress derived from tensile and triaxial tests is that soil-water interaction at different levels of suction and failure modes is dominated by different inter-particle stresses. Tensile failure often creates only a single planar fracture. It seems the tensile failure is more affected by larger scale structures (inter-aggregate pores) and in this region the water is retained by capillary stresses. While, in the shear failure the smaller scale structures (intra-aggregate pores) are more dominating and in this region the water is retained by adsorbed water and physico-chemical stresses (e.g. van der Waals stresses). As a result, based on the proposed boundary conditions, effects of the soil structure lead to differences in upscaling the microscopic interaction effects to macroscopic strength effects.

- It is shown in Figs 6.7 to 6.9 that the predictions of suction stress using the drying or scanning SWCC of the soils investigated failed. When using one of these SWCC curves suction stresses were heavily overestimated compared to the suction stress determined from the experiments. This effect seems to become more pronounced with an increasing content of fines and decreasing degree of saturation.
  It seems that the upscaling function to predict suction stress from Eq. 2.27 ($\chi = S_r$) does not consider the contributions of different interparticle stresses originating e.g. from capillary effects and physico-chemical stresses and therefore, it is not proper for fine grain materials. Also changes in micro structure of the soil samples during drying and wetting may influence the suction stress, which is not reproduced by SWCC. In addition, in macro scale the contribution of matric suction to effective stress could vary with in situ depths or confining stress that are not included in

the proposed equation from SWCC. As a result the boundary conditions has to be accounted in the SWCC.

- If the suction stresses derived from the experiments are used to define a suction stress SWCC that gives a good approximation of those derived suction stresses (σ^s_{SWCC} in Figure 6.10) the resulting curve lies outside the SWCC loop composed of the drying and wetting curves experimentally determined for the soil materials (Fig. 6.11). This indicates that the measured SWCCs on drying path (including scanning SWCCs) can not be used to predict suction stresses of the compacted samples on the drying path.

- Fig. 6.1 shows an increasing in amount of the van der Waals stresses by decreasing in degrees of saturation. This effect becomes more pronounced with increase in the amount of the fines content. The results indicate that in the case of sand the van der Waals stress can be safely ignored and capillary stress is the major reason to exhibit suction stress. For pure kaolin the values of the van der Waals stresses are important even for saturated condition and for two sand-kaolin mixtures the van der Waals stresses have significant contribution in interparticle stresses for degrees of saturation <0.2.

- The capillary model does not reflect the increasing trend of the suction stress derived from the experiments. This maybe explained through the fact that for sand-kaolin mixtures and pure kaolin at high suction levels the suction stress are not more dominated by capillary stresses and physico-chemical stresses (e.g. van der Waals stresses) may start to contribute to suction stresses significantly.

Investigation of the soil structure

- Visual observations derived from ESEM method (Fig. 4.28) show no significant changes in soil structure of the materials used (sand kaolin-mixtures; 70-30 and 50-50) from initial state (optimum water content and Proctor density) to air-dry conditions.

- Figure 4.29 confirmed the existence of bimodal porosity through MIP for initial state (optimum water content and Proctor density) and air-dry conditions comprising inter-aggregate pores that ranged in size >1 μm and intra-aggregate pores ranging from $\approx$ 0.1 μm to 1 μm. Importantly, the bimodal structure was not broken down by compaction, even at initial state and close to the optimum water contents. But for saturated conditions the double pore size distribution is no longer depicted.

- Wetting of the samples (sand kaolin-mixtures; 70-30 and 50-50) from initial state to saturated condition leads to increase of the pore volumes especially for intra-aggregate pores. For samples in the initial state and air-dry conditions the pore volume of the inter-aggregate pores ($>1\mu m$) remain almost constant. At all saturation levels the inter-layer pores (smaller than 0.1 μm) are relatively unaltered.

- As it was mentioned by Romero (1999) in the inter-aggregate region the water is retained by capillary stresses. Fig. 4.31 indicates that the main changes in this region are occurring from saturated to initial state and no further changes in pore volume of the inter-aggregate pores have been observed by increasing of suction level. According to the definition of the suction stress as the summation of the interparticle stresses in form of the capillary stress and physicichemical stresses it can be seen in Figs. 6.2 to 6.5, that by reduction in degrees of saturation the contribution of the capillary stress reduces and the interparticle stresses are more affected by physico-chemical stresses (e.g. van der Waals stresses) (see Figure 6.1).

- MIP testing of samples showed that changes in pore size distribution due to drying occurred almost exclusively for pores of 0.1 μm to 1 μm in size related to the intra-aggregate pores (Fig. 4.31). These pores desaturate at suctions of about 150 kPa to 1500 kPa. This region corresponds to the major part of the fitted suction stress SWCC curve. It could be seen that for suction range less than 1500kPa the interparticle stresses (suction stress) are more relating to capillary stress and for suction range greater than 1500kPa the physicochemical stresses are more contributing to interparticle stresses.

Design of the new hollow cylinder device

- The device explores the possibility of applying matric suction and to study the mechanical behavior in saturated, partially saturated and dry conditions. The device is equipped by double wall cell system which enables to apply matric suction whilst providing accurate measurement of soil volume change.

- Since applying the matric suction and reaching to equilibrium for sandy soil is faster therefore, in this study the sandy soil is used for performing the test.

- Expansion tests in annular sandy soil specimens by injecting water and applying cavity pressure leads to tensile failure. By determining the tangential stresses the tensile strength subjected to the used material are determined. While partially saturated soils are indicating the tensile strength under dry and saturated conditions

no tensile failure was observed (Fig. 7.14). The results show that the tensile strength of sandy soils are depending on degree of saturation as well as matric suction.

Suggested future works

Based on the findings of this study further research could investigate the following lines of study:

- It is recommended to use a suction controlled double wall triaxial test device for low suction levels to assure matric suction remains constant during the tests and to measure the volume changes accurately.
- It is recommended to use the hollow cylinder testing device for cohesive soils to evaluate the effect of suction stress in effective stress.
- The experiments in this research were only conducted for Proctor compacted samples. In order to establish the effect of density on suction stress, a range of compaction densities should be used when performing tests.
- A complete study on the variation of pore size distribution with suction on main drying, wetting and scanning curves is necessary in order to revise the methods for the prediction of soil suction from pore size distribution.
- A study on the influence of fine content on the soil water characteristics by using more active clay than those used in this study is also a topic for investigation.

A. Appendix

A.1. Listing of experimental results

A.2. Used parameters for determination of capillary stress and capillary tensile strength

Table A.1.: Tensile strength for pure sand (Lu et al. 2007), two mixtures of sand-kaolin and pure kaolin (Heibrock 1997).

Sample							
Pure sand		70/30		50/50		Pure kaolin	
Sr [-]	Tensile strength [kPa]	Sr [-]	Tensile strength [kPa]	Sr [-]	Tensile strength [kPa]	Sr [-]	Tensile strength [kPa]
0.00	0.00	0.02	45.79	0.03	66.27	0.02	143.00
0.04	0.69	0.02	39.19	0.03	72.75	0.21	149.00
0.10	0.91	0.02	37.69	0.03	58.75	0.36	223.00
0.15	1.05	0.15	44.34	0.03	60.35	0.55	262.00
0.25	1.43	0.15	39.49	0.25	46.72	0.83	266.00
0.40	1.45	0.30	35.03	0.25	48.22	0.92	80.00
0.55	1.33	0.30	40.87	0.25	50.4	1.00	18.00
0.70	1.26	0.30	38.4	0.53	42.16		
0.85	1.05	0.50	34.88	0.53	38.69		
0.93	0.92	0.50	32.44	0.53	36.29		
1.00	0.00	0.50	36.04	0.53	38.48		
		0.50	38.83	0.70	34.70		
		0.50	36.41	0.70	32.27		
		0.70	29.96	0.70	32.88		
		1.00	0.00	1.00	0.00		

Table A.2.: Results of direct tensile tests and triaxial tests for 70/30 and 50/50 sand-kaolin mixtures

sample	$Sr^1[-]$	σ_3 $[kPa]$	$p=\left(\frac{\sigma_1+\sigma_3}{2}\right)$ $[kPa]$	$q=\left(\frac{\sigma_1-\sigma_3}{2}\right)$ $[kPa]$	φ_t [°]	$-Suction\ stress$ $[kPa]$
70/30 sand-kaolin	0.02	0	-20.44	20.44	50.9	53.51
		25	282.30	257.30		
		50	381.97	331.97		
	0.31	0	-19.05	19.05	38.3	49.86
		25	141.54	116.31		
		50	214.60	164.60		
	0.50	0	-17.86	17.86	36.3	46.75
		25	136.05	111.05		
		50	190.75	140.75		
	0.69	0	-15.34	15.34	33.9	40.14
		25	106.57	81.57		
		50	167.98	117.98		
	1.00	0	0.00	0.00	38.2	1.31
		25	76.36	51.36		
		50	129.64	79.64		
50/50 sand-kaolin	0.03	0	-32.27	32.27	53.1	80.73
		0	359.42	359.42		
		50	514.60	464.60		
	0.24	0	-24.22	24.22	46.3	60.61
		0	207.82	207.82		
		50	315.57	265.57		
	0.52	0	-19.45	19.45	44.7	48.67
		0	166.82	166.82		
		50	269.09	219.09		
	0.71	0	-16.64	16.64	43.6	41.64
		0	127.91	127.91		
		50	249.14	199.14		
	1.00	0	0.00	0.00	41.7	1.25
		0	37.67	37.67		
		50	162.68	112.68		

1: Sr= Degree of saturation

Table A.3.: Results of biaxial tests on pure sand (Alabdullah 2010), triaxial tests on two sand-kaolin mixtures and pure kaolin (Brueggemann 1998)

Sample	Sr^1 [−] or Ψ^2 [kPa]	σ_3 [kPa]	$p=\left(\frac{\sigma_1+\sigma_3}{2}\right)$ [kPa]	$q=\left(\frac{\sigma_1-\sigma_3}{2}\right)$ [kPa]	c [kPa]	φ [°]
Pure sand	Saturated	10	52.01	42.01	5.04	45.7
		50	185.75	135.75		
		100	367.52	267.52		
	2	10	68.72	58.72	9.58	47.5
		50	217.93	167.93		
		100	411.61	311.61		
	4	10	61.16	51.16	8.15	47.1
		50	204.89	154.89		
		100	400.76	300.76		
	Dry	10	41.87	31.87	2.34	46.3
		50	189.51	139.51		
		100	354.99	254.99		
70/30 sand-kaolin	0.02	25	282.30	257.30	95.16	42.2
		50	381.97	331.97		
		100	512.63	412.63		
	0.31	25	141.54	116.31	40.67	37.2
		50	214.60	164.60		
		100	332.84	232.84		
	0.50	25	136.05	111.05	36.03	36.5
		50	190.75	140.75		
		100	319.47	219.47		
	0.69	25	106.57	81.57	26.25	34.6
		50	167.98	117.98		
		100	280.91	181.19		
	1.00	25	76.36	51.36	12.61	34.1
		50	144.64	94.64		
		100	248.47	148.47		

1: Sr= Degree of saturation
2: Ψ = matric suction

sample	Sr^1 $[-]$ or Ψ^2 $[kPa]$	σ_3 $[kPa]$	p $[kPa]$	q $[kPa]$	c $[kPa]$	φ [°]
50/50 sand-kaolin	0.03	0	359.42	359.42	177.37	38.19
		50	514.60	464.60		
		100	617.92	517.92		
	0.24	0	207.82	207.82	118.15	31.10
		50	315.57	265.57		
		100	414.51	314.51		
	0.52	0	166.82	166.82	93.79	31.17
		50	269.09	219.09		
		100	374.11	274.11		
	0.71	0	127.91	127.91	75.68	30.83
		50	249.14	199.14		
		100	330.42	230.42		
	1.00	0	37.67	37.67	22.72	31.23
		50	150.15	100.15		
		100	244.93	144.93		
Pure kaolin	0.38	50	310.65	260.65	173.75	18.6
		100	390.72	290.72		
		200	541.29	341.29		
	0.63	50	335.95	285.95	180.85	21.1
		100	429.42	329.42		
		200	572.32	372.32		
	0.83	50	262.34	212.34	121.72	21.3
		100	351.47	262.18		
		200	520.61	320.61		
	0.92	50	130.35	80.35	43.10	17.3
		100	203.71	103.71		
		200	337.53	137.53		
	1.00	50	87.79	37.79	5.59	20.2
		100	163.05	63.05		
		200	301.71	101.71		

1: Sr= Degree of saturation
2: Ψ = matric suction

Table A.4.: Used parameters for the determination of the capillary stress

Sample	e [-]	Ts [N/m]	d_{10} [m]	k	s/R [-]
Pure sand	0.65	0.0728	0.00025	4	0.005
				8	
				12	
				4	0.025
				8	
				12	
				4	0.05
				8	
				12	
70/30 sand/kaolin	0.43	0.0728	6.78E-06	4	0.005
				8	
				12	
				4	0.0185
				8	
				12	
				4	0.05
				8	
				12	
50/50 sand/kaolin	0.48	0.0728	4.05E-06	4	0.005
				8	
				12	
				4	0.0185
				8	
				12	
				4	0.05
				8	
				12	
Pure kaolin	0.6	0.0728	0.000001	4	0.005
				8	
				12	
				4	0.025
				8	
				12	
				4	0.05
				8	
				12	

Table A.5.: Used parameters for the determination of the capillary tensile strength

Sample	Sr [-]	s/R	k	ϴ [°]	σ_t [kPa]
Pure sand	0.2	0.025	8	26.87	0.86
	0.15			24.89	0.85
	0.1			22.21	0.82
	0.05			18.00	0.74
	0.01			10.10	0.416
	0.001			3.46	0.027
70/30 sand/kaolin	0.7	0.0185	8	33.24	51.49
	0.53			31.51	51.54
	0.27			26.71	51.10
	0.15			22.91	49.82
	0.10			20.45	48.26
	0.009			9.11	25.70
	0.001			3.34	3.44
	0.0001			0.00	0.000
50/50 sand/kaolin	0.7	0.0185	8	33.33	77.22
	0.52			32.23	77.28
	0.26			27.15	76.77
	0.15			23.61	75.18
	0.10			21.10	73.09
	0.008			9.10	38.52
	0.001			3.53	6.07
	0.0002			0.000	0.00
Pure kaolin	0.9	0.05	8	35.78	263.52
	0.8			34.80	261.60
	0.7			33.70	259.15
	0.55			31.67	253.70
	0.37			28.59	242.82
	0.22			24.43	221.53
	0.15			21.71	202.44
	0.10			19.03	178.73
	0.075			17.17	159.18
	0.05			14.72	129.50
	0.01			7.17	20.86
	0.0005			0.000	0.00

Bibliography

Agus, S. & Schanz, T. (2005), Effect of shrinking and swelling on microstructures and fabric of a compacted bentonite-sand mixture, *in* 'International Conference on Problematic Soils'.

Aitchison, G. (1965), Engineering concepts ofmoisture equilibria and moisture changes in soils, *in* 'Statement ofthe review panel, Ed. Moisture Equilibria and Moisture Changes in Soils beneath Covered Areas'.

Al-Hussaini, M. M. & Townsend, F. C. (1973), 'Tensile testing of soils, a literature review', *U.S. Army Engineer Waterways Experiment Station, Soils and Pavement Laboratory* pp. S–73–74.

Al-Hussaini, M. M. & Townsend, F. C. (1974), Investigation of tensile testing of compacted soils, Technical report, U.S. Army Engineer Waterways Experiment Station, Soil and Pavement Laboratory, Vicksburg, Mississippi, USA.

Alabdullah, J. (2010), Testing Unsaturated Soil for Plane Strain Conditions A New Double-Wall Biaxial Device, PhD thesis, Bauhaus-University Weimar.

Albert NG, M. Y. (2008), Modeling of hydraulic fracturing in cement bentonite geomaterials, PhD thesis, University of Cambridge.

Alonso, E. E., Gens, A. & Josa, A. (1990), 'A constitutive model for partially saturated soils', *Géotechnique* **40 (3)**, 405–430.

Alonso, E., Gens, A. & Hight, D. (1987), Special problem soils, *in* 'In Proceedings of the 9th European Conference on Soil Mechanics and Foundation Engineering. Edited by Hanrahan, E.T. and Orr, T.L.L. and Widdis, T.F. Rotterdam, Netherlands'.

Alonso, E. & Romero, E. (2011), Experimental investigation on an effective stress law in compacted clayey-silty soil, *in* 'Proceedings of the Fifth Asia-Pacific Conference on Unsaturated Soils, Pattaya, Thailand. Geotechnical Engineerig Research and Development Centre, Bangkok. pp. 331-336'.

Alsayed, M. (1988), Laboratory testing of thick-walled hollow cylinders of rock, Master's thesis, University of Newcastle upon Tyne, UK.

Alsayed, M. (2002), 'Utilising the hoek triaxial cell for multiaxial testing of hollow rock cylinders', *Journal of Rock Mechanics and Mining Sciences* **39**, 355–366.

Alsherif, N. & McCartney, J. (2014), 'Effective stress in unsaturated silt at low degrees of saturation', *Vadose Zone J.* **13**.

Amanullah Marri, M. (2010), The mechanical behavior of cemented granular materials at high pressures, PhD thesis, University of Nottingham.

Aylmore, L. & Quirk, J. (1971), 'Domains and quasicrystalline regions in clay systems', *Soil sceince society of america* **35**, 652–654.

Bai, S., Shen, X. & Su, B. (1982), Devices for measuring the tensile strength of soils (in chinese), Technical report, Water Conservancy and Hydroelectric Power Research Institute.

Baille, W., Tripathy, S. & Schanz, T. (2014), 'Effective stress in clays of various mineralogy', *Vadose Zone* .

Barden, L. & Sides, G. (1970), 'Engineering behavior and structure of compacted clays', *Soil Mechanics and Foundation Analysis* **96**, 1171–1200.

Barzegar, A. R., Oades, J. M., Rengasamy, P. & Murray, R. S. (1995), 'Tensile strength of dry, remoulded soils as affected by properties of the clay fraction', *Geoderma* **16**, 93–108.

Bishop, A. W. (1959), 'The principle of effective stress', *Teknisk Ukeblad, Oslo, Norway* **106**, 859–863.

Bishop, A. W. & Blight, G. E. (1963), 'Some aspects of effective stress in saturated and partially saturated soils', *Géotechnique* **13 (3)**, 177–197.

Bishop, A. W. & Donald, I. B. (1961), The experimental study of partially saturated soil in the triaxial apparatus, *in* 'in Proc. 5th Int. Conference Soil Mechanic Foundation Engineering (Paris, France), vol. 1, 13-21'.

Blight, G. (1967), 'Effective stress evaluation for unsaturated soils', *Soil mechanics and foundation division* **93**, 125–148.

Bolzon, G., Schrefler, B. A. & Zienkiewicz, O. C. (1996), 'Elastoplastic soil constitutive laws generalised to partially saturated states', *Géotechnique* **46 (2)**, 270–289.

Borja, R. (2006), 'On the mechanical energy and effective stress in saturated and unsaturated porous materials', *International Journal of Solids Structures* **43 (6)**, 1764–1786.

Borja, R. & Koliji, A. (2009), 'On the effective stress in unsaturated porous continua with double porosity', *Mech. Phys. Solids* **57 (8)**, 1182–1193.

Brackley, I. J. A. (1971), Partial collapse in partially saturated expansive clay, *in* 'Proc. 5th Reg. Conference Soil Mech. Found. Eng. (South Africa), pp. 23-30'.

Brueggemann, R. (1998), Zugfestigkeit verdichteter tone als funktion des wassergehalts, Master's thesis, Ruhr-Universität Bochum.

Brye, K. (2003), 'Long-term effects of cultivation on particle size and water-retention characteristics determined using wetting curves', *Soil Science* **168**, 459–468.

Chakrabarty, J. (2006), *Theory of plasticity*, Elsevier Butterworth-Heinemann.

Coleman, J. D. (1962), 'Stress-strain relations for partially saturated soils', *Géotechnique* **12 (4)**, 348–350.

Collins, K. & McGown, A. (1974), 'The form and function of microfabric features in a variety of natural soils', *Géotechnique* **24**, 12–23.

Coulon, E. & Bruand, A. (1989), 'Effects of compaction on the pore space geometry in sandy soils', *Soil and Tillage Research* **15(1-2)**, 137–152.

Croney, D. & Coleman, J. (1961), Pore pressure and suction in soil, *in* 'Conference on Pore Pressure and Suction in Soils London, Butterworths'.

Cui, Y. J. & Delage, P. (1996), 'Yielding and plastic behaviour of a partially saturated compacted silt', *Géotechnique* **46 (2)**, 291–311.

Cuisinier, S. & Laloui, L. (2004), 'Fabric evolution during hydromechanical loading of a compacted silt', *Numerical and Analytical Methods in Geomechanics* **28(6)**, 483–499.

De Las Cuevas, C. (1997), 'Pore structure characterisation in rock salt', *Engineering Geology* **47**, 17–30.

Delage, P. & Lefebvre, G. (1984), 'Study of the structure of a sensitive champlain clay and of its evolution during consolidation', *Canadian Geotechnical Journal* **21**, 21–35.

Den Hartog, J. (1952), *Advanced strength of materials*, Mc Graw. Hill, New York.

Escario, V. & Juca, J. F. T. (1989), Shear strength and deformation of partially saturated soils, *in* 'Proc. 12th Int. Conf. on Soil Mechanics and Foundation Engineering, Vol. 2, Balkema, Rotterdam, The Netherlands 43-46'.

Escario, V. & Saez, J. (1986), 'The shear strength of partially saturated soils', *Géotechnique* **36**, 453–456.

Fredlund, D. G. & Xing, A. (1994), 'Equations for the soil-water characteristic curve', *Canadian Geotechnical Journal* **31**, 521–532.

Fredlund, D. & Morgenstern, N. (1977), 'Stress state variables for unsaturated soils', *Geotechnical Division, ASCE* **103**, 447–466.

Fredlund, D. & Rahardjo, H. (1993), *Soil mechanics for unsaturated soils*, John Wiley and Sons, Inc.

Frydman, S. (1967), Triaxial and tensile strength tests on stabilised soils, *in* 'proceedings of the third asian regional conference on soil mechanics and foundation'.

Fuentes, W. & Triantafyllidis, T. (2013), 'On the effective stress for unsaturated soils with residual water', *Géotechnique* **63 (16)**, 1451–1455.

Futai, M. (2002), Theoretical-experimental study of the behavior of non-saturated tropical soils applied to a gully erosion, PhD thesis, Federal University of Rio de Janeiro Brazil.

Gallipoli, D. A., Gens, R., Sharma & Vaunat, J. (2003), 'An elasto-plastic model for unsaturated soil incorporating the effects of suction and degree of saturation on mechanical behavior', *Géotechnique* **53(1)**, 123–135.

Geiser, F., Laloui, L. & Vulliet, L. (2006), 'Elasto-plasticity of partially saturated soils: laboratory test results on a remoulded silt', *Soils and Foundations* **46(5)**.

Gens, A., Alonso, E., Suriol, J. & Lloret, A. (1995), Effect of structure on the volumetric behaviour of a compacted soil, *in* 'Proceedings of the First International Conference on Partially saturated Soils, UNSAT95, Paris, France. pp. 83-88'.

Ghazi, G., Al-Khateeb & William, G. B. (2000), Hollow-cylinder tensile test for asphaltic paving mixtures, *in* 'Proceedings of the Mid-Continent Transportation Symposium, Ames, Iowa, USA, May 15-16, 2000, 14-19'.

Gray, W. & Schrefler, B. A. (2001), 'Thermodynamic approach to effective stress in partially saturated porous media', *Eur. J. Mech* **20(4)**, 521–538.

Haines, W. B. (1930), 'The hysteresis effect in capillary properties and the modes of moisture distribution associated therewith', *Agricultural Science* **20**, 96–105.

Hassanizadeh, S. & Gray, W. (1990), 'Mechanics and thermodynamics of multiphase flow in porous media including interphase boundaries', *Advanced Water Resources* **13 (4)**, 169–186.

Heibrock, G. (1997), 'Schrumpf ribildung in mineralischen dichtungsschichten unter auflast', *geotechnik* **1 VGE Essen**.

Heibrock, G., Zeh, R. & Witt, K. (2003), Tensile strength of compacted clays, *in* 'International Conference From Experimental Evidence Towards Numerical Modelling of Unsaturated Clays, Weimar'.

Hight, D.W.and Gens, A. & Symes, M. (1983), 'Development of a new hollow cylinder apparatus for investigating the effects of principal stress rotation in soils', *Géotechnique* **33**, 355–83.

Hilf, J. W. (1956), An Investigation of Pore-Water Pressure in Compacted Cohesive Soils, PhD thesis, U.S. Dep. of the Interior, Bureau of Reclamation, Design and Construction Div., Denver.

Houlsby, G. (1997), 'The work input to an unsaturated granular material', *Géotechnique* **47 (1)**, 193–196.

Houlsby, G. T. (1998), Advanced interpretation of field tests, *in* '1st Int. Conf. on Site Investigation, Atlanta, 99-112'.

Jaeger, J. & Cook, N. (1979), *Fundamentals of rock mechanics*, Chapman & Hall, London.

Jennings, J. E. (1961), A revised effective stress law for use in the prediction of the behavior of partially saturated soils in pore pressure and suction in soils, *in* 'conf. organized by the British Nat. Soc. of Int. Soc. Soil Mech. Found. Eng. at the Inst. of Civil Eng. London: Butterworths, 26-30'.

Jennings, J. E. & Burland, J. B. (1962), 'Limitations to the use of effective stresses in partially saturated soils', *Géotechnique* **12 (2)**, 125–144.

Karner, S. L., Chester, F. M., Kronenberg, A. K. & Chester, J. S. (2003), 'Subcritical compaction and yielding of granular quartz sand', *Tectonophysics* **Available online at sciencedirect.com**, 357– 381.

Khalili, N., Geiser, F. & Blight, G. (2004), 'Effective stress in partially saturated soils: A critical review with new evidence', *Geomechanics. ASCE* **4 (2)**, 115–126.

Khalili, N. & Khabbaz, M. (1998), 'A unique relationship for the determination of the shear strength of partially saturated soils', *Géotechnique* **48(5)**, 681–687.

Khalili, N. & Zargarbashi, S. (2010), 'Influence of hydraulic hysteresis on effective stress in unsaturated soils', *Géotechnique* **60 (9)**, 729–734.

Khosravi, A., Ghayoomi, M. & McCartney, J. S. (2010), Impact of effective stress on the dynamic shear modulus of unsaturated sand, *in* 'GeoFlorida (CD-ROM), West Palm Beach, FL, Feb 20-24'.

Khosravi, A. & McCartney, J. (2012), 'Impact of hydraulic hysteresis on the small-strain shear modulus of unsaturated soils', *Geotech. Eng Geoenviron. Eng* **138(11)**, 1326–1333.

Kim, T. (2001), Moisture-induced tensile strength and cohesion in sand, PhD thesis, Dept. of Civil, Environmental and Architectural Engineering, .Univ. of Colorado, Boulder, Colo.

Kim, T. H. & Sture, S. (2008), 'Capillary induces tensile strength in unsaturated sands', *NRC research press* .

Leong, E. & Rahardjo, H. (1997), 'Review of soil-water characteristic curve equations', *Geotechnical and Geoenvironmental Engineering, ASCE* **123**, 1106–1117.

Leong, E., Tripathy, S. & Rahardjo, R. (2003), 'Total suction measurement of unsaturated soils with a device using the chilled-mirror dew-point technique', *Géotechnique* **53**, 173–182.

Li, X. & Zhang, L. (2009), 'Characterization of dual-structure pore size distribution of soil', *Can. Geotech* **46**, 129–141.

Likos, W. J. & Wayllace, A. (2010), 'Porosity evolution of free and confined bentonites during interlayer hydration', *Clays and Clay Minerals* **58**, 399–414.

Lins, Y. (2009), Hydro-Mechanical Properties of Partially Saturated Sand, PhD thesis, Faculty of Civil Egineering University Bochum.

Loret, B. & Khalili, N. (2000), 'A three phase model for partially saturated soils', *Int. J. Numer. Analyt. Meth. Geomech* **24 -11**, 893–927.

Loret, B. & Khalili, N. (2002), 'An effective stress elasto-plastic model for partially saturated soils', *Mech. Material* **44**, 97–116.

Lu, N., Godt, J. W. & Wu, D. T. (2010), 'A closed form equation for effective stress in unsaturated soil', *Water resources research* **46**.

Lu, N., Kim, T. H., Sture, S. & Likos, W. J. (2009), 'Tensile strength of partially saturated sand', *Mechanics of Engineering* **135 (12)**.

Lu, N. & Likos, W. J. (2004), *Unsaturated soil mechanics*, Wiley, New York.

Lu, N. & Likos, W. J. (2006), 'Suction stress characteristic curve for unsaturated soil', *Geotech. Geoenviron. Eng.* **132(2)**, 131–142.

Lu, N., Wu, B. & Tan, C. P. (2007), 'Tensile strength characteristics of unsaturated sands', *Geotech. Geoenviron. Eng* **133(2)**, 144–154.

Maatouk, A., Leroueil, S. & La Rochelle, P. (1995), 'Yielding and critical state of collapsible partially saturated silty soil', *Géotechnique* **45 (3)**, 465–477.

Mair, R. J. & Wood, D. M. (1987), *Pressuremeter testing, methods and interpretation*, Butterworths, London.

Matyas, E. L. & Radhakrishna, H. S. (1968), 'Volume change characteristics of partially saturated soils', *Géotechnique* **18 (4)**, 432–448.

McCartney, J., Villar, L. & Zornberg, J. (2008), Nonwoven geotextiles as hydraulic barriers for capillary rise, *in* 'GeoAmericas, Cancun, Mexico. March. 3-5'.

Menzies, B. K. (1984), 'Soil testing systems', *Geotechnical News* **1, No. 3**, 38–39.

Mitchell, J. K. (1976), *Fundamentals of soil behavior*, Wiley, New York.

Mitchell, J. & Soga, K. (2006), *Fundamentals of soil behaviour. 3rd edition*, John Wiley & Sons, Inc.

Modaressi, A. & Abou-Bekr, N. (1994), A unified approach to model the behaviour of saturated and partially saturated soils, *in* 'Siriwardane, ed., Proc., 8th Int. Conf. on Computer Methods and Advances in Geomechanics, Morgantown, Balkema, Rotterdam, 1507-1513'.

Molenkamp, F. & Nazemi, A. (2003), 'Interactions between two rough spheres, water bridge and water vapour', *Géotechnique* **53 (2)**, 255–264.

Moller, P. C. F., Mewis, J. & Bonn, D. (2006), 'Yield stress and thixotropy: on the difficulty of measuring yield stresses in practice', *Soft material* **2(4)**, 274–283.

Monroy, R., Zdrakovic, L. & Ridley, A. (2010), 'Evolution of microstructure in compacted london clay during wetting and loading', *Géotechnique* **60**, 105–119.

Montanes, J. E. C. (2002), Suction and volume changes of compacted sand-bentonite mixtures, PhD thesis, University of London.

Moo-Young, H. & Ochola, C. (1999), 'Non-destructive testing of fine grained soil behavior utilizing the environmental scanning electron microscope', *American Society for Testing and Materials* **1350**, 29–42.

Murdoch, L. (1993a), 'Hydraulic fracturing of soil during laboratory experiments part 1. methods and observations', *Géotechnique* **43 (2)**, 255–265.

Murray, E. J. (2002), 'An equation of state for unsaturated soils', *Canadian Geotechnical Journal* **39 (1)**, 125–140.

Murray, E. & Sivakumar, V. (2010), *Unsaturated Soils: a fundamental interpretation of soil behaviour*, Wiley-Blackwell.

Nadai, A. (1950), *Theory of flow and fracture of solids*, McGraw-Hill Book Company, Inc., USA.

Nikooee, E., Habibagahi, G., Hassanizadeh, S. & Ghahramani, A. (2013), 'Effective stress in unsaturated soils: A thermodynamic approach based on the interfacial energy and hydromechanical coupling', *Transport in Porous Media* **96 (2)**, 369–396.

Nuth, M. & Laloui, L. (2008), 'Effective stress concept in partially saturated soils: clarification and validation of a unifined framework', *Int Journal of Numerical Methods Geomech* **32**, 771–800.

Oberg, A. & Sallfors, G. (1997), 'Determination of shear strength parameters of partially saturated silts and sands based on the water retention curve', *Geotech Test Journal* **20**, 40–48.

Ohokal, M., Funatol, A. & Takahashi, Y. (1997), 'Tensile test using hollow cylindrical specimen', *Rock Mechanics and Mining Society* **34 (3-4)**.

Penumadu, D. & Dean, J. (2000), 'Compressibility effect in evaluating the pore-size distribution of kaolin clay using mercury intrusion porosimetry', *Canadian Geotechnical* **37(2)**, 393–405.

Pierrat, P. & Caram, H. S. (1997), 'Tensile strength of wet granular material', *Powder Technology* **91**, 83–93.

Pietsch, W. & Rumpf, H. (1967), 'Haftkraft, kapillardruck, flüssigkeitsvolumen und grenzwinkel einer flüssigkeitsbrücke zwischen zwei kugeln', *Chem Ing Tech.* **39(15)**, 885–893.

Poulovassilis, A. & El-Ghamry, W. (1978), 'The dependent domain theory applied to scanning curves of any order in hysteretic soil water relationships', *Soil Science* **126**, 1–8.

Reis, R. (2004), Stress-strain behaviour of two horizons of a residual soil from gneiss, PhD thesis, University of Sao Paulo Brazil.

Richards, B. (1966), The significance of moisture flow and equilibrium in unsaturated soil in relation to the design of engineering structures built on shallow foundations in australia, *in* 'Symposium on Permeability and Capillarity, ASTM, Atlantic City, NJ'.

Romero, E. (1999), Characterisation and Thermo-hydro-mechanical behavior of unsaturated boom clay, an experimental study, PhD thesis, Universidad politecnica de Cataluna Barcelona.

Rumpf, H. (1961), 'The strength of granules and agglomerates', *Agglomeration W.A.Knepper, Interscience* pp. 379–418.

Santamarina, C. (2001), Soil behavior at the microscale particle forces, *in* 'Proc. Symp. Soil Behavior and Soft Ground Construction, in honor of Charles C. Ladd - October, MIT'.

Schanz, T., Agus, S. & Tscheschlok, G. (2004), 'Determination of hydro-mechanical properties of trisoplast', *Laboratory of Soil Mechanics* .

Schnaid, F., Oliveira, L. A. K. & Gehling, W. (2004), 'Unsaturated constitutive surfaces from pressuremeter tests', *Journal of Geotechnical and Geoenvironmental Engineering* **130, No. 2**.

Schubert, H. (1984), 'Capillary force-modeling and application in particulate technology', *Powder Technology* **37**.

Sheahan, T. C., Germaine, J. T. & Ladd, C. C. (1990), 'Automated triaxial testing of soft clays: an upgraded commercial system', *Geotechnical Testing Journal* **13**, 153–163.

Sheng, D., Fredlund, D. & Gens, A. (2008), 'A new modelling approach for unsaturated soils using independent stress variables', *Can. Geotech* **45**, 511–534.

Sivakumar, V. (1993), A critical state framework for partially saturated soils, PhD thesis, Sheffield, University of Sheffield.

Sivakumar, V. & Wheeler, S. (2000), 'Influence of compaction procedure on the mechanical behaviour of an unsaturated compacted clay. part 1: Wetting and isotropic compression', *Géotechnique* **50(4)**, 359–368.

Song, S. Y., Hwang, W. K., Jung, S. J. & Kim, T. H. (2012), 'A comparative study of suction stress between sand and silt under unsaturated conditions', *Engineering Geology* **124**, 90–97.

Song, Y. S. (2014), 'Suction stress in unsaturated sand at different relative densities', *Engineering Geology* **176**, 1–10.

Sridharan, A., Altaschaeffl, A. & Diamond, S. (1971), 'Pore size distribution studies', *Soil Mechanics and Foundations Division* **97 (5)**, 771–787.

Tamagnini, R. (2004), 'An extended cam-clay model for unsaturated soils with hydraulic hysteresis', *Géotechnique* **54(3)**, 223–228.

Tamrakar, S. B., Mitachi, T. & Toyosawa, Y. (2007), 'Measurement of soil tensile stength and factors affecting its measurements', *Soils and foundations* **47**, 911–918.

Tamrakar, S. B., ToyTamr, Y., Mitachi, T. & Itoh, K. (2005), 'Tensile strength of compacted and saturated soils using newly developed tensile strength measuring apparatus', *Soils and* **45**, 103–110.

Tang, C., Xiang, J., Wang, D., Shi, B. & Li, J. (2015), 'Tensile strength of compacted clayey soil', *Geotechnical and Geoenvironmental Engineering* .

Tarantino, A. & Tombolato, S. (2005), 'Coupling of hydraulic and mechanical behaviour in partially saturated compacted clay', *Géotechnique* **55 (4)**, 307–317.

Terzaghi, K. (1936), The shearing resistance of saturated soils, *in* 'Proc., 1st Int. Conf. on Soil Mechanics, Vol. 1, Cambridge, Mass., 54-56'.

Thom, R., Sivakumar, R., Murray, E. & Mackinnon, P. (2007), 'Pore size distribution of unsaturated compacted kaolin the initial states and final states following saturation', *Géotechnique* **57**, 469–474.

Toll, D. & Ong, B. (2003), 'Critical state parameters for an unsaturated residual sandy clay', *Géotechnique* **53(1)**, 93–103.

Topp, G. C. & Miller, E. E. (1966), Hysteretic moisture characteristics and hydraulic conductivities for glass-bead media, *in* 'Proc. Crop Science Society of Americ, vol. 30, 156-162'.

Tuller, M., Or, D. & Dudley, L. M. (1999), 'Adsorption and capillary condensation in porous media: Liquid retention and interfacial configurations in angular pores', *Water Resour. Research* **35**, 1949–1964.

van Genuchten, M. (1980), 'A closed-form equation for predicting the hydraulic conductivity of unsaturated soils', *Soil Sci. Soc* **44**, 892–898.

van Olphen, H. (1991), *Clay colloid chemistry*, 2nd Ed., Krieger, Boca Raton, Fla.

Vanapalli, S. K., Fredlund, D. G., Pufahl, D. E. & Clifton, A. W. (1996), 'Model for the prediction of shear strength with respect to soil suction', *Can. Geotech* **33**, 379–392.

Vesga, L. F. (2009), 'Direct tensile-shear test (dts) in unsaturated kaolinite clay', *Geotechnical Testing Journal* **Vol 32, No. 5**.

Vesga, L. F. Vallejo, L. E. (2006), Direct and indirect tensile tests for measuring the equivalent effective stress in a kaolinite clay, *in* '4th Int. Conf. on Unsaturated Soils, ASCE, Reston, Va., 1290-1301'.

Wheeler, S., Sharma, R. & Buisson, M. (2003), 'Coupling of hydraulic hysteresis and stress-strain behaviour in unsaturated soils', *Géotechnique* **53(1)**, 41–54.

Yu, H. (2000), *Cavity expansion methods in geomechanics*, Kluwer Academic Publishers, The Netherlands.

Schriftenreihe des Lehrstuhls für Grundbau, Boden- und Felsmechanik der Ruhr-Universität Bochum

Herausgeber: H.L. Jessberger

1 (1979) **Hans Ludwig Jessberger**
Grundbau und Bodenmechanik an der Ruhr-Universität Bochum

2 (1978) **Joachim Klein**
Nichtlineares Kriechen von künstlich gefrorenem Emschermergel

3 (1979) **Heinz-Joachim Gödecke**
Die Dynamische Intensivverdichtung wenig wasserdurchlässiger Böden

4 (1979) **Poul V. Lade**
Three Dimensional Stress-Strain Behaviour and Modeling of Soils

5 (1979) **Roland Pusch**
Creep of soils

6 (1979) **Norbert Diekmann**
Zeitabhängiges, nichtlineares Spannungs-Verformungsverhalten von gefrorenem Schluff unter triaxialer Belastung

7 (1979) **Rudolf Dörr**
Zeitabhängiges Setzungsverhalten von Gründungen in Schnee, Firn und Eis der Antarktis am Beispiel der deutschen Georg-von-Neumayer- und Filchner-Station

8 (1984) **Ulrich Güttler**
Beurteilung des Steifigkeits- und Nachverdichtungsverhaltens von ungebundenen Mineralstoffen

9 (1986) **Peter Jordan**
Einfluss der Belastungsfrequenz und der partiellen Entwässerungs-möglichkeiten auf die Verflüssigung von Feinsand

10 (1986) **Eugen Makowski**
Modellierung der künstlichen Bodenvereisung im grundwasserdurchströmten Untergrund mit der Methode der finiten Elemente

11 (1986) **Reinhard A. Beine**
Verdichtungswirkung der Fallmasse auf Lastausbreitung in nichtbindigem Boden bei der Dynamischen Intensivverdichtung

12 (1986) **Wolfgang Ebel**
Einfluss des Spannungspfades auf das Spannungs-Verformungsverhalten von gefrorenem Schluff im Hinblick auf die Berechnung von Gefrierschächten

13 (1987) **Uwe Stoffers**
Berechnungen und Zentrifugen-Modellversuche zur Verformungsabhängigkeit der Ausbaubeanspruchung von Tunnelausbauten in Lockergestein

14 (1988) **Gerhard Thiel**
Steifigkeit und Dämpfung von wassergesättigtem Feinsand unter Erdbebenbelastung

15 (1991) **Mahmud Thaher**
Tragverhalten von Pfahl-Platten-Gründungen im bindigen Baugrund,
Berechnungsmodelle und Zentrifugen-Modellversuche

16 (1992) **Rainer Scherbeck**
Geotechnisches Verhalten mineralischer Deponieabdichtungsschichten
bei ungleichförmiger Verformungswirkung

17 (1992) **Martin M. Bizialiele**
Torsional Cyclic Loading Response of a Single Pile in Sand

18 (1993) **Michael Kotthaus**
Zum Tragverhalten von horizontal belasteten Pfahlreihen aus langen Pfählen in Sand

19 (1993) **Ulrich Mann**
Stofftransport durch mineralische Deponieabdichtungen:
Versuchsmethodik und Berechnungsverfahren

20 (1992) **Festschrift anlässlich des 60. Geburtstages von**
Prof. Dr.-Ing. H. L. Jessberger
20 Jahre Grundbau und Bodenmechanik an der Ruhr-Universität Bochum

21 (1993) **Stephan Demmert**
Analyse des Emissionsverhaltens einer Kombinationsabdichtung im Rahmen der
Risikobetrachtung von Abfalldeponien

22 (1994) **Diethard König**
Beanspruchung von Tunnel- und Schachtausbauten in kohäsionslosem Lockergestein
unter Berücksichtigung der Verformung im Boden

23 (1995) **Thomas Neteler**
Bewertungsmodell für die nutzungsbezogene Auswahl von Verfahren zur Altlastensanierung

24 (1995) **Ralph Kockel**
Scherfestigkeit von Mischabfall im Hinblick auf die Standsicherheit von Deponien

25 (1996) **Jan Laue**
Zur Setzung von Flachfundamenten auf Sand unter wiederholten Lastereignissen

26 (1996) **Gunnar Heibrock**
Zur Rissbildung durch Austrocknung in mineralischen Abdichtungsschichten
an der Basis von Deponien

27 (1996) **Thomas Siemer**
Zentrifugen-Modellversuche zur dynamischen Wechselwirkung zwischen Bauwerken
und Baugrund infolge stoßartiger Belastung

28 (1996) **Viswanadham V. S. Bhamidipati**
Geosynthetic Reinforced Mineral Sealing Layers of Landfills

29 (1997) **Frank Trappmann**
Abschätzung von technischem Risiko und Energiebedarf bei Sanierungsmaßnahmen
für Altlasten

30 (1997) **André Schürmann**
Zum Erddruck auf unverankerte flexible Verbauwände

31 (1997) **Jessberger, H. L. (Herausgeber)**
Environment Geotechnics, Report of ISSMGE Technical Committee TC 5
on Environmental Geotechnics

Herausgeber: Th. Triantafyllidis

32 (2000) **Triantafyllidis, Th. (Herausgeber)**
Boden unter fast zyklischer Belastung: Erfahrung und Forschungsergebnisse (Workshop)

33 (2002) **Christof Gehle**
Bruch- und Scherverhalten von Gesteinstrennflächen mit dazwischenliegenden Materialbrücken

34 (2003) **Andrzej Niemunis**
Extended hypoplastic models for soils

35 (2004) **Christiane Hof**
Über das Verpressankertragverhalten unter kalklösendem Kohlensäureangriff

36 (2004) **René Schäfer**
Einfluss der Herstellungsmethode auf das Verformungsverhalten von Schlitzwänden in weichen bindigen Böden

37 (2005) **Henning Wolf**
Zur Scherfugenbänderung granularer Materialien unter Extensionsbeanspruchung

38 (2005) **Torsten Wichtmann**
Explicit accumulation model for non-cohesive soils under cyclic loading

39 (2008) **Christoph M. Loreck**
Die Entwicklung des Frischbetondruckes bei der Herstellung von Schlitzwänden

40 (2008) **Igor Arsic**
Über die Bettung von Rohrleitungen in Flüssigböden

41 (2009) **Anna Arwanitaki**
Über das Kontaktverhalten zwischen einer Zweiphasenschlitzwand und nichtbindigen Böden

Herausgeber: T. Schanz

42 (2009) **Yvonne Lins**
Hydro-Mechanical Properties of Partially Saturated Sand

43 (2010) **Tom Schanz (Herausgeber)**
Geotechnische Herausforderungen beim Umbau des Emscher-Systems
Beiträge zum RuhrGeo Tag 2010

44 (2010) **Jamal Alabdullah**
Testing Unsaturated Soil for Plane Strain Conditions: A New Double-Wall Biaxial Device

45 (2011) **Lars Röchter**
Systeme paralleler Scherbänder unter Extension im ebenen Verformungszustand

46 (2011) **Yasir Al-Badran**
Volumetric Yielding Behavior of Unsaturated Fine-Grained Soils

47 (2011) **Usque ad finem**
Selected research papers

48 (2012) **Muhammad Ibrar Khan**
Hydraulic Conductivity of Moderate and Highly Dense Expansive Clays

49 (2014) **Long Nguyen-Tuan**
Coupled Thermo-Hydro-Mechanical Analysis: Experimental and Back Analysis

50 (2014) **Tom Schanz (Herausgeber)**
Ende des Steinkohlenbergbaus im Ruhrrevier:
Realität und Perspektiven für die Geotechnik Beiträge zum RuhrGeo Tag 2014

51 (2014) **Usque finem**
Selected research papers

52 (2014) **Houman Soleimani Fard**
Study on the Hydro-Mechanical Behavior of Fiber Reinforced Fine Grained Soils, with Application to the Preservation of Historical Monuments

53 (2014) **Wiebke Baille**
Hydro-Mechanical Behaviour of Clays - Signicance of Mineralogy

54 (2014) **Qasim Abdulkarem Jassim Al-Obaidi**
Hydro-Mechanical Behavior of Collapsible Soils

55 (2015) **Veselin Zarev**
Model Identication for the Adaption of Numerical Simulation Models-
Application to Mechanized Shield Tunneling

56 (2015) **Meisam Goudarzy**
Micro and Macro Mechanical Assessment of Small and Intermediate
Strain Properties of Granular Material

57 (2016) **Oliver Detert**
Analyse einer selbstregulierenden interaktiven Membrangründung für
Schüttkörper auf geringtragfähigen Böden

58 (2016) **Yang Yang**
Analyses of Heat Transfer and Temperature-induced Behaviour in Geotechnics

59 (2016) **Alborz Pourzargar**
Application of Suction Stress Concept to Partially Saturated Compacted Soils